

UNIVERSIDAD POLITÉCNICA DE MADRID

ESCUELA TÉCNICA SUPERIOR
DE INGENIEROS DE TELECOMUNICACIÓN



DEVELOPMENT OF EFFICIENT TECHNIQUES FOR
THE ANALYSIS AND DESIGN OF ANTENNAS IN
DUAL-REFLECTARRAY CONFIGURATION

TESIS DOCTORAL

Carolina Tienda Herrero
Ingeniera de Telecomunicación

Madrid, 2012



DEPARTAMENTO DE ELECTROMAGNETISMO
Y TEORÍA DE CIRCUITOS



ESCUELA TÉCNICA SUPERIOR
DE INGENIEROS DE TELECOMUNICACIÓN

TESIS DOCTORAL

DEVELOPMENT OF EFFICIENT TECHNIQUES FOR THE ANALYSIS AND DESIGN OF ANTENNAS IN DUAL-REFLECTARRAY CONFIGURATION

Autora:

Carolina Tienda Herrero

Ingeniera de Telecomunicación

Director:

José Antonio Encinar Garcinuño

Doctor Ingeniero de Telecomunicación

Catedrático de Universidad

Codirector:

Manuel Arrebola Baena

Doctor Ingeniero de Telecomunicación

Profesor Titular de Universidad

Madrid, 2012

TESIS DOCTORAL: Development of efficient techniques for the analysis and design of antennas in dual-reflectarray configuration.

AUTOR: Carolina Tienda Herrero
Ingeniera de Telecomunicación

DIRECTOR: José Antonio Encinar Garcinuño
Doctor Ingeniero de Telecomunicación
Catedrático de Universidad

CODIRECTOR: Manuel Arrebola Baena
Doctor Ingeniero de Telecomunicación
Profesor Titular de Universidad

DEPARTAMENTO: Electromagnetismo y Teoría de Circuitos
Universidad Politécnica de Madrid

El Tribunal de Calificación, compuesto por:

PRESIDENTE:

VOCALES:

VOCAL SECRETARIO:

VOCALES SUPLENTES:

Acuerda otorgarle la CALIFICACIÓN de:

Madrid, a de Febrero de 2012.

ACKNOWLEDGMENT

First of all I would like to show my most sincere gratitude to my advisor Prof. José A. Encinar. This thesis work could not have been accomplished without his insight, guidance and patience. Thank you for being always there, no matter where, in Madrid or Belfast.

I am indebted to my advisor Manuel Arrebola Baena for his support throughout the whole process of this thesis. Thank you for being available any time, seven days per week. Thank you for encouraging me in the “moments of darkness”.

I would like to thank all the staff of the Departamento de Electromagnetismo y Teoría de Circuitos of Universidad Politécnica de Madrid. Special thanks go to Mariano. Without “his beloved” lab and his great building abilities none of the antenna reflectarrays prototypes would have ever seen the light. From him I learned hands-on laboratory skills and I really enjoyed my time while doing some hardware work.

I owe my gratitude to the external committee members, for the time and effort to read and evaluate this thesis: Robert Cahill, Elena Saenz and Germán León.

This thesis is also the result of an educational visit to the European Space Agency (ESTEC), under the supervision of Dr. Giovanni Toso and Cyril Mangenot. Thank you for hosting me in your department during that period.

I would also like to thank some institutions for financial support during this thesis: Ministerio de Ciencia y Tecnología (MCyT) and Ministerio de Educación y Ciencia (MEC).

I am also grateful to all the colleagues I got the opportunity to interact with during this time at the University of Madrid, either sharing the office, discussing on technical topics or entertaining lunch, coffee breaks and chinos. In particular I would like to mention: Eduardo Carrasco, Carlos Alberto Leal, Bilal Eljaafari, Jose Enrique, Pedro Robustillo, Ignacio Echeveste, Gerardo Pérez Palomino, Leandro de Haro, Jesús María Rebollar, Jose Ramón and Jesús Grajal.

Finally, I would like to thank many friends for their support during the last years. People, who despite the distance, are close to me: Desi, Rosi, Adrián, CaroCo, EvaP, Vane, Marina, Cristi, Bea, Ruth, Loli and Rafael. And also thanks to my friends from here (Madrid) with whom I have shared part of my life: Yayo, Germán, Julio, Gonzalo, Elena, Bea, Pili and Alfonso.

Special thanks to Varo, my partner, he always supports me no matter where.

ABSTRACT

This thesis contributes to the analysis and design of printed reflectarray antennas. The main part of the work is focused on the analysis of dual offset antennas comprising two reflectarray surfaces, one of them acts as sub-reflector and the second one acts as main-reflector. These configurations introduce additional complexity in several aspects respect to conventional dual offset reflectors, however they present a lot of degrees of freedom that can be used to improve the electrical performance of the antenna. The thesis is organized in four parts: the development of an analysis technique for dual-reflectarray antennas, a preliminary validation of such methodology using equivalent reflector systems as reference antennas, a more rigorous validation of the software tool by manufacturing and testing a dual-reflectarray antenna demonstrator and the practical design of dual-reflectarray systems for some applications that show the potential of these kind of configurations to scan the beam and to generate contoured beams.

In the first part, a general tool has been implemented to analyze high gain antennas which are constructed of two flat reflectarray structures. The classic reflectarray analysis based on MoM under local periodicity assumption is used for both sub and main reflectarrays, taking into account the incident angle on each reflectarray element. The incident field on the main reflectarray is computed taking into account the field radiated by all the elements on the sub-reflectarray.. Two approaches have been

developed, one which employs a simple approximation to reduce the computer run time, and the other which does not, but offers in many cases, improved accuracy. The approximation is based on computing the reflected field on each element on the main reflectarray only once for all the fields radiated by the sub-reflectarray elements, assuming that the response will be the same because the only difference is a small variation on the angle of incidence. This approximation is very accurate when the reflectarray elements on the main reflectarray show a relatively small sensitivity to the angle of incidence.

An extension of the analysis technique has been implemented to study dual-reflectarray antennas comprising a main reflectarray printed on a parabolic surface, or in general in a curved surface.

In many applications of dual-reflectarray configurations, the reflectarray elements are in the near field of the feed-horn. To consider the near field radiated by the horn, the incident field on each reflectarray element is computed using a spherical mode expansion. In this region, the angles of incidence are moderately wide, and they are considered in the analysis of the reflectarray to better calculate the actual incident field on the sub-reflectarray elements. This technique increases the accuracy for the prediction of co- and cross-polar patterns and antenna gain respect to the case of using ideal feed models.

In the second part, as a preliminary validation, the proposed analysis method has been used to design a dual-reflectarray antenna that emulates previous dual-reflector antennas in Ku and W-bands including a reflectarray as subreflector. The results for the dual-reflectarray antenna compare very well with those of the parabolic reflector and reflectarray subreflector; radiation patterns, antenna gain and efficiency are practically the same when the main parabolic reflector is substituted by a flat reflectarray. The results show that the gain is only reduced by a few tenths of a dB as a result of the ohmic losses in the reflectarray. The phase adjustment on two surfaces provided by the dual-reflectarray configuration can be used to improve the antenna performance in some applications requiring multiple beams, beam scanning or shaped beams.

Third, a very challenging dual-reflectarray antenna demonstrator has been designed, manufactured and tested for a more rigorous validation of the analysis technique presented. The proposed antenna configuration has the feed, the sub-reflectarray and the

main-reflectarray in the near field one to each other, so that the conventional far field approximations are not suitable for the analysis of such antenna. This geometry is used as benchmarking for the proposed analysis tool in very stringent conditions. Some aspects of the proposed analysis technique that allow improving the accuracy of the analysis are also discussed. These improvements include a novel method to reduce the inherent cross polarization which is introduced mainly from grounded patch arrays.

It has been checked that cross polarization in offset reflectarrays can be significantly reduced by properly adjusting the patch dimensions in the reflectarray in order to produce an overall cancellation of the cross-polarization. The dimensions of the patches are adjusted in order not only to provide the required phase-distribution to shape the beam, but also to exploit the crosses by zero of the cross-polarization components.

The last part of the thesis deals with direct applications of the technique described. The technique presented is directly applicable to the design of contoured beam antennas for DBS applications, where the requirements of cross-polarisation are very stringent. The beam shaping is achieved by synthesising the phase distribution on the main reflectarray while the sub-reflectarray emulates an equivalent hyperbolic subreflector.

Dual-reflectarray antennas present also the ability to scan the beam over small angles about boresight. Two possible architectures for a Ku-band antenna are also described based on a dual planar reflectarray configuration that provides electronic beam scanning in a limited angular range. In the first architecture, the beam scanning is achieved by introducing a phase-control in the elements of the sub-reflectarray and the main-reflectarray is passive. A second alternative is also studied, in which the beam scanning is produced using 1-bit control on the main reflectarray, while a passive subreflectarray is designed to provide a large focal distance within a compact configuration. The system aims to develop a solution for bi-directional satellite links for emergency communications. In both proposed architectures, the objective is to provide a compact optics and simplicity to be folded and deployed.

RESUMEN

Una antena de tipo reflectarray está compuesta de una fuente primaria que ilumina una superficie reflectora plana o curva, formada por una agrupación de elementos radiantes impresos. Un diseño apropiado de estos elementos permite modificar la distribución de fase del campo reflejado, en la superficie reflectora, produciendo un haz colimado o conformado en una dirección determinada. La fase del campo reflejado es el resultado de la combinación de la fase del campo incidente y la del coeficiente de reflexión para cada elemento-.

Los arrays de fase (phased arrays) y los reflectores parabólicos son comúnmente utilizados en la mayoría de las aplicaciones de alta ganancia, como el radar o las comunicaciones de larga distancia. Sin embargo, las antenas reflectarray presentan ciertas características adicionales que las hacen atractivas para estas aplicaciones. Debido a que son antenas impresas, los reflectarrays planos son más ligeros y ocupan menos volumen que los reflectores parabólicos o conformados. Las pérdidas óhmicas en los reflectarrays dependen del factor de disipación del sustrato y de la geometría del parche. En particular, para un reflectarray de dos o tres capas de parches apilados las pérdidas son comparables a las de un reflector parabólico. Por otra parte, los reflectarrays se pueden utilizar para generar haces conformados usando procesos de fabricación sencillos y bien conocidos que se han venido utilizando en circuitos impresos multicapa. Las antenas basadas en reflectores convencionales también pueden

generar haces conformados, pero para su construcción requieren el desarrollo de costosos moldes que deben ser diseñados y fabricados específicamente para cada misión, sin posibilidad de reutilización, además de hacer más lento el proceso de desarrollo de una antena con estas características.

La principal limitación de las antenas reflectarrays es su reducido ancho de banda, provocado por el comportamiento en banda estrecha de los elementos impresos y por la diferencia de caminos desde el alimentador hasta cada uno de los elementos del reflectarray, denominada diferencia espacial de retardo de fase. En los últimos años se han propuesto varias soluciones para aumentar el ancho de banda de los elementos, que es el factor más limitante en los reflectarrays de tamaño moderado. Así se han alcanzado hasta un 15% de ancho de banda por medio de distintas técnicas, como por ejemplo el uso de varias capas impresas, cada una de ellas con parches de diferentes tamaños. Otra posibilidad es el uso de los llamados parches acoplados por ranura a línea de retardo que permiten reducir la diferencia espacial de retardo de fase al insertar una ruta física que produce un retraso de tiempo real.

Las antenas de doble reflectarray proporcionan control de fase en las dos superficies reflectoras gracias a lo cual se extiende la aplicabilidad y el rendimiento de las antenas reflectarray. De esta manera se pueden diseñar antenas con haces múltiples con escasa degradación. También permite utilizar el principio de la antena bifocal o generar haces conformados. Otra gran ventaja de las antenas de doble reflectarray es que están compuestas de reflectores planos que pueden ser fácilmente plegados de manera compacta siendo esta una característica muy conveniente en aplicaciones de satélite. Los sistemas de doble reflectarray también pueden proporcionar capacidades de reconfiguración, gracias al uso de interruptores micro-electro-mecánicos (MEM) o diodos PIN. Algunas de las aplicaciones de estas antenas reconfigurables son los Radars de Apertura Sintética (SAR), misiones de teledetección radiométrica o misiones de transmisión directa vía satélite (DBS) usando antenas de haces conformados y reconfigurables.

Para aplicaciones en bandas milimétricas y sub-milimétricas, el barrido electrónico se puede lograr mediante reflectarrays basados en cristales líquidos, donde la fase del campo reflejado se controla mediante la tensión de polarización aplicada a los cristales líquidos.

La tesis se divide en tres partes principales. La primera se corresponde con la implementación y descripción de una técnica de análisis para configuraciones de doble reflectarray. Se han implementado dos versiones de la técnica: una versión en la que se emplean ciertas aproximaciones que producen un ahorro substancial de tiempo de cálculo y una segunda versión que aunque permite tener mayor precisión en los resultados penaliza la eficiencia computacional. La segunda parte está dedicada a la validación de dicha técnica de análisis, en primer lugar mediante comparaciones con sistemas reflectores equivalentes. Posteriormente, se realiza una validación completa mediante el diseño, fabricación y medida de una antena de doble reflectarray. Por último, se diseñan distintas antenas de doble reflectarray, que muestran el potencial de estas configuraciones para generar haces conformados y hacer barrido electrónico del haz.

Técnica de análisis para antenas de doble reflectarray

Se ha desarrollado una técnica modular de análisis de antenas basadas en configuraciones con dos reflectarrays que incluye el análisis del alimentador, del subreflectarray y del reflectarray principal, así como el cálculo del diagrama de radiación en campo lejano. La Fig. R.1 muestra una configuración genérica de la antena propuesta, en este caso se trata de una configuración offset si bien la formulación puede aplicarse a geometrías centradas. El modelado del alimentador basado en funciones que modelan el campo lejano consigue normalmente una buena precisión. No obstante, hay casos en los que los elementos del subreflectarray se encuentran en la zona de Fresnel del alimentador, por lo que la aproximación de campo lejano deja de ser válida y es conveniente utilizar modelos de campo cercano que pueden estar basados en, por ejemplo, la expansión en modos esféricos del campo radiado por el alimentador.

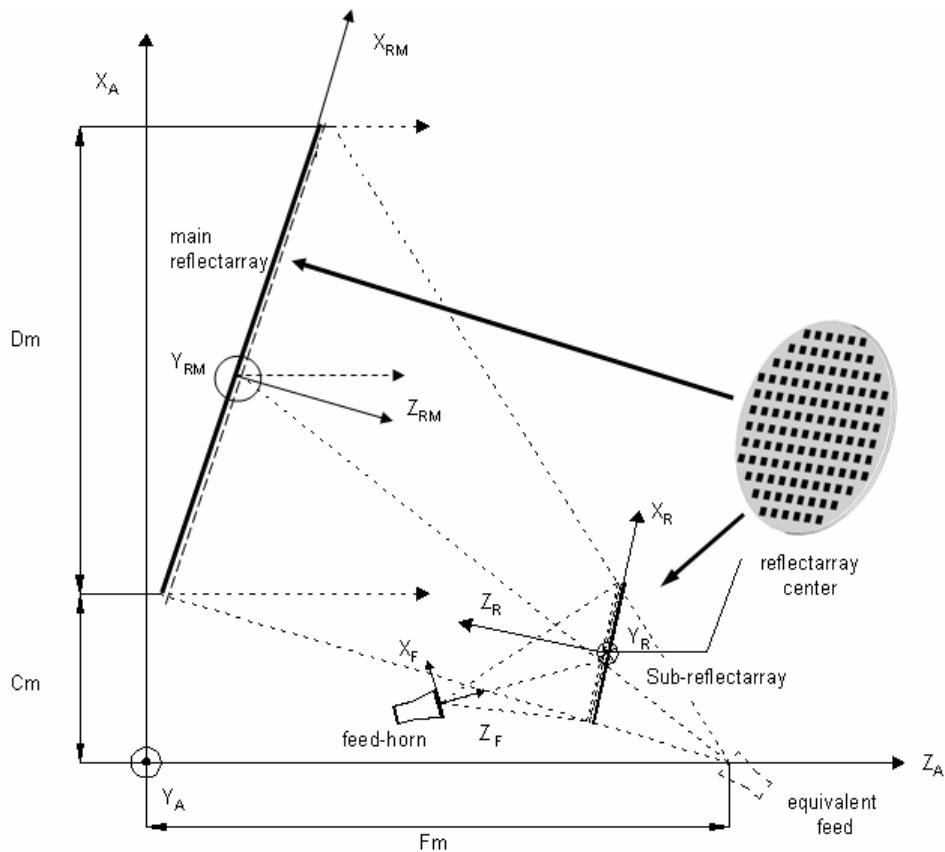


Fig. R.1. Esquema de un sistema de doble reflectarray.

El sub reflectarray se analiza elemento a elemento, teniendo en cuenta la periodicidad local y el ángulo de la onda incidente proveniente del alimentador. El campo total reflejado en los elementos del sub reflectarray se calcula mediante el método de los momentos (MoM) como la superposición de los campos radiados por los parches y el campo reflejado en la estructura dieléctrica multicapa y considerando las pérdidas de disipación del reflectarray.

El reflectarray principal se analiza usando la misma técnica empleada para el sub-reflector. Para calcular el campo incidente en las celdas del reflectarray principal, se tienen en cuenta las contribuciones de todos los elementos del sub-reflector. En principio, los ángulos de incidencia de todos los elementos del sub-reflector se consideran iguales, lo que supone una simplificación en la técnica de análisis. Dicho ángulo de incidencia se calcula utilizando el centro del sub-reflector como origen del campo incidente. Gracias a esta simplificación se reducen drásticamente los tiempos de cálculo manteniendo una precisión suficiente en los resultados obtenidos para las configuraciones estudiadas.

Sin embargo, la técnica de análisis contempla la posibilidad de hacer un análisis más preciso para las configuraciones que así lo requieran. Este es el caso de los sistemas en los que el reflector principal se encuentre en la zona de Fresnel del sub-reflector y cuando la respuesta de los elementos del reflectarray principal es muy dependiente del ángulo de incidencia. Para llevar a cabo dicho análisis, los elementos del sub-reflectarray se agrupan en pequeños sub-arrays de elementos y el campo incidente en el reflector principal se descompone en ondas radiadas por cada grupo con sus ángulos de incidencia correspondientes.

En el cálculo de la polarización cruzada, se tienen en cuenta dos componentes: la generada por los parches impresos y la debida a la geometría de la antena (proyecciones de campo). A pesar de que la componente contrapolar del campo generada por los parches en general es baja, es necesario considerarla en el análisis y diseño del reflectarray, sobre todo en aquellas aplicaciones que tienen requisitos estrictos en el nivel de polarización cruzada.

Finalmente, el diagrama de radiación de la antena completa se calcula a partir del campo reflejado por el reflectarray principal, aplicando el Segundo Principio de Equivalencia y un algoritmo basado en la FFT bidimensional.

Validación de la técnica de análisis

La principal dificultad en la validación de la técnica de análisis recae en el hecho de que no existen en la literatura medidas de antenas de doble reflectarray. Por ello, la validación se ha realizado en dos etapas.

En primer lugar se han usado como referencia dos antenas diferentes de doble reflector, compuestas por un reflector principal parabólico y un sub reflectarray, documentadas anteriormente en la literatura. La validación se lleva a cabo mediante la sustitución del reflector parabólico principal de las antenas de referencia por un reflectarray equivalente, diseñado para emular el comportamiento del reflector parabólico principal.

La primera configuración consiste en un doble reflectarray en banda Ku, donde el sub-reflectarray introduce una constante de fase (que funciona como un reflector plano metálico) y el reflectarray principal colima el haz, emulando el comportamiento del reflector parabólico. Comparando los resultados de la técnica de análisis con los de la literatura queda demostrado que las prestaciones de la antena en términos de ganancia,

eficiencia y los diagramas de radiación son prácticamente las mismas cuando el reflector principal de la antena de referencia se sustituye por un reflectarray plano.

El segundo diseño es un doble reflectarray en configuración dual-offset, que genera un haz colimado a 94GHz que se desvía 5° en azimut introduciendo una fase progresiva en el reflectarray que actúa como subreflector. En este caso se observa que el campo cercano radiado por la bocina debe ser incluido en el análisis para proporcionar resultados similares a los documentados en la literatura.

Ambos ejercicios de validación demuestran la viabilidad de las dos antenas con doble reflectarray, en las que el reflectarray principal se ha diseñado para emular el comportamiento de un reflector convencional.

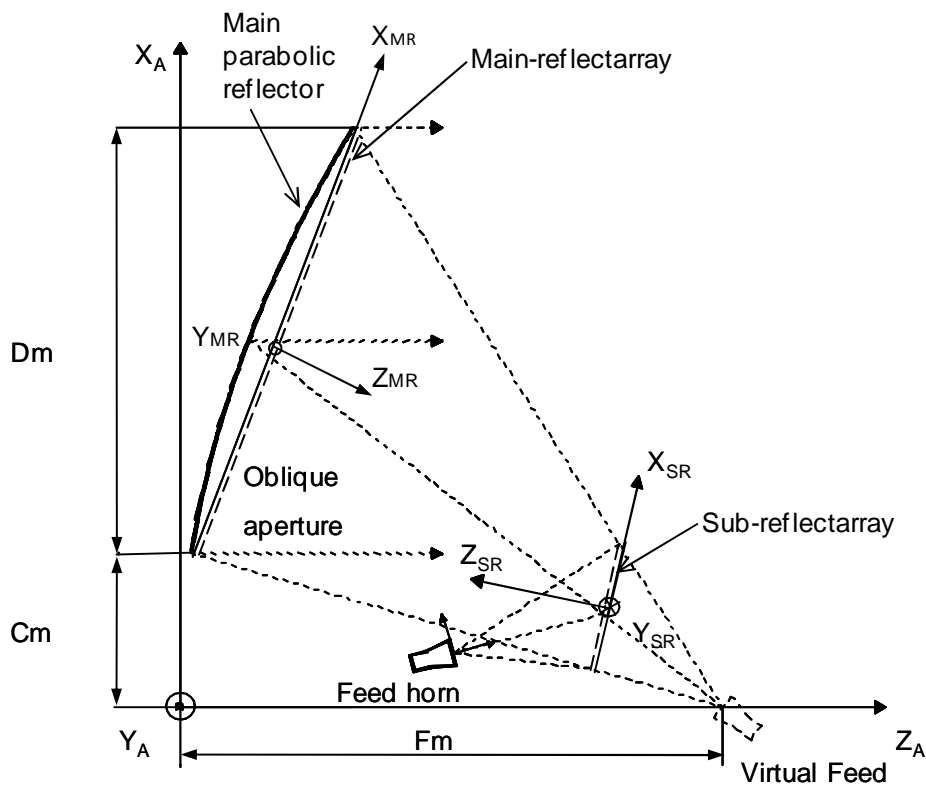


Fig. R.2. Esquema de una configuración de doble reflectarray. El reflectarray principal se ha superpuesto con su reflector parabólico equivalente

Diseño, fabricación y medida de un prototipo de doble reflectarray

La validación de las técnicas de análisis y diseño propuestas en esta tesis se completa en una segunda etapa mediante el diseño, construcción y medida de una antena de doble reflectarray basada en una geometría compacta. Este es el único método posible para validar rigurosamente las técnicas de análisis desarrolladas en esta tesis.

La geometría de la antena se ha seleccionado de forma que sea capaz de llevar al límite la validez de la técnica de análisis. Así la configuración propuesta tiene los tres elementos (bocina, reflectarray principal y sub reflectarray) muy próximos unos de otros, que hace que las aproximaciones convencionales de campo lejano no sean adecuadas para el análisis de esta antena. Asimismo, los dos reflectarrays se han definido para emular los reflectores de la antena equivalente, que producen un haz enfocado dirigido en la dirección dada por $\theta = 28^\circ$, cumpliendo las condiciones Mizugutchi.

Dos diseños con la misma geometría se han llevado a cabo. El primer prototipo usa un sub reflectarray de dos capas con tamaño de parche diferente en cada capa y un reflector principal de una sola capa, debido a que el rango de fase necesario para el reflectarray principal es más reducido. Los elementos se han diseñado con el objetivo de reducir la polarización cruzada, forzando a la cancelación de una parte de dicha componente. El prototipo de doble reflectarray se ha construido y medido en cámara anecoica, ver Fig. R.3. Los resultados de la simulación tienen una concordancia muy buena con las medidas, salvo por algunas pequeñas diferencias en los lóbulos laterales causados por los errores de tolerancia del proceso de fabricación. Este prototipo ofrece una discriminación de la polarización cruzada mayor de 35 dB y funciona en un amplio ancho de banda de frecuencia: de 12,2 GHz a 15 GHz.

Con objeto de mejorar las prestaciones de ancho de banda y polarización cruzada de la antena construida, se ha realizado un segundo diseño en el que se incluyen dos capas en el reflectarray principal. Seleccionando el tamaño adecuado de los parches se puede conseguir que los nulos y el cambio de signo de la polarización cruzada se cancelen en este nuevo diseño de doble reflectarray. De esta manera se consigue una reducción sustancial en los niveles de polarización cruzada, con lo que se obtiene una discriminación contrapolar mejor de 37 dB en un ancho de haz de 3dB para las dos polarizaciones lineales ortogonales.

A partir de la configuración anterior de doble reflector, se ha diseñado una antena que genera un haz conformado para una cobertura Europea utilizada definida por Eutelsat para aplicaciones DBS (Direct Broadcast Satellite). En este caso, la distribución de fase en el reflectarray principal se ha sintetizado de manera que proporcione cobertura sobre toda Europa. La antena puede trabajar en polarización dual lineal y los diagramas resultantes cumplen los requisitos de cobertura en la banda de frecuencia de transmisión. Estos resultados demuestran como la configuración de doble reflectarray cumple con los requisitos de las antenas de DBS tanto en la banda de transmisión como en la de recepción.

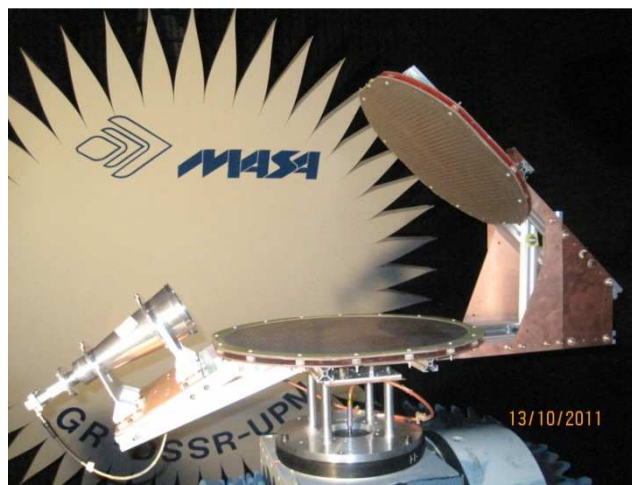


Fig. R.3. Demostrador de doble reflectarray ubicado en la cámara anecoica

Aplicación de un doble reflectarray para barrido en banda Ku

En esta tesis también se ha abordado el análisis de dos arquitecturas de antenas de doble reflectarray en banda Ku capaces de proporcionar barrido electrónico del haz en un rango angular limitado. Los diseños han sido desarrollados en el marco del proyecto RESKUE (contrato de la ESA n ° 22078/08/NL/ST) en colaboración con la Agencia Espacial Europea (ESA) y RF-Microtech. El sistema tiene como objetivo desarrollar una estación portátil para enlaces vía satélite bidireccionales y con capacidad de apuntamiento automática, útiles en comunicaciones de emergencia en lugares remotos, donde las infraestructuras de otros medios de telecomunicación no estén disponibles o sean insuficientes.

Los requisitos impuestos dentro del proyecto RESKUE son que la arquitectura propuesta debe proporcionar una óptica compacta y con cierta facilidad de plegado y desplegado. Igualmente el sistema debe proveer la capacidad automática de apuntamiento a un satélite geostacionario en un rango angular limitado. Finalmente, el sistema se debe diseñar para proporcionar un haz directivo en las bandas de recepción (10.70 - 12.75 GHz) y transmisión (14.0 - 14.5GHz), para lo que se han propuesto dos soluciones. En la primera, el reflectarray principal es pasivo y el barrido del haz se consigue mediante la introducción de control de fase en los elementos del sub-reflectarray. Los principales inconvenientes observados en esta configuración son que el reflectarray principal tiene que ser de gran tamaño y que es difícil diseñar un elemento de reflectarray de polarización dual que abarque las bandas de transmisión y recepción.

Para superar estos problemas, se ha estudiado una segunda configuración que cuenta con un sub-reflectarray pasivo de doble capa y un reflectarray principal con control electrónico de 1-bit. El sub reflectarray pasivo se diseña con el único objetivo de conseguir una configuración compacta para un sistema parabólico con una distancia focal grande. Esta configuración presenta pequeños errores en la fase que han sido evaluadas a diferentes frecuencias. En caso de considerarse necesario, estos errores se pueden reducir mediante la inclusión de una tercera capa en el sub reflectarray pasivo. Los resultados preliminares muestran un rendimiento satisfactorio de la antena en las bandas transmisora y receptora.

Antena de doble reflectarray con reflectarray principal parabólico

Una alternativa a la antena de doble reflectarray consiste en reemplazar el reflectarray plano principal por un reflectarray impreso sobre una superficie curva en general y, en particular, sobre una superficie parabólica. Así se ha propuesto una configuración compuesta de tres componentes: una fuente primaria, un sub-reflectarray plano y un reflectarray principal parabólico, como se muestra en la Fig. R.4 En esta configuración el reflectarray principal sólo necesita introducir pequeños ajustes de fase ya que la geometría de la superficie parabólica enfoca el haz.

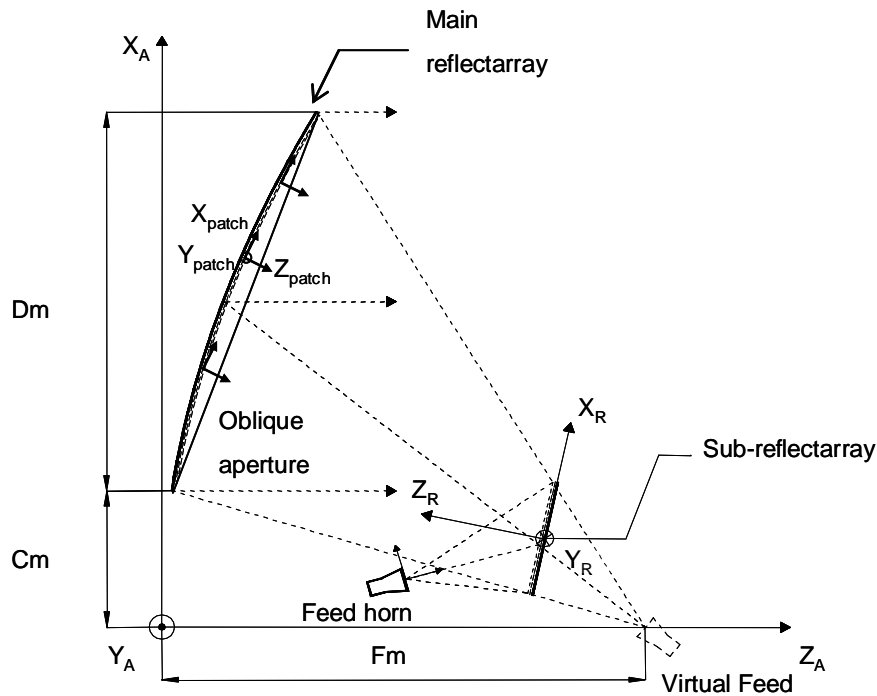


Fig. R.4. Esquema de una configuración de doble reflectarray con reflectarray principal parabólico

Para analizar esta antena, se ha implementado una extensión de la técnica de análisis para antenas planas de doble reflectarray que permite analizar un reflectarray principal parabólico. Dicha extensión también puede aplicarse a configuraciones más genéricas en la que el sub-reflectarray, el reflectarray principal, o ambos están impresos sobre cualquier tipo de superficie curva.

Con objeto de validar la técnica de análisis se ha empleado un único reflectarray sobre una superficie parabólica que proporcionar una cobertura para América del Sur, del cual existían resultados previos en la literatura. El sistema analizado consta de un reflectarray principal parabólico, cuyos parches se han optimizado para obtener la cobertura Europea previamente definida y un sub reflectarray que emula una superficie plana conductora, con objeto de obtener los mismos resultados que los obtenidos con la antena de referencia con único reflector parabólico. Los resultados muestran que los diagramas de radiación están próximos a los requisitos de cobertura. Estos unos resultados preliminares que demuestran la viabilidad de una antena reflectarray sobre una superficie parabólica. Las pequeñas discrepancias de los diagramas con respecto a la cobertura especificada se pueden reducir mejorando la síntesis de diagramas conformados y la optimización de los parches en el reflectarray. La configuración estudiada, en la que no se utiliza el subreflectarray, proporciona una elevada polarización cruzada. e Sin embargo, el sub reflectarray se

puede diseñar para reducir la polarización cruzada de la antena, tal y como se hizo en el demostrador construido y medido.

Table of Contents

1	Introduction	1
1.1	State of the art on reflectarray antennas	3
1.1.1	Reflectarray in single reflector configuration	4
1.1.2	Reflectarrays in dual-reflector configuration	6
1.1.3	Dual- reflectarray antennas	8
1.1.4	Parabolic reflectarray in dual-reflector configurations	9
1.1.5	Reflectarray with low cross-polarization	10
1.2	Goals of the thesis	11
1.2.1	Development of a technique to analyze dual-reflectarray configurations	12
1.2.2	Validation of analysis tool	13
1.2.3	Design, manufacturing and test of a dual reflectarray	14
1.2.4	Evaluation of dual-reflectarray for beam scanning	14
1.2.5	Analysis and design of contoured-beam dual-reflectarray for DBS applications	14
1.2.6	Extension of the analysis technique to include a reflectarray printed on curved surfaces.	15
1.3	Thesis organization	15
2	Analysis technique for a dual-reflectarray antenna	17
2.1	Introduction	17
2.2	Feed-Horn Models	19
2.2.1	Far field models.	19
2.2.2	Near field models	20
2.3	Analysis of the sub reflectarray	23
2.3.1	Number of samples	23
2.3.2	Co- and Cross-polar radiation produced by the sub reflectarray	24
2.4	Analysis of the main-reflectarray	27
2.4.1	Flat main reflectarray	27
2.4.2	Division of the sub reflectarray aperture	30
2.4.3	Number of samples	34
2.5	Calculation of the radiation pattern	35
2.6	Efficient computation of the spectral functions	40
2.7	Conclusions	46
3	Validation of the analysis technique	47
3.1	Introduction	47
3.2	Ku-band dual reflectarray antenna	48
3.2.1	Antenna definition	48

3.2.2	Design of main reflectarray	50
3.2.3	Conclusions	58
3.3	94 GHz dual-reflector antenna	58
3.3.1	Antenna definition	59
3.3.2	Design of sub and main reflectarrays	60
3.3.3	Antenna analysis	62
3.4	Conclusions	66
4	Design manufacture and test of dual-reflectarray demonstrator	67
4.1	Introduction	67
4.2	Design, manufacture and test of a dual-reflectarray demonstrator	68
4.2.1	Equivalent parabolic system	68
4.2.2	Antenna optics	70
4.2.3	Feed-horn	73
4.2.4	Multi-layer configuration of the two reflectarrays	80
4.2.5	Antenna design.	86
4.2.6	Low cross-polarization design	91
4.2.7	Improvement of dual-reflectarray design	98
4.3	Prototype Manufacturing	107
4.3.1	Photo-etching masks	107
4.3.2	Prototype assembling	110
4.4	Electrical test	114
4.4.2	Validation of the analysis technique	119
4.4.3	Conclusions	127
4.5	Improved design of the main-reflectarray using two layers of varying-sized patches.	128
4.5.1	Main-reflectarray multilayer configuration	128
4.5.2	Main-reflectarray design	130
4.5.3	Photo-etching masks	141
4.5.4	Conclusions	142
4.6	Contoured-Beam Dual-Reflectarray Antenna for DBS Applications	143
4.6.1	Coverage requirements and antenna definition	143
4.6.2	Contoured beam synthesis	146
4.6.3	Antenna design	148
4.6.4	Conclusions.	154
4.7	Conclusions	154
5	Dual reflectarray for beam scanning in Ku-band	156
5.1	Introduction	156
5.2	Dual-reflectarray antenna for beam scanning with phase control on the sub reflectarray	157
5.2.1	Antenna definition	157
5.2.2	Antenna design and analysis	159

5.2.3	Conclusions	165
5.3	Dual-reflectarray antenna for beam scanning with 1-bit phase control on the main reflectarray	166
5.3.1	Antenna geometry	166
5.3.3	Feed-horn	169
5.3.4	Phase distribution for both reflectarrays.	170
5.3.5	Analysis considering a real sub reflectarray	177
5.3.6	Sub reflectarray design	178
5.3.7	Main-reflectarray element	182
5.3.8	Analysis of dual reflectarray including the two-layer sub reflectarray	183
5.4	Conclusions	186
6	Dual-Reflector configuration with parabolic main reflectarray	188
6.1	Analysis of a parabolic reflectarray in a dual reflector configuration	193
6.1.1	Antenna geometry	193
6.1.2	Antenna analysis	197
6.1.3	Conclusions	200
7	Conclusions and future research lines	201
7.1	Conclusions	201
7.2	Original contributions	204
7.3	Future research lines	206
7.4	List of publications related to this work	208
7.4.1	Journal papers	208
7.4.2	International conferences	208
7.5	Research projects related to this thesis	209
8	References	210

CHAPTER 1

1 Introduction

A printed reflectarray antenna consists on a primary feed that illuminates a flat or curved reflecting surface made up of radiating printed elements. These elements are designed to re-radiate the incident field with a phase distribution on the aperture to produce a focused or a shaped beam in the far-field. The phases introduced by each of the elements are those that compensate the different path lengths from the primary feed.

Traditionally, for most of high-gain applications, like radar or long distance communications, parabolic reflectors and phased arrays have been used. However, reflectarray antennas present certain characteristics that make them attractive for such applications [1]. Since reflectarrays are printed antennas, they are low profile, they consume less weight and volume than parabolic reflectors and they are cost-effective. Ohmic losses in reflectarrays depend on the dissipative factor of the substrate and on the geometry of the patch. For a printed reflectarray based on stacked patches, losses are comparable to those of a reflector antenna. Moreover, reflectarrays can be used to generate contoured beams using simple manufacturing processes based on photo-etching and other well-known techniques used in printed circuits and multi-layer structures [2],[3]. On the other side, the manufacturing of reflector antennas for contoured beams requires complex and expensive custom moulds that must be designed

and manufactured specifically for each mission.

It is well known that the most severe limitation in reflectarray antennas is their narrow frequency band operation, produced by the bandwidth of the printed elements and by the differential spatial phase delay [4]. In recent years, several solutions have been proposed to overcome the narrow bandwidth of the element, which is the most significant in moderate size reflectarrays. More than 15% bandwidth for microstrip antennas can be achieved using several techniques, such as using several layers of varying-sized patches. In this case, a multi resonant behaviour is obtained and the phase range can be a few times 360° [2]. Other possibility is the introduction of aperture-coupled patches to delay lines that reduce the effect of the differential spatial phase delay by inserting a physical path that produces true time delay [5]. It has been demonstrated that the use of an artificial impedance surface can lead to a reflectarray gain bandwidth of more than 20% with a single layer of printed patches. The artificial impedance surface consists of patch elements that are electrically smaller than the resonant size, they are spaced a distance significantly less than $\lambda/2$ [6]. Several alternatives have been proposed to reduce the effect of differential spatial phase delay in large reflectarray antennas, such as, the compensation of phase dispersion by optimising the dimensions in three layers of varying-sized patches. A three layer configuration provides a range of phases around twice 360° , so any value of the objective phase can be achieved having a third degree of freedom to control the phase difference between the two limits of the frequency band [7]. Other way to reduce the effect of the differential spatial phase delay is designing the elements to provide a linear phase response, proportional to the length of the line in a large range of phase delay (by using true time delay) [8]. A parabolic reflector antenna uses the physical geometry to focus spherical waves coming from the feed to radiate a planar wave front, this effect is independent of the frequency and it is equivalent to the true time delay technique used in phased arrays. The same effect can be achieved by printing the reflectarray on a parabolic surface to enlarge the bandwidth for shaped-beam antennas [9].

A dual-reflectarray provides phase control on both reflectarray surfaces, which can extend the applicability and performance of reflectarray antennas. This can be used to design multiple-beam antennas with almost no degradation of the beam [10], using the principle of the bifocal antenna [11] or to generate shaped beams as demonstrated in

[12] for folded reflectarrays. These configurations are able to work in both polarizations. Reflectarray antennas composed of flat panels can be folded in a compact way and rapidly installed in a given location, which can be very convenient in satellite applications. In addition, they can provide a certain level of beam agility to simplify the antenna pointing, allowing the user to only roughly align the antenna towards a satellite and then leaving the antenna to perform an automatic fine pointing [13]. They also achieve reconfigurable capabilities that may be implemented with micro-electro-mechanic (MEM) switches or PIN diodes. Applications of the proposed antenna configuration can be Synthetic Aperture Radar (SAR) [14], radiometric remote-sensing missions [15] and shaped-beam reconfigurable antennas for Direct Broadcast Satellite (DBS) missions.

For applications in the millimetre and submillimetre wave range, electronic beam scanning can be achieved by using reflectarrays based on Liquid Crystals (LC) [16] where the phase of the reflected field is controlled by the bias voltage applied to the liquid crystal. Several demonstrators reported in the literature have shown the capabilities of beam scanning and beam switching with liquid crystal reflectarrays [17]-[18]. The LC-based reflectarray is a very attractive solution for beam scanning and beam reconfiguration because the simplicity in manufacturing and bias control. The LC-reflectarray can be implemented as a small sub reflector in a dual-reflectarray configuration to provide electronically beam steering antennas for the radiometric instruments [19].

A dual-reflector antenna made of a parabolic reflector and a reflectarray as sub reflector can also be used to produce a contoured beam for DBS antennas, by properly adjusting the phase-shift distribution on the reflectarray. In this sense, this architecture is very attractive, since the general geometry and particularly the main reflector can be reused for several missions and the different radiation patterns are obtained by the design of each specific sub reflectarray.

1.1 State of the art on reflectarray antennas

The review of the state of the art on reflectarray antennas includes conventional single offset reflectarray antennas and those involving a dual-reflector configuration, which is the main topic of this dissertation.

1.1.1 Reflectarray in single reflector configuration

The characteristics of a printed reflectarray in terms of bandwidth, cross-polarization and dissipative losses, depend on several factors, including the reflectarray elements and the dimensions and geometry of the antenna. Different types of printed reflectarray elements have been demonstrated, as shown in Fig. 1-1. The first one uses phase delay lines of different lengths ended in open circuit connected to identical patch elements. In this configuration, the field radiated by the feed is received on the patch, propagated along the line, reflected at the open-end, back propagated and re-radiated by the patch, introducing a phase-shift proportional to twice the length of the line. This kind of elements exhibits high dissipative losses and high levels of cross-polarization due to the spurious radiation of the line.

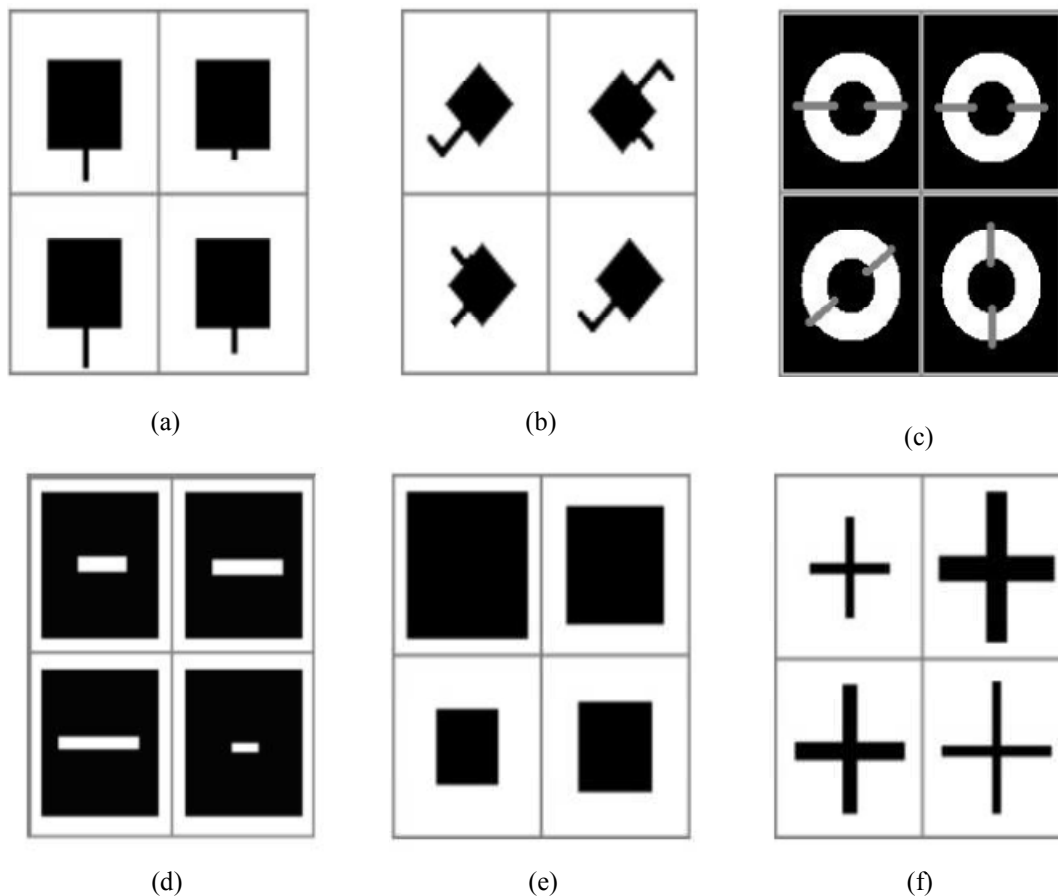


Fig. 1-1. Several phase-shift elements:(a) Squared patches with varying-length stubs, (b) sequential rotation patches with varying-length stubs, (c) resonators with reactive charges and (d) varying-length slots, (e) varying-size rectangular patches, (f) varying-length crossed dipoles.

A technique was developed for the patches using tuning stubs of variable length to reduce the cross-polarization [20]. With this technique, the reflectarray aperture is separated into four quadrants and the elements are located with mirror symmetry as shown in Fig. 1-1 (c), where square patch elements with reverse orientations and reverse phases for the four quadrants are used to cancel the crosspolar radiations.

The second type of elements is made of elements of different size which adjust the phase shift generated by changing the resonant dimensions of the patches. In this case, the patches can be rectangular or cross-shaped [21], [22], [23]. These elements reduce the dissipative losses and the cross-polarization level with respect to the case of delay lines because the radiation from the stubs is eliminated [4]. The margin of the phase shift that can be achieved by modifying the size of the patches depends on the multilayer configuration. Usually, the feasible phase range using this element is less than 360° and the phase variation versus the size is non-linear because of the narrow band margins of the microstrip patches. This realizable phase range limits the performance of the reflectarray since the phase distribution is very sensitive to the manufacturing tolerances and therefore the frequency band is reduced. Actually, practically most of reflectarrays suffer from the limitation of a narrow band imposed by the bandwidth of the radiating element. This drawback can be compensated by using two or more layers of stacked patches, [2], [24], [25]. By using three layers, the phase curve of the patch may achieve a range greater than 700° varying the patch dimensions [7], which improves the versatility of the reflectarray allowing an optimization in a frequency band.

Other kind of elements used for reflectarray applications are stacked metallic rings [26]. In this case, the phase variation introduced by the diameter of the ring is controlled by the difference in the centre resonant frequency of the two arrays. This parameter is used to improve the linearity of the phase curve versus ring size slope. As a consequence, an improvement of the element bandwidth is achieved. However, rectangular patches of variable size [2] provide more linear curves of phase and also better bandwidth than stacked rings.

Some concepts have been demonstrated for reflectarray elements in circular polarisation. One of them consists on elements with variable rotational angle implemented for circular polarization. In this case, the phase shift is achieved by physically rotating the element [2], [27], as the phase shift achieved in circularly polarized (CP) phased arrays, in this case the phase shift applied to the reflectarray signal is doubled because of the reflection process. This approach achieved an improved performance in terms of sidelobe and cross-polarization levels [2]. All the elements are identical and resonating at the same frequency what makes them to achieve better efficiency since there is a lack of specular reflection for the off-broadside incident rays.

The aperture coupled patches to delay lines with variable length have been used for dual linear polarization [28], [29],[30]. The transmission lines are implemented in a different plane from the patch, avoiding space problems to locate the line and spurious radiation of the stubs. The main advantage presented in this configuration is the possibility of introducing reconfigurable elements in the line layer.

A more recent electronic beam scanning reflectarray development uses voltage-controlled Varactor diodes [31], [32], where only one or two control lines are needed to achieve beam scanning with lower losses. The potential of achieving even lower phase shifter losses by using the micro-electro-mechanical (MEM) switches is currently under development [33]. Electronic beam scanning can be also achieved by using reflectarrays based on Liquid Crystals (LC) [16] where the phase shift generated by the element is controlled by the bias voltage applied to the liquid crystal. Several demonstrators implemented show the capabilities of beam scanning and beam switching with liquid crystal reflectarrays [17], [18]. The LC-based reflectarray is a very attractive solution for beam scanning and beam reconfiguration because of the simplicity in manufacturing and bias control.

1.1.2 Reflectarrays in dual-reflector configuration

Geometrical optics (GO) is a simple and time efficient analysis technique of reflector antennas. It is widely used in designing and shaping these antennas. The principles of GO include power conservation and Snell's law. Using these principles, shaping circularly symmetric reflectors have been formulated in [34]-[36]. Although most of the

energy redistribution is accomplished by the shaped sub reflector, some phase errors take place due to the modified sub reflector surface [35]. Therefore, an additional step is required by correcting the main reflector surface to maintain a planar phase front. A relatively simple ray-tracing-based shaping procedure is introduced in [37]. The reflector surfaces are approximated by local planar surface, but two steps are required to adjust the ray path length for the new main reflector surface.

An alternative shaping method for circularly symmetric dual reflector systems to obtain the desired aperture distribution consists on the formulation of several nonlinear algebraic equations based on GO principles and geometrical properties of conventional dual reflector antennas by tracing rays through each local Gregorian or Cassegrain antenna system from the feed to the aperture of the main reflector [38]. Each local dual reflector system, including both surfaces, is simultaneously obtained by reducing these equations to only one non differential linear equation with one unknown.

Reflectarray antennas exhibit certain properties that make them attractive compared to parabolic reflectors and phased array antennas for particular applications, such as radar, long distance communications and contoured beam antennas for Direct Broadcast Satellite (DBS) [1]. For contoured-beam DBS antennas, the manufacture of conventional reflectors requires complex and expensive custom moulds that must be designed and manufactured specifically for each use. On the other side, reflectarrays can be used to generate contoured beams by synthesizing the appropriate phase distribution on its surface and by using simple manufacturing processes based on photo-etching and other well-known techniques used in printed circuits and multi-layer structures [39], [40].

Although single-reflectarray configurations have been deeply studied, dual-reflector configurations present some advantages with respect to single-reflectors such as the reduction of the cross-polarization or the antenna volume. Several dual reflector antennas which use a planar sub reflectarray and a parabolic classic reflector have been proposed for beam scanning applications [1], [19]. This configuration combines the advantages of a parabolic main reflector, high gain and broadband, with the simplicity of manufacturing a small sub reflectarray.

1.1.3 Dual-reflectarray antennas

Other development for a low weight and low-cost reflectarray antenna consists of a linear polarized feed, a polarizing grid and a reflectarray [41]. The planar printed surface achieves beam-forming and also works as a twist reflector. The x-polarized field is radiated by the feed to the grid. Then, the field is reflected by the grid toward the reflectarray. The rectangular patches of different lengths and widths provide a prescribed phase shift and a twisting of the polarization by 90° at the same time. Finally, the wave passes the grid and is radiated into free space. The entire antenna consists of two printed substrates, easy to fabricate, at low cost, low weight and low losses [41]. By combining folded reflectarrays and multilayer shaped pattern reflectarrays, a compact antenna was proposed for LMDS central station antenna [12]. The main drawback of this configuration is that it works only in single linear polarization and therefore the number of applications is limited

A dual-reflectarray antenna made up of a main reflectarray and an offset-placed sub reflectarray, as the one shown in Fig. 1-2 has been proposed in reference [42], for active or reconfigurable antennas by inserting amplifier modules or phase-shifters on the elements of the reflectarray sub reflector, in order to achieve high-power transmission or fine beam pointing adjustment [43]. In addition, dual-reflectarray configuration can be used to scan or reconfigure the beam by using controllable phase-shifters based on MEMS or pin diodes on the elements of a small reflectarray sub reflector, while using a passive reflectarray as main reflector that emulates a parabolic reflector.

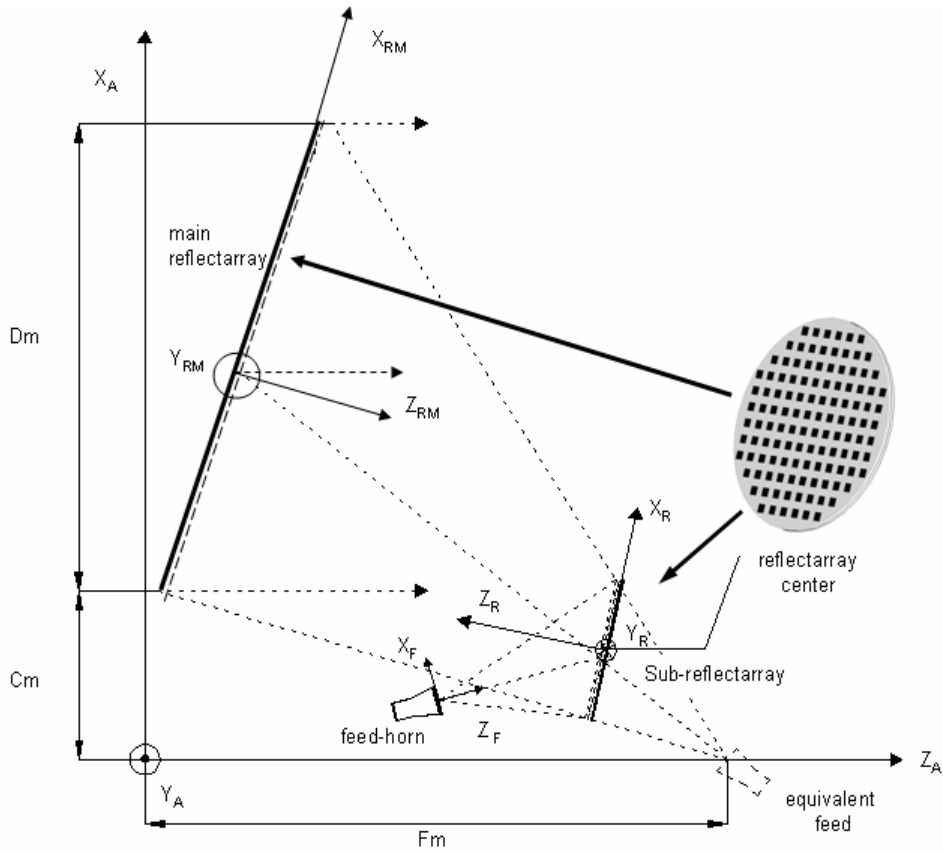


Fig. 1-2. Scheme of a dual reflectarray structure

1.1.4 Parabolic reflectarray in dual-reflector configurations

It has been demonstrated in previous works [39] that reflectarray antennas based on three layers of stacked varying-sized patches can be used to generate contoured beams for Direct Broadcast Satellite (DBS) applications in a 10% bandwidth, however additional bandwidth enlargement is desirable for transmit (Tx) and receive (Rx) antennas[44]. A reflectarray printed on a parabolic surface was first proposed in [45] to overcome the intrinsic narrowband performance of large reflectarrays, resulting from the different path lengths from the feed to the phase front. The bandwidth of the configuration proposed in [45] is limited however by the narrowband behaviour of the single layer reflectarray element. A two-layer parabolic reflectarray based on varying-sized patches was proposed in [9] to enlarge the bandwidth for shaped-beam DBS antennas. In that work, the feed was located near the focus of the paraboloid, so that the beam was focused by the parabolic surface, and the printed patches were used to adjust the phase-shift in order to produce the required contoured beam. A single offset parabolic reflectarray antenna was designed to provide a South American coverage.

However, the main drawback of this configuration is the cross-polarisation produced by the parabolic surface and by the printed patches. Cross polarisation can be reduced by using a sub reflector as in conventional reflector antennas. One of the advantages of this configuration is that manufacturing a parabolic surface is much simpler than a shaped reflector, especially for large apertures.

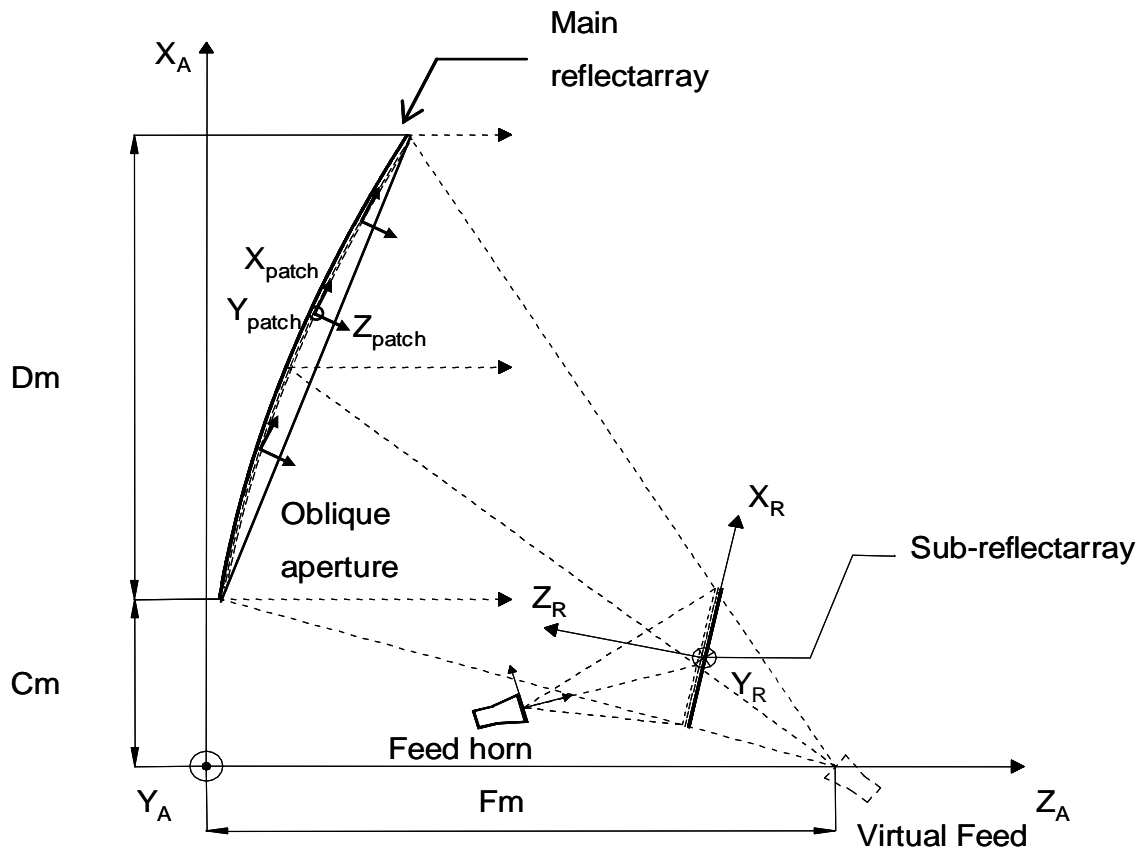


Fig. 1-3. Scheme of a dual-reflectarray structure with a parabolic main reflectarray

1.1.5 Reflectarray with low cross-polarization

The frequency re-use technique is becoming common in satellite communications systems to exploit efficiently the available frequency bands. Consequently the antenna requirements in terms of cross-polarization discrimination are becoming more and more stringent. Parabolic reflectors in offset configuration present low side lobe level and high efficiency, since there is no aperture blockage which simplifies the fulfilment of the cross-polarization requirements. Normally, the antenna must operate in two orthogonal polarizations, a rotational symmetric feed with low cross-polarization is

needed for this purpose. However, the antenna should cover in general an elliptic sector which implies an elliptical antenna aperture. This produces an asymmetrical projection onto the aperture plane and consequently a non-optimal edge illumination. In order to achieve an elliptic shape with low cross-polarization, a shape of the reflector surfaces can maintain a constant illumination on the edges of the reflector [46].

However, when the antenna must cover a larger angular area, the cross-polarization level becomes too high, making questionable the application of shaped dual reflector antennas. The main cause of the high level of cross-polarization is not the reflector shaping but the antenna geometry, the relative position of the sub reflector, the main-reflector and the feed-horn. With an appropriate definition of the antenna geometry, the cross polarization level can be reduced. The polarization characteristics of a reflector system depend mainly on both symmetry and curved surface of the reflectors, as well as on the quality of feed. The cross-polarized component over the aperture plane in a single-offset reflector configuration can be cancelled by making effective use of another asymmetrical reflector and by properly arranging them to fulfill Mizuguchi conditions [47] consisting on a certain relation among the angles formed by the rotational axis of both reflectors, the angle between the feed-horn and the sub reflector rotational axis and the eccentricity of the sub reflector.

Pencil or contoured beams can be easily achieved using reflectarrays by implementing the appropriated phase-shift in the reflectarray elements, using one or more layers of variable-sized patches. Flat reflectarrays produce a lower cross-polarization than offset reflector antennas, mainly because they are flat surfaces. It has been demonstrated that cross-polarization in offset configurations, which provides a pencil or contoured beam, can be reduced drastically by a proper adjustment of the sandwich configuration, modifying the separation between layers and the patch dimensions [48].

1.2 Goals of the thesis

This thesis proposes the development and validation of a general tool for the analysis of a dual-reflector configuration in which the sub reflector, the main reflector or both are reflectarrays. The phase adjustment in the two reflecting surfaces provides an improvement of the antenna performance in applications requiring multiple beams,

electronic beam scanning or contoured beams. The analysis tool is also extended to systems in which the main reflector is a curved reflectarray. In these systems the curvature of the reflector will be used to achieve a good optics of the system and the reflectarray patches will be used to achieve beam forming. Dual reflectarray configurations are also proposed to reduce the crosspolar radiation of the antenna system.

1.2.1 Development of a technique to analyze dual-reflectarray configurations

A modular technique to perform the analysis of an antenna in dual reflectarray configuration has been implemented. The technique uses the Method of Moments (MoM) for the analysis of both the sub and main reflectarray and it is based on the following steps: first, the field radiated by the feed horn is considered as incident field in each element of the sub reflectarray. In some cases, when reflectarray patches are situated in Fresnel zone of the feed, a conventional far-field model (\cos^q) is used. However for a more rigorous analysis, the near-field analysis of the feed will be also implemented. Secondly, the sub reflectarray is analyzed element by element, taking into account the local periodicity and the incident angle of the impinging wave from the feed to every cell of the sub reflector. The total field reflected by the sub reflectarray is calculated as the superposition of the fields re-radiated by the patches and the field reflected by the multilayer structure. Third, the analysis of the main reflectarray is carried out using the same technique as that used for the sub reflectarray. For this calculation, all contributions of the sub reflector patches are taken into account in the analysis of each cell of the main reflectarray. The field reflected by every cell of the main reflector is obtained as the product of the reflection coefficient of the cell and the calculated incident field. Finally, the radiated far field is computed from the field reflected in the main reflectarray using an algorithm based on the Fast Fourier Transform.

As a first approximation, the incident field on each element of the main reflectarray is calculated by adding all the contributions of the field radiated by every cell of the sub reflector. According to this approach, the incident angle of the field from the sub reflector is defined by assuming its origin at the center of the sub reflectarray. This should not affect the accuracy in the analysis of the main reflector, when the variation of the incident angle from each element in the sub reflectarray does not produce a

significant variation in the phase-shift produced on the element of the main reflector. This condition depends on the optics of the antenna as well as on the sensitivity of the reflectarray to the incident angle.

Specific cases of dual reflectarray antennas will be studied, for instance, one in which the sub reflector is located near the main reflector (violating the far-field condition) or other where the sub reflector has a large size with respect to the main reflector. To analyze these cases, a more accurate analysis technique than the one previously described will be implemented. The analysis of the feed and the sub reflector will be similar to the previous technique, however, for the analysis of the main reflector, the sub reflectarray is divided into sub-arrays. The incident field on each cell of the main reflector is computed for each group with their respective angles of incidence, and the MoM is used to analyze each element of the main-reflector. The size of the groups in the sub reflector is calculated in order to meet the far-field conditions of each sub-group on the elements of the main reflectarray. All field contributions coming from the same group of cells is considered to have the same angle of incidence in each cell of the main reflector (which corresponds to the case where the origin of the electric field is at the center of the corresponding sub group). Each group of cells produces a field contribution in each cell of the main-reflectarray. Note that these contributions have different incidence angles, to be taken into account in calculating the reflected field by each cell of the main reflectarray. It should be highlighted that the technique does not introduce any restriction on the size of the subgroups, being possible to consider from a single group (fast and approximated) to the same number of groups as the total number of sub reflectarray elements (for a very accurate and time consuming analysis). Finally, the technique will also be extended to consider a curve main-reflectarray.

The analysis techniques previously described will be implemented in FORTRAN code, resulting in a versatile tool where the sub-, the main- or both reflectors can be reflectarrays.

1.2.2 Validation of analysis tool

For the preliminary validation of the analysis tool, several antennas will be designed to emulate previous dual-reflector antennas. In a first case, the sub reflectarray will introduce a constant phase (as a metallic flat reflector) and the main-reflectarray will work as a parabolic reflector. The second antenna configuration will be an offset dual-

reflectarray configuration where the sub reflectarray produces a beam deflected 5° in azimuth, while the main reflectarray collimates the beam.

A more rigorous validation is provided by the design, manufacture and test of a dual-reflectarray demonstrator.

1.2.3 Design, manufacturing and test of a dual reflectarray

Using the design techniques developed during this work, a compact range prototype has been designed, manufactured and tested first to validate the analytical tools, and secondly to demonstrate the improvement in performance by the implemented techniques. Low cross-polarization levels and large bandwidth are the most critical parameters in the antennas used on satellites for communications, broadband multimedia applications, or direct broadcast. For this reason, the antenna demonstrator is designed to provide a large bandwidth and a reduction of the crosspolar radiation. The measurement of the antenna demonstrator has corroborated the very good performance in both bandwidth and cross-polarization.

1.2.4 Evaluation of dual-reflectarray for beam scanning

A preliminary design and evaluation of dual-reflectarray antennas for bi-directional satellite links with beam scanning capabilities is one of the objects of this work. The antenna optics should be compact and capable of being folded and deployed. The antenna should provide a solution for emergency communications for bi-directional satellite links in remote locations. The antenna should be designed to provide a directive beam in receive (10.70 - 12.75 GHz) and transmit (14.0 - 14.5 GHz) frequency bands with electronic scanning capabilities within a limited angular range.

1.2.5 Analysis and design of contoured-beam dual-reflectarray for DBS applications

Since one potential application of reflectarrays is in contoured-beam antennas for DBS applications, a dual-reflectarray antenna will be design to provide a DBS coverage, and their capabilities will be evaluated.

1.2.6 Extension of the analysis technique to include a reflectarray printed on curved surfaces.

Finally, the technique will be extended to non-flat main reflectarrays. As a particular case, it will be implemented for a parabolic reflectarray. The new technique will be validated by analysing a single offset parabolic reflectarray previously designed for a South American coverage. The reflectarray sub reflector will be substituted by a flat metal plate, in order to simulate the case of a single parabolic reflectarray.

1.3 Thesis organization

This thesis is organized in seven chapters; all of them present an introduction, one section with conclusions, and their respective sections about the specific concepts that are studied within. This chapter and the last one summarize the main ideas and conclusions of the work. The rest of the chapters present the methodology applied to analyse several configurations of dual-reflectarray antennas and the validation of the technique.

The second chapter describes a general method to analyse a dual reflectarray configuration, in which both the sub and the main reflectors are flat reflectarrays. Each reflectarray is analysed by using MoM and applying local periodicity. The incident field on the main reflectarray is computed as the contribution from all the elements on the sub reflectarray. Several approaches are proposed to provide accurate results and computation efficiency.

The third chapter shows the validation of the analysis technique described in chapter 2. First, to demonstrate that the designed reflectarray can substitute the main reflector, it is checked that both single offset configurations, reflectarray and reflector, provide virtually identical radiation patterns at the design frequency. After demonstrating such equivalence, the radiation patterns of the dual-reflectarray antenna are compared with those obtained for two reference antennas, made of a parabolic reflector and a sub reflectarray, in Ku- and W-bands.

The fourth chapter shows the design, manufacturing and test of a dual-reflectarray antenna with a compact optics. Both reflectarrays have been designed to reduce the

cross-polarization level of the complete antenna. Two more designs are shown in this chapter; they present the same optics than the previous system: one of them is designed to cancel completely the cross-polarization of the antenna and to improve the bandwidth and the last design generates a contoured beam that provides an European coverage for DBS (Direct Broadcast Satellite) applications.

Chapter five deals the preliminary design of a Ku-band antenna based on a dual planar reflector configuration that provides electronic beam scanning.

Two possible architectures have been studied. In the first architecture, the main reflectarray is passive and the beam scanning is achieved by introducing a phase-control in the elements of the sub reflectarray. In the second one, the antenna consists on a passive reflectarray as sub reflector and a reconfigurable reflectarray with 1-bit electronic control as main reflector.

Finally, in chapter six the technique is extended to analyse an antenna that includes a flat sub reflectarray and main parabolic reflectarray. The technique has been used to parabolic reflector that provides a contoured beam for a DBS application.

CHAPTER 2

2 Analysis technique for a dual-reflectarray antenna

2.1 Introduction

In this chapter, a modular technique is proposed for the analysis of a general dual-reflectarray antenna, which comprises the analysis of the feed and the sub and main reflectarrays as well as the calculation of the far-field radiation pattern. A general scheme of the proposed antenna configuration is shown in Fig. 2-1. In this work an offset configuration is considered but the analysis technique is general and can be applied to centered geometries.

Normally, a conventional far-field model of feed $\cos^q(\theta)$ can be used providing good accuracy. However, sometimes the sub reflectarray elements are placed in the Fresnel zone of the primary feed, so the approximation of the far field can not be used and the near field of the feed must be taken into account, which can be obtained through full-wave simulations, characterized through spherical wave mode expansion or measurements of the feed, [19][49].

The sub reflectarray is analyzed element by element, considering local periodicity and the real angle of incidence of the wave coming from the feed for each periodic cell. The total field reflected by the sub reflectarray elements is computed by MoM as the superposition of the fields reradiated by the patches and the field reflected by the multi-layer dielectric structure[2]. The calculation of the reflected field includes dissipative losses on the reflectarray.

The main reflectarray is analyzed using the same technique as for the sub reflectarray.

This analysis can be divided in two parts: the computation of the incident field on the reflectarray surface and the calculation of the reflected field for each reflectarray cell.

For the calculation of the cross polarization there are two components that are taken into account, the cross polarization due to the printed patches and the crosspolar field due to the antenna geometry. Although, the crosspolar field generated by the patches is very low it must be considered in the analysis and design of the reflectarray antennas, particularly in those applications that have stringent requirements on crosspolar level.

There are full-wave techniques based in Method of Moment that make an electromagnetic analysis of the complete reflectarray, considering all mutual couplings among the different elements [50], [51]. These methods provide an accurate analysis of reflectarrays but they are time-consuming and they are not useful for designing purposes. However, they can be used for virtual prototyping, not requiring the manufacture of a breadboard to validate a design.

The radiation pattern of the entire antenna is computed starting from the electric field reflected by the main reflectarray. Once the reflected field is calculated, the far field radiation pattern is computed applying the Second Equivalence Principle and a FFT-based algorithm.

The details of each step in the analysis technique are provided in the following sections of this chapter.

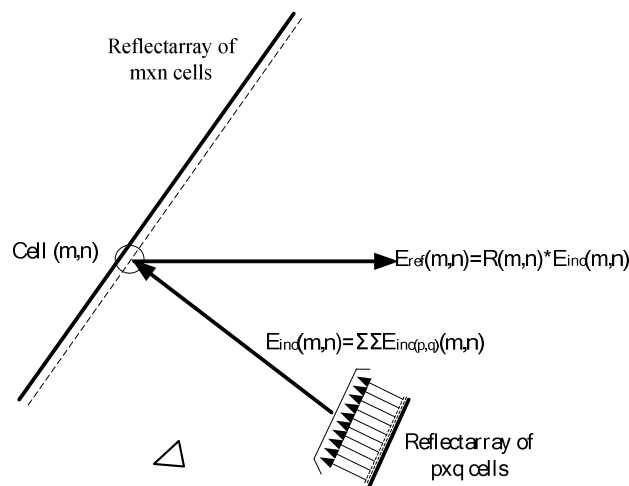


Fig. 2-1. Scheme of a dual-reflectarray structure for the method of analysis

2.2 Feed-Horn Models

2.2.1 Far field models.

2.2.1.1 Model based on $\cos^q(\theta)$ function.

A simple and accurate model of the far field radiated by a horn antenna is provided in[52]. In this reference, the electric field radiated by an aperture using the approximation of $\cos^q(\theta)$ for both X and Y polarized antennas is given by the following expressions:

$$E^X(r) = A_0 \frac{k_0}{2\pi r} e^{-jk_0 r} (\hat{\theta} C_X(\theta) \cos \phi - \hat{\phi} C_Y(\theta) \sin \phi) \quad (2-1)$$

$$E^Y(r) = A_0 \frac{k_0}{2\pi r} e^{-jk_0 r} (\hat{\theta} C_X(\theta) \sin \phi - \hat{\phi} C_Y(\theta) \cos \phi) \quad (2-2)$$

Where k_0 is the wave number in vacuum, A_0 is the complex constant in (watts)^{1/2} and C_X and C_Y model the feed horn pattern and they are given by these expressions:

$$C_X(\theta) = \cos^{qX}(\theta) \quad (2-3)$$

$$C_Y(\theta) = \cos^{qY}(\theta) \quad (2-4)$$

The q-factors provide the gain of the feed, the beamwidth in the main planes and the power radiated by the feed is adjusted through the A_0 constant.

The total power radiated by the feed is calculated in order to compute the incident field in the sub reflectarray and it is given by equation (2-5) .

$$P_{feed} = \int_{\theta=0}^{\theta=\pi/2} \int_{\phi=0}^{2\pi} \frac{|E^{X/Y}(\theta, \phi)|^2}{2\eta_0} r^2 \sin \theta d\theta d\phi \quad (2-5)$$

Where $E^{X/Y}(\theta, \phi)$ is the electric field radiated by the feed-horn. Substituting equations (2-1) and (2-2) in equation (2-5), the power radiated by the feed is:

$$P_{feed} = \frac{A_0^2 \pi}{\eta_0 \lambda^2 (2q+1)} \quad (2-6)$$

2.2.1.2 Gaussian beam model

The Gaussian beam is a simple and useful model of a typical feed in reflector antenna systems such as corrugated horn. One of its advantages is that it is easy to specify, radiates a typical beam and provides a good model of not only the far field of the feed but also the near field, which is important when a reflector is in the near field of the horn [53].

The pattern is generated as a Gaussian beam, which is a point source radiating a tapered beam. The field of the source satisfies Maxwell's equations in the near field as well as in the far field. The point source consists on a x-directed electrical short dipole and a y-directed short magnetic dipole resulting a z-directed Huygens source with certain polarization [54]. The expression for the Huygens source for large distances r , is given by

$$\mathbf{E}(r, \theta, \phi) = -\frac{E_0^e}{\sqrt{2}} \frac{e^{-jkr}}{kr} (1 + \cos \theta)(\cos \phi \hat{\theta} - \sin \phi \hat{\phi}) \quad (2-7)$$

E_0^e is the amplitude of the electric field radiated by the x-directed electric short dipole when it is excited by a real factor $1/\sqrt{2}$ for the Huygens source to radiate a total power of 4π watts.

2.2.2 Near field models

In some configurations, the far field approximation is inappropriate because the reflectarray elements are placed in the Fresnel zone of the primary feed. This occurs, for example, when the reflectarray is illuminated with a high gain feed, or in the case of dual-reflector configurations in which the sub reflectarray is located in the near field of the feed.

The incident field on the reflectarray can be obtained through different methods such as the direct measure of the NF (Near Field) or FF (Far Field) measurements and FF to NF transformation. Alternatively, the feed can also be calculated through a full-wave simulation with commercial tools, such as CHAMP from Tiera [55] for horns with revolution symmetry.

2.2.2.1 Source reconstruction

One of the techniques used in this thesis, consists on a source reconstruction from the far field measurements, the complete far field radiation pattern (amplitude and phase) of the feed horn is measured in spherical range in an anechoic chamber. Then, an integral-equation-based method for the antenna diagnosis and FF-NF (Far Field-Near Field) transformation are used to obtain a set of equivalent currents that will characterize the radiation pattern of the antenna, then the NF on the reflectarray surface is calculated from these currents [49][56]. Fig. 2-2 shows a scheme of the methodology.

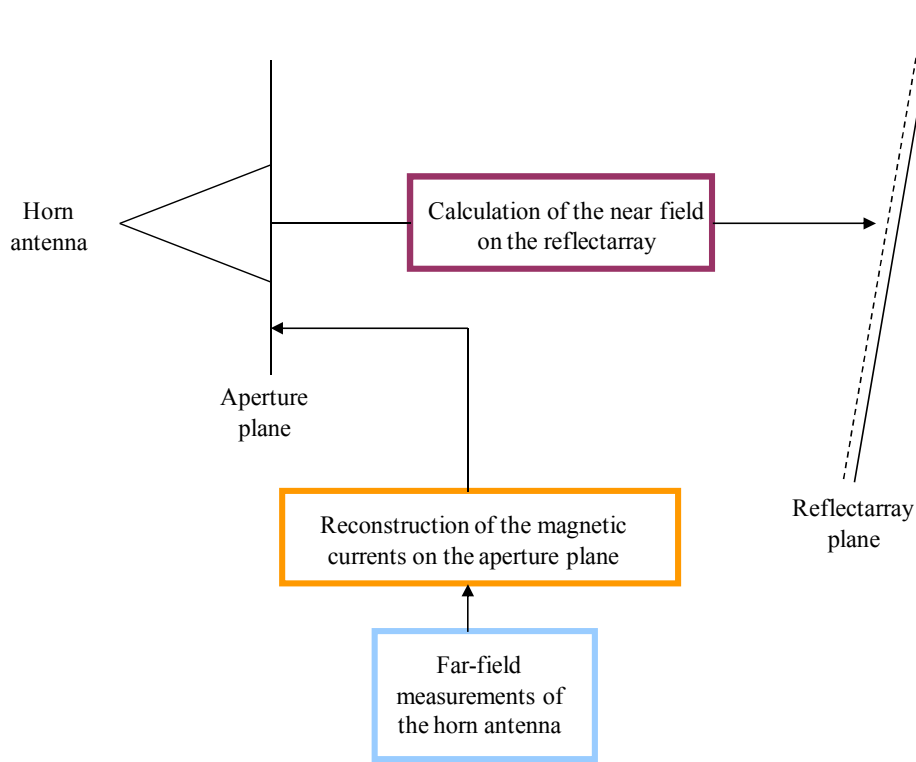


Fig. 2-2. Scheme of the process to obtain the NF on the reflectarray plane, starting from the FF measurements of the horn antenna

2.2.2.2 Feed defined by spherical wave expansion

A general electromagnetic field may be written as a spherical wave expansion [53], which in the notation of the ab-modes may be written as

$$\mathbf{E}(r, \theta, \phi) = k\sqrt{2\eta_0} \sum_{m=-M}^M \sum_{\substack{n=|m| \\ n>0}}^{N(m)} \{a_{mn} \mathbf{m}(r, \theta, \phi) + b_{mn} \mathbf{n}(r, \theta, \phi)\} \quad (2-8)$$

$$\mathbf{H}(r, \theta, \phi) = jk \sqrt{\frac{2}{\eta_0}} \sum_{m=-M}^M \sum_{\substack{N(m) \\ n=|m| \\ n>0}} \{a_{mn} \mathbf{n}(r, \theta, \phi) + b_{mn} \mathbf{m}(r, \theta, \phi)\} \quad (2-9)$$

a_{mn} and b_{mn} are the spherical –wave expansion coefficients and η_0 is the free-space impedance. The spherical vector expansion functions $\mathbf{m}_{mn}(r, \theta, \phi)$ and $\mathbf{n}_{mn}(r, \theta, \phi)$ are defined by

$$\begin{aligned} \mathbf{m}_{mn}(r, \theta, \phi) = & -h_n^{(2)}(kr) \frac{j m P_n^{|m|}(\cos \theta)}{\sin \theta} e^{-j m \phi} \hat{\theta} \\ & - h_n^{(2)}(kr) \frac{j m P_n^{|m|}(\cos \theta)}{d \theta} e^{-j m \phi} \hat{\phi} \end{aligned} \quad (2-10)$$

and

$$\begin{aligned} \mathbf{n}_{mn}(r, \theta, \phi) = & \frac{n(n+1)}{kr} h_n^{(2)}(kr) P_n^{|m|}(\cos \theta) e^{-j m \phi} \hat{r} \\ & + \frac{1}{kr} \frac{d}{d(kr)} \{k r h_n^{(2)}(kr)\} \frac{d P_n^{|m|}}{d \theta} e^{-j m \phi} \hat{\theta} \\ & - \frac{1}{kr} \frac{d}{d(kr)} \{k r h_n^{(2)}(kr)\} \frac{j m P_n^{|m|}}{\sin \theta} e^{-j m \phi} \hat{\phi} \end{aligned} \quad (2-11)$$

$P_n^m(\cos \theta)$ are the associated Legendre functions given by

$$P_n^{|m|}(\cos \theta) = (\sin \theta)^{|m|} \frac{d^{|m|} P_n(\cos \theta)}{d \cos(\theta)^{|m|}}, \quad |m| \leq n \quad (2-12)$$

Where

$$P_n(\cos \theta) = \frac{1}{2^n n!} \frac{d^n}{d(\cos \theta)^n} (\cos^2 \theta - 1)^n, \quad n \geq 0 \quad (2-13)$$

P_n is the Legendre polynomial. $h_n^{(2)}(kr)$ are the Hankel functions of the second kind given by a recursion relation as defined in [57].

The power of the mode-expanded field is given by the ab coefficients as

$$P = 4\pi \sum_{m=-M}^M \sum_{n=|m|}^{N(m)} \frac{n(n+1)}{2n+1} \frac{(n+|m|)!}{(n-|m|)!} (|a_{mn}|^2 + |b_{mn}|^2) \quad (2-14)$$

2.3 Analysis of the sub reflectarray

The analysis of the sub reflectarray is carried out element by element, considering local periodicity and the angle of incidence of the wave coming from the feed for each periodic cell. The Floquet's Theorem is applied locally and the total field reflected by the sub reflectarray elements is computed by MoM as the superposition of the fields reradiated by the patches and the field reflected by the multi-layer dielectric structure. The technique has been described in Chapter 3 (Section 3.6.2) of [1].

2.3.1 Number of samples

For the calculation of the incident and reflected field on a reflectarray cell, the module and the phase are usually considered constant on the surface of each cell being the fields calculated in the centre of each cell. However, there are cases in which the reflectarray is located in the Fresnel zone of the feed-horn, producing a variation of the incident field within the periodic cell that must be considered. To take into account this effect in the computation of the incident and reflected fields, the cell is divided in a number of subcells. Although, the incident field is calculated for each subcell, the reflection coefficient per cell is calculated only once as previously discussed. The division in four subcells is considered enough for a reflectarray illuminated in the Fresnel zone of a conventional feed-horn, see Fig. 2-3, but a larger number of samples can be taken if necessary.

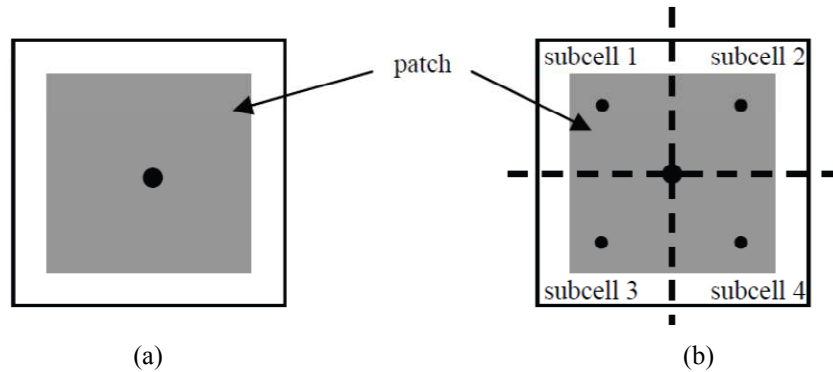


Fig. 2-3. Scheme of a reflectarray cell with one (a) or four samples (b) per cell

The analysis of each reflectarray cell assumes that the incident field on the cell is a locally plane wave on the center of the periodic cell. Consequently, if the field varies

abruptly within the reflectarray the analysis may not work. The minimum distance where the sub reflectarray must be located respect to the feed-horn is the one in which the spherical wave is considered locally plane in the reflectarray cell.

2.3.2 Co- and Cross-polar radiation produced by the sub reflectarray

There are two sources of cross-polar radiation in the antenna configuration, which are the antenna geometry and the printed patches. The first component is produced by the projection (decomposition) of the polarization vector of the field on the patch dimensions, while the second is generated by the patches themselves. This section shows the co- and cross-polar components of the radiated field radiation when a feed illuminates the reflectarray.

Both co-polar and cross-polar components are computed with the analysis technique summarized in the previous section. The two following expressions show the x and y components of the reflected field, for X/Y linear polarisation (either X or Y polarisation):

$$E_{x \text{ ref}}^{X/Y} = \rho_{xx} \cdot E_{x \text{ inc}}^{X/Y} + \rho_{xy} \cdot E_{y \text{ inc}}^{X/Y} \quad (2-15)$$

$$E_{y \text{ ref}}^{X/Y} = \rho_{yx} \cdot E_{x \text{ inc}}^{X/Y} + \rho_{yy} \cdot E_{y \text{ inc}}^{X/Y} \quad (2-16)$$

Fig. 2-4 shows a scheme of the incident field vector decomposed in their two orthogonal components (x-component and y-component) and how each of these components generates a contribution in the orthogonal direction.

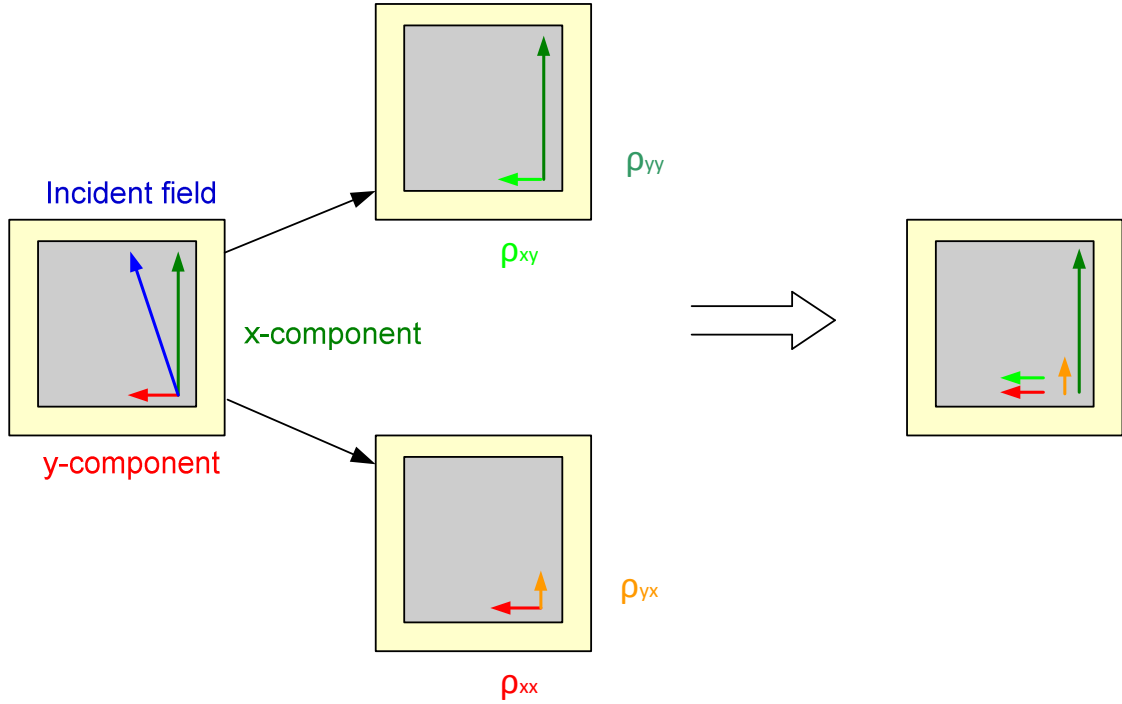


Fig. 2-4. Scheme of the incident electric field vector on each cell of the reflectarray divided in their x and y components, assuming a feed with the electric field polarised in x-direction

Assuming X-polarisation, the co-polar reflected field is given by the equation (2-17).

$$E_{x\ ref}^X = E_{cp\ ref}^X = \rho_{xx} \cdot E_{x\ inc}^X + \rho_{xy} \cdot E_{y\ inc}^X \quad (2-17)$$

The equation (2-17) can be simplified thanks to the following inequalities:

$$\left. \begin{array}{l} |\rho_{xx}| \gg |\rho_{xy}| \\ |E_{x\ inc}^X| \gg |E_{y\ inc}^X| \end{array} \right\} \Rightarrow |\rho_{xx} \cdot E_{x\ inc}^X| \gg |\rho_{xy} \cdot E_{y\ inc}^X| \quad (2-18)$$

The co-polar component of the reflected field can be simplified to one component

$$E_{x\ ref}^X = E_{cp\ ref}^X \approx \rho_{xx} \cdot E_{x\ inc}^X \quad (2-19)$$

The cross-polar component of the reflected field is given by equation (2-16) and can be written as:

$$E_{y\ ref}^X = E_{xp\ ref}^X = \rho_{yx} \cdot E_{x\ inc}^X + \rho_{yy} \cdot E_{y\ inc}^X = E_{xp\ ref}^X \Big|_{patch} + E_{xp\ ref}^X \Big|_{geometry} \quad (2-20)$$

The first term of the sum corresponds to the cross-polar generated by the patches themselves and the second is due to the geometry. The geometry produces cross radiation since the incidence of the X-polarized impinging out of the symmetry axes of the antenna generates a component in the orthogonal direction (Y).

In this case, none of the terms of the sum can be neglected since the comparison of the modules is:

$$\left. \begin{aligned} |\rho_{yx}| &\ll |\rho_{yy}| \\ |E_{x\ inc}^X| &\gg |E_{y\ inc}^X| \end{aligned} \right\} \quad (2-21)$$

If only single linear polarisation is required, the orthogonal dimension of the patch can be adjusted to control the phase of the reflected coefficient to produce a partial cancellation between the cross-polar term due to the patch and the term produced by the geometry.

In the case of having Y polarisation, the co-polar radiation corresponds to the equation (2-16) and the inequalities fulfilled are:

$$\left. \begin{aligned} |\rho_{yy}| &\gg |\rho_{yx}| \\ |E_{x\ inc}^Y| &\ll |E_{y\ inc}^Y| \end{aligned} \right\} \Rightarrow |\rho_{yx} \cdot E_{y\ inc}^Y| \ll |\rho_{yy} \cdot E_{y\ inc}^Y| \quad (2-22)$$

The co-polar component of the reflected field can be simplified to one component:

$$E_{y\ ref}^Y = E_{cp\ ref}^Y \approx \rho_{yy} \cdot E_{y\ inc}^Y \quad (2-23)$$

The cross-polar radiation of the reflected field is given by equation (2-15) and can be written as:

$$E_{x\ ref}^Y = E_{xp\ ref}^Y = \rho_{xx} \cdot E_{x\ inc}^Y + \rho_{xy} \cdot E_{y\ inc}^Y = E_{xp\ ref}^Y \Big|_{geometry} + E_{xp\ ref}^Y \Big|_{patch} \quad (2-24)$$

No terms of the sum can be neglected since the comparison of the modules is:

$$\begin{aligned} |\rho_{xx}| &\gg |\rho_{xy}| \\ |E_{x\ inc}^Y| &\ll |E_{y\ inc}^Y| \end{aligned} \quad (2-25)$$

2.4 Analysis of the main-reflectarray

2.4.1 *Flat main reflectarray*

The main reflectarray is analyzed using the same technique described previously for the sub reflectarray, which implies an analysis element by element, assuming local periodicity and the local application of the Floquet's Theorem. The total field reflected by the main-reflectarray elements is computed by MoM as the superposition of the fields reradiated by the patches and the field reflected by the multi-layer dielectric structure [2].

In general, the analysis can be divided into two parts: the computation of the incident field on the reflectarray surface and the calculation of the reflected field for each reflectarray cell.

In a standard case, the cells of the main reflectarray will be placed in the Fresnel zone of the sub reflectarray. However, they are placed in the Far-Field region of the sub reflectarray cells since they are considered small apertures. Consequently, the computation of the incident electric field on the main reflectarray surface can be computed as the superposition of all the contributions from the sub reflector elements. Assuming each sub reflectarray cell as a small aperture uniformly illuminated, the incident field on a cell (m,n) of the main reflectarray produced by the (p,q) element of the sub reflectarray is given by:

$$E_{in\theta}^{p,q}(m,n) = L \cdot (E_{ref\ x_{SR}}(p,q) \cos \phi + E_{ref\ y_{SR}}(p,q) \sin \phi) \quad (2-26)$$

$$E_{in\phi}^{p,q}(m,n) = -L \cdot \cos \theta \cdot (E_{ref\ x_{SR}}(p,q) \sin \phi - E_{ref\ y_{SR}}(p,q) \cos \phi) \quad (2-27)$$

Where $E_{ref\ x_{SR}}(p,q)$ and $E_{ref\ y_{SR}}(p,q)$ are the x_{SR} and y_{SR} components of the reflected field on the cell (p,q) of the sub reflectarray and L is

$$L = \frac{jk_0}{2\pi R_{(p,q)-(m,n)}} e^{-jk_0 R} p_{Sx} p_{Sy} \cdot \sin c\left(\frac{k_u p_{Sx}}{2}\right) \cdot \sin c\left(\frac{k_v p_{Sy}}{2}\right) \quad (2-28)$$

In equation (2-28), $R_{(p,q)-(m,n)}$ is the distance from the cell (p,q) of the sub reflectarray to the cell (m,n) of the main reflector, p_{Sx} and p_{Sy} are the dimensions of the periodic cell on the sub- reflectarray and k_u and k_v are given by

$$\begin{aligned} k_u &= k_0 u = k_0 \sin \theta \cos \phi \\ k_v &= k_0 v = k_0 \sin \theta \sin \phi \end{aligned} \quad (2-29)$$

Where k_0 is the wave number in free space, and θ, ϕ the spherical angles. Since the cells of the main reflectarray are located in the Far Field Zone of the sub reflectarray patches, the total incident field on an element (m,n) of the main reflectarray can be computed as the sum of the contributions of all the cells of the sub reflectarray.

$$\mathbf{E}_{in}(m,n) = \sum_{p=1}^P \sum_{q=1}^{Q(p)} \mathbf{E}_{in}^{p,q}(m,n) \quad (2-30)$$

Where $E_{in}(m,n)$ is the incident field in the cell (m,n) of the main reflector and $E_{in}^{p,q}(m,n)$ is the incident field on the cell (m,n) of the main due to the cell (p,q) of the sub reflectarray. P and $Q(p)$ are the number of rows and columns of the sub reflectarray, taking into account that the shape of the reflectarray can be arbitrary and thus the number of columns $Q(p)$ in general depends on the row, as it is the case for a circular or elliptical reflectarray. Only the tangential components are considered in the analysis of the main as it was done for the sub reflectarray.

Once the incident field has been computed, the reflected field has to be calculated at element level. The incident and reflected fields are related through a matrix $\mathbf{R}^{m,n}$, as can

be seen in equation 2-32. The mentioned matrix depends on the incidence angle and therefore depends on the placement of each (p,q) contribution of the sub reflectarray. For a very accurate analysis of the main reflectarray, the $\mathbf{R}^{m,n/p,q}$ matrix, which represents the reflection coefficients of every cell of the main reflectarray (m,n) for a plane wave coming from each cell of the sub reflectarray (p,q) , should be computed for each pair of elements $(m,n) - (p,q)$. Note that all the cells of the sub reflectarray are considered as origin of the incident field, which requires a very large computational effort. Nevertheless, the incidence angles for different contributions of the sub reflectarray cells on the same main reflectarray element are only slightly different and therefore the $\mathbf{R}^{m,n/p,q}$ matrices are very similar for all the elements (p,q) on the sub reflectarray. Thus they can be approximated as:

$$\mathbf{R}^{m,n/p,q} \approx \mathbf{R}^{m,n} \quad (2-31)$$

Where $\mathbf{R}^{m,n}$ is computed assuming for the incidence angle that the impinging wave comes from the sub reflectarray center or the equivalent focal point of the main reflectarray. With this approximation the reflected field for each cell of the main reflectarray can be approximated as.

$$\mathbf{E}_{ref}(m,n) = \mathbf{R}^{m,n} \mathbf{E}_{in}(m,n) \quad (2-32)$$

The approximation produces a significant reduction in the computation effort, since each $\mathbf{R}^{m,n}$ matrix should be computed by MoM. As a result, the numerical analysis is applied only once per element of the main reflectarray, instead of N_{SR} times, being N_{SR} the number of elements in the sub reflectarray. This approximation assumes that all the field contributions on the main reflectarray surface have the same angle of incidence for each cell.

This approach will not affect the accuracy in the analysis of the main reflector, if the variation in the angle of incidence from the different elements in the sub reflectarray does not produce a significant variation of the phase-shift on the cells of the main reflectarray. This condition depends on the antenna optics and also on the sensitivity of the reflectarray cells to the angle of incidence. Note that in many practical configurations, incidence angles up to 30 degrees will produce practically no effect on the reflected field of the main-reflectarray. When this condition is not fulfilled, the

reflector can be subdivided in sub-arrays, and the phase-center of each sub reflectarray can be used for a more accurate computation, as it is discussed in the next subsection.

2.4.2 *Division of the sub reflectarray aperture*

In a standard dual-reflectarray antenna, the angles of incidence for all the contributions coming from each cell of the sub reflectarray are very similar. Thus, there is practically no difference in the computation of the reflection coefficient if the origin of the incident field is considered to be the centre of the sub reflectarray. However, if the main-reflectarray cells are located in the near field zone of the sub reflectarray, the incidence angle can vary strongly for two sub reflectarray cells. This effect is strong if the two sub reflectarray cells are far but it can be neglected if they are neighbours. To take into account this effect, the sub reflectarray can be divided in sub-arrays of elements. The field is decomposed in waves radiated by each group with their different incident angles and MoM is used to analyze each element of the main-reflectarray for the wave coming from each sub-array of elements of the sub reflectarray. The size of the sub-array in the sub reflectarray is calculated such that the main-reflectarray cells fulfill the far field conditions with respect to the sub-array.

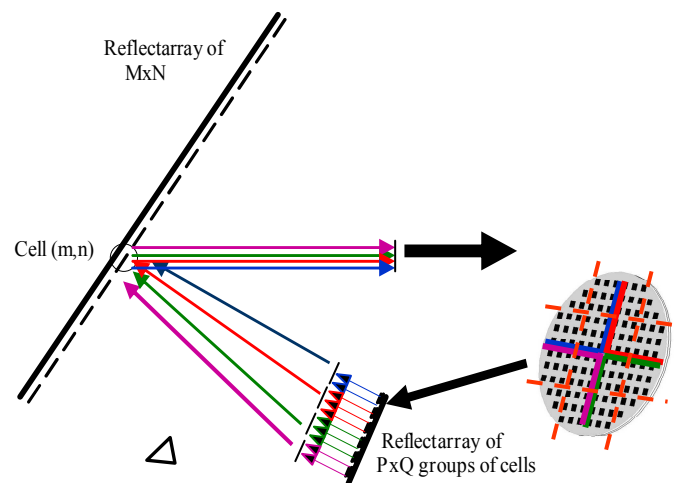


Fig. 2-5. Scheme of a dual reflectarray structure with the sub reflectarray divided in groups of elements

Each group of cells of the sub reflectarray produces an electric field contribution in each cell of the main. Each of these contributions has a different incidence angle, which is taken into account in the computation of the reflected coefficient of each cell in the

main reflector. Therefore, for every cell of the main-reflectarray, a number of PxQ reflected coefficients are calculated, see Fig. 2-5.

The incident field in each cell of the main due to each sub-array cell is added before calculating the reflection coefficient of any cell of main. All the field contributions that come from the same sub-array of cells are considered as they have the same incident angle in each cell of the main (the one that corresponds to the case in which the origin of the incident field is in the centre of the sub-array). Each incident electric field contribution is computed by adding the field radiated by each sub reflectarray element (r,s) as it is shown in equation 2-33.

$$\mathbf{E}_{inc(p,q)}^{X/Y}(m,n) = \sum_{r=1}^{Size_x} \sum_{s=1}^{Size_y} \mathbf{E}_{inc(r,s)}^{X/Y}(m,n) \quad (2-33)$$

Size_x and Size_y are the number of elements for each sub-array in the x and y axis respectively. $\mathbf{E}_{inc(p,q)}^{X/Y}(m,n)$ is the electric field impinging on the cell (m,n) of the main from the group of cells (p,q) of the sub reflectarray, for X or Y polarization.

$$\mathbf{E}_{ref}^{X/Y}(m,n) = \sum_{p=1}^P \sum_{q=1}^Q \mathbf{R}_{(p,q)}(m,n) \cdot \mathbf{E}_{inc(p,q)}^{X/Y}(m,n) \quad (2-34)$$

where

$$\mathbf{R}_{(p,q)}(m,n) = \begin{pmatrix} \rho_{(p,q)xx}^{(m,n)} & \rho_{(p,q)yx}^{(m,n)} \\ \rho_{(p,q)xy}^{(m,n)} & \rho_{(p,q)yy}^{(m,n)} \end{pmatrix} \quad (2-35)$$

The components of the \mathbf{R} matrix are complex reflection coefficients defined for the total reflected field and they characterize the behavior of the reflectarray element for the contribution of each sub-array of sub reflectarray cells. The components ρ_{xx} and ρ_{yx} are the direct and cross reflection coefficients for an incident wave polarized with the electric field on x_R direction (without component in y_R). On the other hand, ρ_{yy} and ρ_{xy} are the reflection coefficients for an incident electric field on y_R direction. They depend on the angle of incidence of the impinging wave coming from the centre of each group of elements in the sub reflectarray. The matrix is different for each element of the main-reflectarray. Hence, the term $\mathbf{R}_{(p,q)}(m,n)$ is the reflected coefficient for the cell (m,n) of the main reflectarray due to the incident field that comes from the centre of the sub-array (p,q) of the sub reflectarray. The term $\mathbf{E}_{inc(p,q)}$ is the incident field in the cell (m,n) of main-reflectarray due to the group of cells (p,q) of the sub reflectarray and the

term $E_{ref}(m,n)$ is the reflected field in the cell (m,n) of the main reflector as Fig. 2-6 shows.

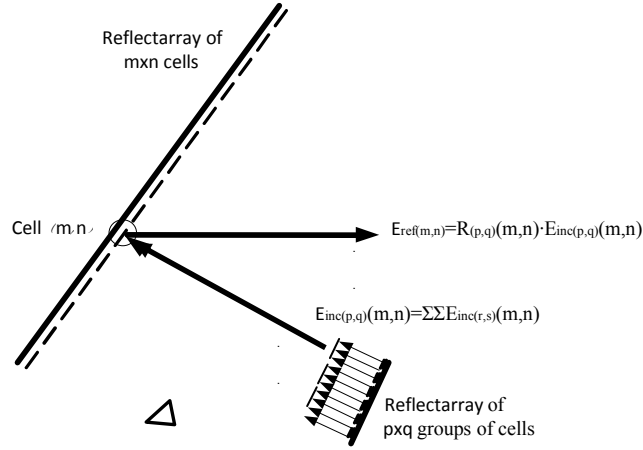


Fig. 2-6. Scheme of a dual-reflectorarray structure for the analysis method

For this general analysis method, there are two possible limit cases: the full-wave case, in which each group of elements has only one cell; and the case in which there is only one group of elements constituted by all the cells of the sub reflectarray, resulting in a single incident plane wave on each main reflectarray cell.

2.4.2.1 Full-wave analysis

In a full-wave analysis, the electric field coming from each cell of the sub reflector impinges on each cell of the main reflectarray with different angle, which is taken into account in the computation of the field reflected by each cell in the main reflectarray, as shown in Fig. 2-7.

$$\mathbf{E}_{ref}^{X/Y}(m,n) = \sum_p \sum_q \mathbf{R}_{(p,q)}(m,n) \cdot \mathbf{E}_{inc(p,q)}^{X/Y}(m,n) \quad (2-36)$$

Where

$$\mathbf{R}_{(p,q)}(m,n) = \begin{pmatrix} \rho_{(p,q) \ xx}^{(m,n)} & \rho_{(p,q) \ yx}^{(m,n)} \\ \rho_{(p,q) \ xy}^{(m,n)} & \rho_{(p,q) \ yy}^{(m,n)} \end{pmatrix} \quad (2-37)$$

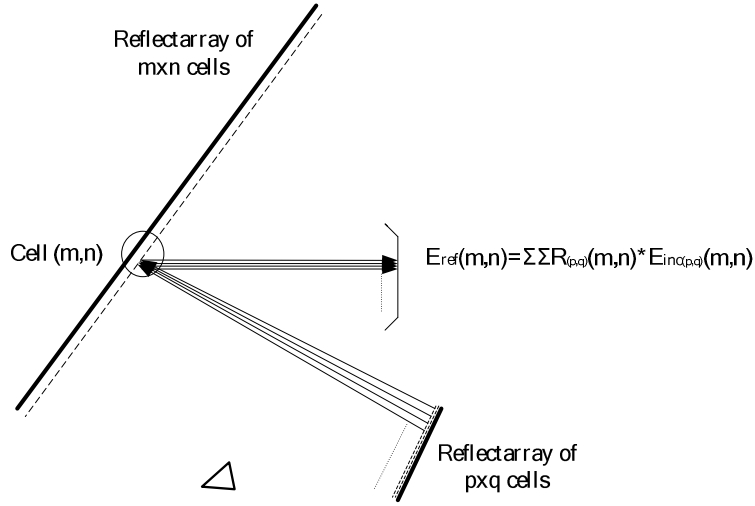


Fig. 2-7. Scheme of a dual reflectarray structure for the accurate case of the analysis method

As it was mentioned before the computation time to obtain the radiation pattern of this dual reflectarray configuration with the explained method is too high, therefore a simplification is proposed as an alternative.

2.4.2.2 Approximation of the incident field by a single plane wave

In an approximate case, the incident field in each cell of the main due to each cell of sub reflector are added before calculating the reflection coefficient of each cell of main and all the field contributions that come from the sub reflector are considered as they have the same angle of incidence in each cell of the main (the one that corresponds to the case in which the origin of the electric field is in the centre of the sub reflectarray), as shown in Fig. 2-8. The incident electric field is computed by adding the contributions of the field radiated by each sub reflectarray element (p, q) as it is shown in equation (2-38).

$$\mathbf{E}_{in}^{X/Y} = \sum_p \sum_q \mathbf{E}_{in(p,q)}^{X/Y} (m, n) \quad (2-38)$$

The reflected field for each cell of the main reflectarray is calculated using the equation,

$$\mathbf{E}_{ref}^{X/Y} (m, n) = \mathbf{R}(m, n) \cdot \sum_p \sum_q \mathbf{E}_{inc(p,q)}^{X/Y} (m, n), \quad (2-39)$$

where

$$\mathbf{R}(m,n) = \begin{pmatrix} \rho_{xx}^{m,n} & \rho_{yx}^{m,n} \\ \rho_{xy}^{m,n} & \rho_{yy}^{m,n} \end{pmatrix} \quad (2-40)$$

In this case the reflection coefficients for an incident electric field depend on the angle of incidence of the impinging wave coming from center of the sub reflectarray so that the matrix is different for each element (m,n) of the main reflectarray and it is different from the matrix of the previous method. So, the term $\mathbf{R}(m,n)$ is the reflected coefficient of the cell (m,n) of the main reflectarray due to the incident field that comes from the center of the sub reflectarray. The radiated field is calculated using the field at the aperture plane, applying the Second Principle of Equivalence.

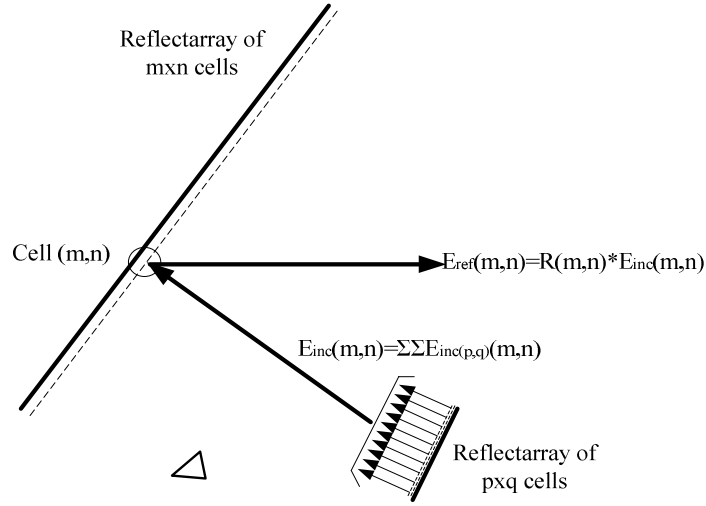


Fig. 2-8. Scheme of a dual-reflectarray structure for the approximate case of the analysis method

2.4.3 Number of samples

For the calculation of the incident and reflected field on a reflectarray cell of the main reflector, the module and the phase are considered constant on the surface of each cell. Normally, the fields are calculated in the centre of each cell. However, there are certain cases in which the calculation of the radiation pattern requires a major number of samples of the reflected field on the main reflectarray surface to achieve an accurate result. Taking this into account, the cell may be divided in four or nine sub-cells, as shown in Fig. 2-9, and the same analysis previously performed for each cell is now done for each piece. Although, the incident field is calculated for each subcell, the reflection coefficient per cell is calculated only once.

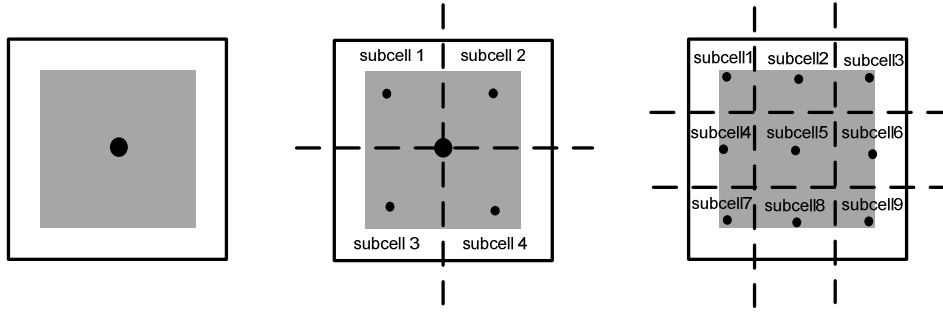


Fig. 2-9. Scheme of a reflectarray cell with one (a) four (b) or 9 samples (c) per cell

2.5 Calculation of the radiation pattern

The last stage in the analysis of the dual reflectarray antenna consists on the calculation of the radiation pattern starting from the field reflected by the main reflectarray. The radiated field is calculated using the field equivalence principles on an arbitrary surface. The field equivalence is a principle by which actual sources are replaced by equivalent sources. They are equivalent within a region because they produce the same fields within that region.

The equivalence principle is based on the theorem: “*a field in a lossy region is uniquely determined by the sources within the region plus the tangential components of the electric field over the boundary, or the tangential components of the magnetic field over the boundary, or the former over part of the boundary and the latter over the rest of the boundary*”. This principle is the most rigorous formulation of the Huygens principle which says: “*each point on a primary wave front can be considered to be a new source of a secondary spherical wave and that a secondary wavefront can be constructed as the envelope of these secondary spherical waves* [58].

The equivalence principle is developed considering an electric source, which electrically is represented by current densities \mathbf{M}_s . Fig. 2-10 (a) represents the problem model and the Maxwell equations are applied outside of the volumen V to describe the electromagnetic field generated by the sources inside V . Fig. 2-10 (b) shows the the equivalent model, where the sources are eliminated. The fields \mathbf{E} and \mathbf{H} outside the volume V do not change due to the introduced surface currents \mathbf{J}_s and \mathbf{M}_s .

$$\mathbf{J}_s = \hat{n} \times (\mathbf{H} - \mathbf{H}_{in})|_s \quad (2-41)$$

$$\mathbf{M}_s = -\hat{n} \times (\mathbf{E} - \mathbf{E}_{in})|_s \quad (2-42)$$

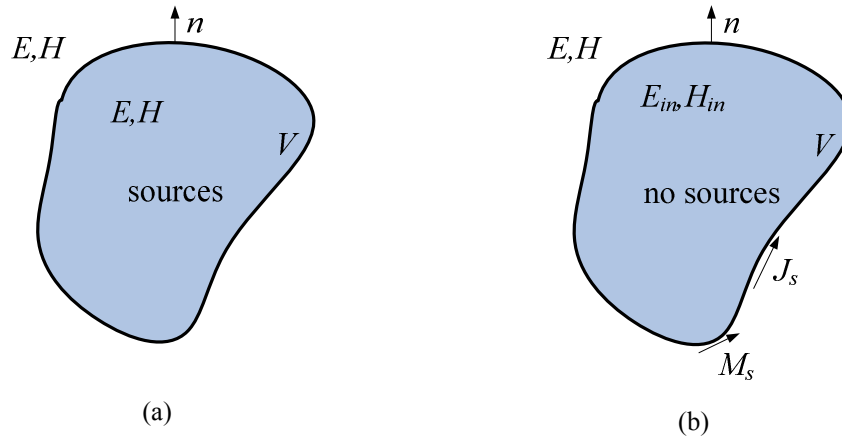


Fig. 2-10. Original (a) and equivalent (b) model

In the First Equivalence Principle, also known as Love's Equivalence Principle, no sources are considered, the electric and magnetic fields inside the volume V are assumed to be zero. The electric and magnetic surface currents calculated for this case are:

$$\mathbf{J}_s = \hat{n} \times \mathbf{H}|_s \quad (2-43)$$

$$\mathbf{M}_s = -\hat{n} \times \mathbf{E}|_s \quad (2-44)$$

In the case of assuming a perfect electric conductor, the current \mathbf{J}_s is zero and there is only \mathbf{M}_s , which corresponds to the Second Equivalence Principle, see Fig. 2-10 (b).

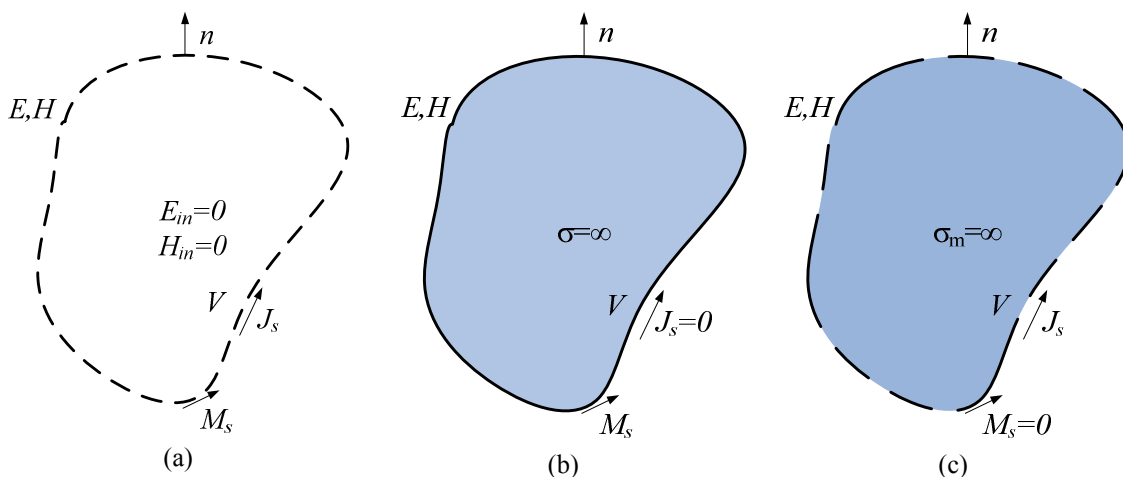


Fig. 2-11. First (a), Second (b) and Third (c) principle of equivalence

In the Third Equivalence Principle, the volume is a perfect magnetic conductor. In this case, \mathbf{M}_s is zero and the electromagnetic field outside V is produced by \mathbf{J}_s . Table 2-1 resumes the three Equivalence Principles.

Table 2-1. Equivalent currents for the equivalence principles

Principle of equivalence	V	\mathbf{J}_s	\mathbf{M}_s
Love's Equivalence Principle (First)	No sources	$\hat{n} \times H _s$	$-\hat{n} \times E _s$
Electric Conductor Equivalence Principle (Second)	$\sigma _{in} = \infty$	0	$-2\hat{n} \times E _s$
Magnetic Conductor Equivalence Principle (Third)	$\sigma_m _{in} = \infty$	$2\hat{n} \times H _s$	0

Using the equivalence principles, the potential vector functions are given by:

$$\mathbf{A}(r) = \frac{\mu}{4\pi r} e^{-jkr} \iint_{S'} \mathbf{J}_s(r') e^{jk\hat{r} \cdot r'} dS' \quad (2-45)$$

$$\mathbf{F}(r) = \frac{\varepsilon}{4\pi r} e^{-jkr} \iint_{S'} \mathbf{M}_s(r') e^{jk\hat{r} \cdot r'} dS' \quad (2-46)$$

The radiated fields in the far-field zone are:

$$\mathbf{E}_A = -j\omega(\mathbf{A}_\theta \hat{\theta} + \mathbf{A}_\phi \hat{\phi}) \quad (2-47)$$

$$\mathbf{H}_F = -j\omega(\mathbf{F}_\theta \hat{\theta} + \mathbf{F}_\phi \hat{\phi}) \quad (2-48)$$

The electric field related to the potential \mathbf{F} can be found in the following equation:

$$\mathbf{E}_F = \eta \mathbf{H}_F \times \hat{r} = -j\omega\eta(\mathbf{F}_\phi \hat{\theta} - \mathbf{F}_\theta \hat{\phi}) \quad (2-49)$$

The total electric field is constituted by the addition of components produced by the electric and magnetic surface currents:

$$\begin{aligned} \mathbf{E} = \mathbf{E}_A + \mathbf{E}_F &= -j\omega(\mathbf{A}_\theta \hat{\theta} + \mathbf{A}_\phi \hat{\phi}) - j\omega\eta(\mathbf{F}_\phi \hat{\theta} - \mathbf{F}_\theta \hat{\phi}) = \\ &= -j\omega[(\mathbf{A}_\theta + \eta\mathbf{F}_\phi) \hat{\theta} + (\mathbf{A}_\phi - \eta\mathbf{F}_\theta) \hat{\phi}] \end{aligned} \quad (2-50)$$

A flat reflectarray is a planar aperture antenna. Thus, the discussed formulation will be particularized for the case of an aperture in an infinite ground plane and the radiated field from the fields at the aperture is calculated.

The First Principle of Equivalence could be used, but it requires the computation of both the electric and magnetic tangential fields. The Second Principle of Equivalence is accurate and only requires the computation of the tangential electric field.

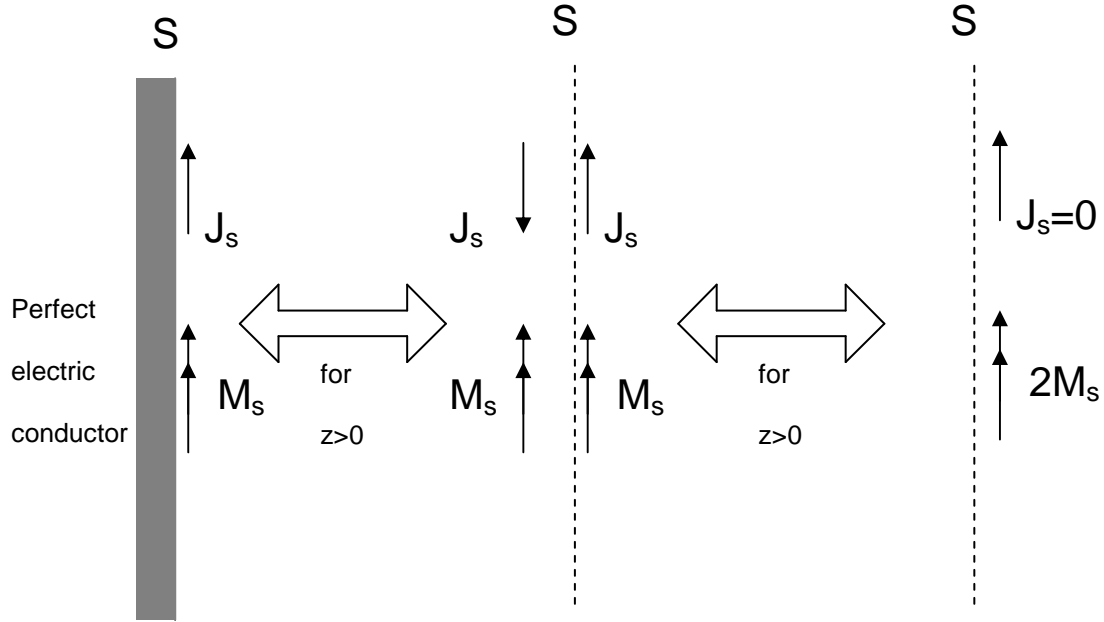


Fig. 2-12. Electric Conductor Equivalence Principle

The Second Principle of Equivalence is shown in the Fig. 2-11 (b) and Fig. 2-12. As can be checked, the electric currents are zero and only the magnetic potential vector must be calculated. According to this principle and considering the normal vector to the surface \hat{n} as the vector \hat{z} , the equivalent electric and magnetic superficial currents are:

$$\mathbf{J}_s = 0 \quad (2-51)$$

$$\mathbf{M}_s = -2\hat{z} \times \mathbf{E}_a \quad (2-52)$$

Substituting these equations in (2-45) and (2-46) the magnetic vector potentials become:

$$\mathbf{A}(r) = 0 \quad (2-53)$$

$$\mathbf{F}(r) = -\frac{\mathcal{E}}{2\pi r} e^{-jk_r r} \hat{z} \times \iint_S \mathbf{E}_a(r') e^{jk_{\hat{r}} \cdot r'} dS' \quad (2-54)$$

And the radiated field given by equation (2-50) is rewritten as:

$$\mathbf{E} = -j\omega\eta(\mathbf{F}_\phi \hat{\theta} - \mathbf{F}_\theta \hat{\phi}) \quad (2-55)$$

In order to simplify the expressions (2-54), the integral can be calculated separately,

$$\mathbf{P} = \iint_S \mathbf{E}_a \cdot e^{jk\hat{r}\cdot\mathbf{r}'} dS' \quad (2-56)$$

Considering the aperture shown in Fig. 2-13, the electric field can be expressed as

$$\mathbf{E}_a = \hat{x} \cdot E_{ax}(x', y') + \hat{y} \cdot E_{ay}(x', y') \quad (2-57)$$

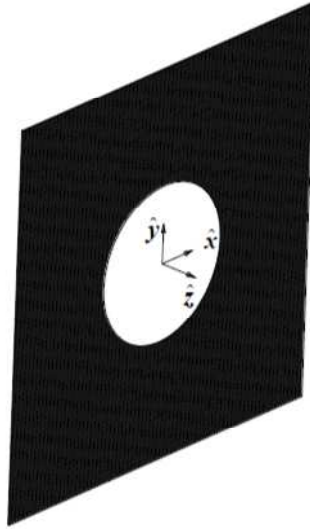


Fig. 2-13. Aperture in an perfect electric conductor with the coordinate system

Being:

$$\hat{r} = \hat{x} \sin\theta \cos\phi + \hat{y} \sin\theta \sin\phi + \hat{z} \cos\theta \quad (2-58)$$

$$r' = x' \cdot \hat{x} + y' \cdot \hat{y} \quad (2-59)$$

$$u = \sin\theta \cos\phi \quad (2-60)$$

$$v = \sin\theta \sin\phi \quad (2-61)$$

The x and y components of the P function can be calculated separately as:

$$\mathbf{P}_x(u, v) = \iint_S E_{ax} \cdot e^{jk(ux'+vy')} dx' dy' \quad (2-62)$$

$$\mathbf{P}_y(u, v) = \iint_S E_{ay} \cdot e^{jk(ux'+vy')} dx' dy' \quad (2-63)$$

If \mathbf{P}_x and \mathbf{P}_y given by equations (2-62) and (2-63) are introduced in equation (2-54) and the result is taken into account in the expression of the far field (2-55), the resulting θ and ϕ components of the radiated field at a distance R are given by:

$$E_{\theta}(u, v) = \frac{jk_0}{2\pi R} e^{-jk_0 R} \cdot (P_x(u, v) \cos \phi + P_y(u, v) \sin \phi) \quad (2-64)$$

$$E_{\phi}(u, v) = -\frac{jk_0}{2\pi R} e^{-jk_0 R} \cdot \cos \theta \cdot (P_x(u, v) \sin \phi - P_y(u, v) \cos \phi) \quad (2-65)$$

Finally, the co-polar and cross-polar components of the radiated field in a linear polarization are given by the Ludwig's Third Definition. The definition of the copolar and crosspolar from the θ and ϕ components in X-polarisation are given by:

$$\begin{pmatrix} E_{CP}^X \\ E_{XP}^X \end{pmatrix} = \begin{pmatrix} \cos \phi & -\sin \phi \\ -\sin \phi & -\cos \phi \end{pmatrix} \begin{pmatrix} E_{\theta}^X \\ E_{\phi}^X \end{pmatrix} \quad (2-66)$$

In the case of Y-polarisation, the copolar and crosspolar components are given by,

$$\begin{pmatrix} E_{CP}^Y \\ E_{XP}^Y \end{pmatrix} = \begin{pmatrix} \sin \phi & \cos \phi \\ \cos \phi & -\sin \phi \end{pmatrix} \begin{pmatrix} E_{\theta}^Y \\ E_{\phi}^Y \end{pmatrix} \quad (2-67)$$

2.6 Efficient computation of the spectral functions

In a dual reflectarray configuration with planar main reflectarray, the radiation pattern of the entire antenna is computed starting from the electric field reflected by the main reflectarray. Considering the aperture as the main reflectarray surface (MR), the field reflected by the reflectarray surface (\mathbf{E}_{ref}) and the coordinate system of the main reflectarray (\mathbf{x}_{MR} , \mathbf{y}_{MR} , \mathbf{z}_{MR}), the two components of \mathbf{P} given by equations (2-62) and (2-63) can be written as:

$$P_x(u, v) = \iint_{MR} E_{ref, x_{MR}}(x_{MR}, y_{MR}) \cdot e^{jk_0(ux_{MR} + vy_{MR})} dx_{MR} dy_{MR} \quad (2-68)$$

$$P_y(u, v) = \iint_{MR} E_{ref, y_{MR}}(x_{MR}, y_{MR}) \cdot e^{jk_0(ux_{MR} + vy_{MR})} dx_{MR} dy_{MR} \quad (2-69)$$

Taking into account that in a reflectarray antenna the reflected field is computed at the centre of each element, the field is calculated considering a regular mesh of period p_{Mx} and p_{My} in the x_{MR} and y_{MR} (being the sub-index MR, main reflectarray) directions respectively. Moreover, the reflectarray cell is considered as a small aperture uniformly

illuminated, so the field is considered constant both in phase and amplitude in each element.

Then, the following variable change can be applied, which relates the cell index (m,n) with the physical placement of the reflected field (x_{MR} , y_{MR}):

$$x_{MR} = x + \left(m - \frac{M-1}{2}\right)p_{Mx} \quad -\frac{p_{Mx}}{2} \leq x \leq \frac{p_{Mx}}{2} \quad m=0,1,2,\dots,M-1 \quad (2-70)$$

$$y_{MR} = y + \left(n - \frac{N-1}{2}\right)p_{My} \quad -\frac{p_{My}}{2} \leq y \leq \frac{p_{My}}{2} \quad n=0,1,2,\dots,N-1 \quad (2-71)$$

Thus, the reflected field can be written as a function of the cell index (m,n):

$$E_{ref \ x_{MR}}(x_{MR}, y_{MR}) = A_x(m, n) \cdot e^{j\phi_x(m, n)} \quad (2-72)$$

$$E_{ref \ y_{MR}}(x_{MR}, y_{MR}) = A_y(m, n) \cdot e^{j\phi_y(m, n)} \quad (2-73)$$

As a result, the integrals 2-68 and 2-69 can be written as summations,

$$P_x(u, v) = K \cdot K' \cdot \sum_{m=0}^{M-1} \sum_{n=0}^{N-1} A_x(m, n) \cdot e^{j\phi_x(m, n)} \cdot e^{jk_0(um \cdot p_{Mx} + vn \cdot p_{My})} \quad (2-74)$$

$$P_y(u, v) = K \cdot K' \cdot \sum_{m=0}^{M-1} \sum_{n=0}^{N-1} A_y(m, n) \cdot e^{j\phi_y(m, n)} \cdot e^{jk_0(um \cdot p_{Mx} + vn \cdot p_{My})} \quad (2-75)$$

Where K is the radiation pattern of the uniformly illuminated reflectarray periodic cell. and K' a phase term as follows:

$$K = p_{Mx} p_{My} \operatorname{sinc}\left(\frac{k_0 u p_{Mx}}{2}\right) \operatorname{sinc}\left(\frac{k_0 v p_{My}}{2}\right) \quad (2-76)$$

$$K' = e^{-j\frac{k_0}{2}(u(M-1)p_{Mx} + v(N-1)p_{My})} \quad (2-77)$$

The expressions (2-74) and (2-75) are very similar to a Two Dimensional Discrete Fourier Transform (DFT2). In fact, the general expressions for the DFT2 and for the Two Dimensional Inverse Discrete Fourier Transform (IDFT2) are

$$F(p, q) = DFT2[f(m, n)] = \sum_{m=0}^{M-1} \sum_{n=0}^{N-1} f(m, n) \cdot e^{-j\frac{2mp\pi}{M}} \cdot e^{-j\frac{2nq\pi}{N}} \quad (2-78)$$

$$f(m, n) = IDFT2[F(p, q)] = \frac{1}{MN} \sum_{m=0}^{M-1} \sum_{n=0}^{N-1} F(p, q) \cdot e^{j\frac{2mp\pi}{M}} \cdot e^{j\frac{2nq\pi}{N}} \quad (2-79)$$

The relationship between equations (2-74, 2-75) and (2-79) is given by the following variable changes:

$$u = \frac{2\pi p}{Mp_{M_x}k_0} \quad p = 0, 1, 2, \dots, M-1 \quad (2-80)$$

$$v = \frac{2\pi q}{Np_{M_y}k_0} \quad q = 0, 1, 2, \dots, N-1 \quad (2-81)$$

If these changes are applied, the P_x and P_y functions can be written as

$$P_x(p, q) = K \cdot K' \cdot \sum_{m=0}^{M-1} \sum_{n=0}^{N-1} A_x(m, n) \cdot e^{j\phi_x(m, n)} \cdot e^{j\frac{2mp\pi}{M}} \cdot e^{j\frac{2nq\pi}{N}} \quad (2-82)$$

$$P_y(p, q) = K \cdot K' \cdot \sum_{m=0}^{M-1} \sum_{n=0}^{N-1} A_y(m, n) \cdot e^{j\phi_y(m, n)} \cdot e^{j\frac{2mp\pi}{M}} \cdot e^{j\frac{2nq\pi}{N}} \quad (2-83)$$

By identifying terms between these functions and the expression (2-79), the double summation in m and n of P_x and P_y functions can be written as a IDFT and remains as [59]

$$P_x(p, q) = K \cdot K' \cdot M \cdot N \cdot IDFT2 [A_x(m, n) \cdot e^{j\phi_x(m, n)}] \quad (2-84)$$

$$P_y(p, q) = K \cdot K' \cdot M \cdot N \cdot IDFT2 [A_y(m, n) \cdot e^{j\phi_y(m, n)}] \quad (2-85)$$

The IDFT2 function can be implemented by a time-efficient Two-dimensional Fast Fourier Transform (FFT) based algorithm [28] [60], so that the radiation pattern is computed in all the space at once.

The Discrete Fourier Transform can be computed in two different ways. If the number of points in the field at the aperture and the radiated field are the same, a spectral function with the same number of points is obtained, which can be the case of large antennas. If the resolution of the radiation pattern is required to be higher, like for small antennas, the mesh size of the field at the aperture has to be increased to a larger surface than the reflectarray. In this case, the points of the mesh that are outside the reflectarray are set equal to zero, see Fig. 2-14. In general, the number of points of the lattice, M and

N_x and N_y are desirable to be a power of 2, in order to get a more efficient FFT2 algorithm. For instance, if the number of elements of the grid is twice the number of elements of the reflectarray, the radiation patterns obtained will have double resolution, see Fig. 2-14.

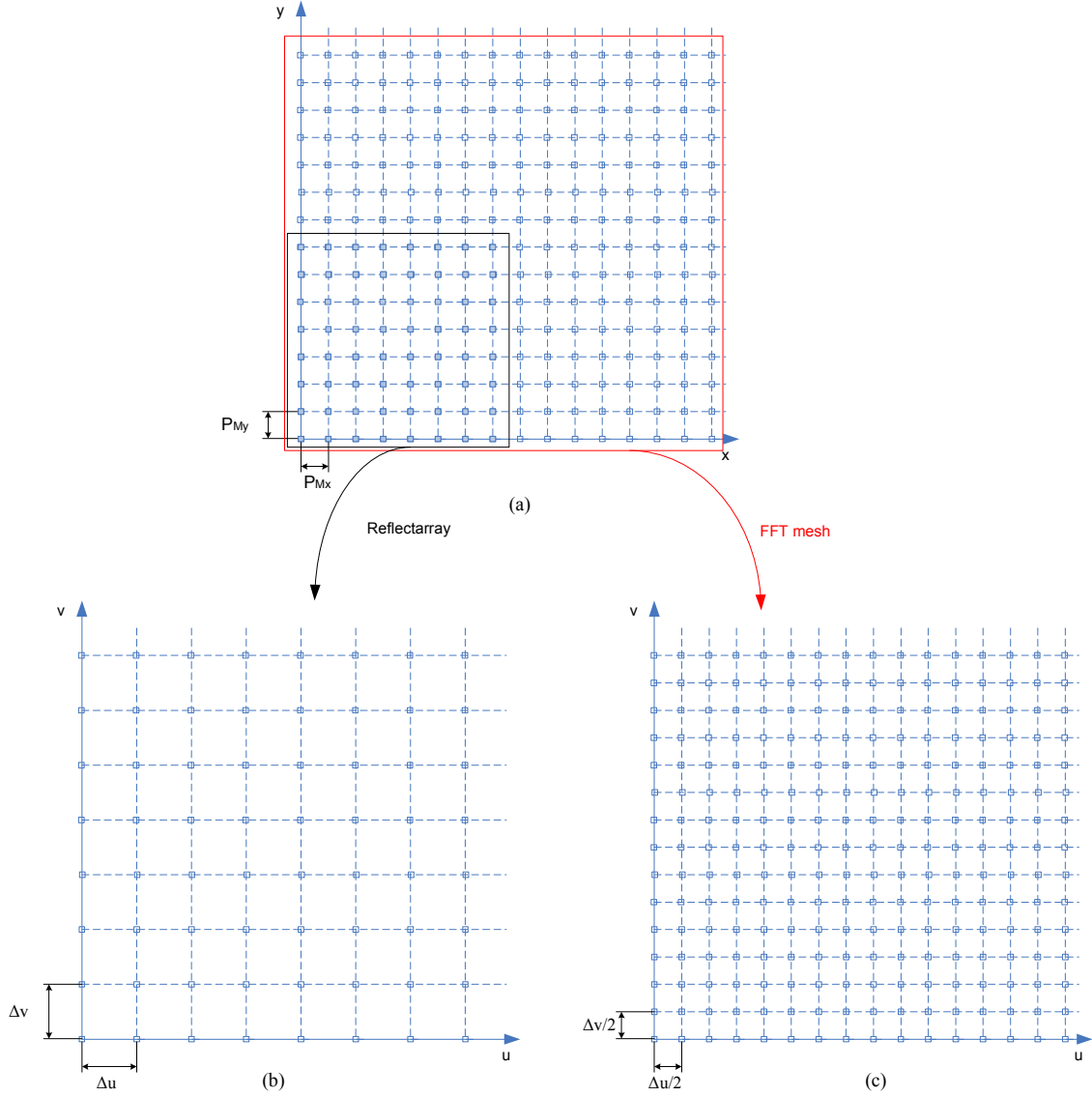


Fig. 2-14. Meshes used for Discrete Fourier Transform, from (x, y) domain to (u, v) domain. Reflectarray mesh (a) and (u, v) mesh considering the reflectarray size (b) or 2x2 times the reflectarray size (c)

Another important point is the angular range where the radiated field is computed. According to the spectral functions defined by equations (2-74) and (2-75) the following conditions are fulfilled,

$$0 \leq u \leq \lambda_0 / p_{Mx} \quad (2-86)$$

$$0 \leq v \leq \lambda_0 / p_{My} \quad (2-87)$$

However, the expressions (2-88) and (2-89) imply that the radiated field is computed only in a quarter of sphere, which corresponds to the hemi space established in origin ($z > 0$). In order to compute the radiation pattern in the entire required hemisphere, the following conditions must be accomplished,

$$-\lambda_0 / 2p_{Mx} \leq u \leq \lambda_0 / 2p_{Mx} \quad (2-88)$$

$$-\lambda_0 / 2p_{My} \leq v \leq \lambda_0 / 2p_{My} \quad (2-89)$$

Therefore, a displacement of p and q indexes is necessary in order to centre the FFT2 mesh and the visible region.

$$p' = p - \frac{M}{2} \Rightarrow u' = u - \frac{\lambda_0}{2p_{Mx}} \quad (2-90)$$

$$q' = q - \frac{N}{2} \Rightarrow v' = v - \frac{\lambda_0}{2p_{My}} \quad (2-91)$$

A displacement in the space domain is equivalent to multiply by an exponential in the transform domain, so the spectral functions are written as,

$$P_x(p, q) = K \cdot K' \cdot M \cdot N \cdot IDFT2 [A_x(m, n) \cdot e^{j\phi_x(m, n)} \cdot e^{-j\pi(m+n)}] \quad (2-92)$$

$$P_y(p, q) = K \cdot K' \cdot M \cdot N \cdot IDFT2 [A_y(m, n) \cdot e^{j\phi_y(m, n)} \cdot e^{-j\pi(m+n)}] \quad (2-93)$$

The last point is to determine the part of the visible hemisphere where the radiated field is being computed and the part of the DFT2 mesh which corresponds to a part of visible hemisphere (real angles). This problem is the intersection of a circle, which corresponds to the hemisphere, and a rectangle, which corresponds to the DFT2 mesh. First, the maximum θ angle of the hemisphere is 90 degrees. Second, the IDFT2 is computed in a rectangular mesh in which the maximum u and v coordinates are determined by (2-94), and depends on the sampling period and the wavelength, the part of the u - v plane which corresponds to the hemisphere is the circle whose equation is $u^2 + v^2 \leq 1$.

$$\begin{aligned} u^2 + v^2 = \sin^2 \theta \\ \theta \leq 90^\circ \end{aligned} \Rightarrow u^2 + v^2 \leq 1 \Rightarrow \begin{cases} u_{\max} = 1 \\ v_{\max} = 1 \end{cases} \quad (2-94)$$

$$u_{\max} = \frac{\lambda_0}{2p_{Mx}} \tag{2-95}$$

$$v_{\max} = \frac{\lambda_0}{2p_{My}}$$

Depending on the different parameters, there are two possibilities:

- 1) If $p_{Mx}, p_{My} < \lambda_0/2$ is fulfilled, the diagram is computed in a lattice larger than the required for the visible region (hemisphere), and so, in points (u,v) that do not have a valid (θ, φ) , see Fig. 2-15(a).
- 2) If $p_{Mx}, p_{My} > \lambda_0/2$ is fulfilled, there are (θ, φ) directions where the diagram is not computed. Also, the IDFT2 can be computed in (u,v) points without (θ, φ) equivalence, see Fig. 2-15(b)

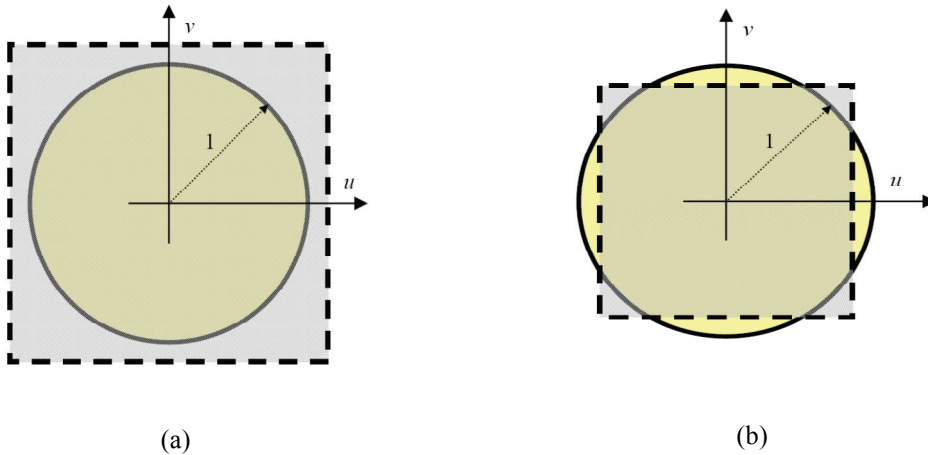


Fig. 2-15. Visible region (yellow hemisphere) and region where the IDFT2 is calculates (grey square).
 (a) $p_{Mx}, p_{My} < \lambda_0/2$, (b) $p_{Mx}, p_{My} > \lambda_0/2$

The case represented in Fig. 2-15 (b) is more frequent than the case shown in Fig. 2-15 (a), since periodicities between $0.5\lambda_0$ and $0.7\lambda_0$ are very common in the design of reflectarray antennas. In this case, the radiation pattern is not computed in all the valid directions (the entire hemisphere with positive z coordinate). A possible solution consists of taking 4 or 9 samples of electric field per reflectarray cell, dividing by 2 or 3 the sampling period of the field on the reflectarray surface both in x and y directions.

2.7 Conclusions

A modular technique based on the Method of Moments for the analysis of dual-reflectarray antennas has been described. Two different configurations are considered in the mentioned methodology. The first one consists on two flat reflectarrays in a dual offset configuration. The second one consists on one flat reflectarray as sub reflector and one curved-shape reflectarray as main-reflector.

A significant improvement is achieved by using the actual incident field on each element obtained from the near field radiated by the horn, which brings the possibility of an accurate analysis of reflectarrays illuminated in the Fresnel zone of the primary feed.

To compute the incident field on the cells of the main reflectarray, the contributions of the field radiated by all the elements in the sub reflectarray are taken into account. At this stage, a simplification has been introduced in the analysis method, considering the same angle of incidence for all the elements in the sub reflectarray. The incidence angle is calculated using the centre of the sub reflectarray as the origin of the incident field. This simplification yields a drastic reduction in the computation times and provides accurate results in practical configurations as presented in this work.

To provide an accurate analysis of the dual offset configuration when the main-reflectarray is located in the near field of the sub reflectarray, the sub reflectarray elements are grouped in small arrays of elements. Then, the field is decomposed in waves radiated by each group with their different incident angles.

Also, the computation of radiation patterns is carried out through the Fast Fourier Transform and its formulation is obtained from the Second Equivalent Principle.

CHAPTER 3

3 Validation of the analysis technique

3.1 Introduction

For the preliminary validation of the analysis technique presented in Chapter 2, two different configurations have been designed to emulate previously reported dual-reflector antennas [19][61], comprising a parabolic main reflector and a reflectarray sub reflector. Since there are no results available in the literature for dual-reflectarray antennas, a preliminary validation of the analysis technique is carried out in this chapter by replacing the main parabolic reflector in the reference antennas by an *equivalent* reflectarray, designed to emulate the behaviour of the main parabolic reflector. The technique used for the design of the main reflectarray has been already validated with several prototypes [2], [39], [62]. The results are presented for two cases, [19], [61], in Ku- and W-bands respectively. For a more accurate validation of the analysis and design techniques proposed in this thesis, a dual-reflectarray antenna is designed, manufactured and tested, as described in a later chapter.

The first reference antenna, is a dual Ku-band reflectarray in which the sub reflectarray introduces a constant phase (it works as a metallic flat reflector) and the main-reflectarray collimates the beam, as a parabolic reflector; then, the results are compared with those obtained in [61], comprising a parabolic main reflector and a reflectarray sub reflector.

The second antenna is an offset dual-reflectarray configuration working in the 94GHz-band where the sub reflectarray produces a beam deflected 5° in azimuth, while the main-reflectarray collimates the beam, showing the simulated results a good agreement with the measurements reported in [19], considered as the reference antenna.

3.2 Ku-band dual reflectarray antenna

Thus, a dual-reflector antenna previously reported [61], comprising a parabolic main reflector and a reflectarray sub reflector, is used as reference for comparison with the results of the proposed dual-reflectarray configuration. The first configuration consists of a dual-offset dual-reflectarray antenna which has been designed to emulate at 11.95 GHz a parabolic antenna with a flat metallic sub reflector, considered as reference antenna. The validation of the analysis technique is carried out by replacing the main parabolic reflector in the reference antenna with an equivalent reflectarray, which has been designed to emulate the behavior of the parabolic reflector using the technique proposed in [2], previously validated [2], [39], [62].

3.2.1 *Antenna definition*

In this first antenna, the primary feed is a horn antenna modeled as a $\cos^q(\theta)$ function, where the q factor has been chosen to have an illumination of -18 dB at the edges of the sub reflectarray. A general scheme of the proposed antenna configuration is shown in Fig. 3-1: a parabolic reflector which is used as reference antenna has been overlapped with the main flat reflectarray. The antenna is made up of three components; a primary feed, a sub reflectarray and a main reflectarray. The two reflectarrays used as sub and main reflectors are considered as planar arrays in rectangular lattices of printed stacked patches of variable size above a ground plane. For the analysis of the dual-reflectarray antenna, four coordinate systems are used: the feed reference system, (x_F, y_F, z_F) , which is centered at the phase-center of the primary feed; the sub- and main reflectarrays reference systems, defined by (x_{SR}, y_{SR}, z_{SR}) and (x_{MR}, y_{MR}, z_{MR}) respectively, whose origins are placed at the centers of the reflectarray surfaces; and the antenna coordinate system (x_A, y_A, z_A) , with the Z_A axis on the direction of the focussed beam, as it is

usually done in reflector antennas. Table 3-1 shows the main parameters that describe the antenna geometry, according to Fig. 3-1.

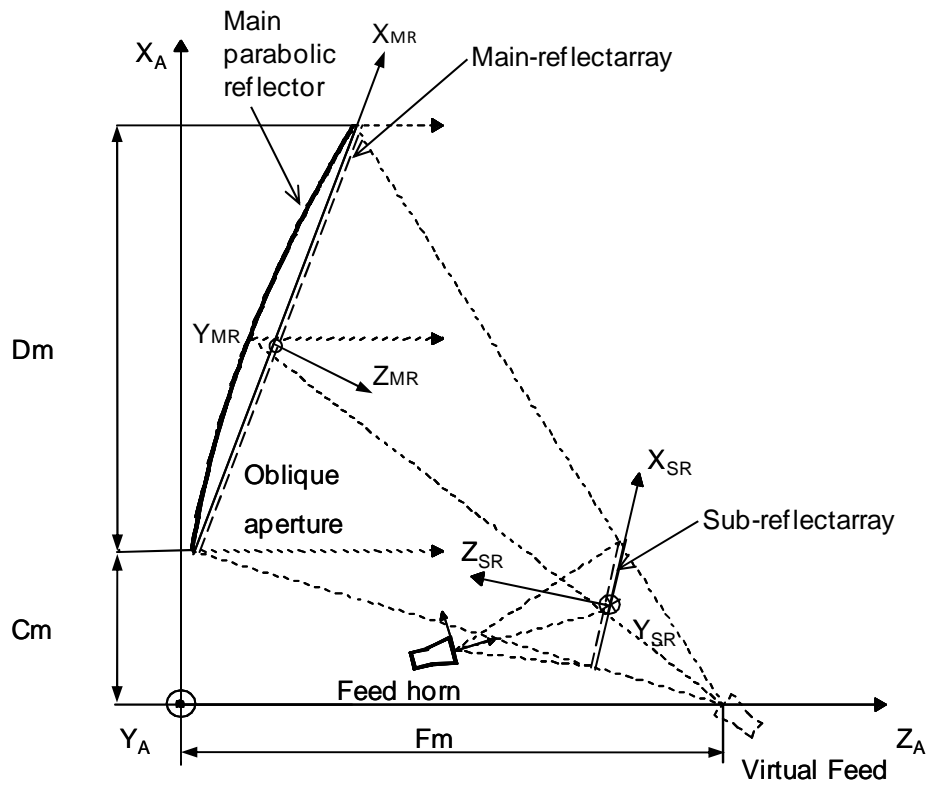


Fig. 3-1. Scheme of a dual-reflectarray structure

The diffraction at the edges is ignored in the analysis tool in both the sub reflectarray and the main reflectarray. In practical cases, particularly for space applications, the illumination at the edges in both the main and the sub reflectarray are lower than -12dB, and therefore, the edge diffraction effect can be negligible in practical cases.

Table 3-1. Main data of the studied geometry

EQUIVALENT PARABOLIC GEOMETRY	
Diameter of the aperture (Dm)	1.5m
Clearance (Cm)	0.2m
Focal distance (Fm)	1.5m
MAIN REFLECTARRAY <i>(data in antenna coordinate system)</i>	
Centre (x _{fm} ,y _{fm} ,z _{fm})	(0.95,0.0,0.244) m
Main reflectarray dimensions	1566 x 1494mm
Matrix of direction cosines <i>(Relationship between Antenna and Main reflectarray Coordinate Systems)</i>	$\begin{bmatrix} 0.953 & 0 & 0.302 \\ 0 & 1 & 0 \\ 0.302 & 0 & 0.953 \end{bmatrix}$
FLAT SUB REFLECTOR <i>(data in antenna coordinate system)</i>	
Centre (x _{fm} ,y _{fm} ,z _{fm})	(0.294, 0, 1.174) mm
Sub reflectarray size	520 × 494 mm
Matrix of direction cosines <i>(Relationship between Antenna and Sub reflectarray Coordinate Systems)</i>	$\begin{bmatrix} 1 & 0 & 0 \\ 0 & -1 & 0 \\ 0 & 0 & -1 \end{bmatrix}$
FEED-HORN <i>(data in sub reflectarray coordinate system)</i>	
Phase centre	(-294, 0, 326)mm
Pointing <i>(on the reflectarray surface)</i>	(-56, 0, 0)mm
Illumination level at the sub reflectarray edges	-18 dB

3.2.2 Design of main reflectarray

The design of the main reflectarray started considering the antenna shown in Fig. 3-1 as reference antenna, which includes a main parabolic reflector of 1.5-m diameter and a focal distance equal to 1.5-m, the first step was to design the main reflectarray to emulate the behaviour of the parabolic reflector. A reflectarray comprising 174 rows × 166 columns is designed by using one layer of variable-sized patches arranged in a periodic lattice with a period smaller than half a wavelength ($a_m=b_m=9$ mm) to increase the bandwidth according to [6], see Fig. 3-2. The reflectarray antenna has been designed for dual-polarization and the radiation patterns of Fig. 3-4 are those corresponding to the X-polarization. The reflectarray is designed to produce the same beamwidth in both planes, so the ratio between both axes is $\cos(\alpha)$, being α the angle formed by the beam and the Z_{MR} axis. Space qualified materials have been used for the design of the main reflectarray, since one potential application is in space antennas. The array of patches are printed on a 0.787 mm-thick prepreg Quartz composite sheet characterized by $\epsilon_r=2.2$

and $\tan(\delta)=0.0009$. Fig. 3-3 shows a very linear phase shift curve and the ohmic losses of the one layer structure which are lower than 0.12 dB.

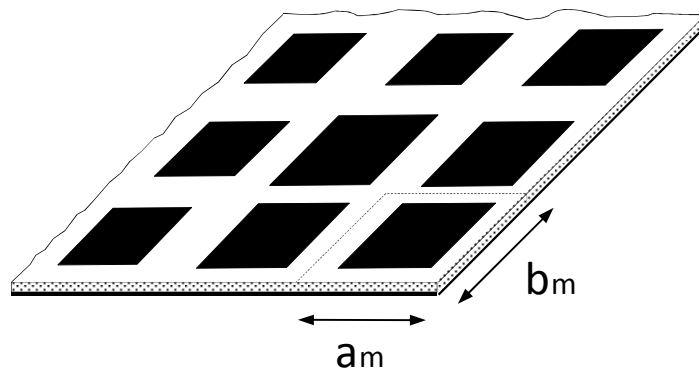


Fig. 3-2. One-layer reflectarray structure

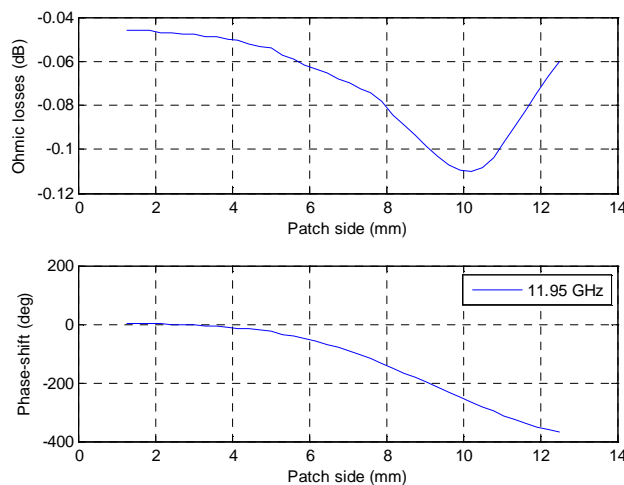


Fig. 3-3. Ohmic losses and phase shift of the patches designed at 11.95 GHz

First, to demonstrate that the designed reflectarray can substitute the main parabolic reflector, it is checked that both the reflectarray and the reflector, without the sub reflector, provide very similar radiation patterns at the design frequency. To evaluate the performance of the designed reflectarray, the radiation patterns of the single offset reflectarray obtained by the analysis technique validated in [2], [39], [62] are compared with those of the parabolic reflector obtained using the GRASP[®] tool from TICRA. The results show virtually identical radiation patterns for the co-polar component at 11.95 GHz and smaller values of cross-polarization for the reflectarray. As a result of the

ohmic losses and small phase errors in the reflectarray, there is a reduction of gain of 0.36 in the reflectarray, compared with the parabolic reflector. The reflectarray has also been analyzed at different frequencies (11.7-12.2 GHz), showing that the gain is reduced in 0.16 dB at 11.7GHz and it is increased in 0.07 dB at 12.2GHz with respect to the reflectarray at central frequency, because of the bandwidth limitation of the reflectarray, although this bandwidth can be improved by using two or three layers of patches as proved in [2] and [39]. Fig. 3-4 (a) and (b) show the elevation and azimuth radiation patterns of the single-reflectarray antenna compared with the reference parabolic reflector. The radiation pattern for the system with a parabolic reflector corresponds to the one obtained in [61].

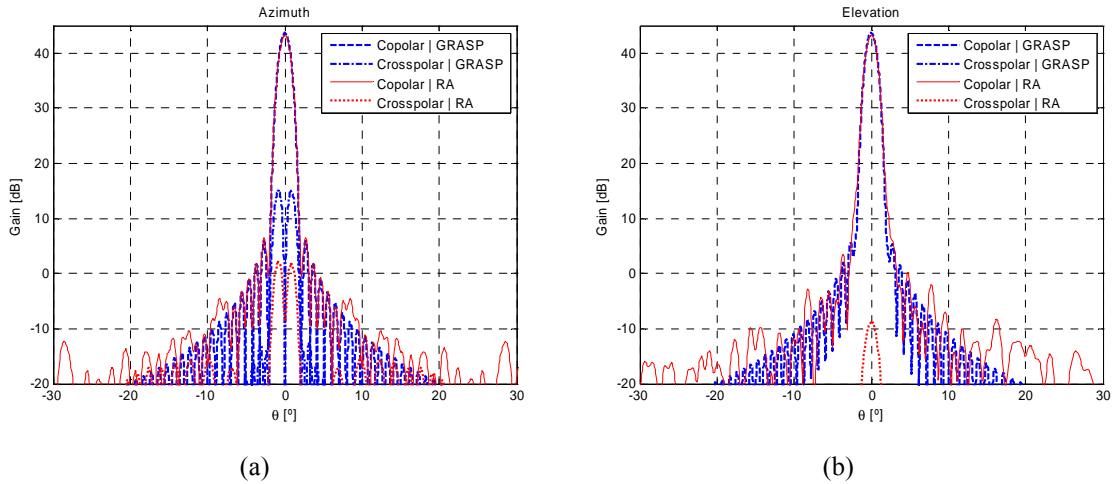


Fig. 3-4. Comparison of the radiation patterns obtained with a reflectarray and with a parabolic reflector (GRASP[®]) in a single offset system at 11.95 GHz (for X-polarization) (a) azimuth and (b) elevation

After demonstrating that the performance of the designed reflectarray and the parabolic reflector are very similar in the prescribed frequency band, the main reflector of the reference antenna [61] is replaced by the reflectarray in the dual-reflector antenna, and the reflectarray sub reflector is designed using two layers of stacked patches over a ground plane. Each array of patches is printed on a 0.125 mm-thick Kapton film ($\epsilon_r=2.98$, $\tan\delta=0.005$) bonded to a 0.125 mm-thick prepreg Quartz fabric layer ($\epsilon_r=2$, $\tan\delta=0.0058$). Then, the two layers and the ground plane are separated by a 3.5 mm-thick Quartz honeycomb ($\epsilon_r=1.046$, $\tan\delta=0.00076$). In this case, the dimensions of the periodic cells are $a_s=b_s=13$ mm, resulting in a reflectarray of 40 rows \times 38 columns. Fig.

3-5 shows the phase curve of the two-layer structure. The sub reflectarray is designed to provide a constant phase-shift of -45° in each cell to emulate a metallic flat surface, so the dimensions of the patches are adjusted slightly to compensate the phase variation produced by the different angles of incidence. Fig. 3-6 points out the masks for the two layers of printed patches for the sub reflectarray.

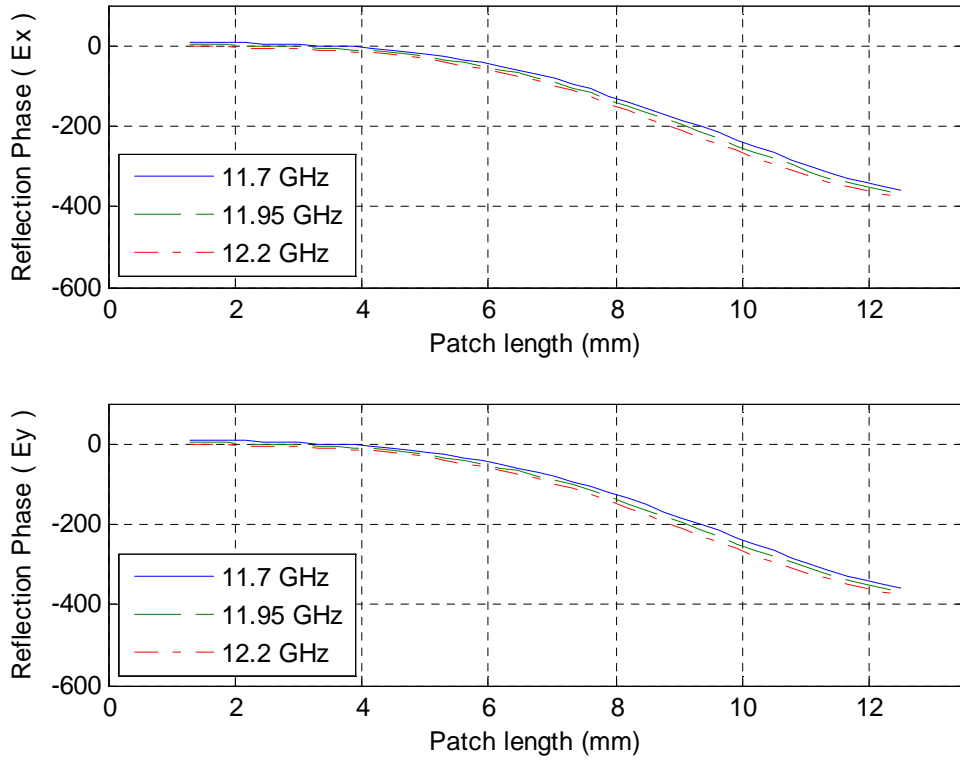
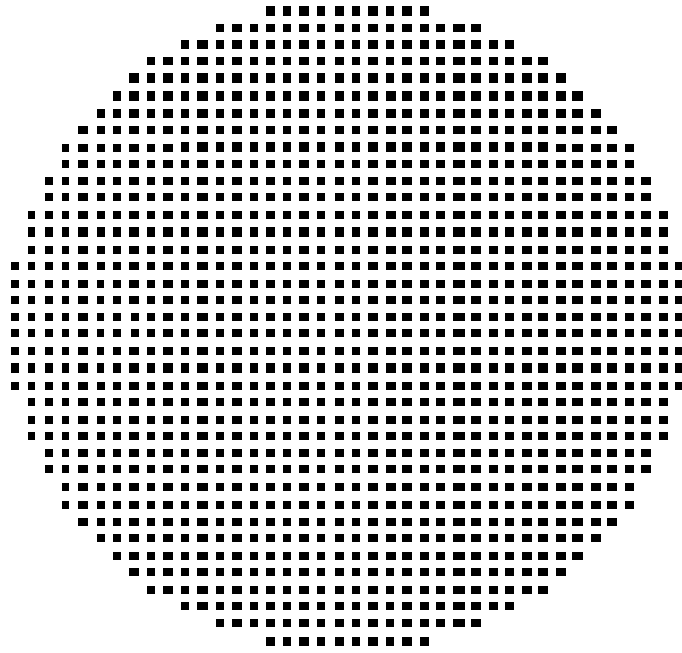
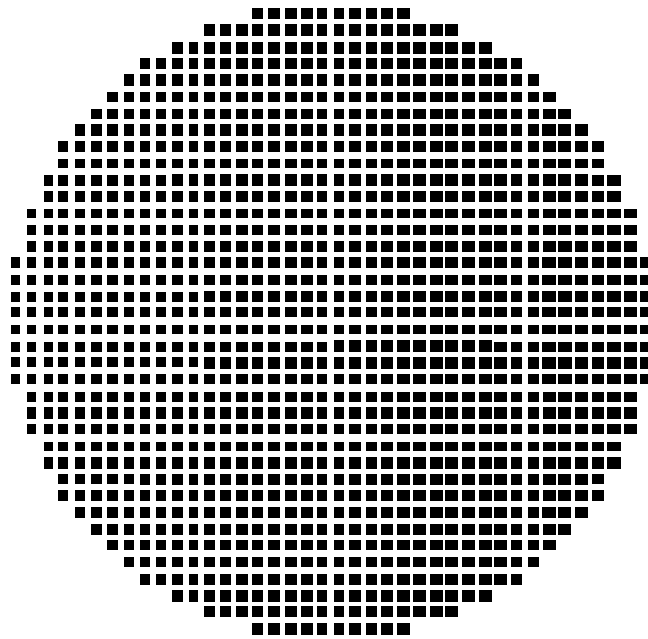


Fig. 3-5. Phase curve for the two layers sub reflectarray



(a)



(b)

Fig. 3-6. Photo-etching masks of the sub reflectarray: (a) top layer, (b) bottom layer

The dual-reflectarray antenna has been analysed using the technique described in chapter 2. The CPU time for the analysis is 22 minutes (Dual Core Processor 2.61 GHz, 1.93 GB de RAM), while the simulation without the approximation stated in Eq. 3-1

takes 42 days and 17 hours in the same PC. It has been checked that the radiation patterns with and without the approximation in equation 3-1, only show slight differences in the side lobes that are 25 dB below the maximum.

$$\mathbf{R}^{m,n/p,q} \approx \mathbf{R}^{m,n} \quad (3-1)$$

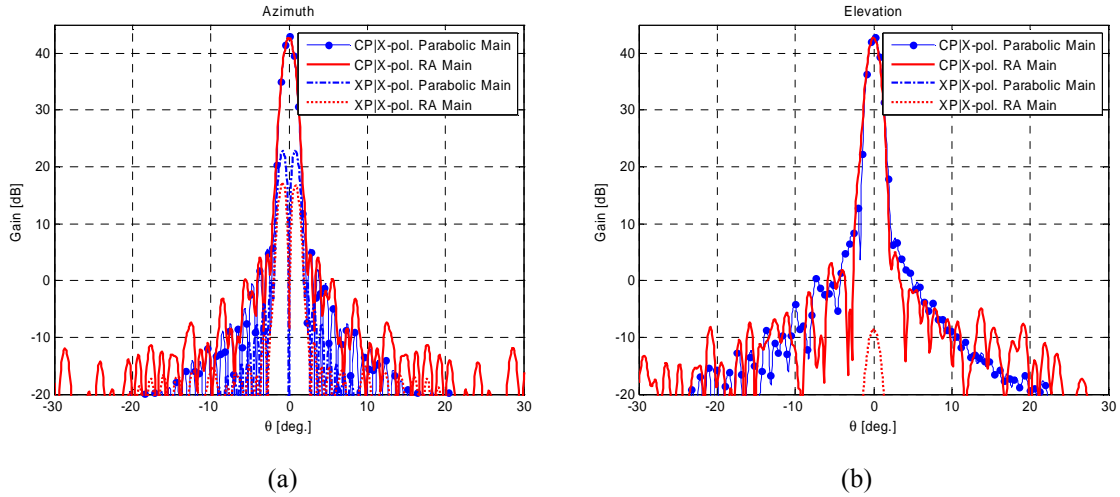
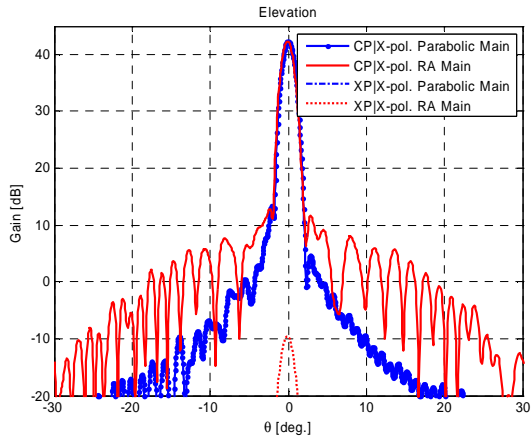
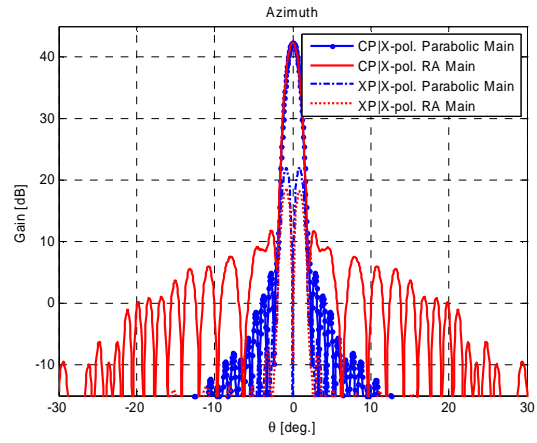


Fig. 3-7. Comparison of the radiation patterns obtained with a main reflectarray and with a parabolic main reflector in a dual reflector system at 11.95 GHz (a) azimuth and (b) elevation

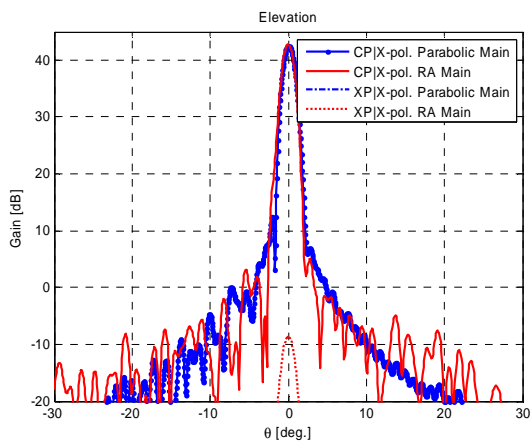
Fig. 3-7 (a) and (b) shows the azimuth and elevation radiation patterns of X-polarization at 11.95 GHz. Only a slight difference in the side lobe zone in the case of using a flat reflectarray with respect to the reference parabolic antenna is observed. The gain calculated for the dual-reflectarray configuration is 42.75 dB, obtaining a difference of 0.38 dB with the reference antenna. Note that this difference is the result of the ohmic losses in the substrate of the main reflectarray and in the sub reflectarray Fig. 3-8 shows the comparison between the radiation patterns and gains in elevation and azimuth for the cases of parabolic reflector and main flat reflectarray at different frequencies. Note that the agreement at extreme frequencies is still very good on the main beam, although the level of side lobes is increased for the dual-reflectarray, because the reflectarray was only design at 11.95 GHz and the true time delay introduced by the reflectarray present some phase-errors at other frequencies, these errors derive in the increase of the side lobe level at the extreme frequencies of the band as can be checked in Fig. 3-8. This problem can be eliminated by an appropriate design of the reflectarray in the prescribed operation frequency, using two or three layers of varying-sized patches, as described in [24].



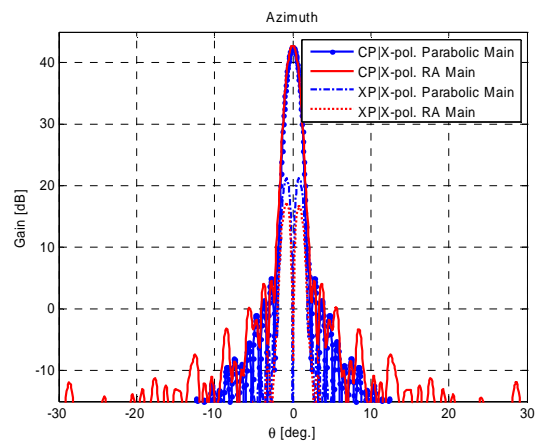
(a)



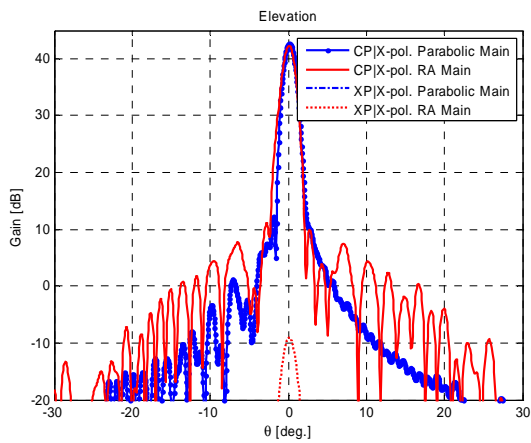
(b)



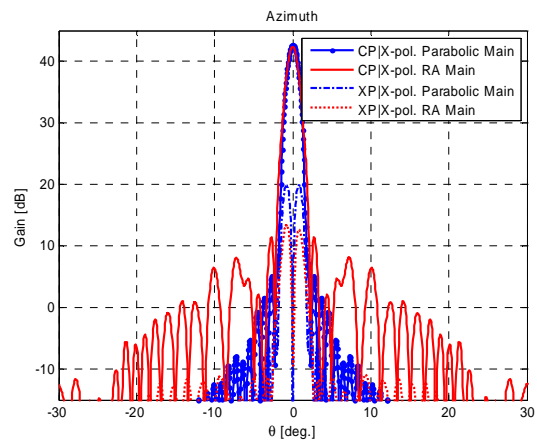
(c)



(d)



(e)



(f)

Fig. 3-8. Comparison of the radiation patterns obtained with a main reflectarray and with a parabolic main reflector in a dual reflector system at 11.7 GHz (a) azimuth and (b) elevation, 11.95 GHz (c) azimuth and (d) elevation, 12.2 GHz (e) azimuth and (f) elevation GHz

Table 3-2. Maximum gain of the system when a parabolic reflector or a main reflectarray is used as main (dB)

f(GHz)	Parabolic reflector	Main flat reflectarray	Difference
11.7	42.93	42.33	0.60
11.95	43.13	42.75	0.38
12.2	43.30	42.25	1.05

The sensitivity of the proposed dual-reflectarray antenna to manufacturing tolerances has been evaluated by computing the radiation patterns considering errors in the patch dimensions for both reflectarrays as well as in the inclination angle of the sub reflectarray. Fig. 3-9 shows a comparison of the radiation patterns obtained for the dual reflectarray system at 11.95 GHz, for four cases: a first case using nominal values, a second case including a deviation of 2 degrees in the sub reflectarray inclination, a third case including a systematic error of $\pm 100\mu\text{m}$ in the printed patches, and the fourth case including a random error of $\pm 100\mu\text{m}$ in the patches for both reflectarrays. These results show that the errors in the patch dimensions produce a slight increase in the side lobes, which is more noticeable when the errors are systematic, while the error in the sub reflectarray pointing produces a small beam deviation. Note that for conventional manufacturing tolerances (less than $50\mu\text{m}$ in the photo-etched patches) the effect on the radiation patterns is practically negligible.

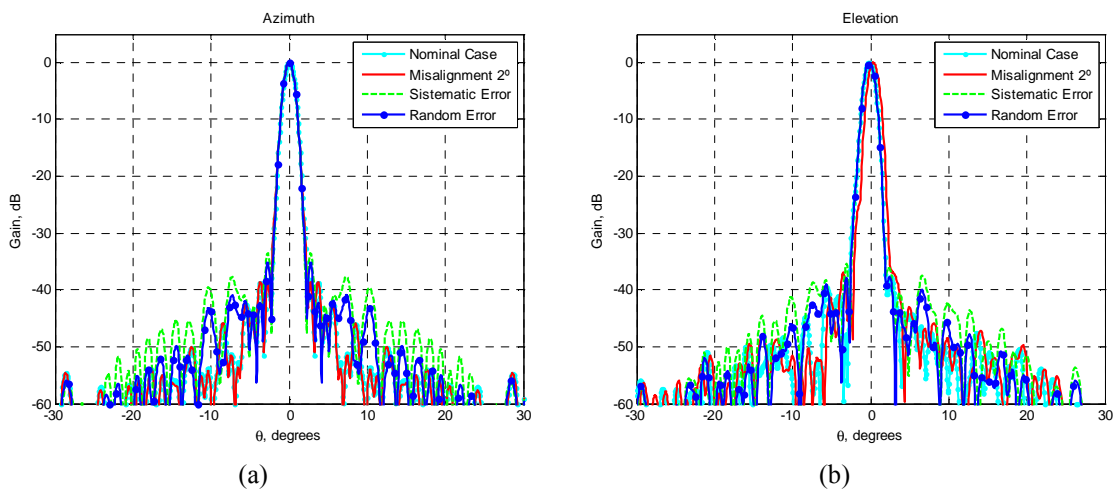


Fig. 3-9. Radiation patterns of the dual-reflectarray antenna at 11.95 GHz in azimuth (a) and elevation (b) planes for a sensitivity analysis.

3.2.3 *Conclusions*

A previously reported dual-reflector antenna, which comprises a main parabolic reflector and a reflectarray as sub reflector, has been considered as reference antenna for comparison in this configuration. The sub reflectarray introduces a constant phase (it emulates a metallic flat reflector) and the main-reflectorarray produces a collimated beam, as a parabolic reflector. The results are compared with those obtained for the reference antenna [61], only a slight difference in the side lobe area can be appreciated. The gain calculated for the dual-reflectorarray configuration is 0.38 dB lower than the one obtained for the reference antenna, due to the ohmic losses in both reflectarrays.

These results show that dual-reflectorarray antennas can provide similar performance in terms of antenna gain and efficiency than conventional dual reflector antennas. The main reflector can be designed for a bandwidth larger than 10% using stacked patches as shown in [2] and [39], The dual-reflectorarray configuration can be designed to produce other functioning such as beam shaping, beam scan, or a reduction in cross-polarization.

3.3 94 GHz dual-reflector antenna

The second configuration corresponds to a dual-reflector antenna comprising a 120-mm diameter parabolic main reflector and a 28-mm diameter reflectarray sub reflector that produces a fix beam deflection in azimuth at 94 GHz [19]. The parabolic reflector generates a focused beam in the boresight direction (Z_a) with a half power beamwidth of 2.4° and a peak gain of 38.7 dBi at 94 GHz when a flat metal sub reflector is used. It produces a beam deflection of 5 degrees when the metal sub reflector is replaced by a passive reflectarray. As in the previous case, the main parabolic reflector is replaced by a flat reflectarray, which has been designed to produce the same radiation patters as the parabolic reflector.

3.3.1 Antenna definition

To produce the beam deviation, the sub reflectarray introduces a progressive phase shift, while the main reflectarray focuses the beam emulating the parabolic reflector. The main reflectarray is designed using two layers of variable-sized patches over a ground plane in order to improve the bandwidth [2]. Each array of patches is printed on a 115 μm -thick metal backed SiO_2 wafer ($\epsilon_r=3.78$, $\tan\delta=0.008$). The dimensions for all periodic cells are $a_m=b_m=1$ mm, resulting a reflectarray of 140 rows \times 120 columns.

The sub reflectarray has been designed using a single layer of patches closely disposed in periodic square lattice ($a_s=1$ mm. and $b_s=0.95$) in order to increase the bandwidth according to [6] , resulting in a reflectarray of 50 rows \times 52 columns. The patches are printed on a metal backed SiO_2 wafer of 115 μm thickness with a ($\epsilon_r=3.78$, $\tan\delta=0.008$). Main data of the geometry are summarized in Table 3-3.

Table 3-3. Main data of the studied geometry	
EQUIVALENT PARABOLIC GEOMETRY	
Diameter of the aperture (Dm)	120mm
Clearance (Cm)	35mm
Focal distance (Fm)	80mm
MAIN REFLECTARRAY <i>(data in antenna coordinate system)</i>	
Centre (x _{fm} ,y _{fm} ,z _{fm})	(95,0,0,39.4) mm
Main reflectarray dimensions	140 x 120mm
Matrix of direction cosines <i>(Relationship between Antenna and Main reflectarray Coordinate Systems)</i>	$\begin{bmatrix} 0.859 & 0 & 0.51 \\ 0 & 1 & 0 \\ -0.51 & 0 & 0.859 \end{bmatrix}$
FLAT SUB REFLECTOR <i>(data in antenna coordinate system)</i>	
Centre (x _{fm} ,y _{fm} ,z _{fm})	(25.2, 0, 68.4) mm
Sub reflectarray size	50 \times 47 mm
Matrix of direction cosines <i>(Relationship between Antenna and Sub reflectarray Coordinate Systems)</i>	$\begin{bmatrix} 0.891 & 0 & 0.454 \\ 0 & -1 & 0 \\ -0.454 & 0 & -0.891 \end{bmatrix}$
FEED-HORN <i>(data in sub reflectarray coordinate system)</i>	
Phase centre	(-17.2, 0, 21.75)mm
Pointing <i>(on the reflectarray surface)</i>	(-2.32, 0, 0)mm

3.3.2 *Design of sub and main reflectarrays*

The main-reflectarray emulates the behaviour of the parabolic reflector in the reference antenna and the sub reflectarray deflects the beam 5°. The required phase-shift for the main and the sub reflectarrays are presented in Fig. 3-10. The masks corresponding to both reflectarray surfaces are shown in Fig. 3-11 and Fig. 3-12.

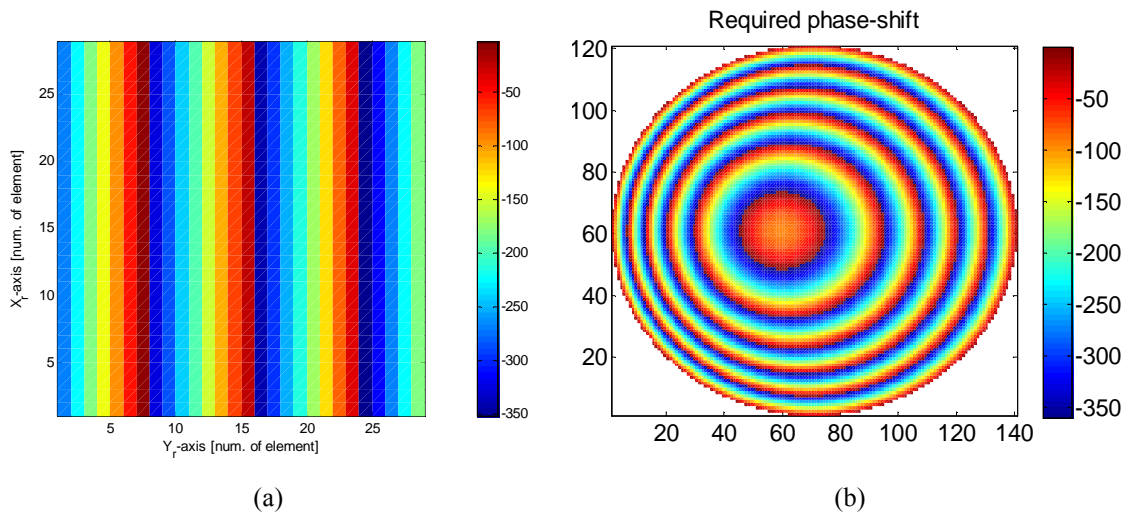


Fig. 3-10. Required phase shift for the (a) sub reflectarray and for the (b) main-reflectarray

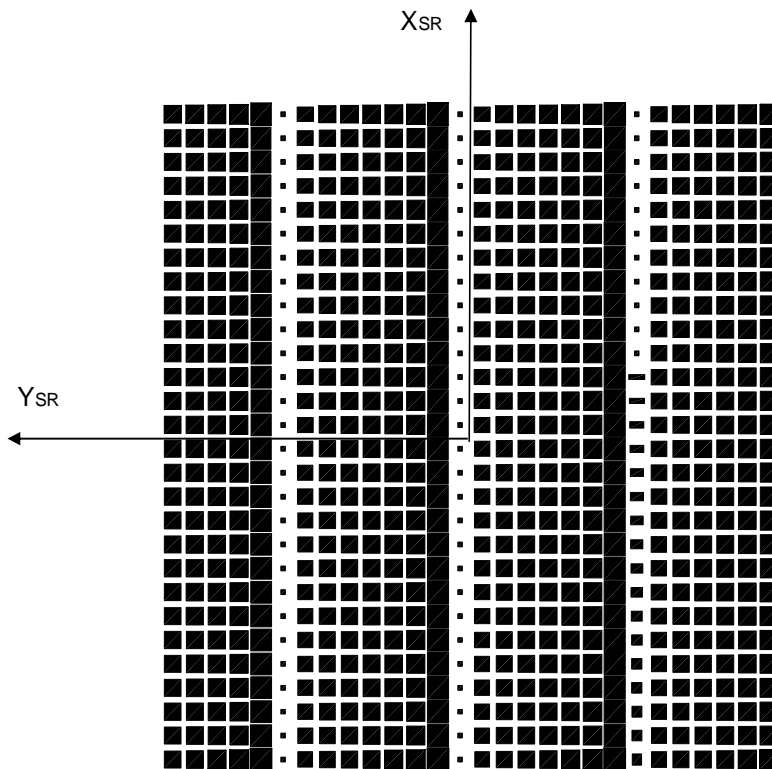
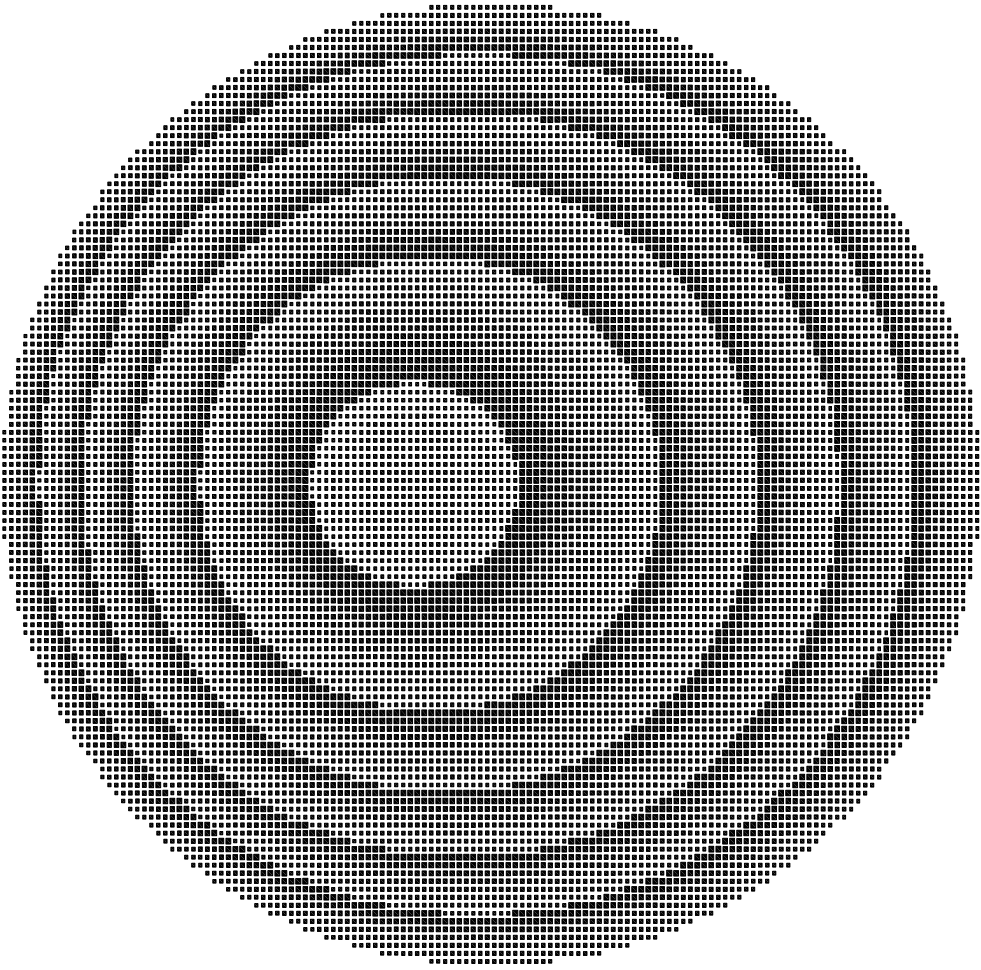
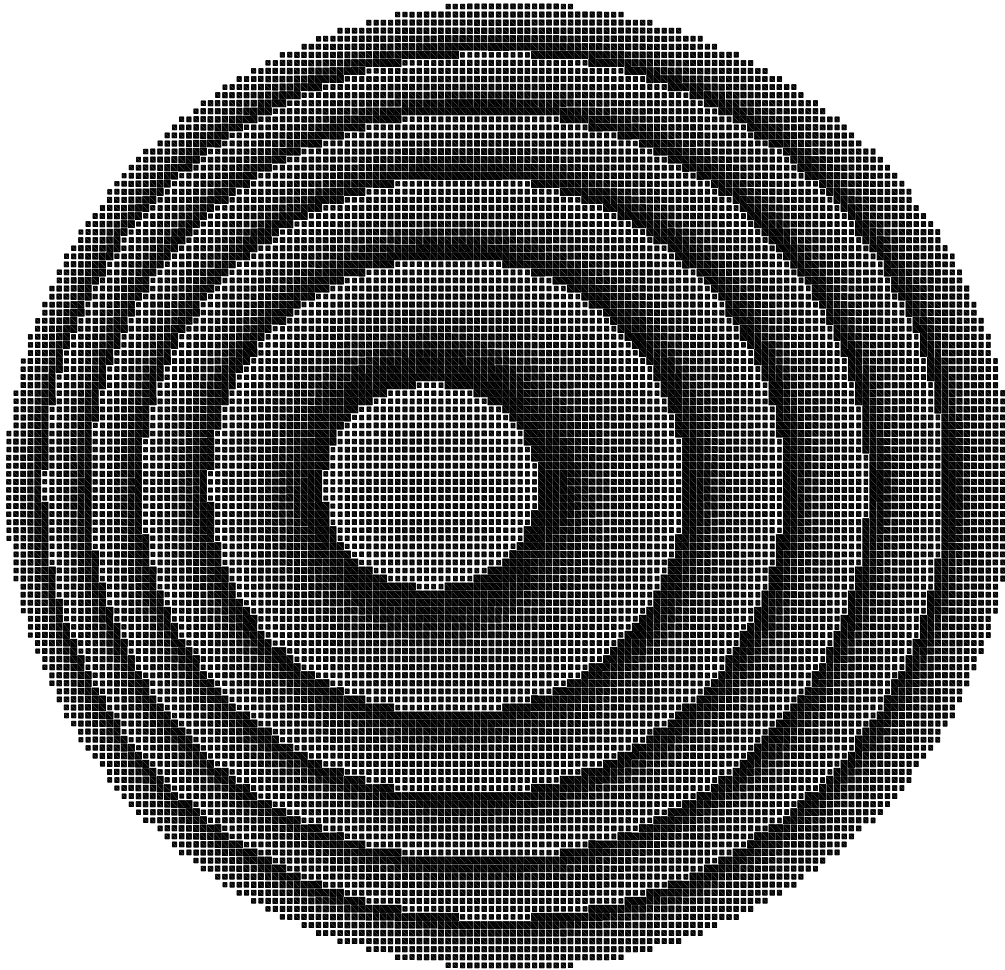


Fig. 3-11. Photo-etching mask for the sub reflectarray



(a)



(b)

Fig. 3-12. Photo-etching masks for the main-reflectarray (a) bottom layer (closer to the ground layer) (b) top layer

3.3.3 *Antenna analysis*

The antenna has been analyzed through the technique discussed in chapter 2, but assuming an ideal far field model based on $\cos^4\theta$ function for the primary feed. Fig. 3-13 shows the comparison of simulated radiation patterns for the centre and the deflected beam in two cases: when a parabolic main reflector is used [19] and when a flat reflectarray is used as main reflector. The results presented in Fig. 3-13 show a general good agreement in the co-polar radiation patterns, particularly in the main lobe zone. The level of the cross-polarization is about 5dB lower for the case of DRA,

because the cross-polarisation in general is lower for a flat reflectarray than for a single-offset reflector.

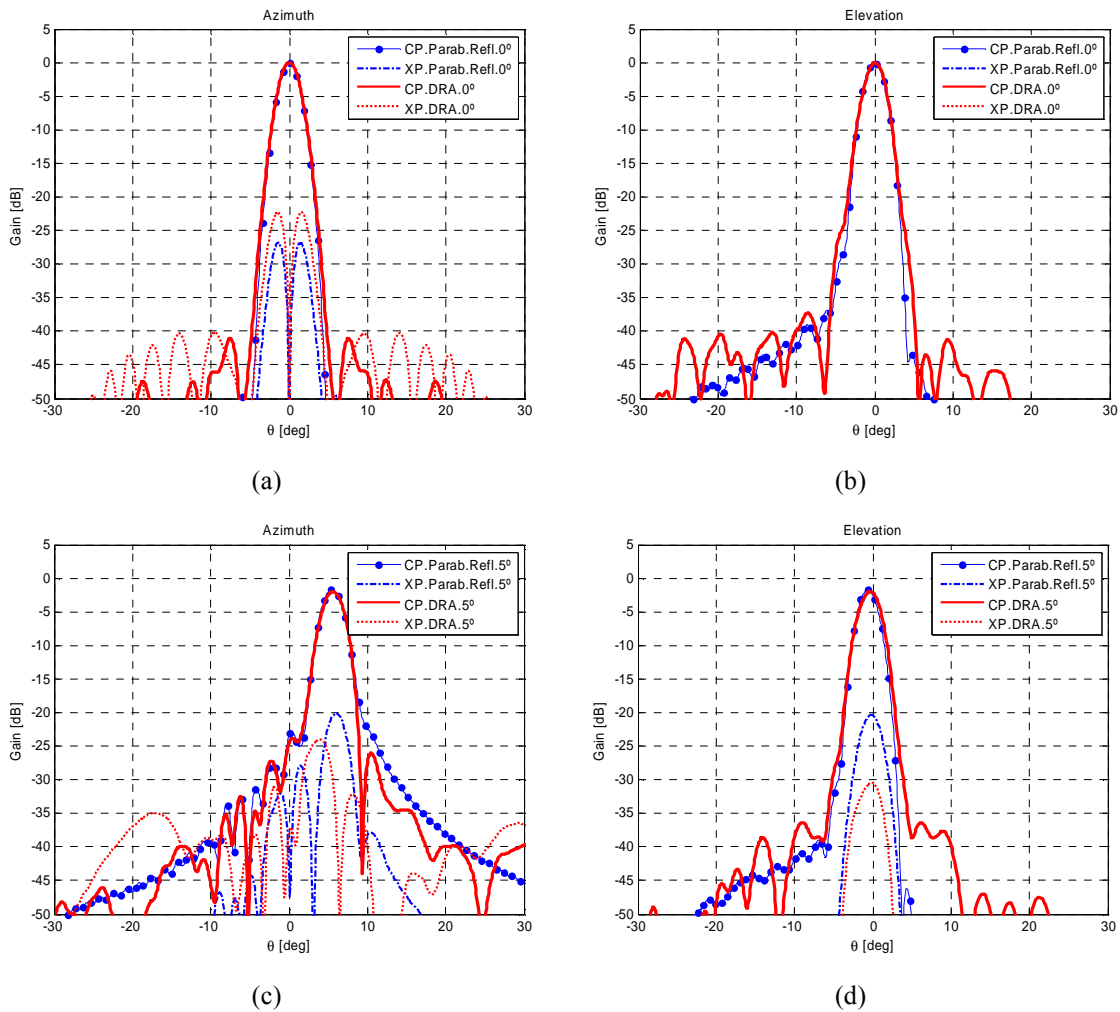


Fig. 3-13. Simulated radiation patterns of the dual reflector antenna with reflectarray sub reflector and main parabolic reflector (Sim.Parab.Refl.) or main reflectarray (Sim.DRA) at 94 GHz (a) azimuth for the centered beam, (b) elevation. for the centered beam, (c) azimuth for the tilted beam and (d) elevation for the tilted beam.

The bandwidth performance of the DRA is also evaluated. Fig. 3-14 shows the radiation pattern of the DRA in a 3 % bandwidth dual reflector antenna, in which both surfaces are reflectarrays. As it can be seen, the radiation patterns are very similar for the three frequencies analyzed: 93 GHz, 95 GHz and 96 GHz, showing a small increase in the side lobes for the higher frequency [19].

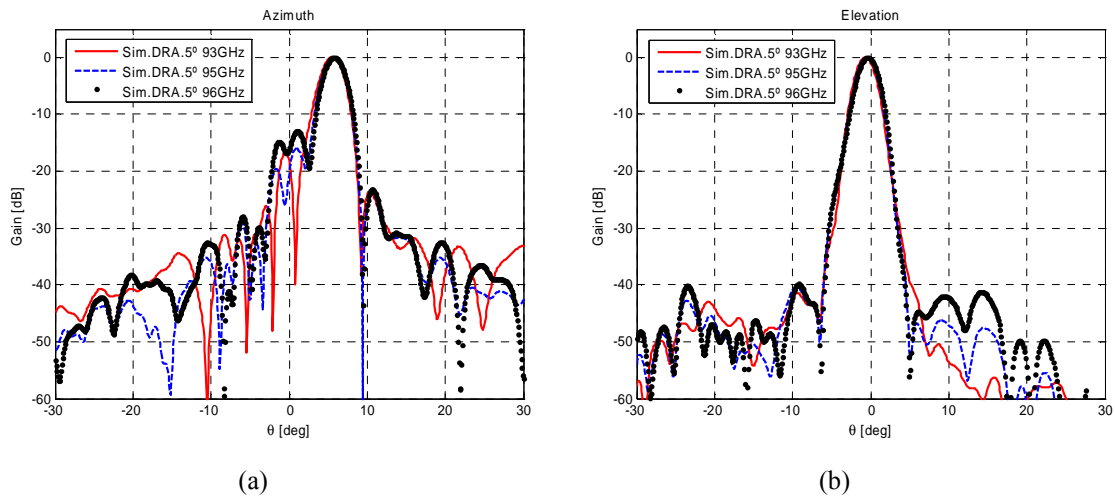


Fig. 3-14 Radiation patterns of the dual reflector antenna with reflectarray sub reflector and main reflectarray (simulations DRA) at 93 GHz, 95 GHz and 96 GHz (a) Azimuth (b) Elevation.

The reference antenna made of a parabolic main reflector and a reflectarray sub reflector has been manufactured at the Institute of Electronics, Communications and Information Technology of Queen’s University in Belfast [19]. Fig. 3-15 shows a picture of the manufactured prototype. The antenna has been measured in the anechoic chamber at Queen’s University, and the results are compared with the designed dual-reflectarray antenna.

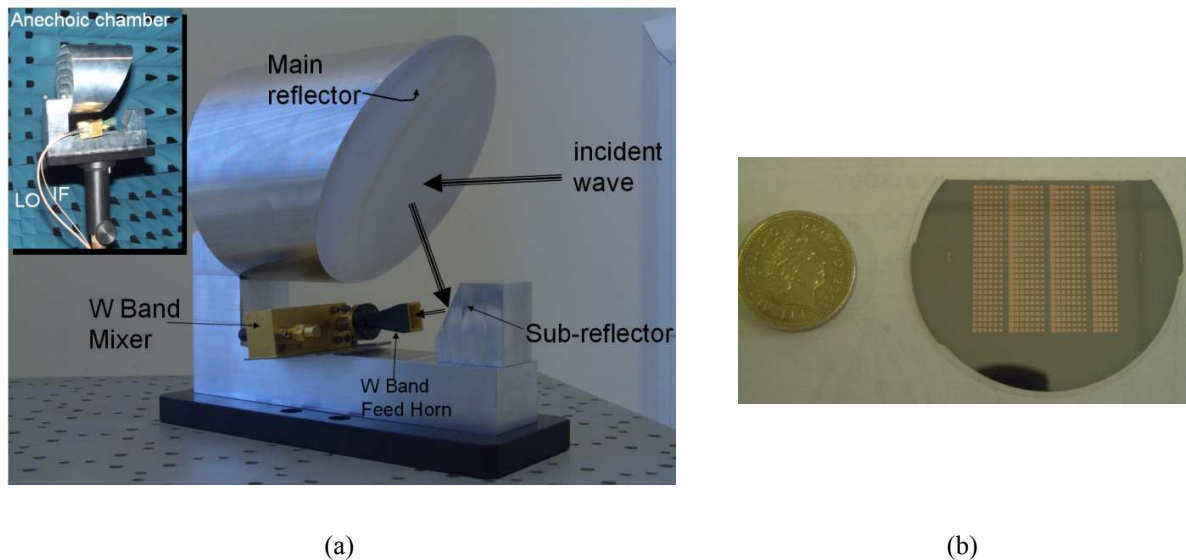


Fig. 3-15. 94-GHz reference dual-reflector antenna. (a) Photograph of the breadboard and (b) reflectarray sub reflector printed on a 2 inch diameter quartz wafer, courtesy of Queen’s University Belfast

Fig. 3-16 shows the comparison of the normalized radiation patterns obtained from measurements of the dual reflector antenna and from the simulations of the dual reflectarray system. Since the sub reflectarray elements are not illuminated in the far

field region of the feed horn, the far field model of the feed horn used in the simulation produces slight discrepancies, particularly for the tilted beam. To overcome this problem, a near field model of the feed is introduced in the simulations [49], and the new simulations are shown in Fig. 3-16. According to these plots, the simulation results successfully match the measurements.

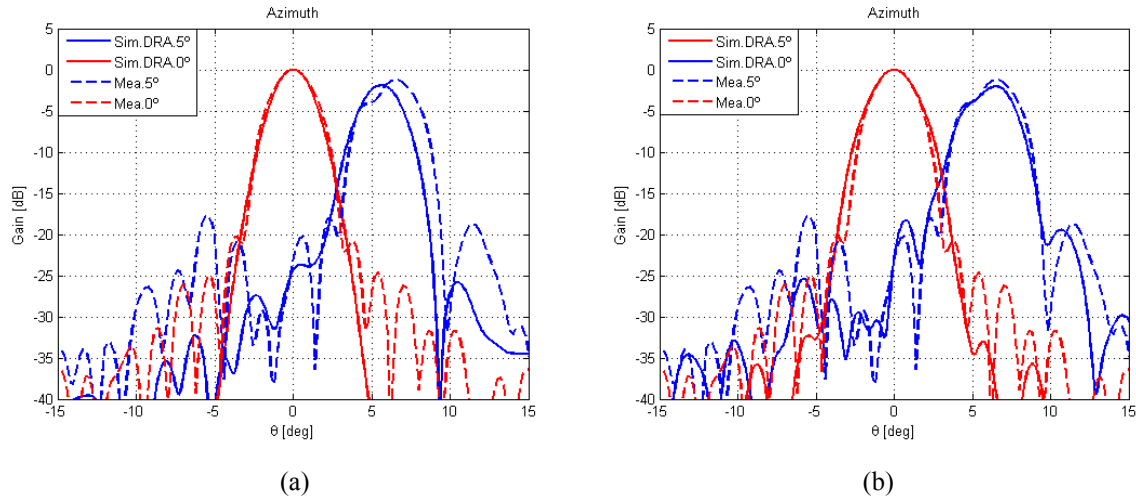


Fig. 3-16. Radiation patterns of the dual reflector antenna with reflectarray sub reflector and main parabolic reflector (measurements) or main reflectarray (simulations DRA) at 94 GHz. (a) A far field model of the feed is used in the simulation. (b) A near field model is used in the simulation.

A sensitivity study has also been carried out for the tilted beam, which is the most critical to tolerance errors. The study includes the same four cases as in the Ku-band antenna, but considering $+5\mu\text{m}$, for the systematic and random errors in the printed patches for both reflectarrays, which is higher than the manufacturing tolerances obtained in [19] ($\pm 2\mu\text{m}$). The resulting radiation patterns show slight variations in the side-lobes and in the beam direction when the sub reflectarray is tilted 2 degrees, as shown in Fig. 3-17. These results confirm that manufacturing tolerances do not produce a significant distortion of the radiation patterns, even in the W-band.

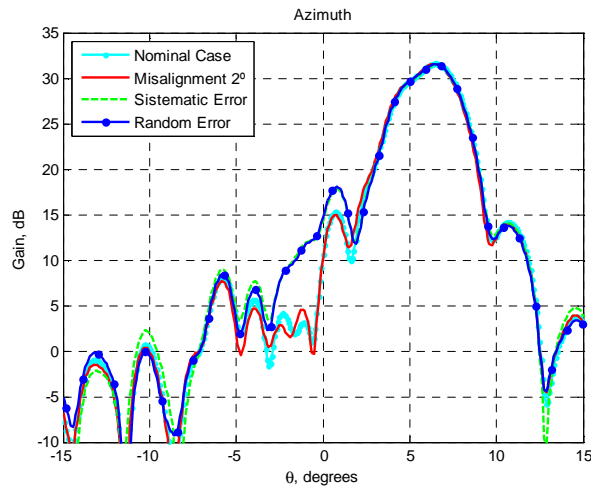


Fig. 3-17. Radiation patterns of the dual-reflector antenna at 94 GHz in azimuth (a) and elevation (b) planes for a sensitivity analysis.

3.4 Conclusions

Two dual-reflector antennas previously reported in the literature, which comprise a main parabolic reflector and a reflectarray as sub reflector, have been considered as reference antennas for comparison. The proposed analysis method for dual-reflector antennas has been applied to demonstrate that the antenna performance in terms of gain, efficiency and radiation patterns are practically the same when the main reflector in the reference antennas is substituted by a flat reflectarray. In the case of the dual reflectarray antenna at 94 GHz, where the main reflectarray focuses the beam and a sub reflectarray introduces a progressive phase to tilt the beam 5° , it was shown that the near field radiated by the horn must be included in the analysis to provide accurate results. The results presented show the feasibility of dual-reflector antennas, which can be designed to improve the antenna performance by properly adjusting the phase on both reflectarray surfaces.

CHAPTER 4

4 Design manufacture and test of dual-reflectarray demonstrator

4.1 Introduction

After the preliminary validation of the proposed analysis technique, a very challenging dual-reflectarray antenna demonstrator has been designed, manufactured and tested for a more rigorous validation of the analysis technique presented in chapter 2. In the antenna configuration presented in this chapter, the feed, the sub-reflectarray and the main-reflectarray are very close one to each other, so that the conventional approximations of far field are not suitable for the analysis of the present antenna. The purpose of choosing this geometry is mainly to be used as benchmarking for the proposed analysis tool in very stringent conditions. Some aspects of the proposed analysis technique that allow improving the accuracy of the analysis are also discussed in this chapter.

The selected antenna optics is based on a dual-offset compact-range Cassegrain reflector. The two reflectarrays are defined to emulate the reflectors of the equivalent antenna, which produce a focussed beam directed to 28° , fulfilling Mizuguchi conditions [47], [63].

Two designs for the same geometry have been carried out. The first one consists of a two-layer sub reflectarray and a single-layer main-reflectarray, being the antenna designed to produce low levels of crosspolarization. In the second case, the crosspolar component of the complete antenna is further reduced with respect to the previous case by designing a main-reflectarray of two layers. In the last section of this chapter a

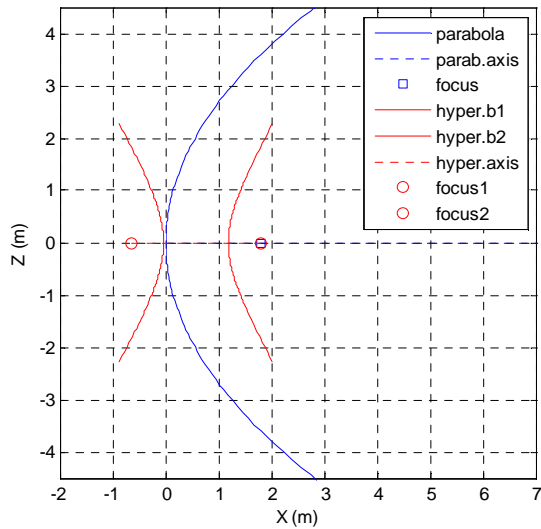
contoured-beam antenna implemented with two reflectarrays for DBS application is proposed using similar optics.

4.2 Design, manufacture and test of a dual-reflectarray demonstrator

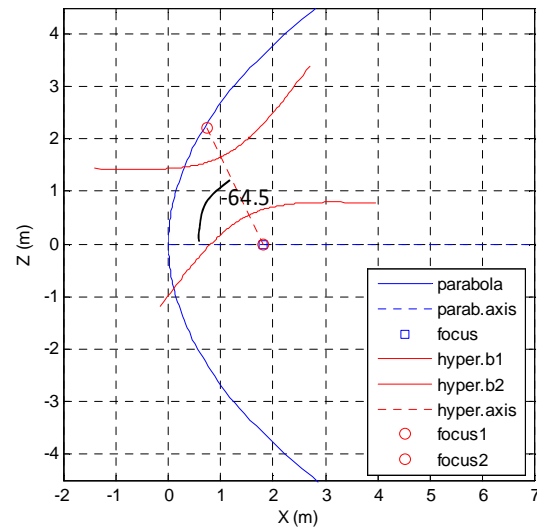
In the first design, the dual reflectarray antenna produces a pencil beam in the 14 GHz band. The geometry derives from a dual offset Cassegrain reflector in compact-range configuration. The main goal of this design consists on the practical validation of the analysis technique proposed in chapter two as well as the reduction of the crosspolar component introduced by the entire antenna (geometry and patches of the two reflectarrays).

4.2.1 Equivalent parabolic system

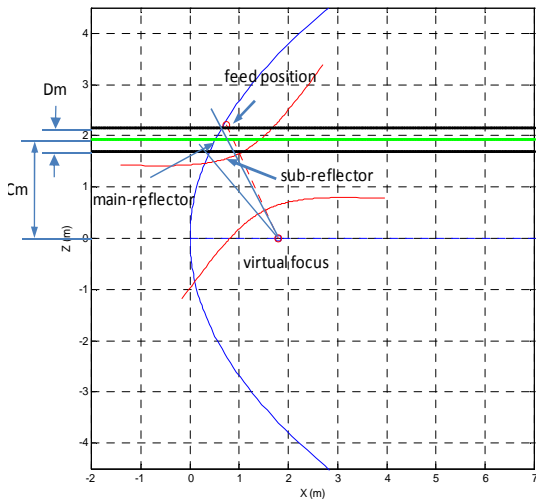
As starting point of the design, the optics of a parabolic system is defined. The antenna fulfils Mizuguchi conditions to ensure a low level of cross-polarisation [63]. The entire antenna geometry has been defined using GRASP[®] tool from Tiera[53]. The system is made up of a main parabolic reflector and a hyperbolic sub reflector. The focal distance of the paraboloid (F_m) is 1.8 m and the diameter of the antenna aperture (D_m) is 0.45m, with a clearance (C_m) of 1.7 m. The sub reflector is a hyperbolic with eccentricity -2 and an aperture diameter of 0.38 m. The pointing of the feed is established to minimize the spillover (equal illumination level at the edges), defining an illumination of -12 dB for an angle of 15.94° for the sub reflector. In the case of the main reflector, the illumination at edges is -15 dB. The angle between the axis of the main and sub reflectors is -64.5° . The process to define the antenna optics is summarized in Fig. 4-1.



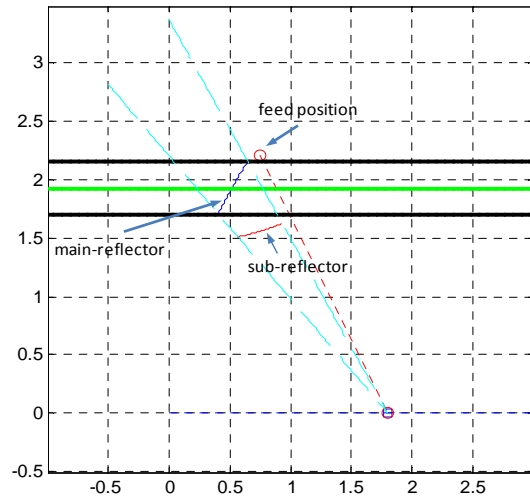
(a)



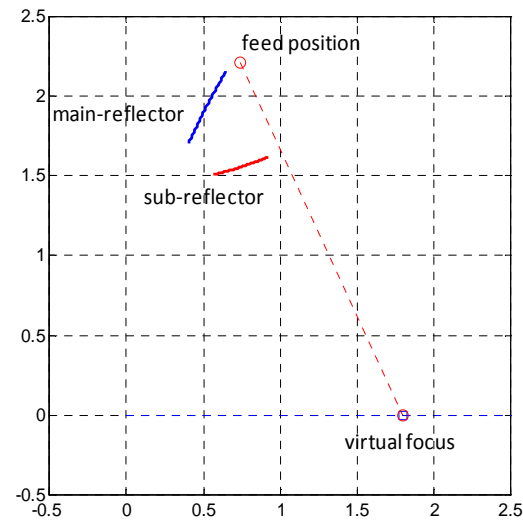
(b)



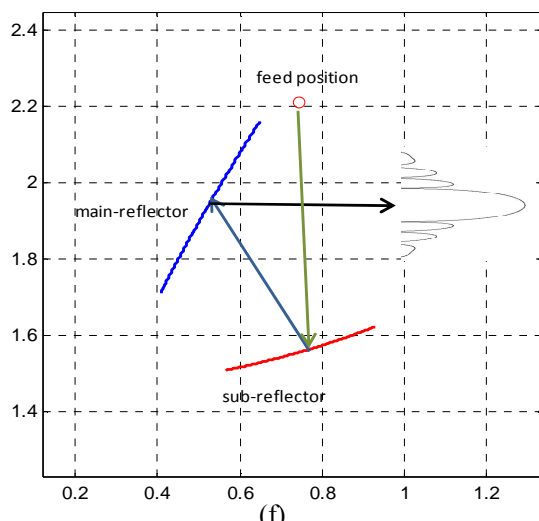
(c)



(d)



(e)



(f)

Fig. 4-1. Dual offset definition step by step. (a)Parabola and hyperbola definition (b) Inclination between the axis of the parabola and the axis of the hyperbola (c) Identification of the reflectors (d) Segmentation of the dual-offset system (e) Dual-offset configuration (f)Dual-offset antenna pointing to boresight

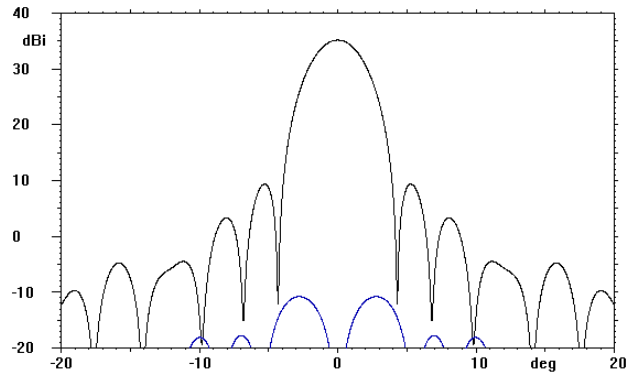


Fig. 4-2. Radiator pattern of the dual offset parabolic antenna defined in GRASP[®] tool.

4.2.2 Antenna optics

The proposed antenna configuration is shown in Fig. 4-3. It is derived from a compact range dual-reflector antenna that fulfils Mizuguchi conditions to achieve a low level of cross-polarization. Fig. 4-4 shows the dual-reflectarray antenna in the coordinate system of the equivalent parabolic dual offset antenna. This configuration, defined in the previous section, produces a focussed beam in the direction $\theta=28.24^\circ$ and $\varphi=0^\circ$ assuming the main reflectarray coordinate system (broadside direction in the antenna coordinate system). The main geometrical parameters are given in Table 4-1.

The antenna is made up of three components: a primary feed and two reflectarrays composed of a circular sub reflectarray (SRA) and an elliptic main reflectarray (MRA). Both reflectarrays are considered as planar arrays in rectangular lattices made of printed stacked patches of variable size above a ground plane. The phase-shift distribution required on each reflectarray is defined to emulate the equivalent reflectors, as it will be explained in section 4.2.5.

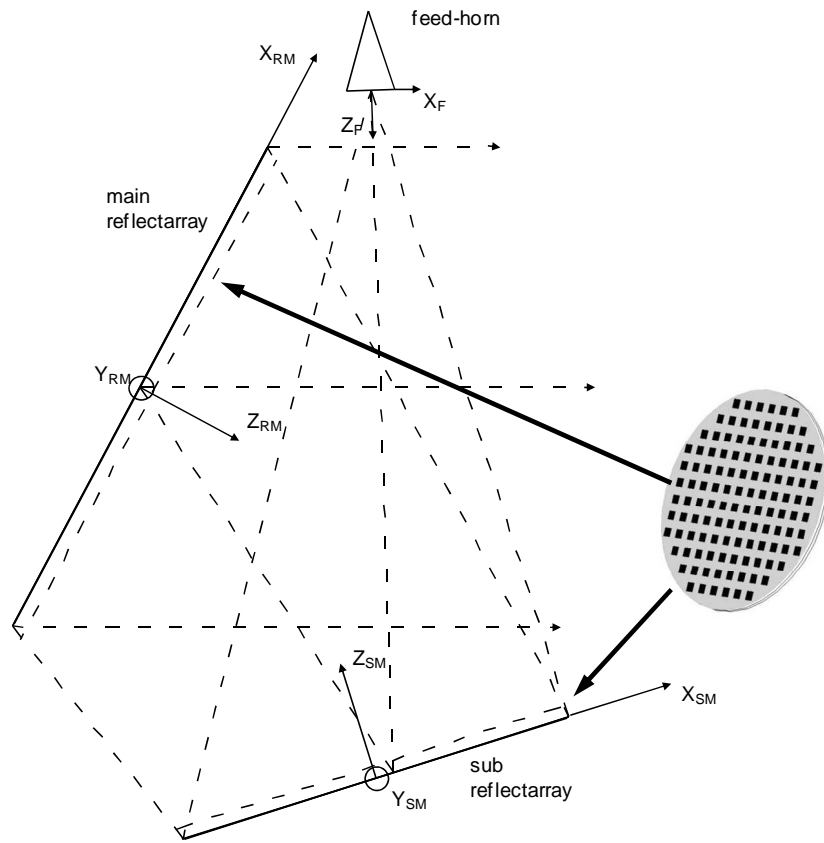


Fig. 4-3. Top view of the antenna configuration.

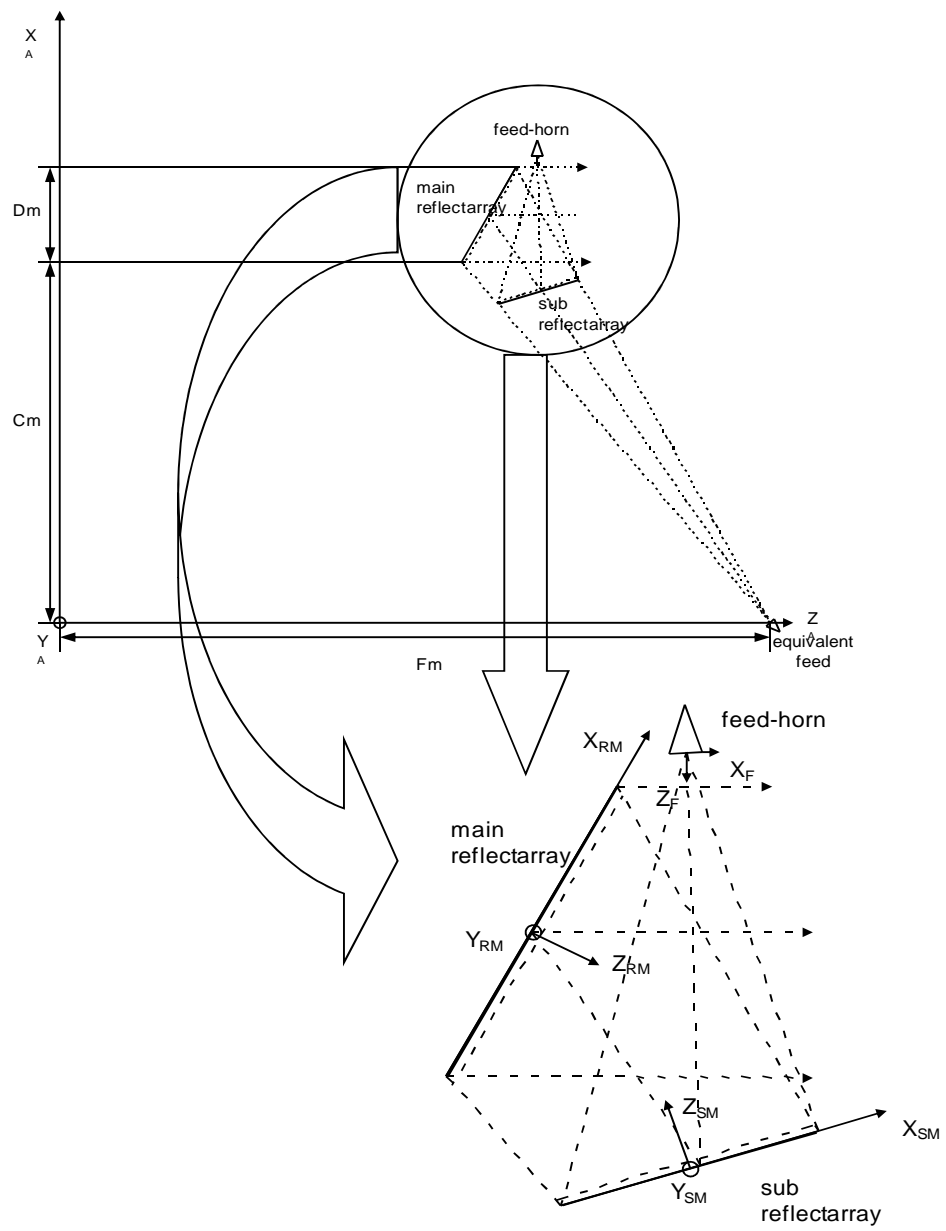


Fig. 4-4. Top view of the antenna configuration

Table 4-1. Main data of the antenna geometry

Main Reflectarray	
Main reflectarray size	504mm × 448mm 63 × 56 elements
Periodicity	8 mm × 8 mm
Sub reflectarray (data in main-reflectarray coordinate system)	
Centre	(-217, 0, 370)mm
Direction cosines matrix Relation between MRA and SRA Coordinate Systems	$\begin{bmatrix} 0.715 & 0 & 0.698 \\ 0 & -1 & 0 \\ 0.698 & 0 & -0.715 \end{bmatrix}$
Sub reflectarray size	380mm × 380mm 38 × 38 elements
Periodicity	10mm × 10mm
Feed-Horn (data in sub reflectarray coordinate system)	
Phase centre	(193, 0.0, 635)mm
Pointing (on the sub reflector surface)	(15, 0, 0)mm

4.2.3 *Feed-horn*

In principle, the sub reflectarray can be illuminated by different types of feeds such as a horn antenna, a dipole, a small array or a cluster of horns. A simple far-field model based on $\cos^q(\theta)$ function is used in the analysis of the geometry for preliminary designs. The model permits to vary the q-factor throughout the different frequencies analyzed and this implies more control in the characterization of the system. In the last stage of the design a full-wave simulation of horn is used to obtain a more accurate simulation of the behaviour of the antenna.

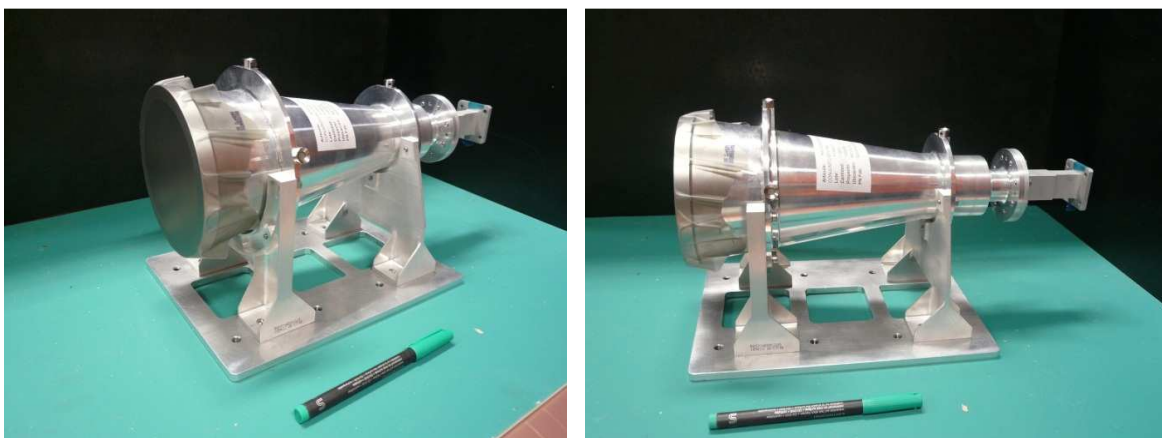


Fig. 4-5. Feed-horn antenna

The horn antenna was designed by EADS-CASA Espacio in the framework of Demorata project supported by ESA [44]. It is a conic and corrugated horn with a length of 268 mm and a diameter in the aperture of 116 mm. The main electrical parameters of the horn antenna at different frequencies are summarized in Table 4-2. The horn has been simulated using the software tool CHAMP from Ticra [64] at seven frequencies (11.7-11.95-12.2-12.975-13.75-14.0-14.5 GHz). The radiation patterns of the feed are plotted in figures Fig. 4-6 to Fig. 4-8. These plots also show the low level of cross-polarization for the frequencies simulated.

Table 4-2. Data of the Feed-horn designed by EADS-CASA Espacio

Freq (GHz)	Directivity (dBi)	X-polar (dB)	Taper at 21,7°
11.7	19,9	-44,2	-16,2
11.95	20,1	-46,0	-17,2
12.2	20,3	-47,0	-17,9
12.975	20,8	-48,7	-20,2
13.75	21,3	-49,1	-21,5
14.0	21,4	-46,3	-22,0
14.25	21,6	-43,5	-22,5

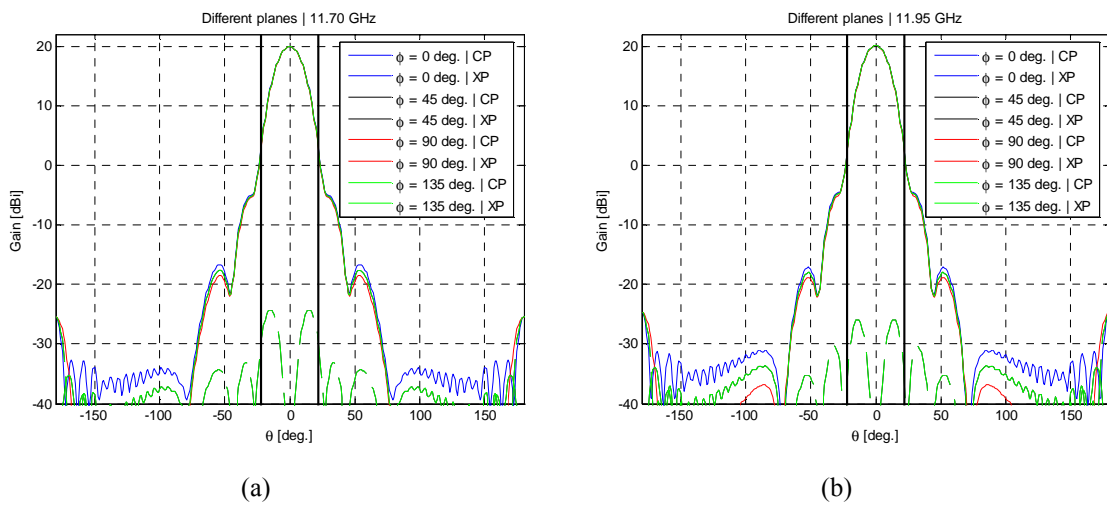
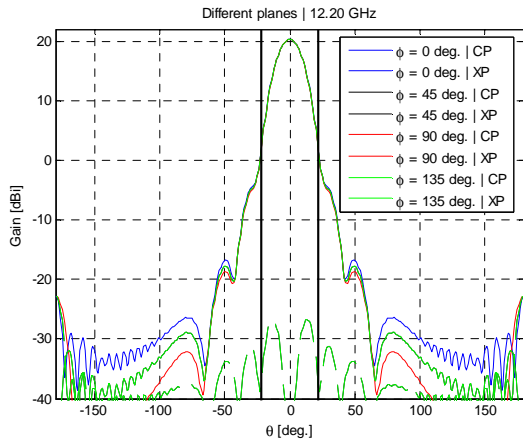
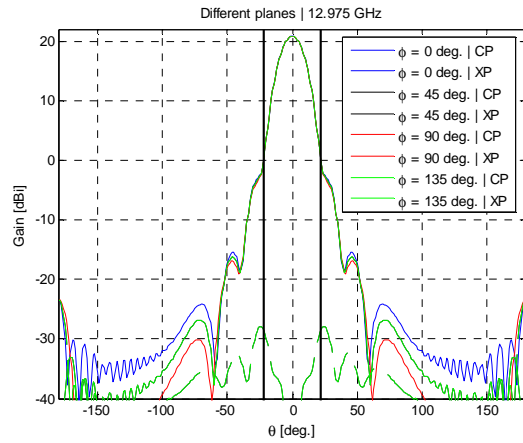


Fig. 4-6. Feed-horn pattern at 11.70 GHz (a) and 11.95 GHz (b)

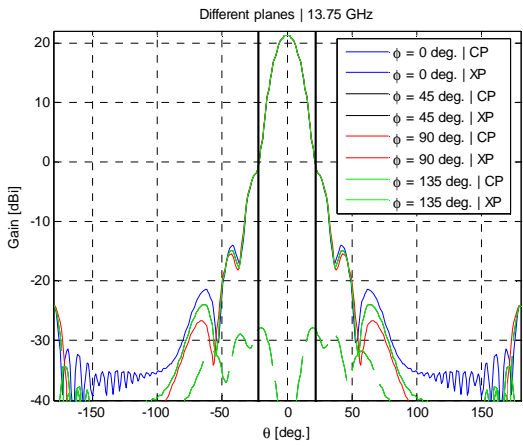


(a)

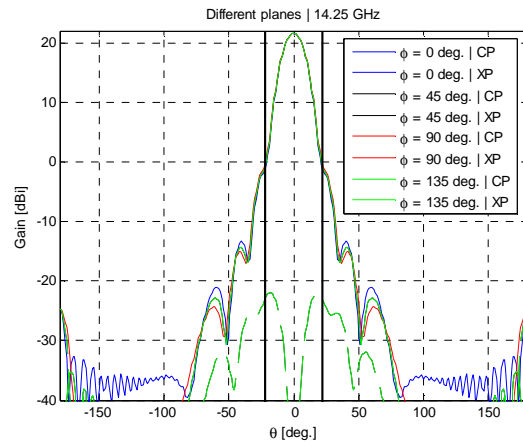


(b)

Fig. 4-7. Feed-horn pattern at 12.2 GHz (a) and 12.975 GHz (b)



(a)



(b)

Fig. 4-8. Feed-horn pattern at 14 GHz (a) and 14.25 GHz (b)

The radiation patterns for $\phi=0^\circ$ and $\phi=90^\circ$ (E and H planes respectively) are compared for different frequencies in the next figures. In each figure seven patterns are superimposed and they are the co-polar component at seven frequencies: 11.70, 11.95, 12.20, 12,975, 13.75, 14.00 and 14.25 GHz. The beamwidth decreases with the frequency as clearly shown in the figures.

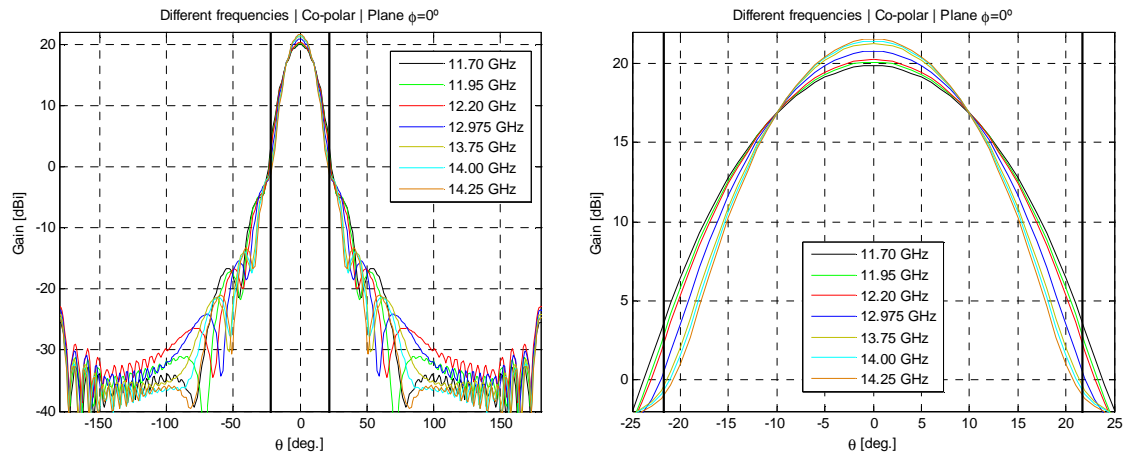


Fig. 4-9. Feed-horn pattern at $\phi = 0^\circ$ and different frequencies

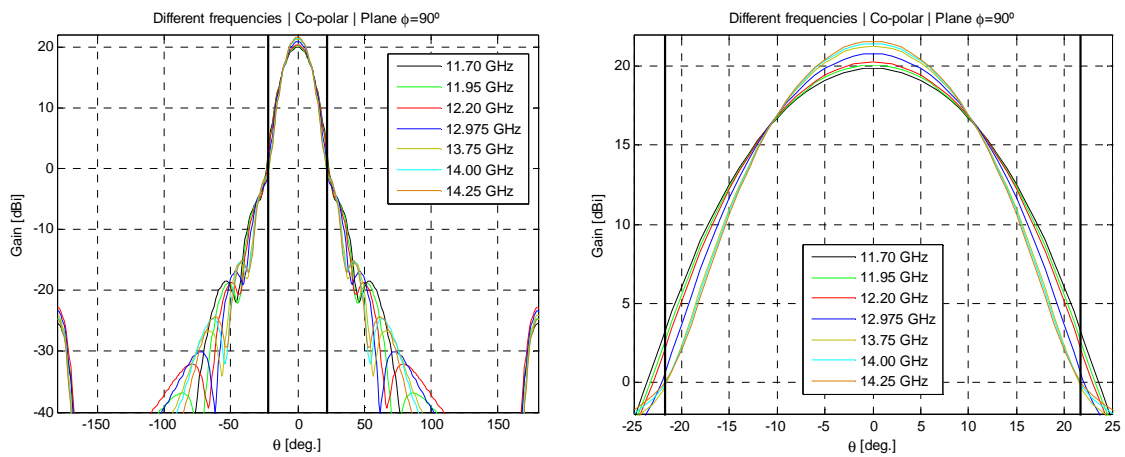


Fig. 4-10. Feed-horn pattern at $\phi = 90^\circ$ and different frequencies

Finally, the phase of the co-polar component at seven frequencies and different planes is compared in the following figures in order to validate the phase-centre approximation of the ideal feed model. The phase is practically constant for all frequencies; this means that the phase centre considered (40 mm inside the aperture plane) is good enough for all frequencies and angle range considered.

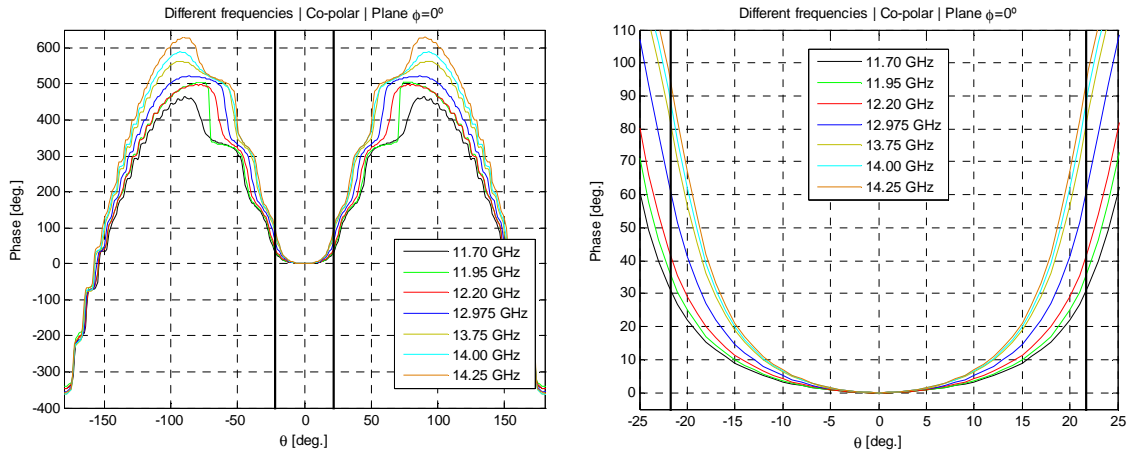


Fig. 4-11. Phase of the co-polar component at $\phi = 0^\circ$ and different frequencies

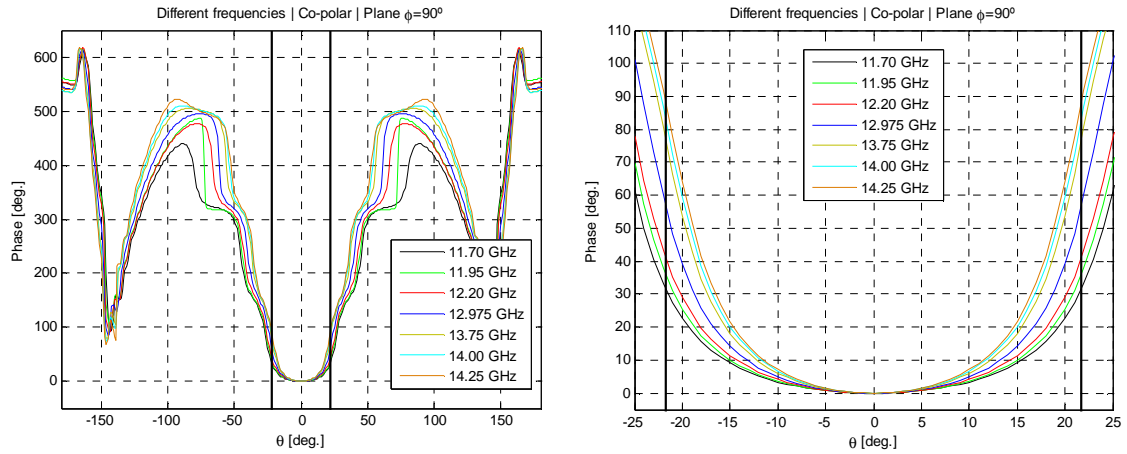


Fig. 4-12. Phase of the co-polar component at $\phi = 90^\circ$ and different frequencies

4.2.3.1 *q*-factor for different frequencies and planes

For preliminary designs, the *q*-factor of the far-field horn antenna model is calculated at each frequency to match the simulated radiation patterns at the two main planes, $\phi = 0^\circ$ and $\phi = 90^\circ$ (E and H planes respectively), showing that the error introduced with the model is minimum. The obtained values are summarized in the table below.

Table 4-3. Q-factor to model the feed-horn at different frequencies

Frequency (GHz)	11.70	11.95	12.20	12.975	13.75	14.00	14.25
$\phi = 0^\circ$	24	26	27	31	34	36	37
$\phi = 90^\circ$	25	26	27	31	34	35	36

For some frequencies the q-factor value is slightly different for E and H planes. So, in these cases the average value can be used. As a second option, one of the two values can be chosen since the results show that the error is marginal. Fig. 4-13 shows both the model pattern (using a different q-factor in each plane: $q_x=36$ and $q_y=35$) and the simulated radiation patterns together and compared at 14 GHz, which is the central frequency of the band defined for the design.

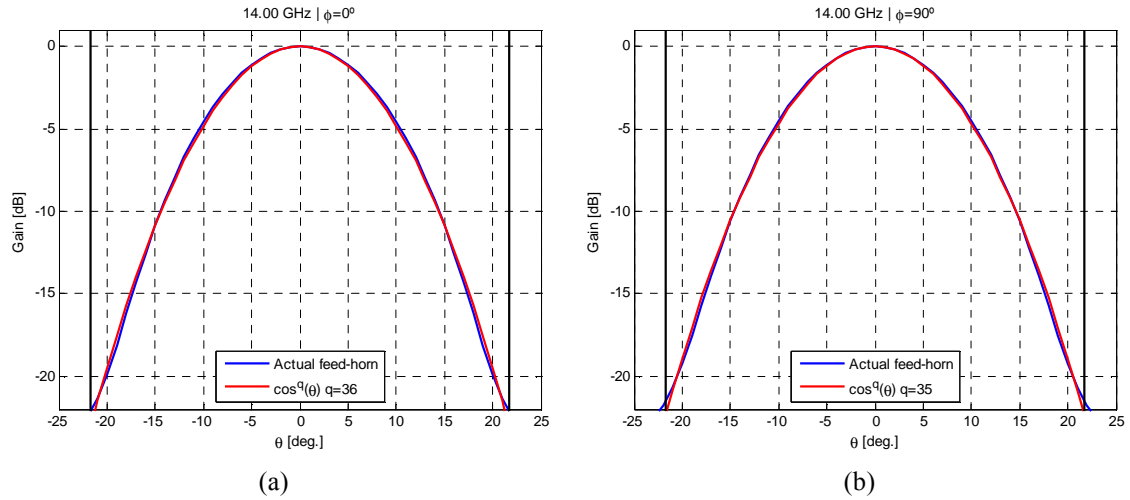


Fig. 4-13. Comparison of horn antenna pattern and $\cos^q(\theta)$ model at 14.00 GHz, $\phi = 0^\circ$ (a), $\phi = 90^\circ$ (b)

Although the cross-polar radiation introduced by the corrugated horn is very low, the reflectarray elements are placed in the near field of the feed-horn, since

$$0.62\sqrt{\frac{D^3}{\lambda}} = 992\text{mm}$$

and the distances from the feed to the sub reflectarray elements are in the range of $636\text{ mm} < r < 755\text{ mm}$. Thus, the computation of the incident field based on the spherical mode expansion of the horn is desirable to compute accurately the behaviour of the antenna.

4.2.3.2 Feed defined by spherical wave expansion

For the accurate analysis of the system a spherical wave expansion of the feed horn has been carried out for an accurate computation of the incident field on the sub reflectarray according to the section 2.2.2.2 of chapter 2.

The phase centre of the feed is placed at the focal point of the equivalent sub reflector and it is pointed to illuminate the edges of the sub reflectarray with -11dB below the maximum within the subtended angle of $\pm 16^\circ$. In principle the phase centre of the feed in the sub reflectarray coordinate system was (188, 0, 616) mm. These coordinates correspond to $f/D=4$. However, the feed was slightly displaced to avoid the blockage of the field radiated by the main reflectarray, since the phase centre of the horn is located 40 mm inside the aperture plane. Therefore the feed-horn is moved 20mm away from the sub reflectarray on its z-axis and the new location in the sub reflectarray coordinate system is (193, 0, 635) mm, which produces a small variation of the antenna with negligible effect in the radiation patterns. Fig. 4-14 shows the coordinates and orientation of the feed, the pointing on the sub reflectarray surface and the radiation angles of the sub and main reflectarray. The most critical incidence angle on this geometry is given by the path defined between the bottom limit of the sub reflector and the top edge of the main-reflector, as it can be checked in the Fig. 4-14.

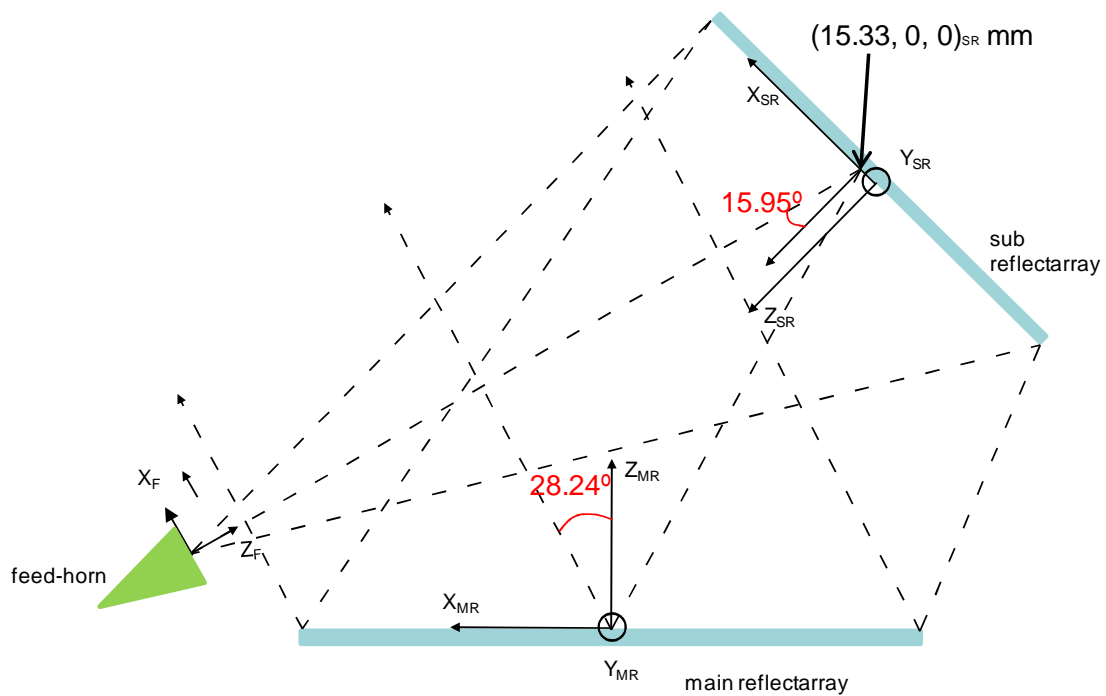


Fig. 4-14. Lateral view of the antenna configuration

4.2.4 Multi-layer configuration of the two reflectarrays

(a) Sub reflectarray

The sub reflectarray consists of a two-layer circular array of rectangular printed stacked patches in a rectangular lattice, being the diameter of the sub reflectarray 380 mm. The period is defined to have a maximum range in the curve of the phase shift to cover all the possible phases needed in the sub reflector distribution and to avoid grating lobes for the angles of incidence from the feed. According to this criterion, the sub reflectarray is organized in 38×38 elements, resulting in a period of $10 \text{ mm} \times 10 \text{ mm}$ ($0.46 \lambda \times 0.46 \lambda$). The required phase shift of each element is achieved adjusting the patch dimensions with relative dimensions of $a_2=0.7a_1$, as shown in Fig. 4-15.

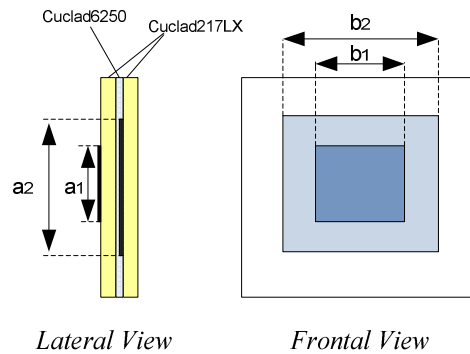


Fig. 4-15. Periodic cell of two layers

CuClad217LX substrate has been chosen for its simplicity of manufacturing and low losses. The sandwich configuration for the two layers sub reflectarray is shown in Fig. 4-16. The copper patches are printed on a dielectric substrate of 60-mil thickness and then both layers are glued through a proper thermoplastic bonding film: Cuclad6250. Table 4-4 shows the main radio-electric characteristics.

Table 4-4. Radio-electric characteristics of the materials

Dielectric	Nominal ϵ_r	tag δ	Thickness (mm)
(SRA) Cuclad 217LX	2.17	0.0009	1.524
(MRA) Arlon AD255	2.55	0.0015	1.580
(SRA) Cuclad6250 (Thermoplastic bonding film)	2.32	0.0013	0.038

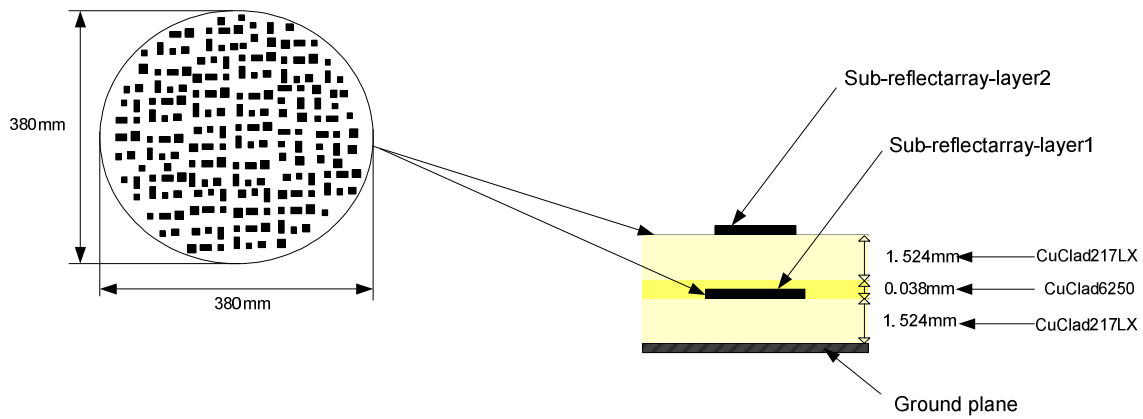


Fig. 4-16. Sandwich configuration of the sub reflectarray using CuClad217LX and CuClad6250

The phase-shift and losses as a function of the patch size for the design frequency (14 GHz) and for ± 1 .GHz bandwidth are shown in Fig. 4-17 for normal incidence. The dissipative losses in the reflectarray will be an average value of those shown in Fig. 4-17, which is approximately 0.07dB.

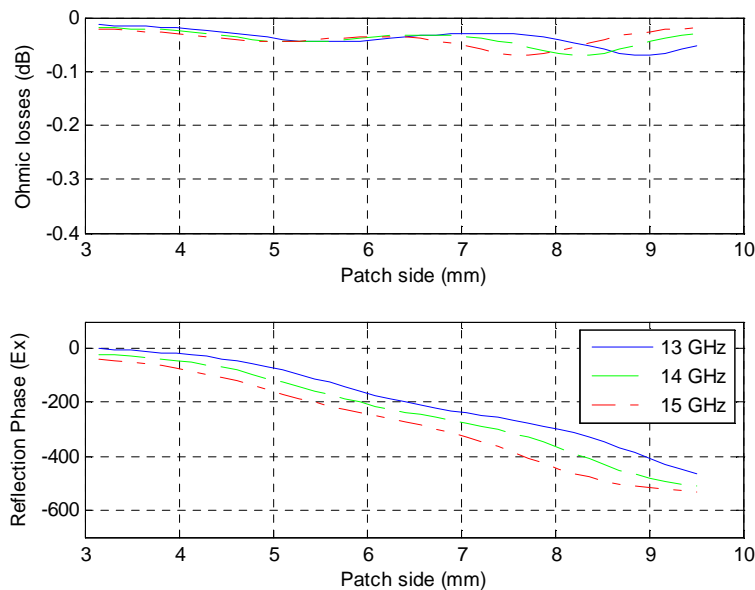
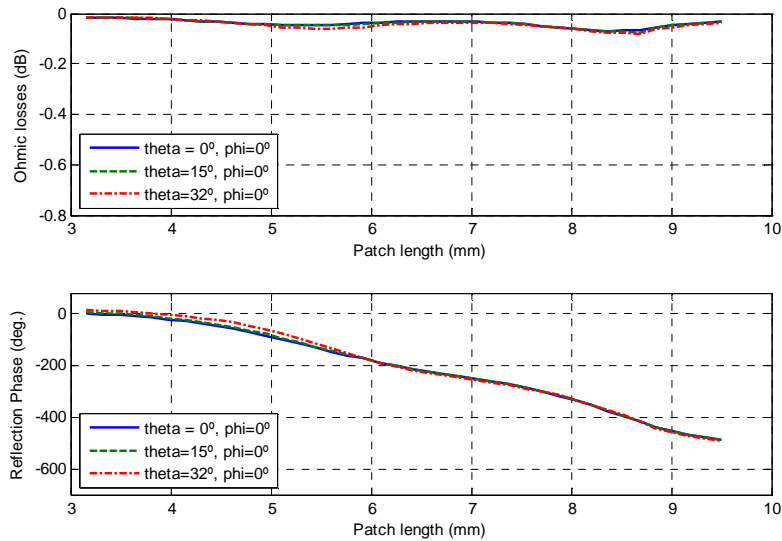


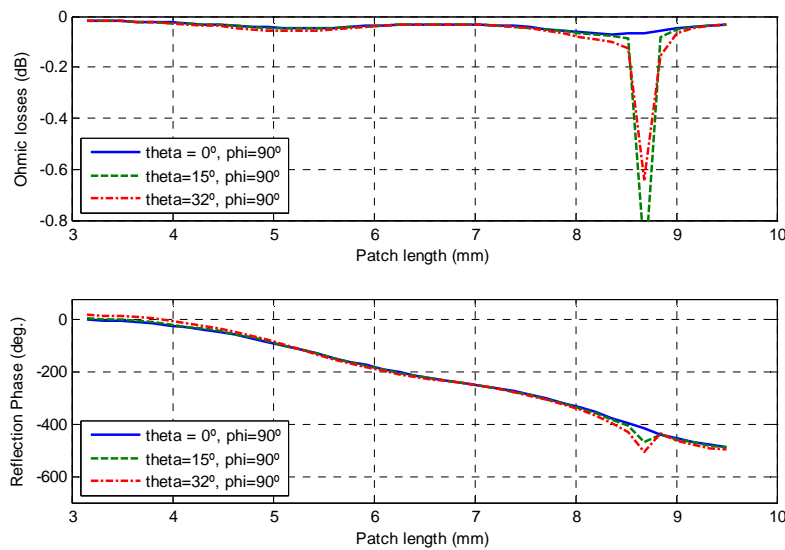
Fig. 4-17. Ohmic losses and phase of the co-polar component at $\phi = 0^\circ$ and different frequencies for the sandwich configuration of the sub reflectarray

Fig. 4-18 shows the phase of reflection coefficient for three incidence angles (the two extreme limits and an intermediate value) of the impinging wave on the sub reflectarray for X and Y polarization. The period of the array is 10 mm and the patches dimensions lie on the range from 3mm to 8.5 mm. As it can be checked, the ohmic losses get worst for y-polarization at $\theta=15^\circ$ and $\theta=32^\circ$ for patches between 8 and 9 mm.

A solution to reduce these losses in the final design consists on avoiding large patches close to the edges, where the incidence angles are large. On the other hand, the larger patches are preferred to be placed around the centre of the reflectarray, where the incident angles become lower than $\theta=10^\circ$.



(a)



(b)

Fig. 4-18. Phase of the co-polar component for the sub- reflectarray for $\phi = 0^\circ$ (Horizontal polarization)(a) and $\phi = 90^\circ$ (Vertical polarization)

(b) Main-reflectarray

In the main reflectarray, the patches are also arranged in a rectangular lattice. Now, the shape of the reflectarray is elliptic with axes of 504 mm and 448 mm. In this case, the incidence angles are much more critical since they can be larger than 70° in the worst case as shown in Fig. 4-19. A period of $8\text{ mm} \times 8\text{ mm}$ has been chosen since a smaller period is less sensitive to the angle of incidence. Thus, the main-reflectarray is organized in a matrix of 63×56 elements. The resulting sandwich configuration is shown in Fig. 4-20 and the nominal dielectric properties and thickness of each layer on sub and main reflectarray are in Table 4-4. Fig. 4-21 shows the phase-shift and losses at normal incidence as a function of the patch size for $\pm 1\text{GHz}$ bandwidth at the design frequency. The dissipative losses in the reflectarray are expected to be around 0.08 dB, as it can be checked in Fig. 4-21.

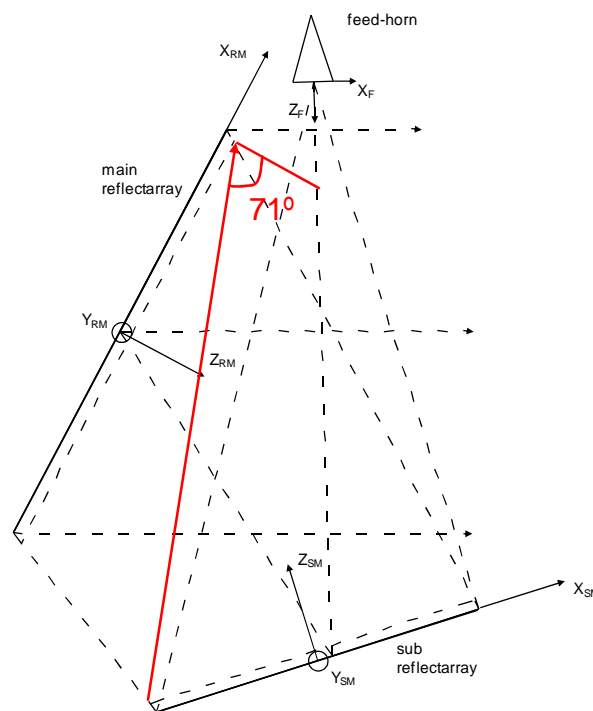


Fig. 4-19. Top view of the antenna configuration. The most critical incident angle is shown in red.

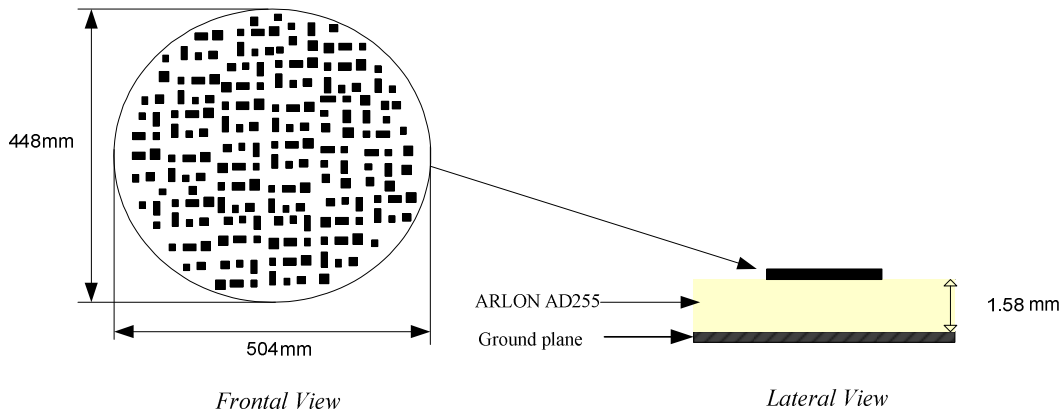


Fig. 4-20. Sandwich configuration of the main-reflectorarray using Arlon AD255

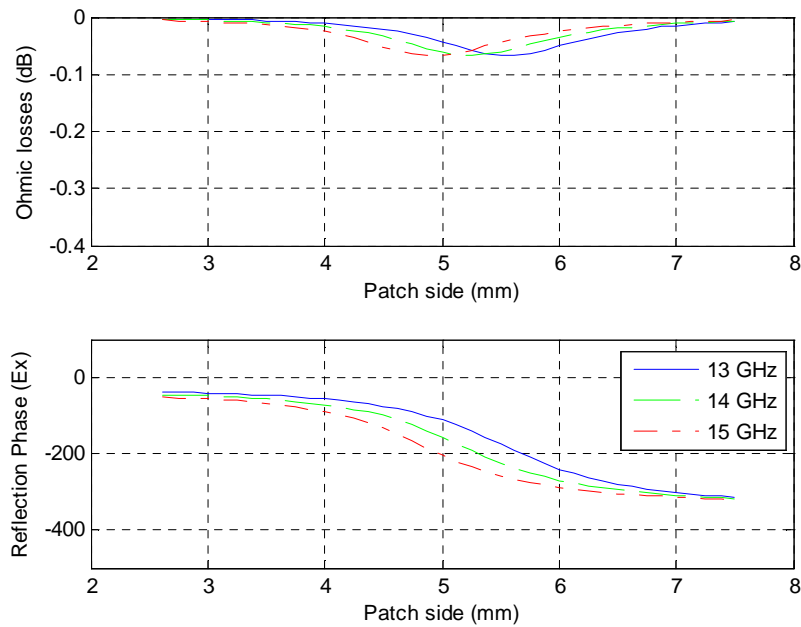
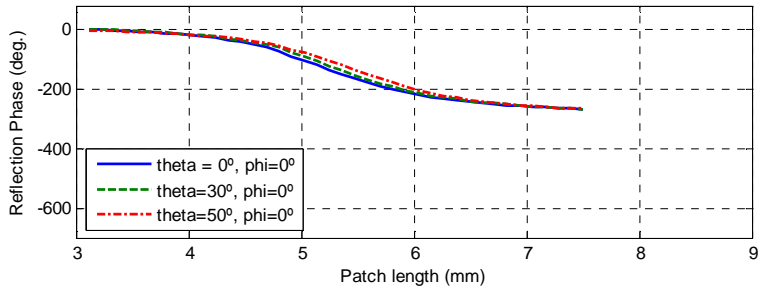
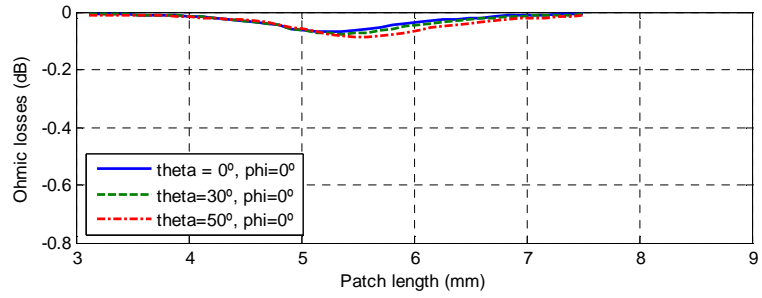
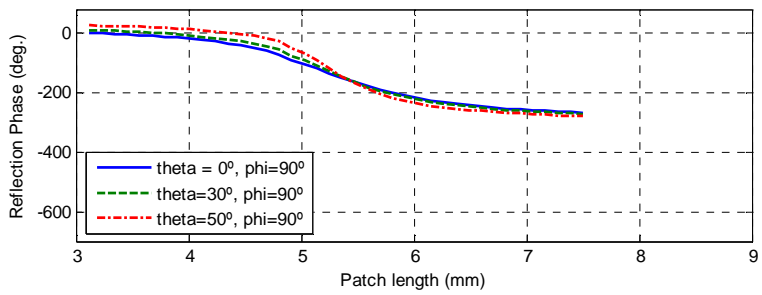
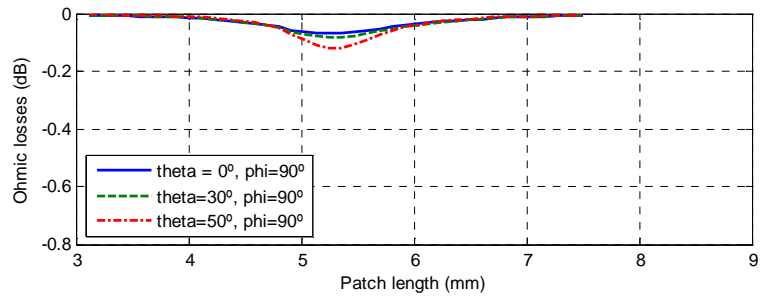


Fig. 4-21. Ohmic losses and phase of the co-polar component at $\theta = 0^\circ$ and $\phi = 0^\circ$ at different frequencies for the main-reflectorarray

In the case of the main reflectarray the period is 8 mm and the patches dimensions are in the range of 3 mm to 7.5 mm. Fig. 4-22 shows the phase of reflection coefficient at 14GHz for three incidence angles in the main reflectarray for X and Y polarization. The ohmic losses are below 0.15 dB.



(a)



(b)

Fig. 4-22. Phase of the co-polar component for the main reflectarray for $\phi = 0^\circ$ (Horizontal polarization)(a) and $\phi = 90^\circ$ (Vertical polarization) (b) at 14 GHz

4.2.5 Antenna design.

4.2.5.1 Preliminary design

For the preliminary design of the antenna, the incident field on the sub reflectarray should be computed. In a first approximation, a $\cos^q(\theta)$ model is used. Once the reflectarray is designed, an accurate near-field model of the feed-horn is used for an accurate prediction of the electric behaviour. A spherical mode expansion of the field radiated by the feed is used to calculate the incident field on the sub reflectarray, see section 2.2.2.2. As a result, the feed-horn produces an illumination of -13.48 dB at the sub reflectarray edges, see Fig. 4-23 and Fig. 4-24.

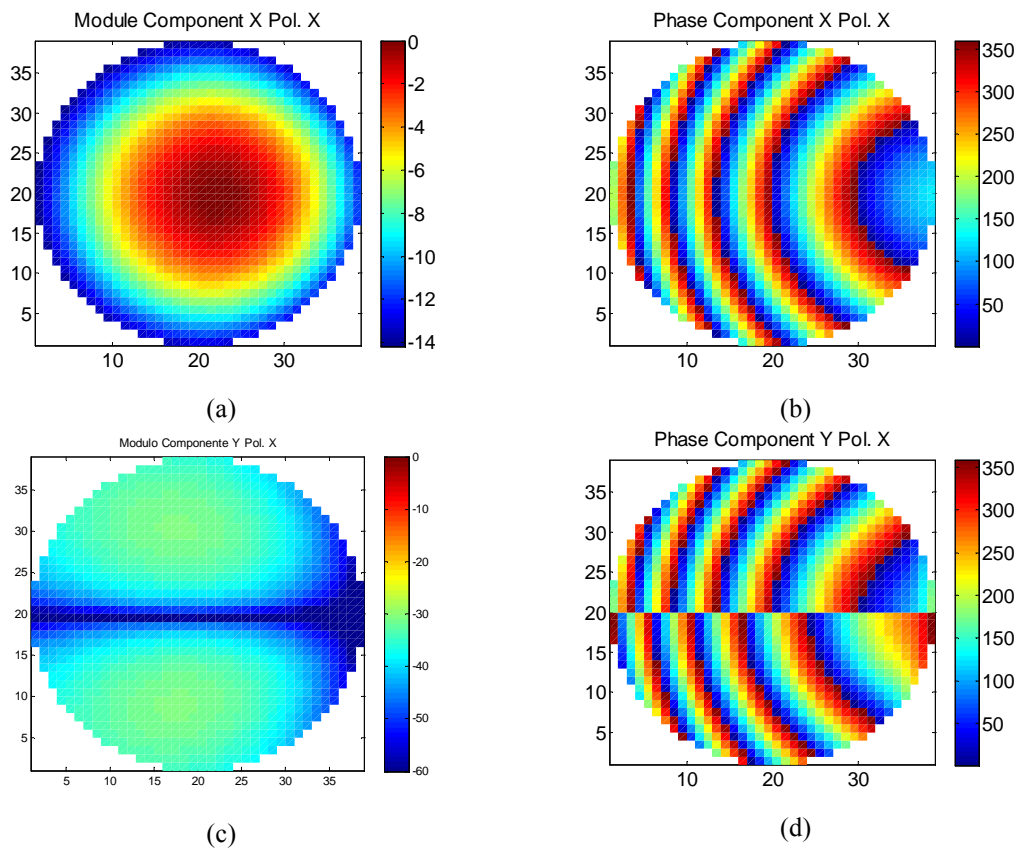


Fig. 4-23. Module (a) and phase (b) of the copolar component and module (c) and phase (d) of the crosspolar component for X- polarisation for the incident field on the sub reflectarray at 14 GHz

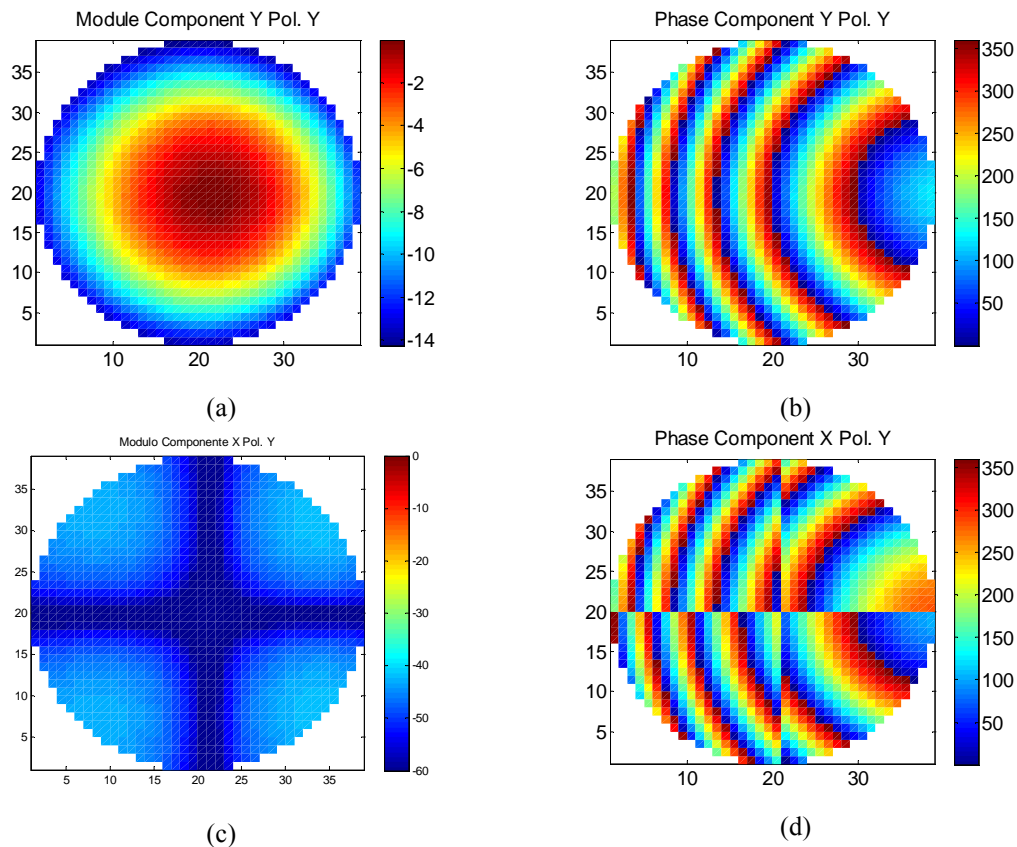


Fig. 4-24. Module (a) and phase (b) of the copolar component and module (c) and phase (d) of the crosspolar component for Y- polarisation for the incident field on the sub reflectarray at 14 GHz

On the other hand, the phase shift required for ideal reflectarray elements is calculated through ray tracing as a function of the difference between two distances: the distance from the feed to the each cell of the sub reflectarray and the distance from the virtual focus to each cell of the sub reflectarray. Fig. 4-25 shows the resulting goal phase shift of the sub reflectarray and main-reflectarray, which is calculated in a similar way, using geometrical optic (GO).

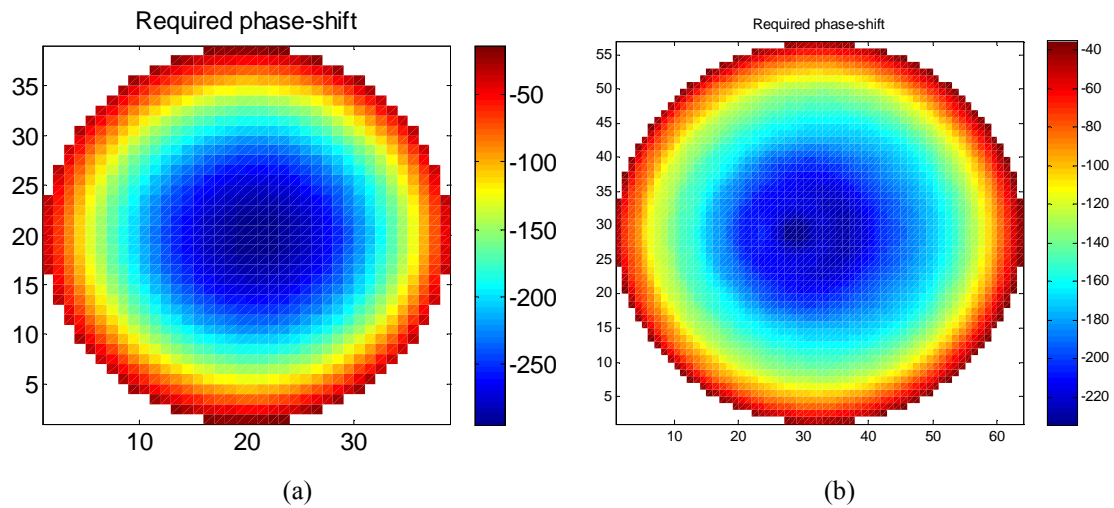


Fig. 4-25. Required phase shift for the sub reflectarray (a) and for the main-reflectarray (b)

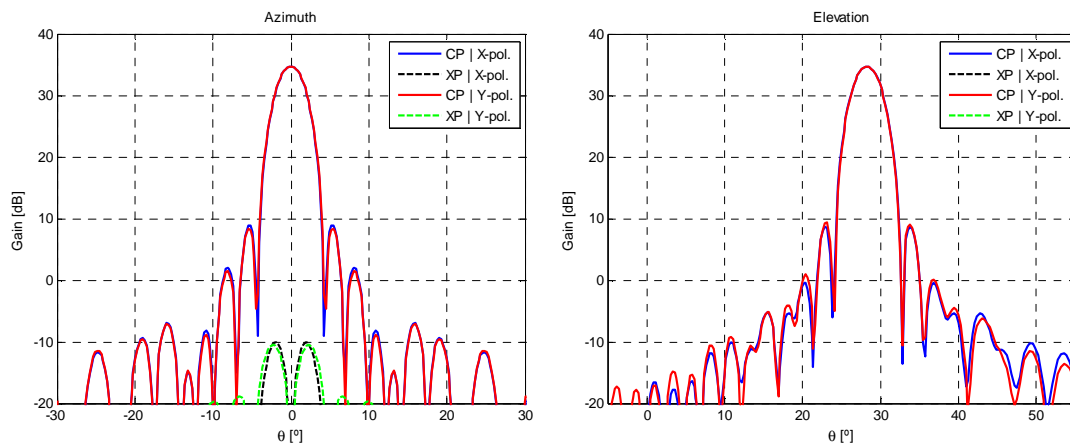


Fig. 4-26. Radiation patterns obtained for V- and H-polarization at 14 GHz using ideal phases on both reflectarray surfaces.

Once the illumination and the phase distribution are determined, the radiation patterns of the antenna considering ideal phase shift elements are computed. Fig. 4-26 points out the radiation pattern obtained when the dual-offset reflectarray system is analyzed using the required ideal phases shown in Fig. 4-25.

The design is carried out for the two reflectarrays, considering dual-linear polarizations at 14 GHz. Both x and y dimensions of the printed patches are adjusted to fulfill the required phase shift previously defined. The phase distribution is different for the two orthogonal polarizations since the incidence is oblique in each element and the phase of the incident field is different in both linear polarisations, resulting in rectangular patches. A fixed relative size of the stacked patches is maintained between the two

layers of the sub reflectarray ($a_1=0.7a_2$, $b_1=0.7b_2$, being a_1 , a_2 , b_1 and b_2 the dimensions of the patches, see Fig. 4-15). For each element, the patch dimensions are adjusted by using a zero finding routine that iteratively calls an analysis routine, assuming local periodicity. Each element is analysed assuming it is embedded in a periodic structure by Spectral-Domain Method of Moments (SD-MoM). This design is used to make a first evaluation of the behavior of the antenna. The resulting crosspolar component of the reflected field obtained in the sub reflector is shown in Fig. 4-27.

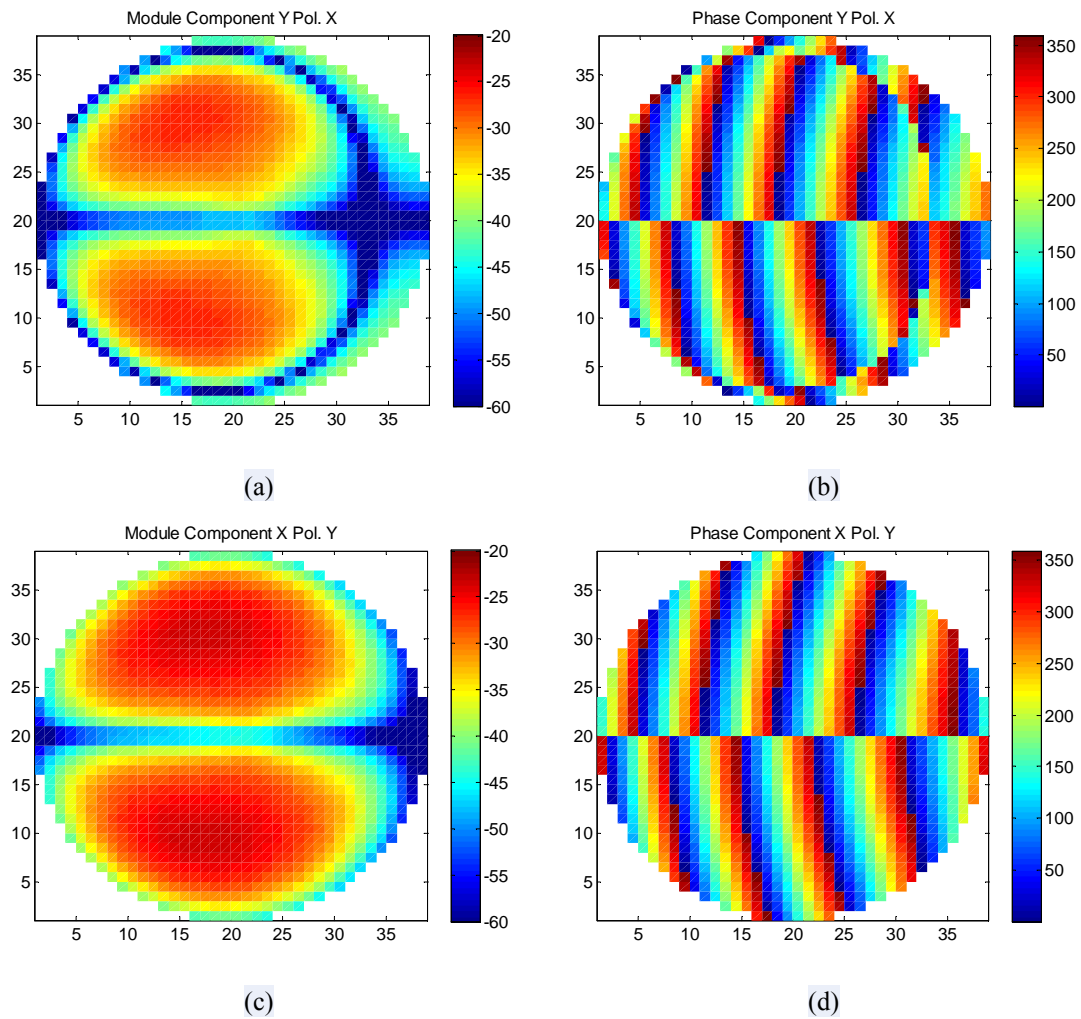


Fig. 4-27. Module (a) and phase (b) of the crosspolar components for the reflected field on the sub reflectarray at 14 GHz for V-polarization. Module (c) and phase (d) of the crosspolar components for the reflected field on the sub reflectarray at 14 GHz for H-polarization

In a similar way, for the design of the main reflectarray, the sandwich configuration used is the one shown in Fig. 4-20, the substrate is AD255 from ARLON and its characteristics are given in Table 4-4. The resulting crosspolar component of the reflected field obtained in the main-reflector is shown in Fig. 4-28.

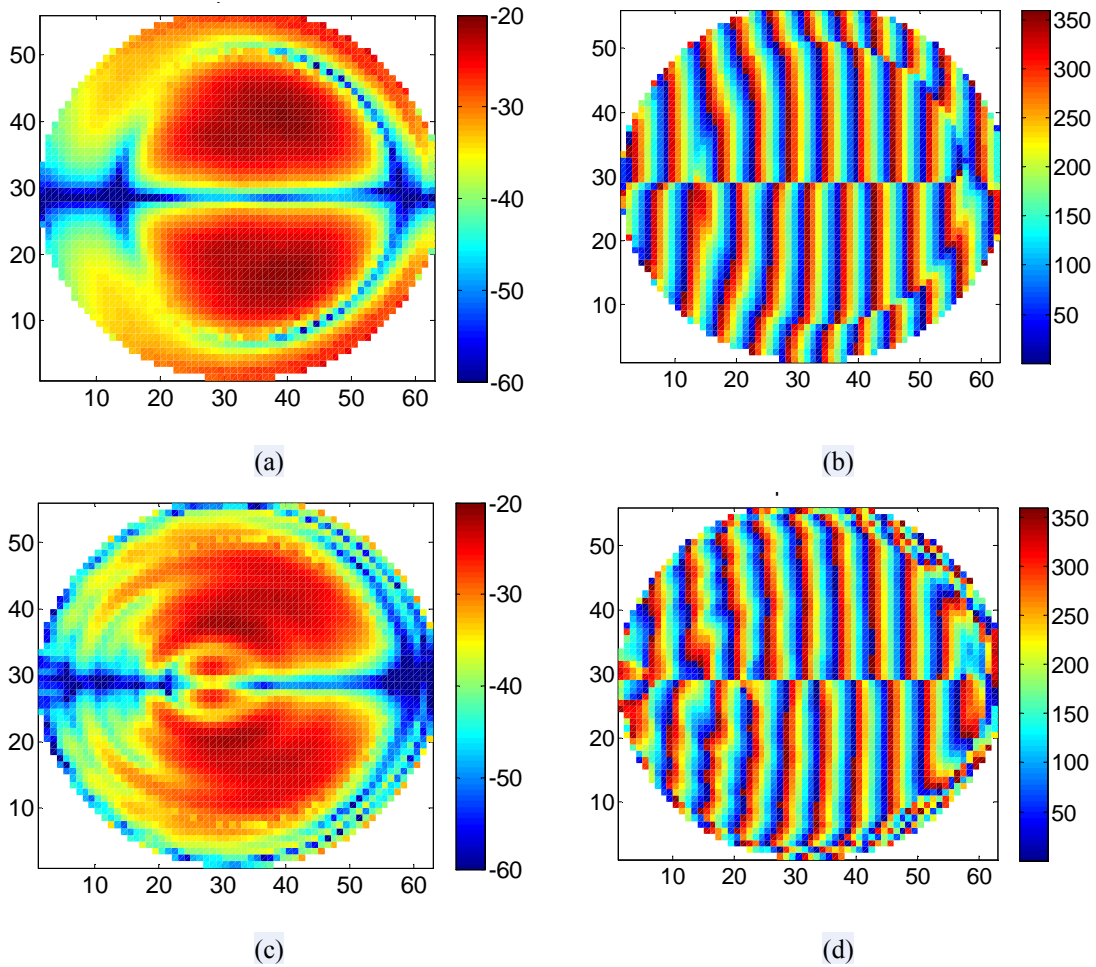


Fig. 4-28. Module (a) and phase (b) of the crosspolar components for the reflected field on the main-reflectarray at 14 GHz for V-polarization. Module (c) and phase (d) of the crosspolar components for the reflected field on the main-reflectarray at 14 GHz for H-polarization

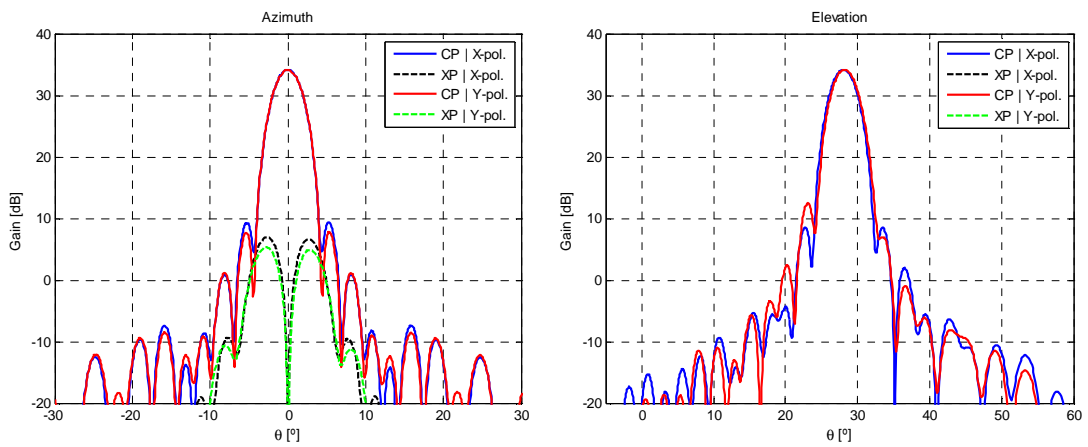


Fig. 4-29. Radiation patterns obtained for V- and H-polarization at 14 GHz.

The sandwich configuration selected for the sub reflectarray, as it is shown in section 4.2.2.4, generates very linear phase curves, see Fig. 4-16. The dual-reflectarray antenna is analyzed at 14 GHz considering the designed patches, and the resulting radiation patterns are shown in Fig. 4-29. Despite having designed a dual reflectarray geometry equivalent to a dual offset parabolic system that fulfils Mizuguchi conditions, the crosspolar generated by the dual reflectarray antenna is higher than expected, as can be checked comparing Fig. 4-26 (expected results performed with ideal phases) and Fig. 4-29. The crosspolar level increases in more than 15 dB.

4.2.6 Low cross-polarization design

The crosspolar component generated in a dual reflectarray system is due to two facts: the geometry of the antenna and the patches themselves. In the configuration analyzed, the crosspolar component produced by the first source (geometry) has been minimized since the antenna optics is defined according to Mizuguchi conditions. Therefore, the resulting crosspolar is mainly produced by the patches of both reflectarrays. To reduce this undesirable component, the phase-curve of the crosspolar is adjusted to locate a null in the area of the sub reflector where the maximum crosspolar is located, as proposed in [48]. Then, the phase curve is adjusted (adding or subtracting a constant in the phase curve) to locate one of the cross by zero matching the patch size where maximum crosspolar is produced, see Fig. 4-30.

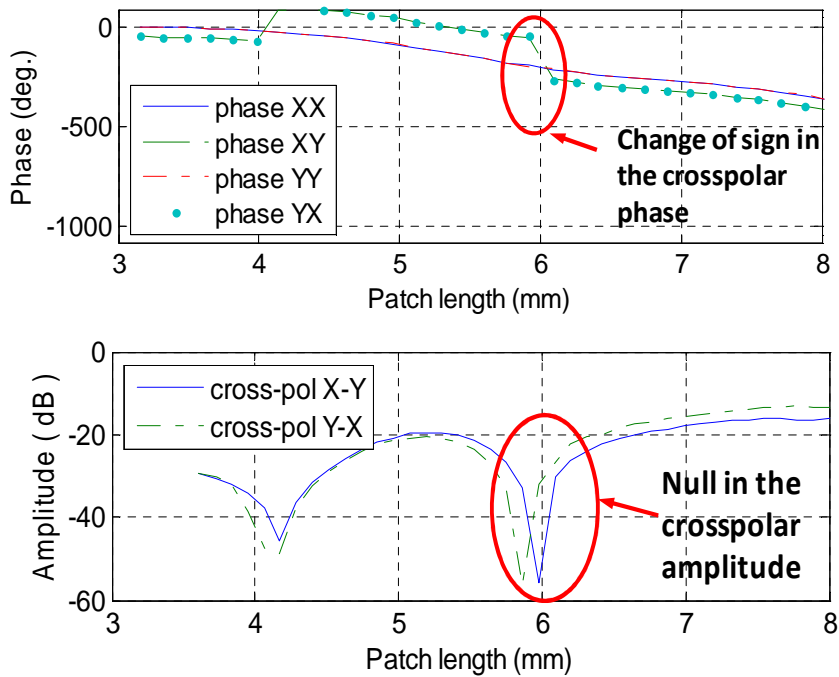


Fig. 4-30. Phase curves as a function of the patch sizes for the sub reflectarray sandwich, considering an angle of incidence: $\theta=36.7^\circ$, $\varphi=19^\circ$

Note that the phase-curve of the crosspolar component depends on the incident angle and therefore it should be calculated for each angle. The incident angles on the patches where the maximum crosspolar is produced are different from the incident angles in the rest of the patches of the same surface. Therefore, it is expected that placing one of the nulls of the phase curve on the size patches where the maximum crosspolar is found, will produce a displacement of the null in the crosspolar of the reflected field for the sub reflector, making necessary a further fine tuning of the crosspolar cancellation. To make this fine adjustment, the reflectarray is analyzed and the constant added to the phase curve is re-adjusted to ensure the maximum cancellation of the crosspolar component in the reflected field. A flow chart with the steps followed for reducing the cross-polarization generated by a reflectarray is shown in Fig. 4-31.

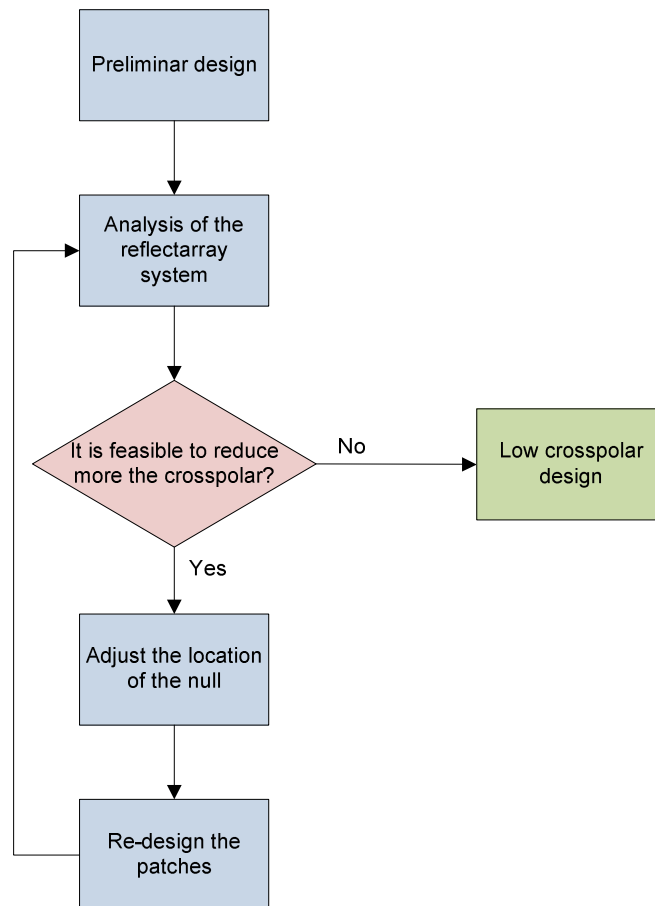


Fig. 4-31. Diagram with the steps of the iterative process to reduce the crosspolar level produces by the patches of a reflectarray

As it can be seen, the null in the phase-curve for the cross-polarization happens for patches of sizes between 5.7 mm and 6 mm, see Fig. 4-30. Fig. 4-32 shows the patch dimensions of the sub reflectarray. To reduce the crosspolar contribution of the sub reflectarray patches, a constant has been added to the phase distribution, so that the area where this contribution is higher (see Fig. 4-33 (a)) is superimposed with the area where the patches of sizes between 5.7 mm and 6 mm are located. This results in a sub reflectarray design with a lower crosspolar contribution: a reduction better than 5 dB in the levels of cross-polarisation is achieved for both polarizations, see Fig. 4-33 (b).

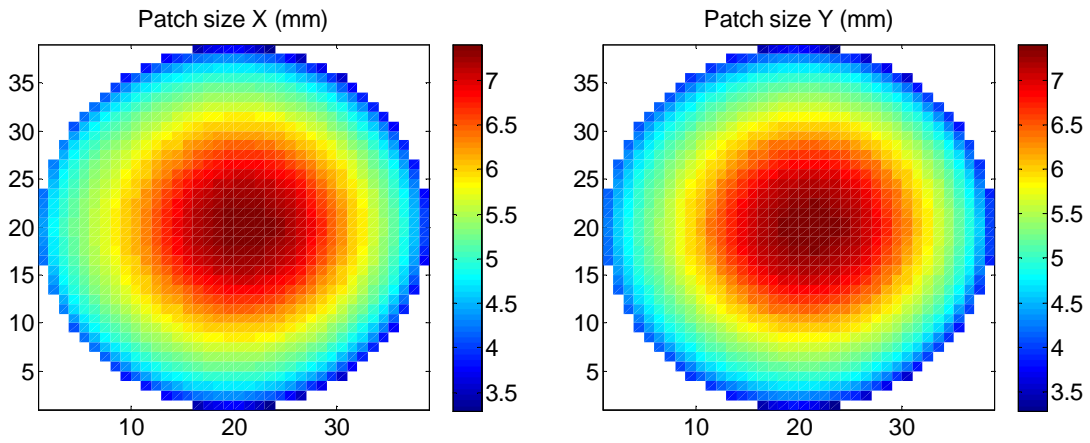


Fig. 4-32. x and y dimensions for the sub reflectarray patches

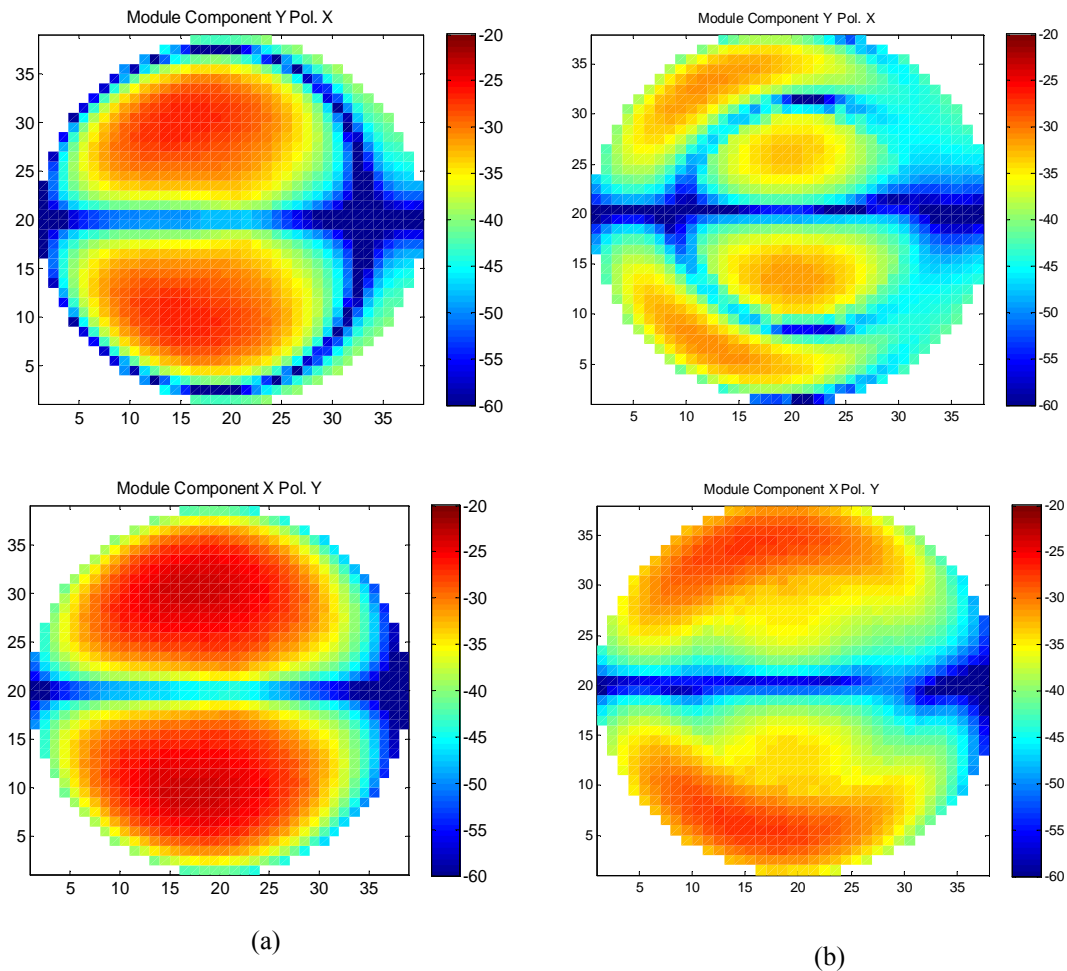


Fig. 4-33. Module of crosspolar component of reflected field for the sub reflectarray (a)preliminary design (b)design with reduction of the crosspolar

Note that the error in phase (difference between required phase distribution and phase simulated by MoM) is very low, less than a few degrees for most of the elements, particularly in the central region of the reflectarray, where the amplitude of the field is

more significant. The average value of this error for X and Y polarization is pointed out in Fig. 4-34.

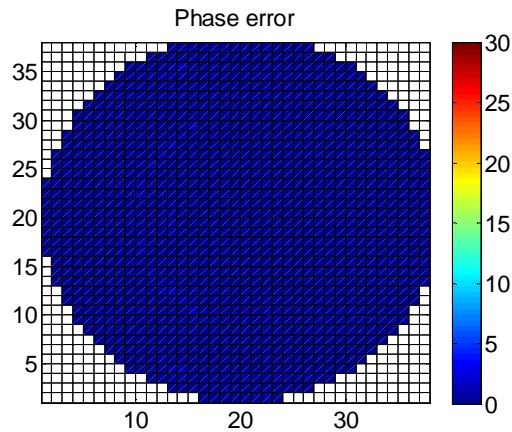


Fig. 4-34. Average error phase for the sub reflectarray patches

Once the sub reflectarray is designed with low crosspolar contribution, a similar process is followed to design the main reflectarray. The first step consists on a preliminary design of the main reflectarray without applying any correction in the cross-polarization, obtaining already a small cancellation of the cross-polarization at this stage, see Fig. 4-35 (a). Then, a constant is added to the phase distribution, so that one of the nulls of the phase curve in the crosspolar component is located at the position of the maximum contribution of the crosspolar on main. Fig. 4-35 shows the cross-polarization on the reflected field of the main-reflector and the azimuth plane of the resulting radiation pattern for three iterations following the steps explained in Fig. 4-31. After several iterations, a significant reduction of 5 dB is achieved in the crosspolar of the complete design, as shown in Fig. 4-35. The radiation pattern in this case has been calculated taking one sample per cell on the main-reflector. A more accurate analysis taking nine samples per cell on main-reflector will be performed for a detailed prediction of the antenna radiation pattern.

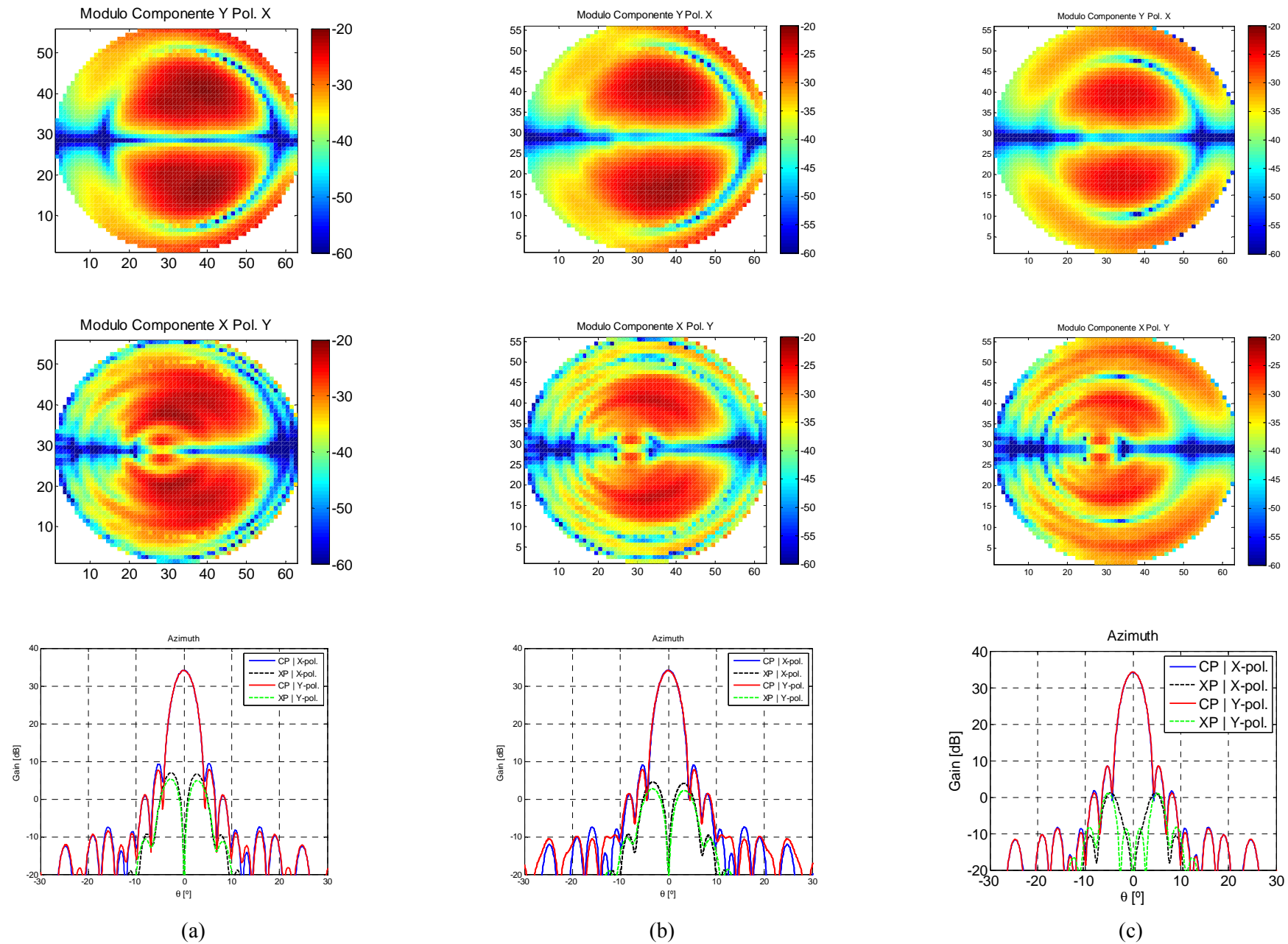


Fig. 4-35. Amplitude of crosspolar component of reflected field for the main-reflectarray and azimuth cut of radiation pattern generated (a) preliminary design (Iteration 1) (b) design with reduction of the crosspolar (Iteration 2) (c) design with higher reduction of the crosspolar (Iteration 3)

Table 4-5. Comparison of gain level when reducing the cross-polarization for both V and H polarizations

Gain(dBi)	Iteration 1	Iteration 2	Iteration 3
Gain for V-polarization	34.19	34.19	34.19
Max. Crosspolar for V-polarization	4.49	4.85	1.26
Gain for H-polarization	34.08	34.08	34.22
Max. Crosspolar for H-polarization	5.32	3.73	1.16

For the resulting patch dimensions after iteration 3, that fulfils the required phase shift at 14 GHz for both polarisations (see Fig. 4-36) and minimizes the crosspolar level, the error in phase is calculated and it is negligible. The patch dimensions and the phase error are shown in Fig. 4-37 and Fig. 4-38 respectively.

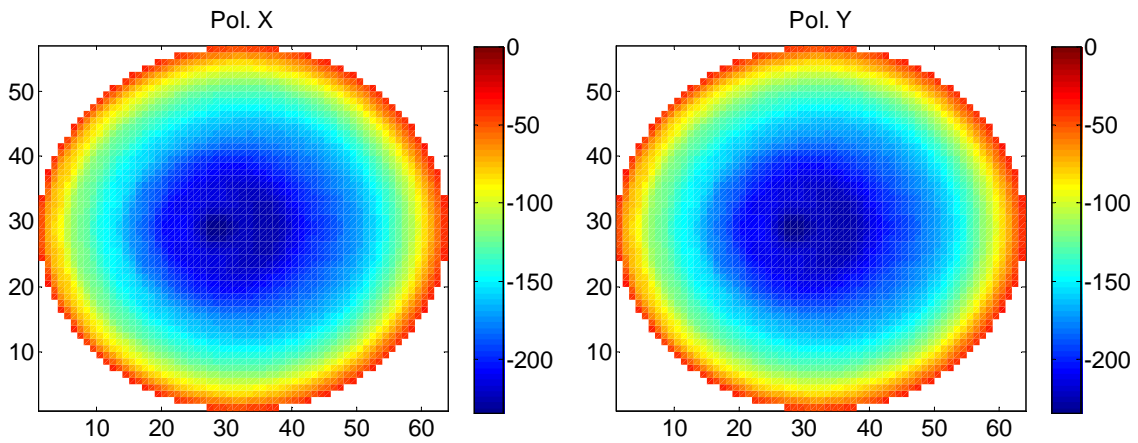


Fig. 4-36. Required phase shift of main-reflectarray for vertical and horizontal polarization

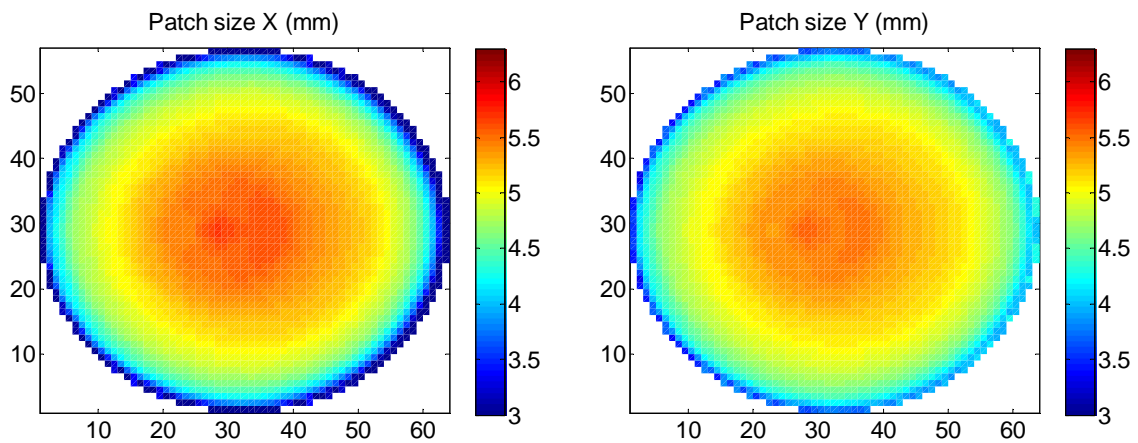


Fig. 4-37. x and y dimensions for the main-reflectarray patches

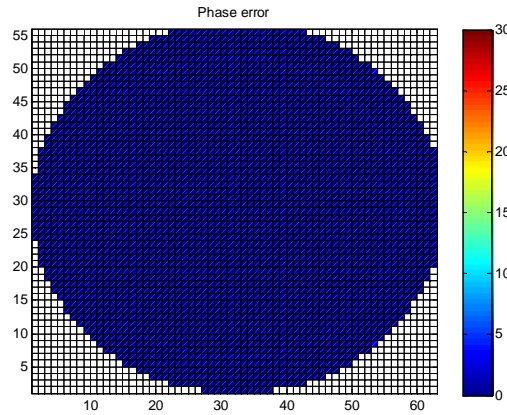


Fig. 4-38. Average phase error for the main-reflector patches

4.2.7 Improvement of dual-reflector design

After the design of the dual-reflector antenna for low cross-polarization, a more accurate analysis of the antenna is discussed in this section. First of all, it must be noticed that the proposed antenna configuration is very challenging, because the feed, the sub reflector and the main reflector are very close to each other, so that the conventional approximations of far field are not suitable for the analysis of the present antenna. The purpose of choosing this geometry is mainly to be used as benchmarking for the proposed analysis tool in very stringent conditions. Some aspects of the proposed analysis technique that allow improving the accuracy of the analysis are discussed here.

In previous section, the analysis of the main-reflector has been performed considering the centre of the sub reflector as origin of the incident field. This approach is appropriate for dual offset systems in which the sub reflector is relatively close to the virtual focus which is equivalent to select the branch 2 of the scheme in Fig. 4-39. However, branch 1 of the hyperbola has been selected for the configuration analyzed, since it is a compact range antenna which implies that the location of the sub reflector centre is far away from the virtual focus. The approach may introduce some errors in the incidence angle with respect to the values for which the patches have been designed. The patches are designed considering the origin of the field coming from the virtual focus. The difference between the incident angles on the main reflector for these two cases is shown in Fig. 4-40. Being the single offset configuration, the case to

which the dual offset configuration should converge. The difference between the incident angles for both cases can go up to 30 °.

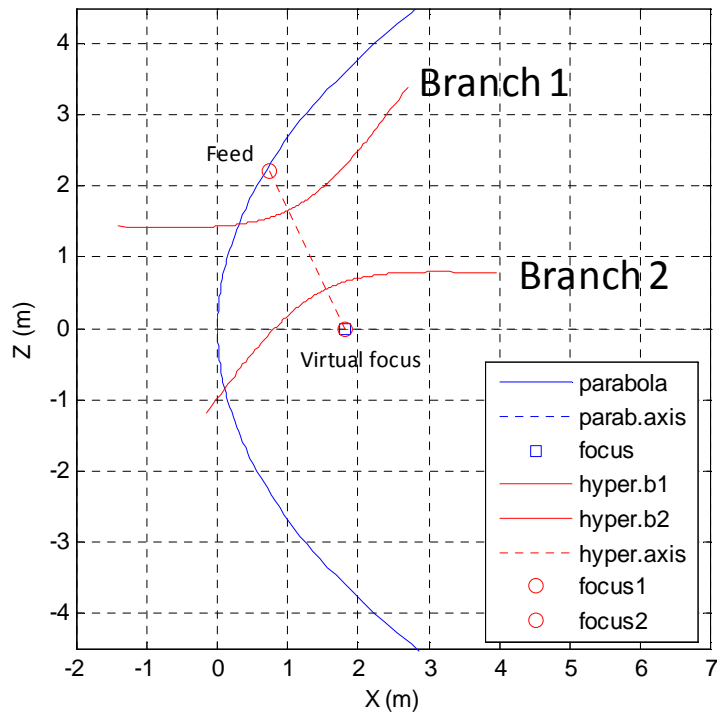


Fig. 4-39. Scheme of the parabola and the two branches of the hyperbola which defines the antenna configuration analysed

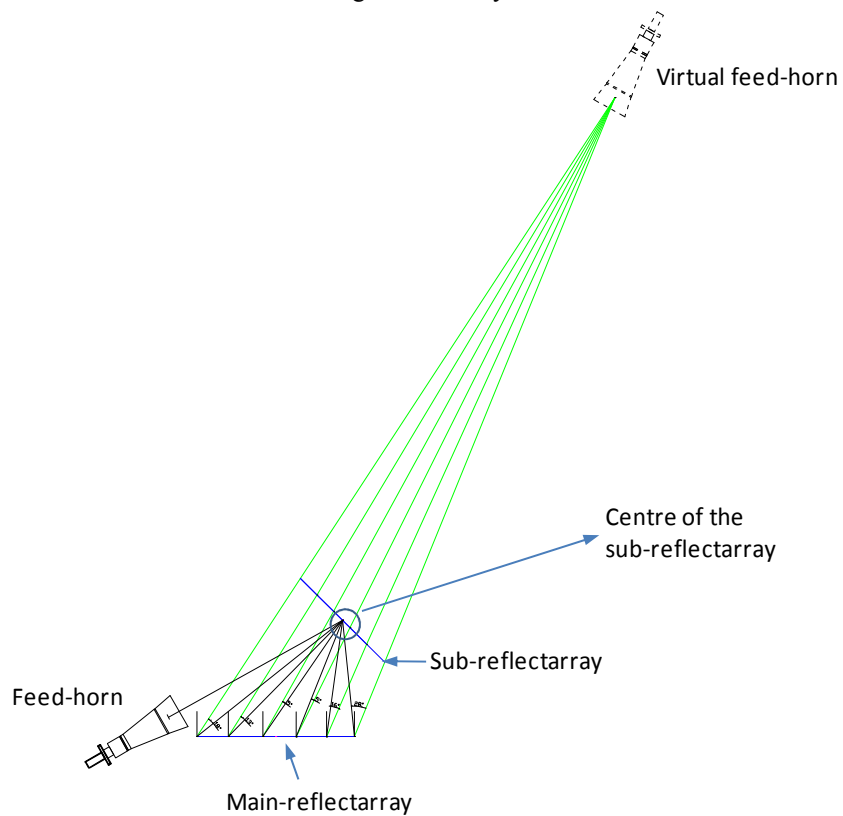


Fig. 4-40. Scheme of the dual-reflectorarray system with the path of the field from the centre of the sub-reflectorarray and from the virtual feed-horn

After analyzing the dual offset reflectarray, the radiation pattern must be similar to the results obtained in the single offset design formed by the main-reflectarray and the virtual feed-horn. Fig. 4-41 shows the comparison of the two cases. As it can be checked, the level of the cross-polarization for both cases differs in 10 dB approximately, due to errors in the incident angles of the field on the main reflectarray when using the approximation discussed above.

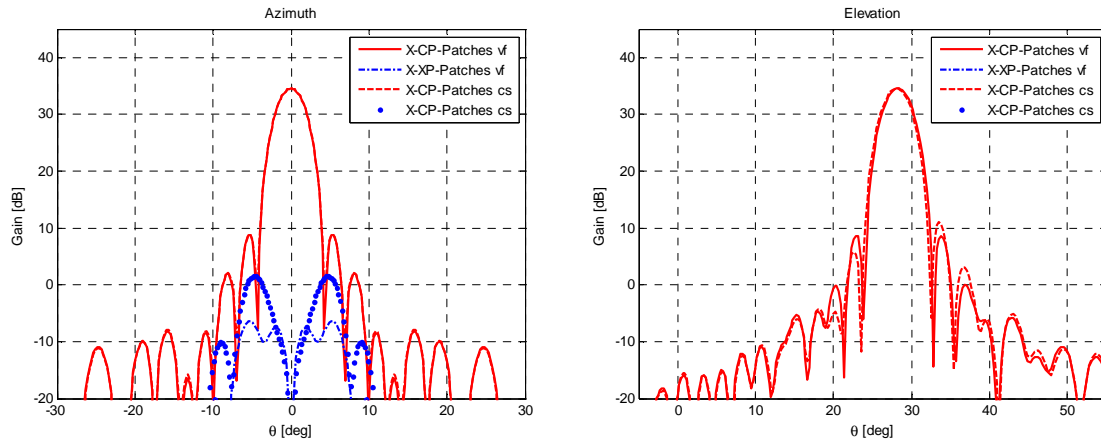


Fig. 4-41. Comparison of radiation patterns for the goal case and for the approximate case

To avoid the errors in the incident angles of the field on the main reflector, it is necessary to apply the technique explained in section 2.4.2 of Chapter 2, which consists on dividing the aperture of the sub reflectarray in groups of elements (sub-arrays) and consider each group as a sub reflectarray. The radiation patterns for vertical polarisation (with the electric field in X direction) are shown in Fig. 4-41. They represent the actual gain, including taper efficiency, spillover and dissipative losses in both reflectarrays. In order to evaluate the losses in both reflectarrays, the radiation patterns have also been computed assuming the ideal phase on each reflectarray, excluding the losses of the materials. Practically the same patterns are obtained, but the maximum value for gain is increased in 0.1dB. Therefore, this is the estimated value for the losses. Apart from the ideal pattern, considered as reference, the rest of the patterns are calculated by analyzing the antenna using Cuclad880 and AD255 for sub and main reflectarray respectively in several cases, which include: without dividing the sub reflectarray and dividing the sub reflector aperture in 4, 9 and 25 groups respectively. Note that the main beam is well reproduced even considering the whole sub reflectarray, but when the sub reflectarray is divided in groups we can see some differences in the sidelobes in cross-polarization. In the azimuth cut, the crosspolar level when the analysis is performed without dividing

the sub reflectarray is much higher than the level obtained when ideal phases are assumed. However when the sub reflectarray is divided, the crosspolar component is getting closer to the ideal case, showing a good convergence of the technique.

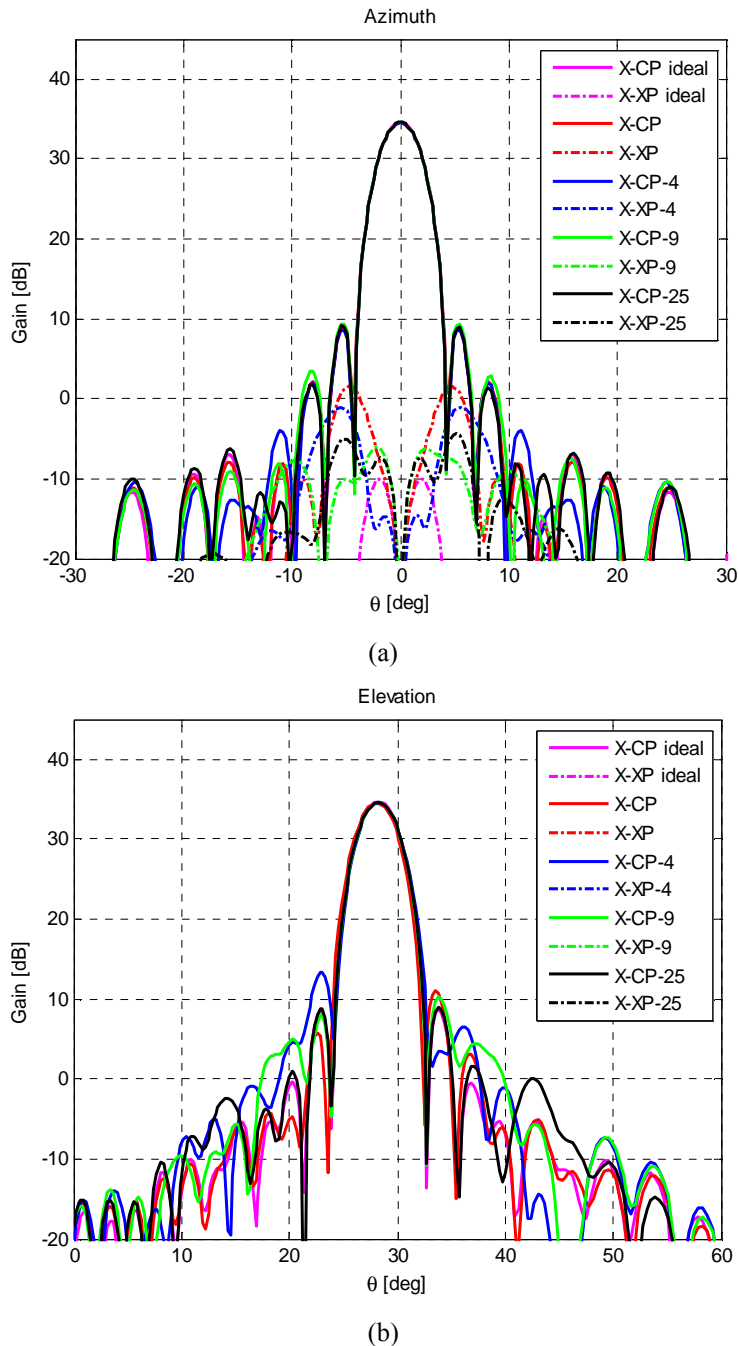


Fig. 4-42. Azimuth (a) and elevation (b) radiation patterns for vertical polarization when using material without losses and when using Cuclad880 and AD255 for sub and main respectively, without dividing the sub reflectarray aperture and dividing the sub reflectarray aperture in 4, 9 and 25 groups at 14GHz

Fig. 4-41 and Fig. 4-42 show the gain and the maximum crosspolar level calculated for the different cases in both polarizations. Crosspolar isolation of 40 dB is achieved for

the designed antenna. Nine samples per cell on the main reflectarray are considered in the calculation of the radiation pattern, because it provides a more accurate prediction of the gain.

Table 4-6. Comparison of gain level when dividing the sub reflectarray aperture for V-polarisation

Material	Number of groups in the sub-RA aperture	Gain (dBi)	Maximum crosspolar (dBi)
Ideal phases	-	34.73	-10.07
Lossy multilayer structure	1 group	34.58	1.67
	4 groups	34.56	-1.14
	9 groups	34.61	-6.23
	25 groups	34.62	-5.17

Table 4-7. Comparison of gain level when dividing the sub reflectarray aperture for H-polarisation

Material	Number of groups in the sub-RA aperture	Gain (dBi)	Maximum crosspolar (dBi)
Ideal phases	-	34.73	-10.07
Lossy multilayer structure	1 group	34.60	1.57
	4 groups	34.61	-0.7
	9 groups	34.63	-5.37
	25 groups	34.62	-4.45

The results when the sub-aperture is divided into 25 groups and those obtained considering the virtual focus as origin of the field are also compared. The first case converges to the goal as it can be checked in Fig. 4-43. Also a good agreement is observed in the cross-polarization, as shown in Fig. 4-43. Fig. 4-44 shows the amplitude of the cross-polar component for the field reflected by the main reflectarray. It can be seen how this component becomes lower when the accurate analysis technique is applied. Fig. 4-45 shows the cuts in elevation and azimuth when the sub reflectarray aperture is iteratively divided in 4, 9 or 25 groups of elements, increasing the accuracy of the prediction of the cross-polarization.

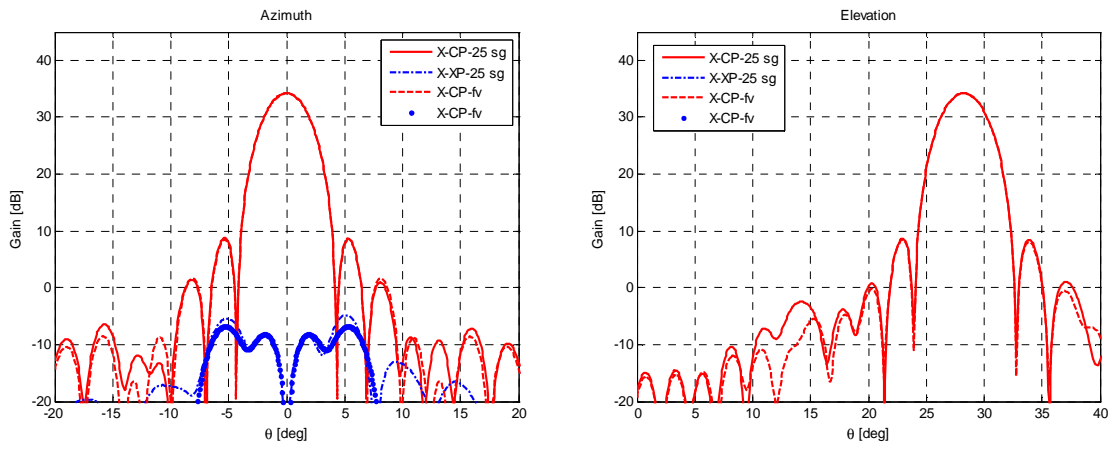


Fig. 4-43. Comparison between radiations patterns for vertical polarization for two cases: the virtual focus is considered the origin of the field and the sub reflectarray aperture is divided into 25 groups

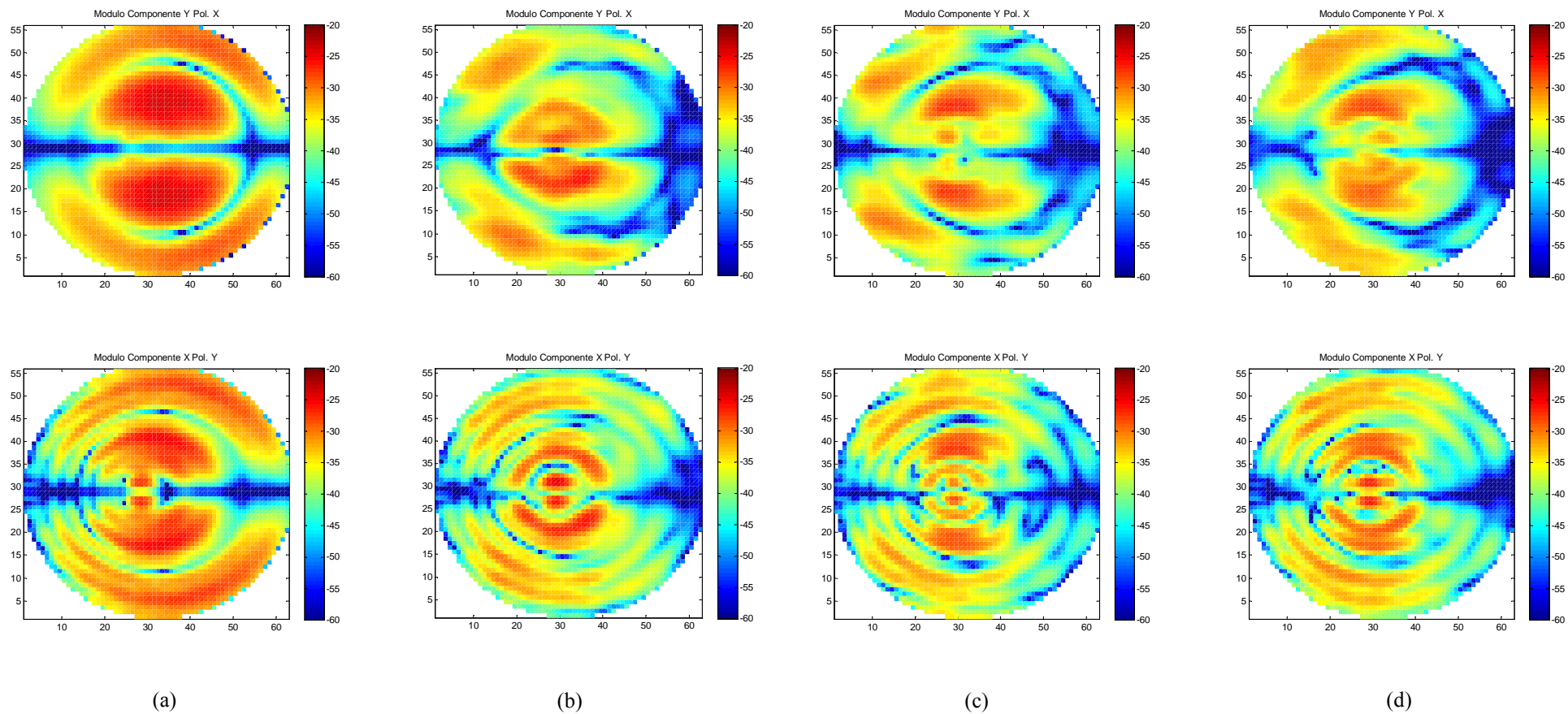


Fig. 4-44. Module of crosspolar component of reflected field for the main-reflectorarray (a) without dividing the sub reflectarray aperture (b)dividing the sub reflectarray aperture in 4 groups (c) dividing the sub reflectarray aperture in 9 groups (d) dividing the sub reflectarray aperture into 25 groups

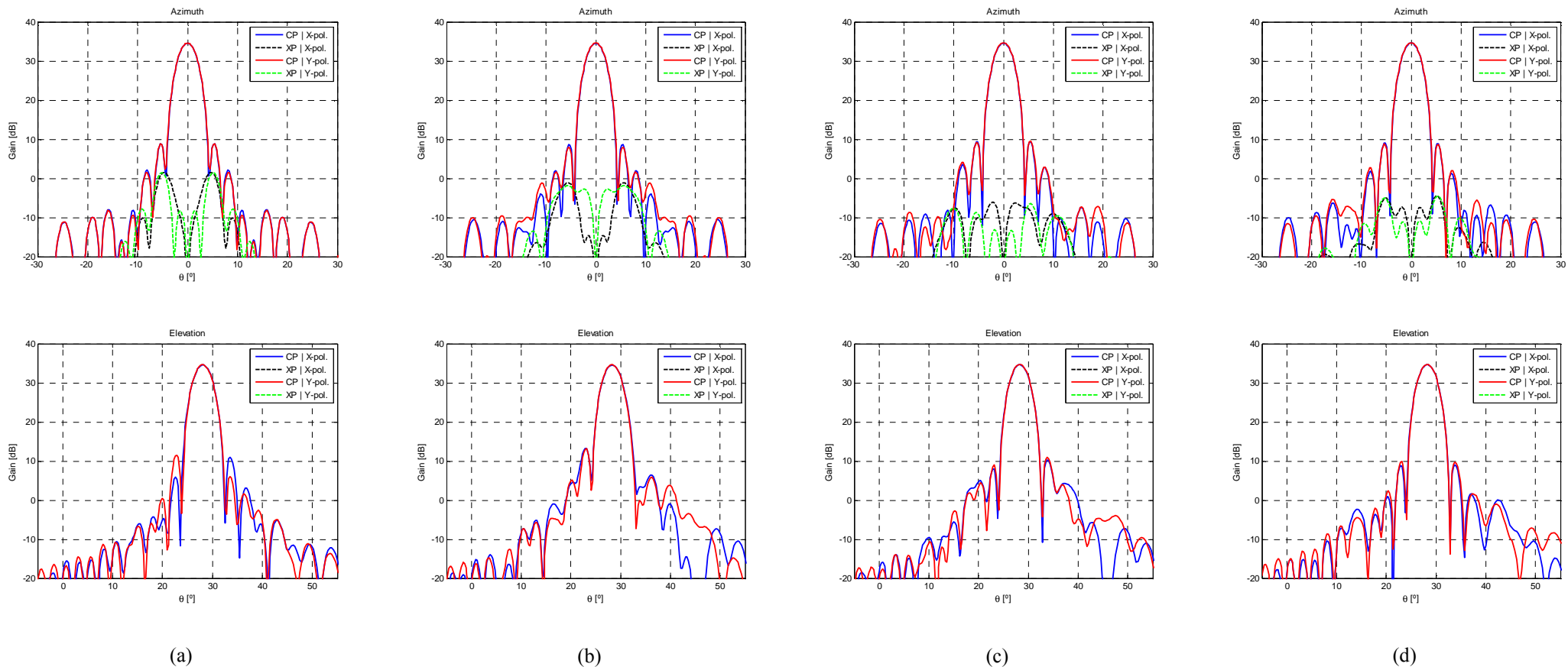
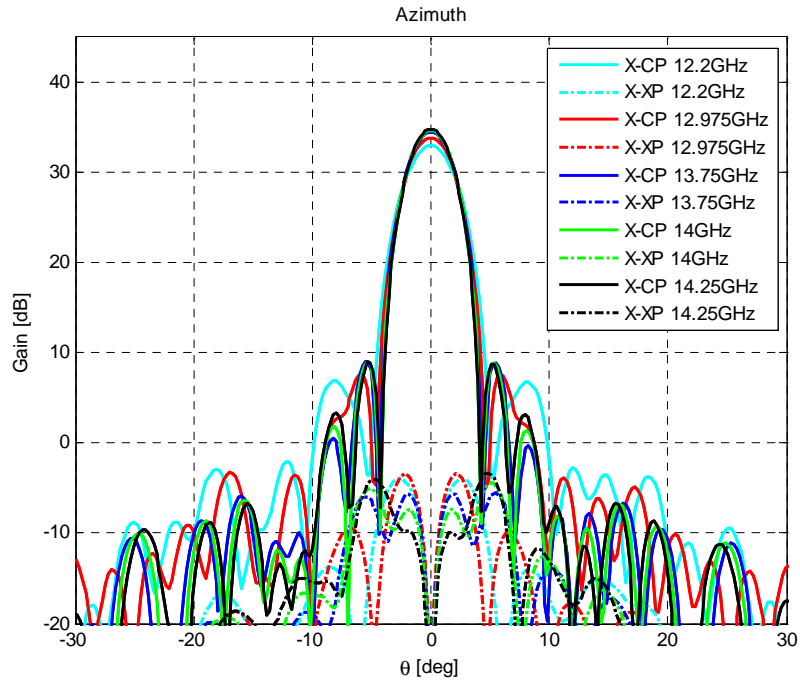
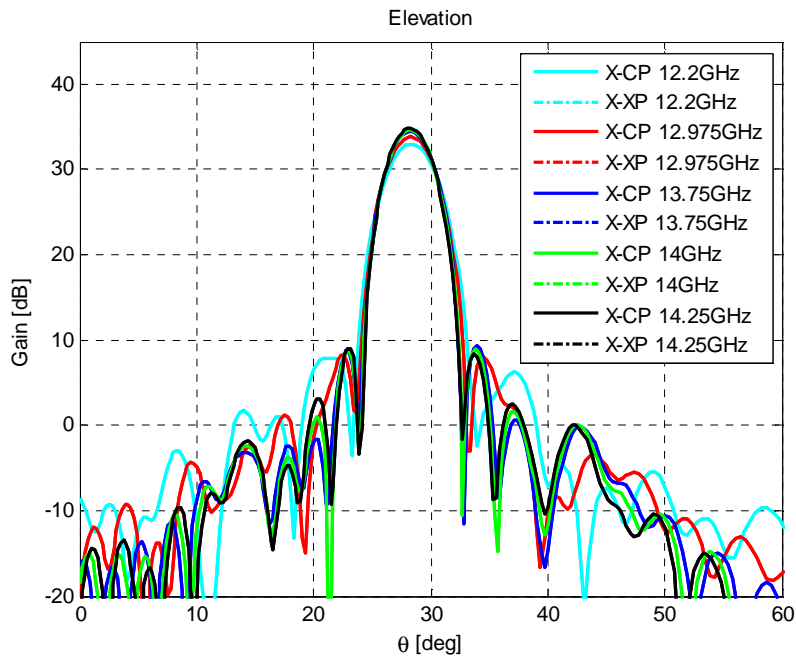


Fig. 4-45. Cuts in elevation and azimuth (a) without dividing the sub reflectarray aperture (b)dividing the sub reflectarray aperture in 4 groups (c) dividing the sub reflectarray aperture in 9 groups (d) dividing the sub reflectarray aperture into 25 groups

Fig. 4-46 shows the co- and cross-polar patterns at 12.2, 12.975, 13.75, 14 and 14.25 GHz for vertical polarization. All the values are given in gain, and the dissipative losses in the reflectarrays are considered. These simulations are run considering the aperture divided into 25 groups taking 9 samples per patch. The main data of these patterns are summarized in Table 4-8.



(a)



(b)

Fig. 4-46. Azimuth (a) and elevation (b) radiation patterns for vertical polarization at 12.2, 12.975, 13.75, 14 and 14.25GHz

Table 4-8. Comparison of gain level when dividing the sub reflectarray aperture for H-polarisation

Gain (dBi)	12.2GHz	12.975GHz	13.75GHz	14GHz	14.25GHz
V-pol-CP	32.99	33.8	34.44	34.62	34.78
V-pol-XP	-3.85	-3.29	-5.14	-4.4	-3.39

Finally, it must be noted that although the breadboard has been design at 14GHz the radiation pattern at other frequencies in the band is not distorted.

4.3 Prototype Manufacturing

The antenna demonstrator has been manufactured and tested in an anechoic chamber. The printed arrays are produced by conventional photo etching techniques, and are then attached to a support structure to ensure the correct positioning of all the elements in the antenna.

4.3.1 *Photo-etching masks*

The patches are printed on the Arlon substrates in a single piece for each layer in both main and sub reflectarray. The layouts with the dimensions of the patches are generated in AutoCAD using the patch sizes computed in the electrical design. For the sub reflectarray, there are two masks corresponding to the two layers, the bottom and the upper one, see Fig. 4-47 and Fig. 4-48. The mask of the main-reflectarray is depicted in Fig. 4-49

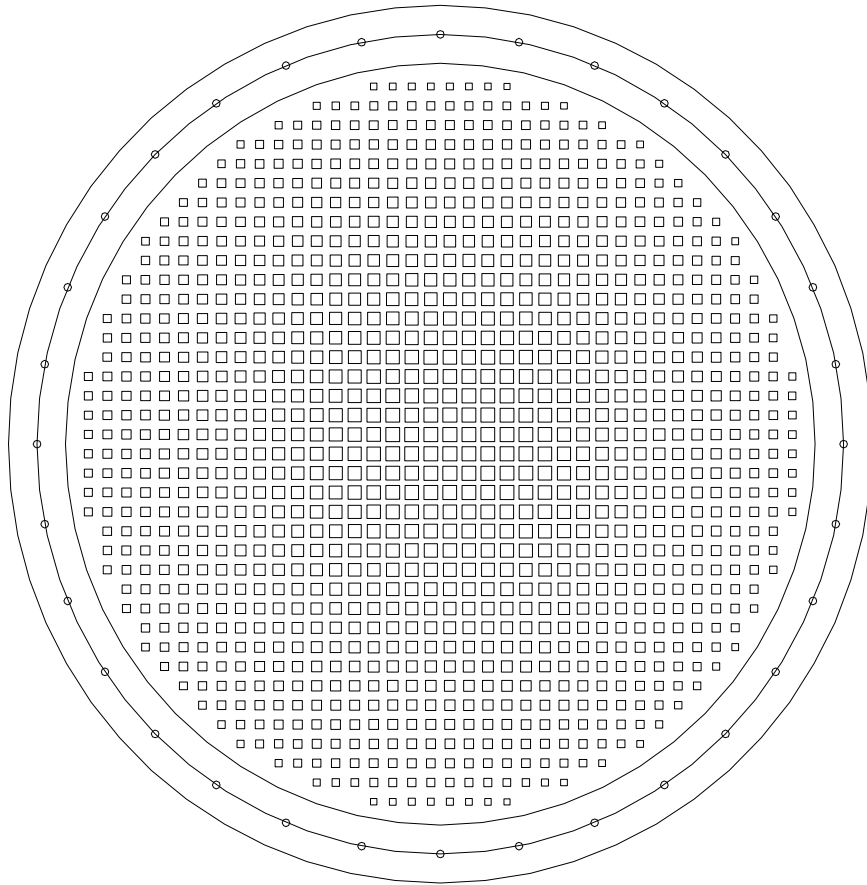


Fig. 4-47. Photo etching mask of the bottom layer for the sub reflectarray

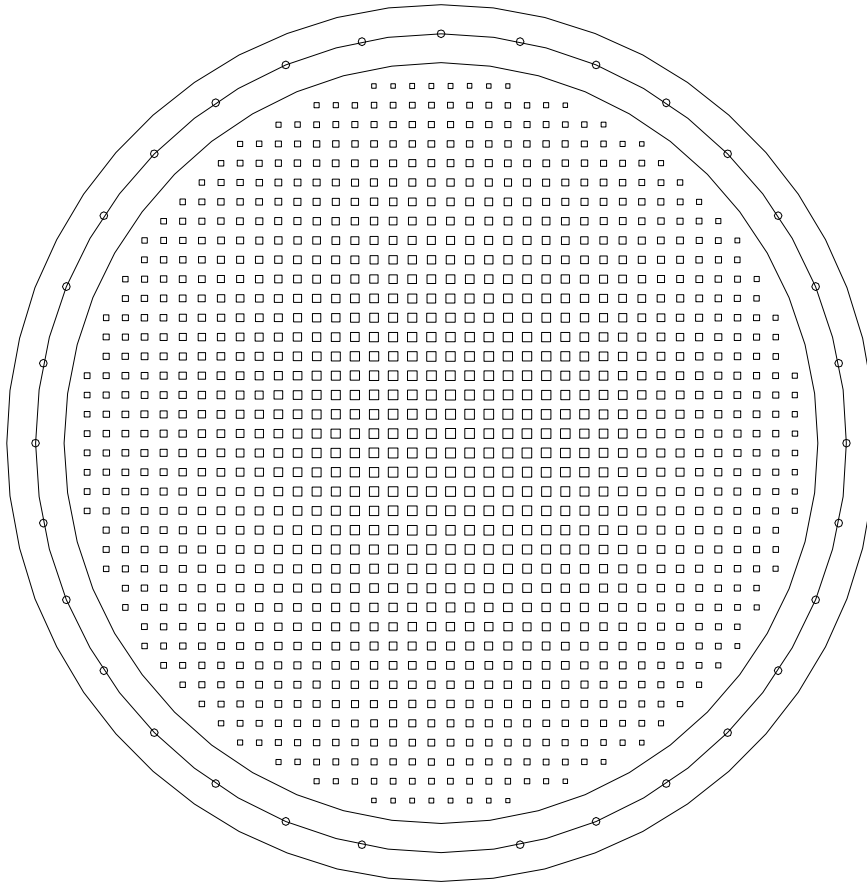


Fig. 4-48. Photo etching mask of the upper layer for the sub reflectarray

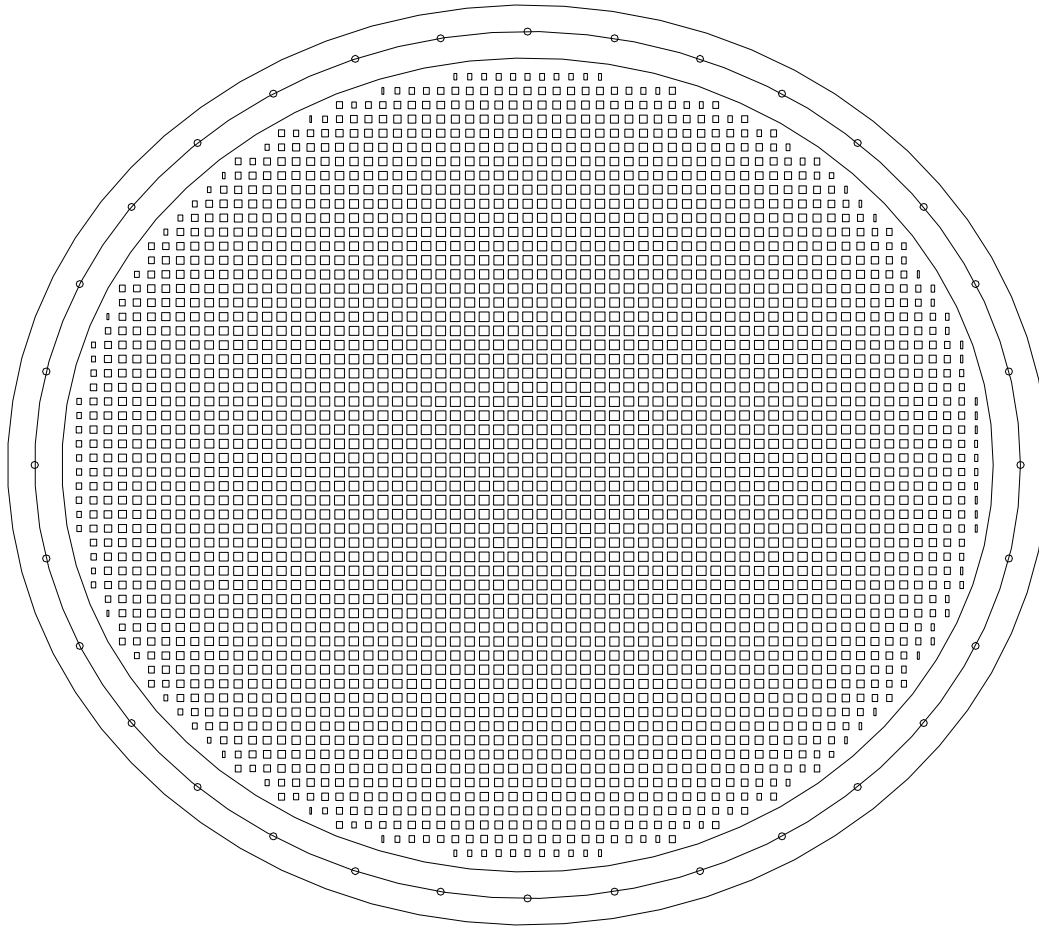


Fig. 4-49. Photo etching mask for the main-reflectorarray

4.3.2 *Prototype assembling*

The dual-reflectorarray antenna has been manufactured and assembled on a support structure (see Fig. 4-50) at the facilities of the Department of Electromagnetism and Circuit Theory at Universidad Politécnica de Madrid (UPM), Spain. The sub reflectarray (sub-RA) breadboard consists of two layers of cuclad-copper foils (CuClad217LX) and thermoplastic bonding film (CuClad6250 TBF) used to glue both layers of cuclad. A backside stiffening sandwich with FR4 is used to support the reflecting layers. The main reflectarray is made up of a single layer of Arlon (AD255) and the same FR4 sandwich as the one used for the sub reflector, see Fig. 4-51.

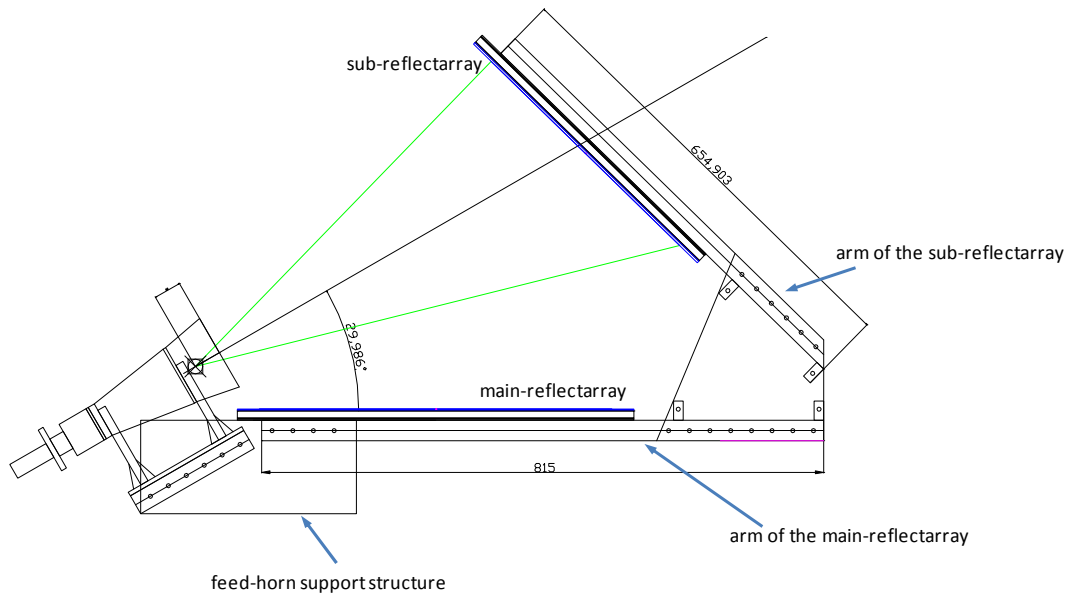


Fig. 4-50. AutoCAD scheme for the dual-reflectarray infrastructure

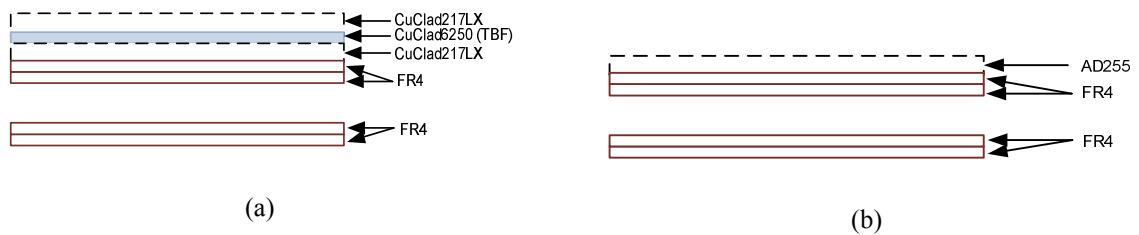


Fig. 4-51. Design of the sub reflectarray panel (a) and main-reflectarray panel (b)

The manufacturing of the sub reflectarray panel was performed according to the established cure cycles for the Thermo Plastic Bonding film of Arlon. Two aluminum plates were used to produce pressure to the curing sandwich (CuClad217LX-CuClad6250-CuClad217LX). Then the FR4 layers were assembled into the sandwich. The manufactured sub reflectarray breadboard panel is shown in Fig. 4-51 (a). For the main reflectarray the four layers of FR4 were assembled according to the Fig. 4-51 (b). The result is the antenna breadboard of Fig. 4-52.

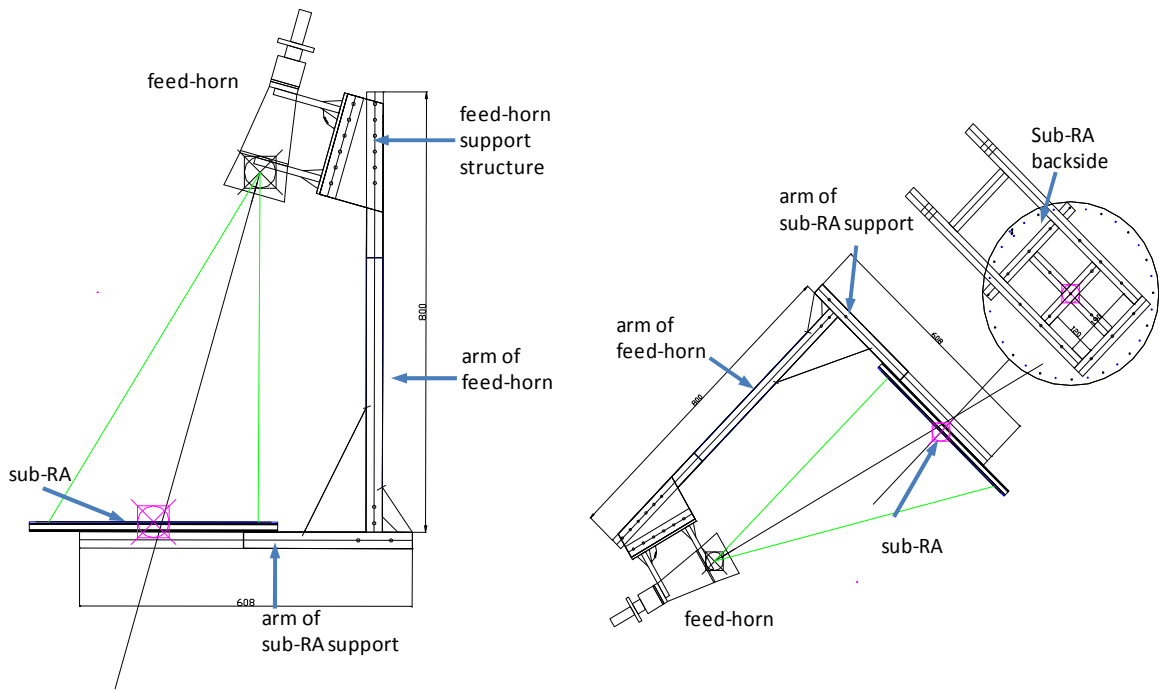


Fig. 4-53. AutoCAD scheme for the sub reflectarray support structure



Fig. 4-54. Sub reflectarray breadboard

4.4 Electrical test

The breadboard has been measured in the anechoic chamber of LEHA-UPM (Laboratorio de Ensayos y Homologación de Antenas- Universidad Politécnica de Madrid). The measurements in the compact antenna test range provided the main cuts in elevation and azimuth for both polarizations.

4.4.1.1 Sub reflectarray test

As a first step, a validation of the sub reflectarray is carried out. Fig. 4-55 shows a picture of the sub reflectarray breadboard in the anechoic chamber of UPM and Fig. 4-56 and Fig. 4-57 point out the measured radiation patterns obtained. Table 4-9 and Table 4-10 resume the levels of gain and the maximum values of cross-polarization for both polarizations in the sub reflectarray. As it can be checked in the radiation pattern, the sub reflectarray presents a stable performance in the measured frequency band (12.97-14.25 GHz).



Fig. 4-55. Sub reflectarray breadboard in the compact range anechoic chamber

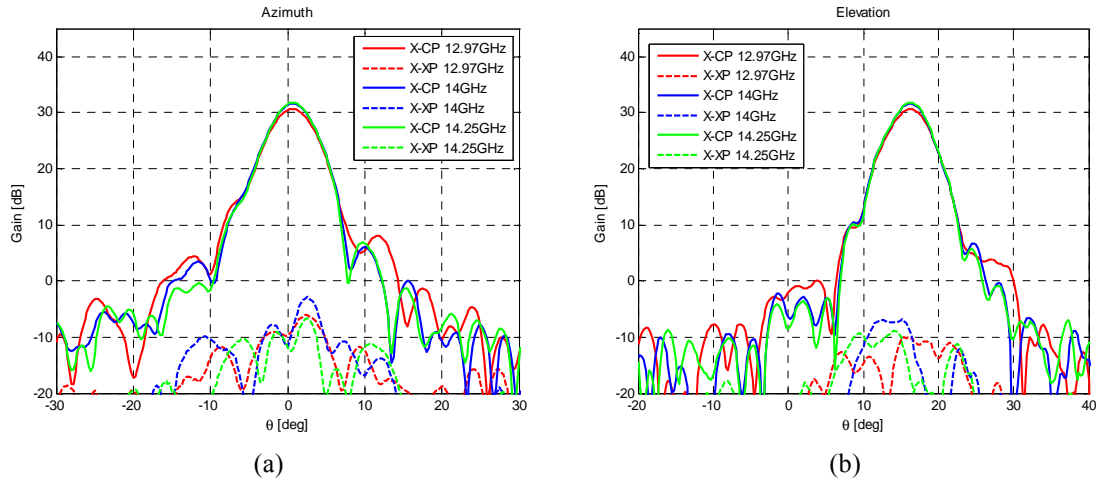


Fig. 4-56. Azimuth (a) and elevation (b) cuts of the measured radiation pattern for vertical polarization at 12.97, 14 and 14.25GHz

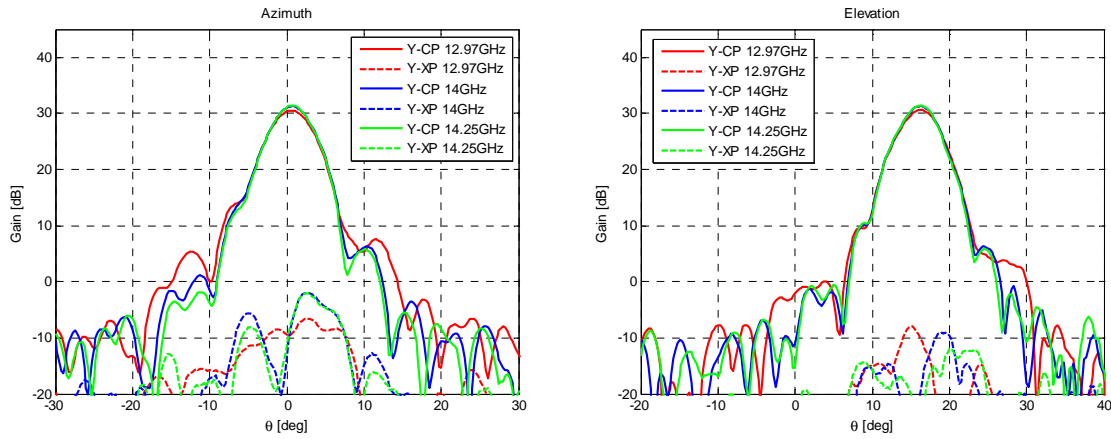


Fig. 4-57. Azimuth (a) and elevation (b) cuts of the measured radiation pattern for horizontal polarization at 12.97, 14 and 14.25GHz

Table 4-9. Values of measured gain for V polarisation at several frequencies for the sub-RA

Frequency(GHz)	Gain (dBi)	Maximum Crosspolar (dBi)
12.97	30.63	-6.1
14.0	31.68	-2.88
14.25	31.8	-6.6

Table 4-10. Values of measured gain for H polarisation at several frequencies for the sub-RA

Frequency(GHz)	Gain (dBi)	Maximum Crosspolar (dBi)
12.97	30.55	-6.51
14.0	31.32	-1.95
14.25	31.4	-2.07

4.4.1.2 Antenna test

Finally, a measurement of the azimuth and elevation cuts of the dual-reflectarray antenna for vertical and horizontal polarizations at five different frequencies is performed. Fig. 4-58 shows a picture of the antenna breadboard in the compact range anechoic chamber. The antenna shows a good performance in the whole measured frequency band (12.2-15 GHz). As it can be checked in the radiation patterns shown in Fig. 4-59 and Fig. 4-60 , the dual reflectarray antenna presents a stable and satisfactory behavior at all frequencies. Table 4-11 and

Table 4-12 summarize the levels of gain and the maximum values of cross-polarization in the antenna system.



Fig. 4-58. Installation of the breadboard in the compact range anechoic chamber

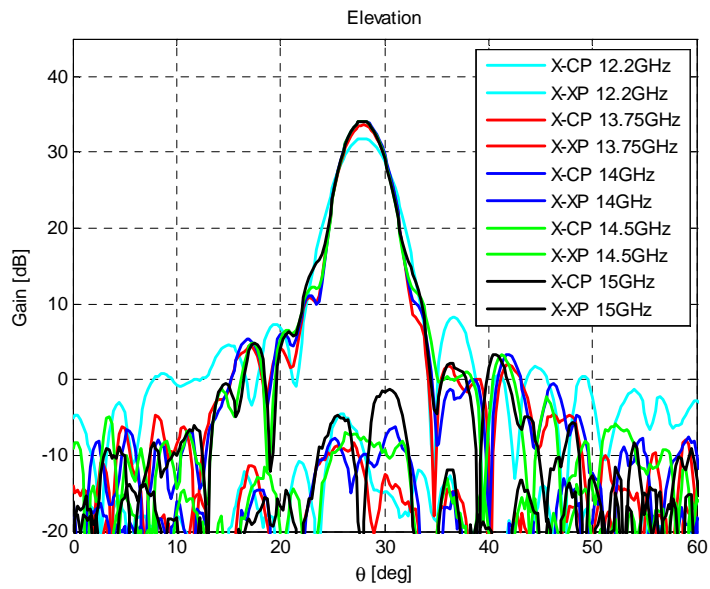
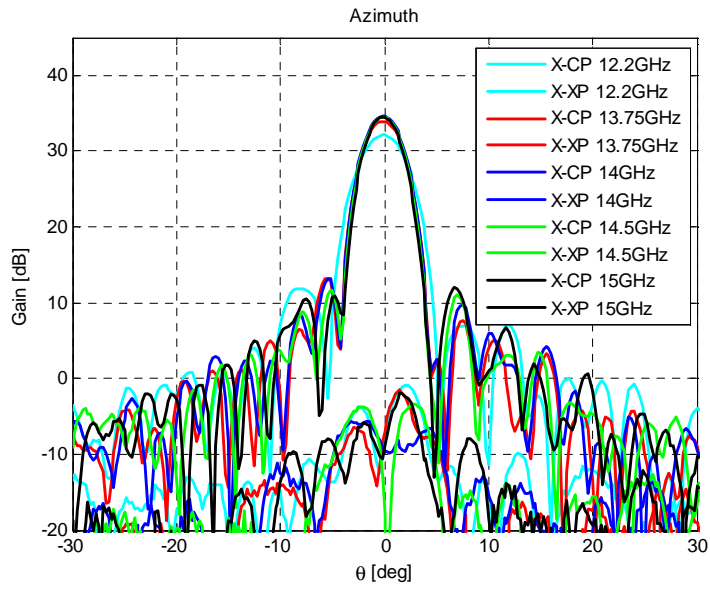
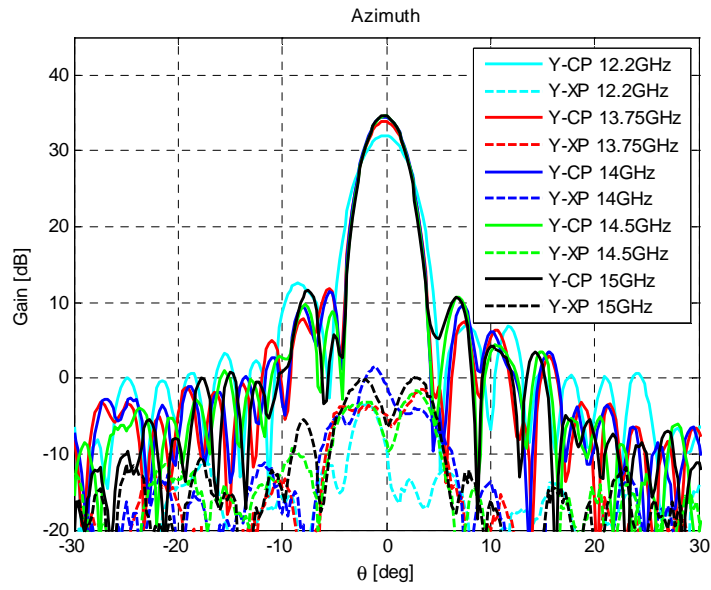
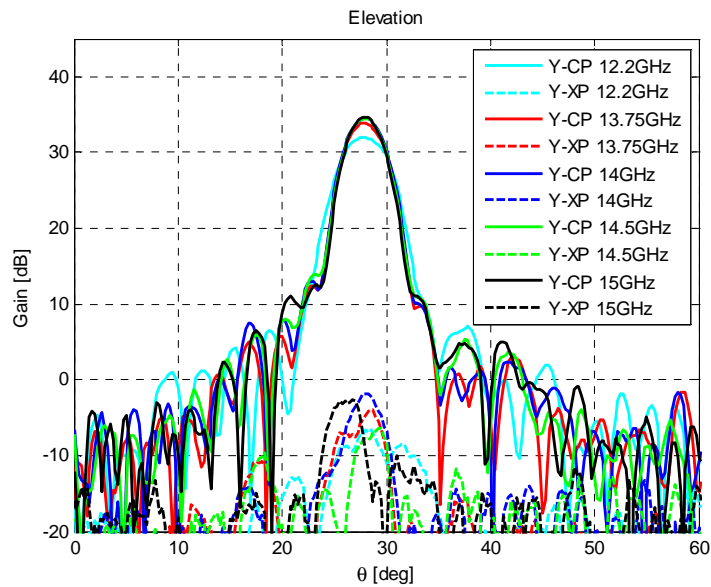


Fig. 4-59. Azimuth (a) and elevation (b) cuts of the measured radiation pattern for vertical polarization at 12.2, 13.75, 14, 14.5 and 15GHz



(a)



(b)

Fig. 4-60. Azimuth (a) and elevation (b) cuts of the measured radiation pattern for horizontal polarization at 12.2, 13.75, 14, 14.5 and 15GHz

Table 4-11. Values of measured gain for V polarisation at several frequencies

Frequency(GHz)	Gain (dBi)	Maximum Crosspolar (dBi)
12.2	32.12	-0.89
13.75	33.94	-1.49
14.0	34.56	-5.56
14.5	34.53	-3.36
15.0	34.51	-1.88

Table 4-12. Values of measured gain for H polarisation at several frequencies

Frequency(GHz)	Gain (dBi)	Maximum Crosspolar (dBi)
12.2	32.05	-3.41
13.75	33.94	-1.48
14.0	34.54	1.49
14.5	34.56	-1.68
15.0	34.65	0.27

4.4.2 Validation of the analysis technique

The validation of the analysis technique consists of two parts: a first comparison between the simulated and tested radiation patterns of the sub reflectarray and secondly a validation of the simulated and measured radiation patterns of the antenna system is performed.

4.4.2.1 Sub reflectarray validation

As a first step for the validation of the analysis technique, a measurement of the sub reflectarray radiation pattern is carried out. The measured radiation patterns are superimposed onto the simulated radiation patterns in the principal planes at 12.97 GHz, 14 GHz and 14.25 GHz as shown in Fig. 4-61, Fig. 4-62 and Fig. 4-63 respectively.

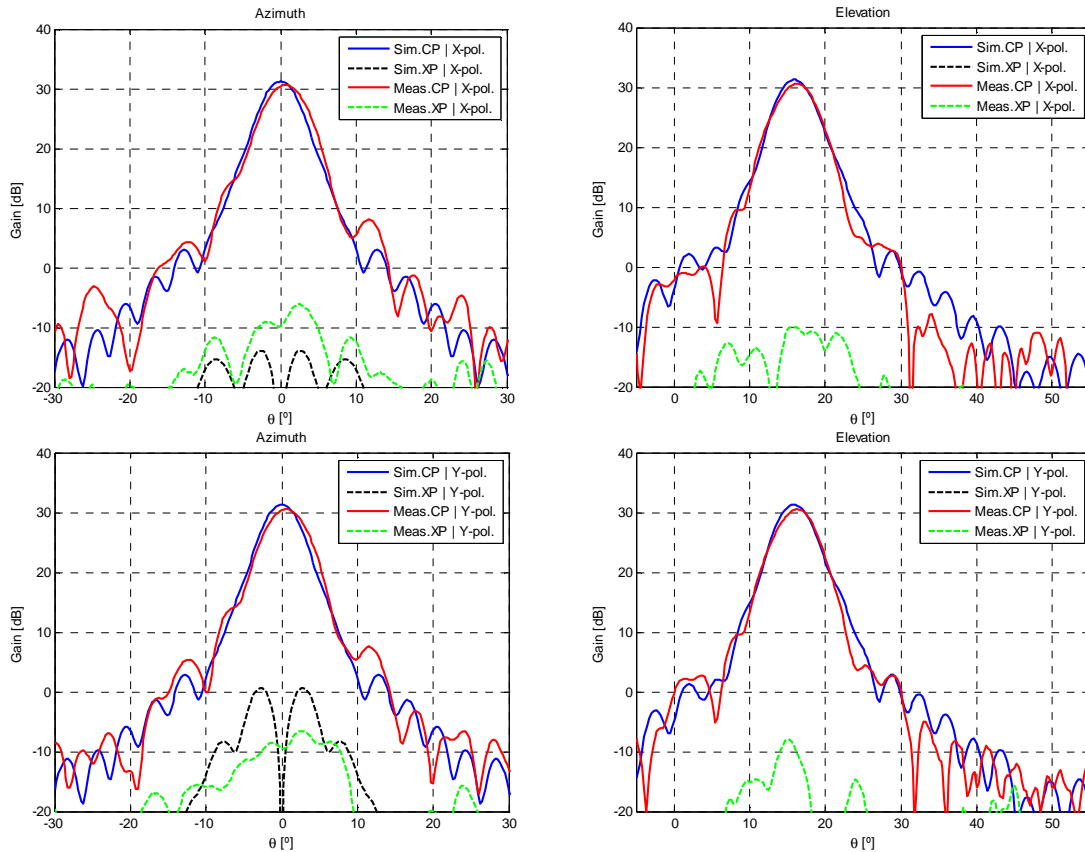


Fig. 4-61. Comparison of simulated and measured azimuth and elevation cuts at 12.97 GHz

The measured radiation patterns show some discrepancies with respect to the simulations, basically slight differences in the side lobes. These distortions in the radiation patterns are the result of some phase errors produced by tolerance errors in the dimensions of the patches. It was checked that to make a proper bonding of the two dielectric layers in the sub reflectarray, two layers of thermoplastic bonding film were needed. Table 4-13 and Table 4-14 show the comparison between the maximum levels of the co-polar and cross-polar components of the simulated and measured radiation patterns of the sub reflectarray.

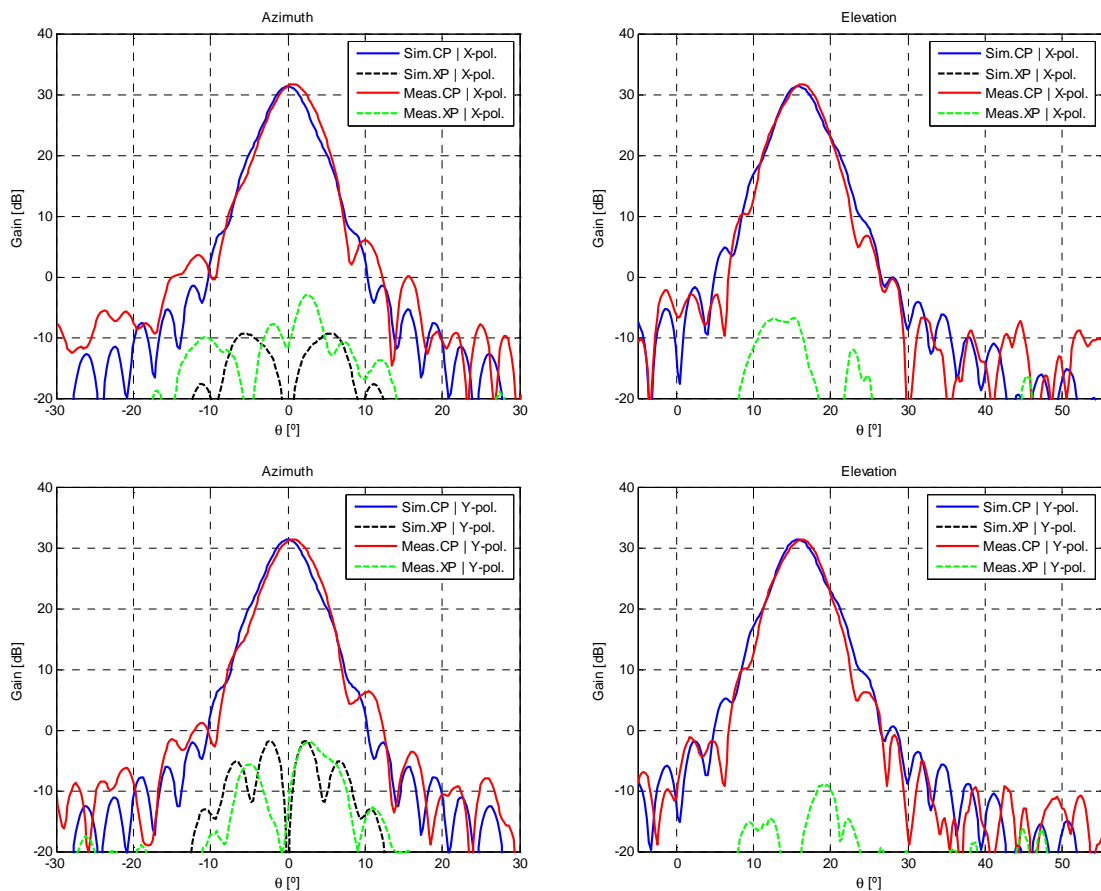


Fig. 4-62. Comparison of simulated and measured azimuth and elevation cuts at 14 GHz

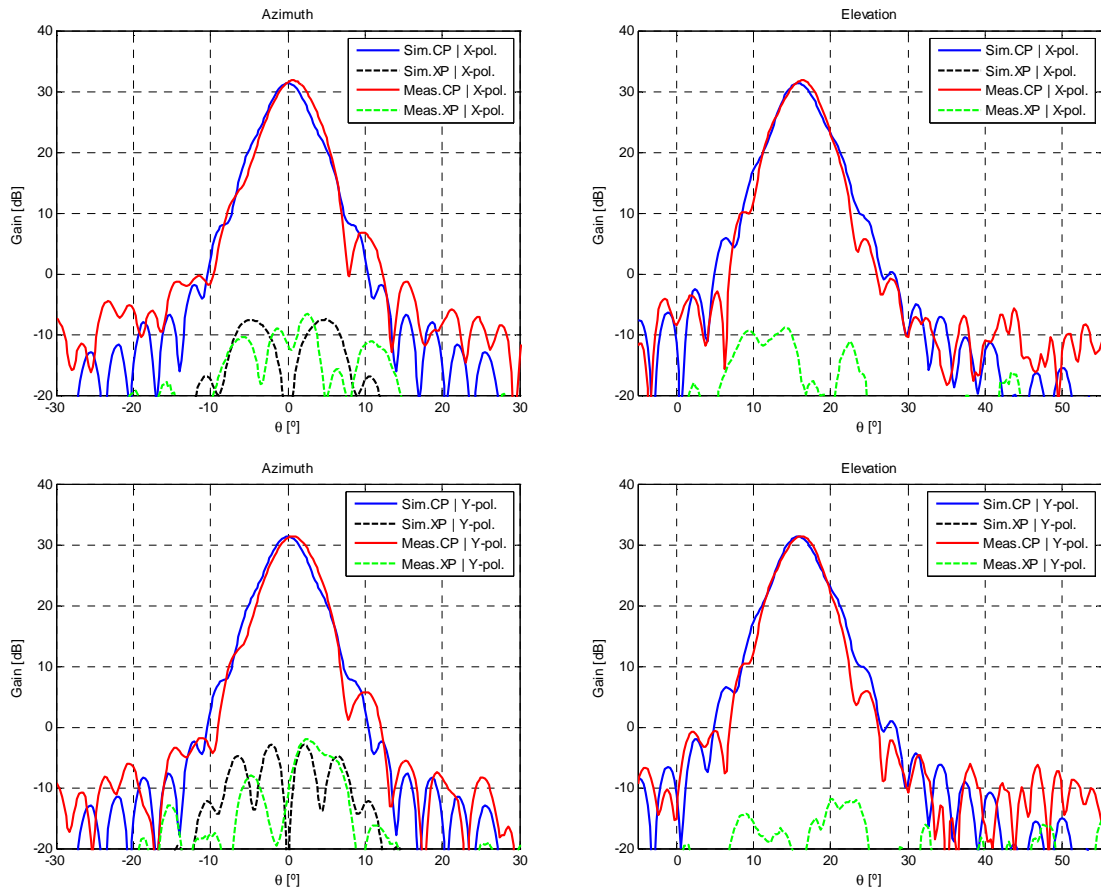


Fig. 4-63. Comparison of simulated and measured azimuth and elevation cuts at 14.25 GHz

Table 4-13. Comparison of gain levels and maximum cross-polarization between the simulated and measured radiation patterns of the sub reflectarray for vertical polarization

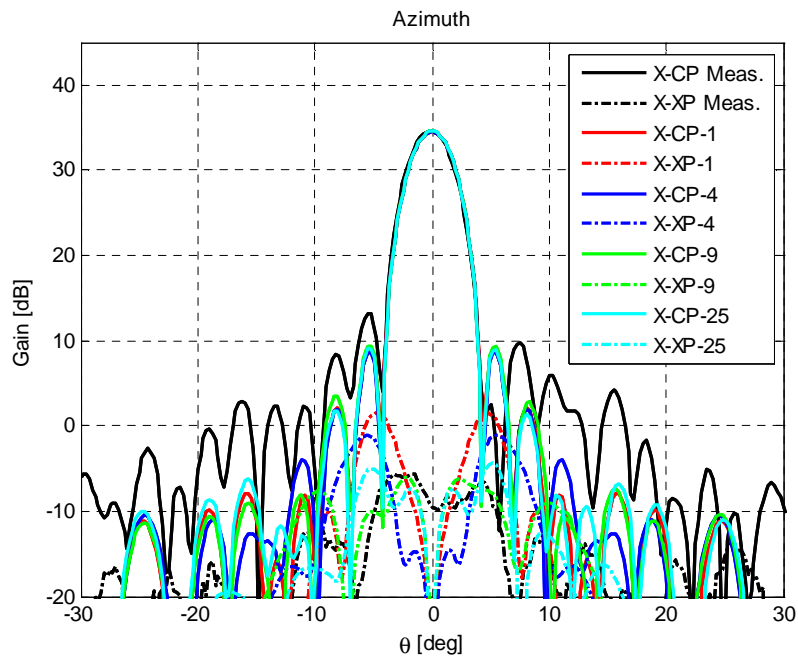
Frequency(GHz)	Sim. Gain (dBi)	Mea. Gain (dBi)	Max. XP.Sim (dBi)	Max. XP.Mea. (dBi)
12.97	31.24	30.63	-11.39	-6.1
14.0	31.34	31.68	-6.1	-2.88
14.25	31.33	31.8	-4.63	-6.6

Table 4-14. Comparison of gain levels and maximum cross-polarization between the simulated and measured radiation patterns of the sub reflectarray for horizontal polarization

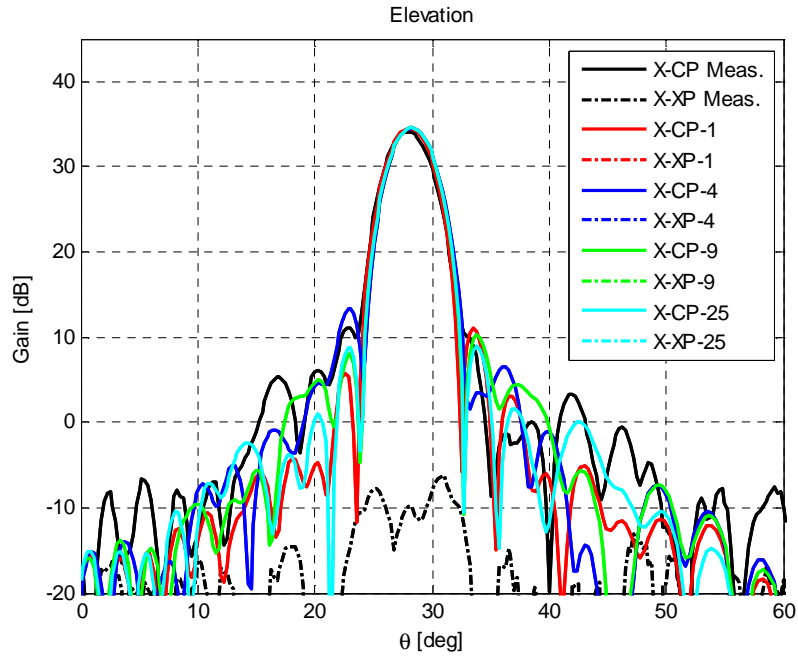
Frequency(GHz)	Sim. Gain (dBi)	Mea. Gain (dBi)	Max. XP.Sim (dBi)	Max. XP.Mea. (dBi)
12.97	31.33	30.55	0.61	-6.51
14.0	31.33	31.32	-1.76	-1.95
14.25	31.32	31.4	-2.8	-2.07

4.4.2.2 Antenna validation

For the validation of the analysis technique, the measured radiation patterns of the antenna are superimposed onto the simulated radiation patterns when the sub reflectarray is divided in several groups. Fig. 4-64 shows the convergence of the simulated azimuth and elevation cuts to the measured radiation patterns at 14 GHz. Then, the radiation pattern simulated dividing the sub reflectarray in 25 groups are superimposed with the measurements for all the measured frequencies: 12.2 GHz, 13.75 GHz, 14 GHz and 14.25 GHz, as it can be checked in Fig. 4-65 to Fig. 4-68. The simulated cross-polarization is zero in elevation because it is a symmetry plane. However, Fig. 4-64(b) shows certain level of cross-polarization in the elevation cut of the measurements, this corresponds to the floor noise of the test-bed used in the compact range anechoic chamber of UPM, since only signals with levels of gain that are less than 40 dB below the maximum can be measured.



(a)



(b)

Fig. 4-64. Comparison of simulated (dividing the sub reflectarray in 1,4,9 and 25 groups) and measured azimuth (a) and elevation (b) cuts at 14 GHz

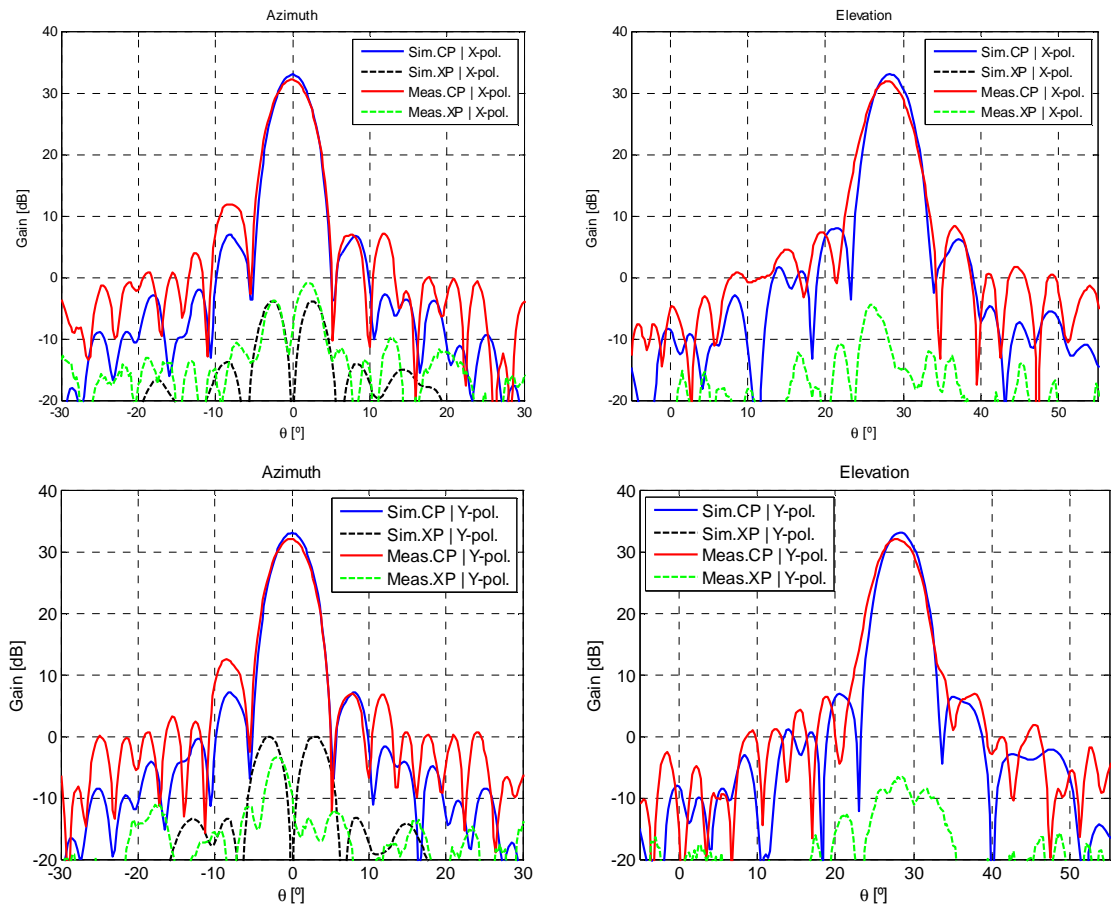


Fig. 4-65. Comparison of simulated and measured azimuth and elevation cuts at 12.2 GHz

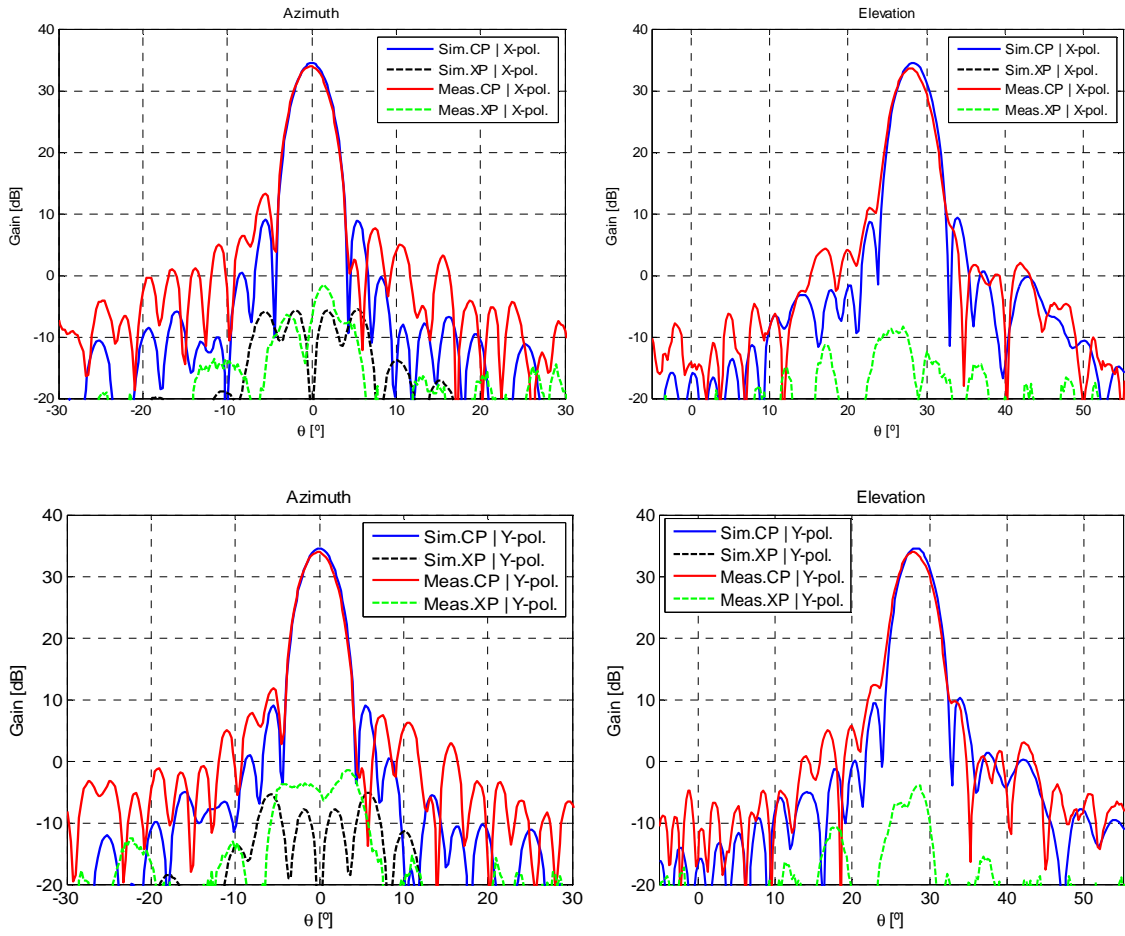


Fig. 4-66. Comparison of simulated and measured azimuth and elevation cuts at 13.75 GHz

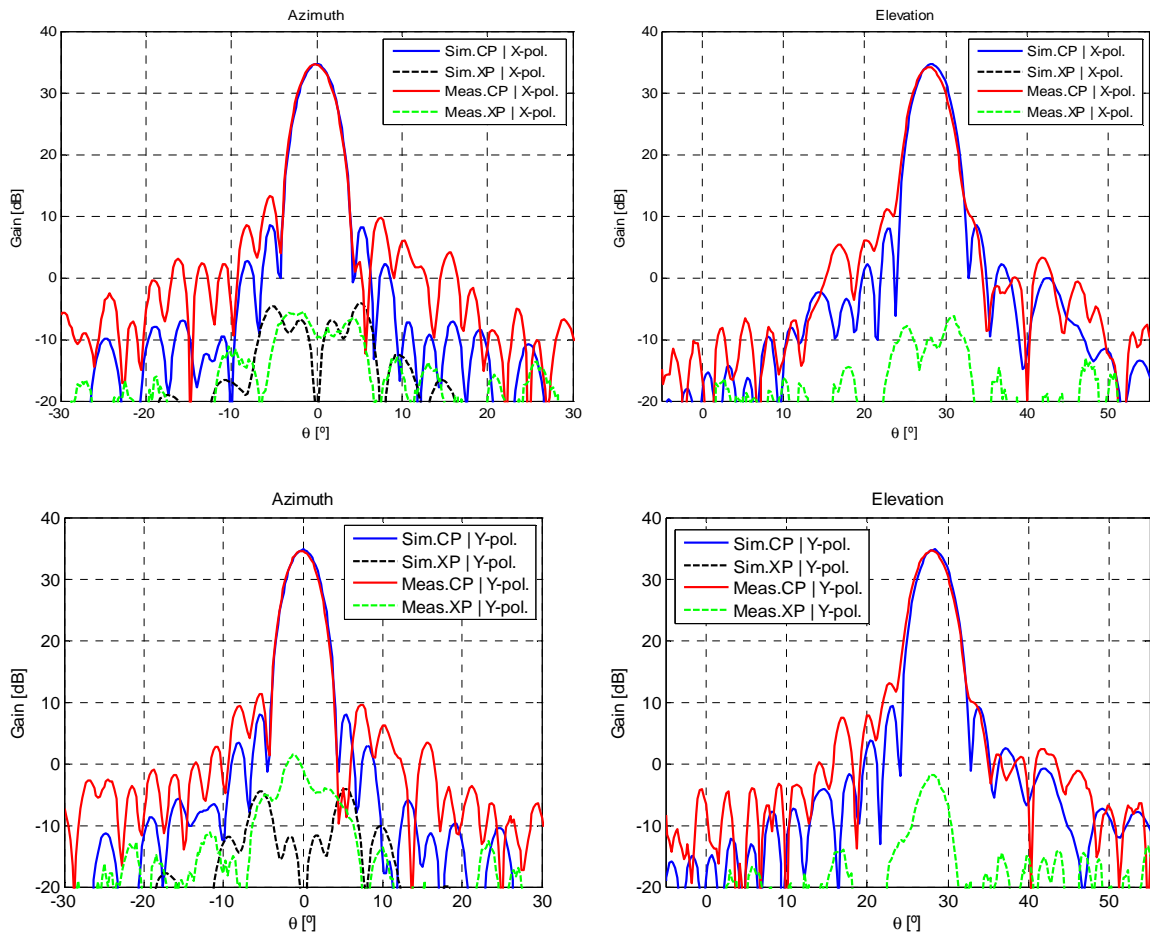


Fig. 4-67. Comparison of simulated and measured azimuth and elevation cuts at 14GHz

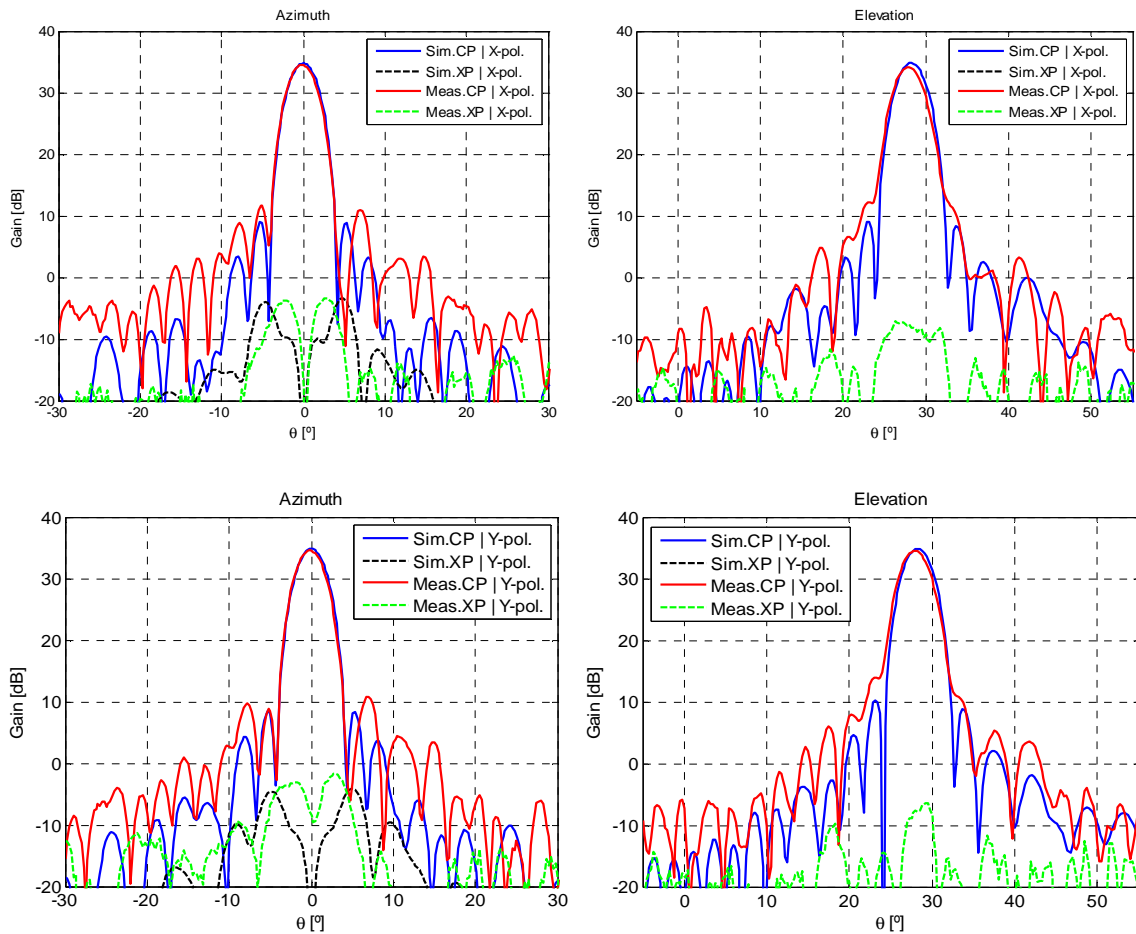


Fig. 4-68. Comparison of simulated and measured azimuth and elevation cuts at 14.25GHz

Although the radiation patterns simulated are in very good agreement with the measurements, there are some discrepancies basically in the side lobes which are more significant at lower frequencies. The distortions in the side lobe levels and the cross-polarization of the radiation patterns is due to the manufacturing tolerances that produce slightly asymmetric diagrams in the azimuth cut even when the antenna is symmetric. The patch dimensions have been measured in some selected patches of the two layers of the sub reflectarray and on the single layer main-reflectarray, showing that the patch dimensions are always smaller than the nominal values. Note that the radiation patterns behave slightly worse for lower frequencies since the patch dimensions in the two layers are 50 microns smaller than expected, which is an average value for the measured errors. On the other hand, the random tolerance errors produce a slight asymmetry in the azimuth cut of the radiation patterns.

Table 4-15. Comparison of gain levels and maximum cross-polarization between the simulated and measured radiation patterns for vertical polarization

Frequency(GHz)	Sim. Gain (dBi)	Mea. Gain (dBi)	Max. XP.Sim (dBi)	Max. XP.Mea. (dBi)
12.2	32.99	32.12	-3.85	-0.89
13.75	34.44	33.94	-5.14	-1.49
14.0	34.65	34.56	-4.12	-5.56
14.25	34.78	-	-3.39	-
14.5	-	34.53	-	-3.36
15	-	34.51	-	-1.88

Table 4-16. Comparison of gain levels and maximum cross-polarization between the simulated and measured radiation patterns for horizontal polarization

Frequency(GHz)	Sim. Gain (dBi)	Mea. Gain (dBi)	Max. XP.Sim (dBi)	Max. XP.Mea. (dBi)
12.2	33.04	32.05	-0.02	-3.41
13.75	34.53	33.94	-5	-1.48
14.0	34.74	34.54	-4.01	1.49
14.25	34.85	-	-3.96	-
14.5	-	34.56	-	-1.68
15	-	34.65	-	0.27

4.4.3 *Conclusions*

A dual-flat-reflectarray antenna has been designed, manufactured and tested to generate a focused beam. The antenna is derived from a compact range dual-reflector antenna, where the sub reflectarray emulates a hyperbolic sub reflector and the main-reflectarray emulates a parabolic surface. The antenna has been designed to reduce the cross-polarization levels of the dual-reflectarray antenna in dual linear polarization. The simulation results show a reduction of 9 dB in the levels of cross-polarization, providing a cross-polar discrimination better than 38 dB, which is sufficient for space Telecom antennas. In the measurements, spillover and diffraction effects have been observed at the edges of the sub reflectarray. The comparison of the simulated results with the measurements shows good agreement, however, slight differences in the side lobe levels are observed as a consequence of the tolerance errors of the manufacturing process.

These results provide a powerful validation of the analysis technique proposed in this thesis for dual-reflectarray antennas.

4.5 Improved design of the main-reflectarray using two layers of varying-sized patches.

In this section, the design of a dual-reflectarray antenna with minimum crosspolar based on the geometry described in section 4.2 is improved by using a two-layer reflectarray also in the main reflector. The goal of this design consists on the cancellation of the cross-polarisation introduced by the geometry and the patches of both the sub and the main reflectarray by means of using a two-layer main reflectarray. In addition, the two-layer reflectarray also provides a wider antenna bandwidth.

4.5.1 *Main-reflectarray multilayer configuration*

The sandwich configuration for the two-layer main-reflectarray is shown in Fig. 4-69. The copper patches are printed on a 60-mil dielectric substrate (DiClad880B). Both layers are glued through a thermoplastic bonding film (CuClad6250).

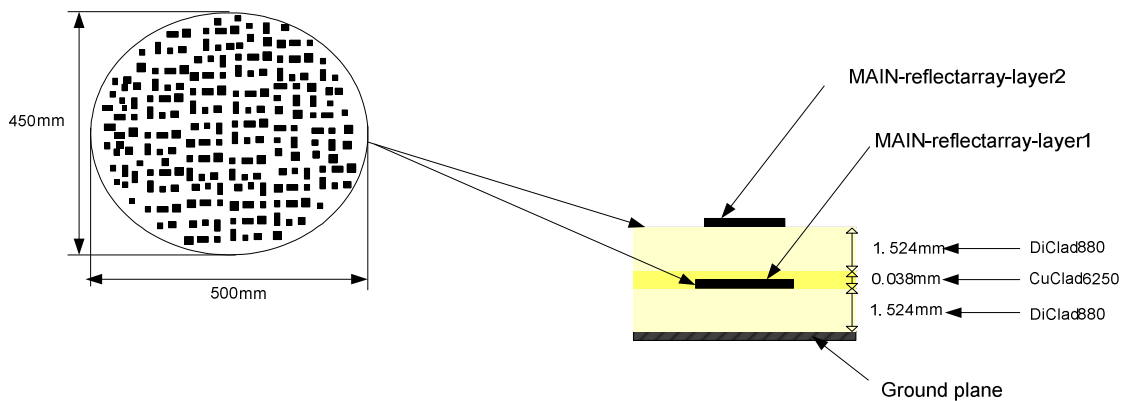


Fig. 4-69. Sandwich configuration of the 2 layers main-reflectarray using DiClad880 and CuClad6250

The phase-shift and losses as a function of the patch size for the design frequency (14GHz) and for ± 1 GHz bandwidth are shown in Fig. 4-70. The dissipative losses in this reflectarray are expected to be around 0.07dB. Fig. 4-71 shows the phase curves and ohmic losses for the main-reflectarray at different incident angles.

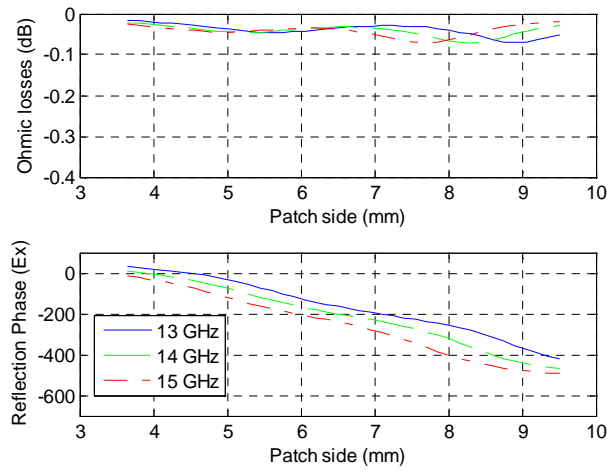
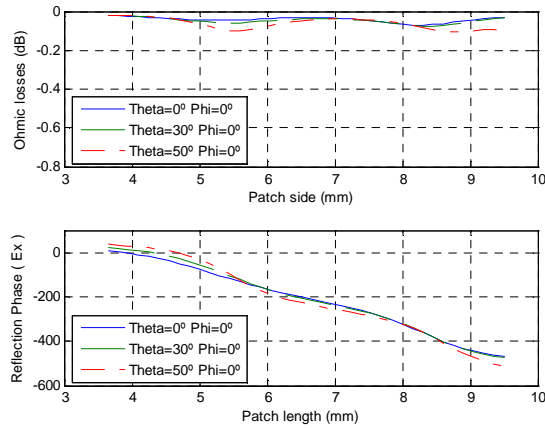
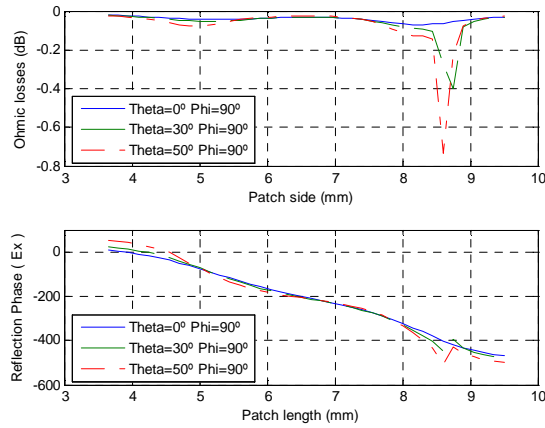


Fig. 4-70. Ohmic losses and phase of the co-polar component at $\phi = 0^\circ$ and different frequencies for the sandwich configuration of the 2-layers main-reflectarray



(a)



(b)

Fig. 4-71. Phase of the co-polar component for the 2-layers main-reflectarray for $\phi = 0^\circ$ (Horizontal polarization)(a) and $\phi = 90^\circ$ (Vertical polarization)

In the two-layer main-reflectarray, the patches are distributed in a rectangular lattice with an elliptical shape of $500 \text{ mm} \times 450 \text{ mm}$. The selected period is 10 mm in x and y axes. This period and the two layers provide a larger phase range which is very

convenient for having more flexibility in the design of the patches. Thus, the main-reflectarray is arranged in 50×45 elements. The resulting sandwich configuration is shown in Fig. 4-69 and the nominal dielectric properties and thickness of each layer on sub and main reflectarrays are in Table 4-17.

Table 4-17. Radio-electric characteristics of the materials for the 2 layers main reflectarray

Dielectric	Nominal ϵ_r	tag δ	Thickness (mm)
Diclad880B	2.17	0.0009	1.524
Cuclad6250 (Thermoplastic bonding film)	2.32	0.0013	0.038

4.5.2 *Main-reflectarray design*

First, a preliminary design of the main reflectarray without applying any correction in the cross-polarization is carried out. The required phase-shift distribution for the main-reflectarray is shown in Fig. 4-72. Then, applying the same technique described in section 4.2 and [48], the patches are designed locating the nulls of the phase curve of the crosspolar component at the patches where the maximum contribution of the crosspolar is detected. The cross-polarization produced by the patches changes becomes null, changing the sign, for patches with sizes between 5.5 mm and 6 mm, as shown in Fig. 4-73.

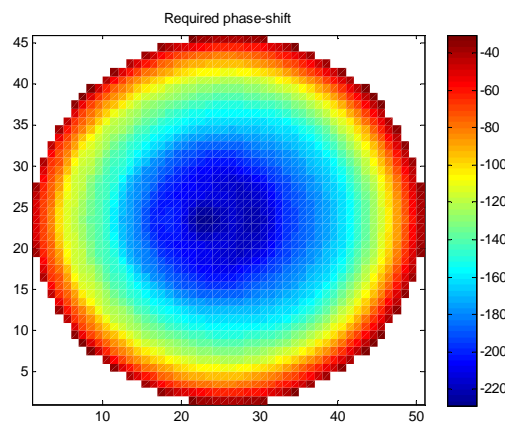


Fig. 4-72. Required phase shift for the 2 layers main-reflectarray

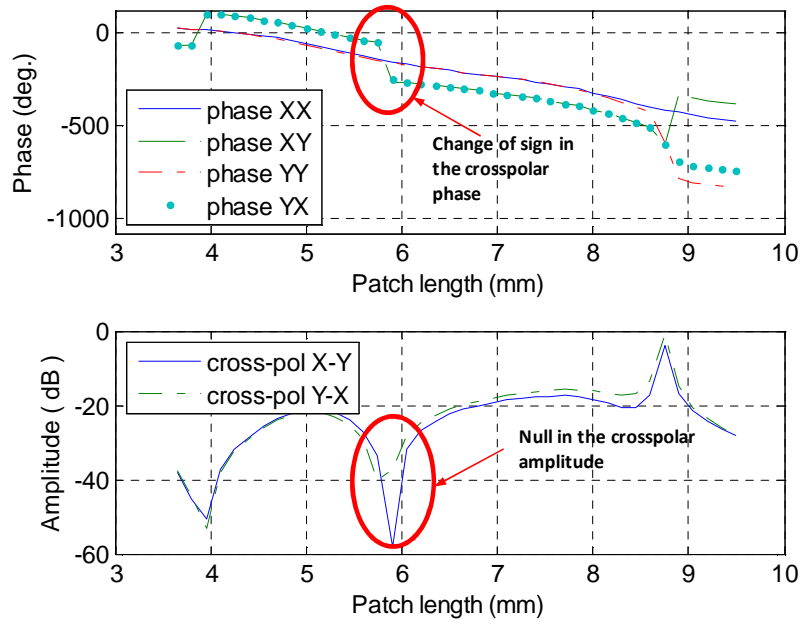


Fig. 4-73. Phase curves as a function of the patch sizes for the 2 layers main-reflector array sandwich

After two iterations following the steps explained in the scheme of Fig. 4-31, a significant reduction of 6 dB is achieved in the crosspolar of the complete design, as it can be checked in Fig. 4-74. The radiation pattern in this case has been calculated taking one sample of incident and reflected field per cell of the main reflector in order to reduce the computation time. A more accurate analysis taking 9 samples per cell on main reflector will be finally performed.

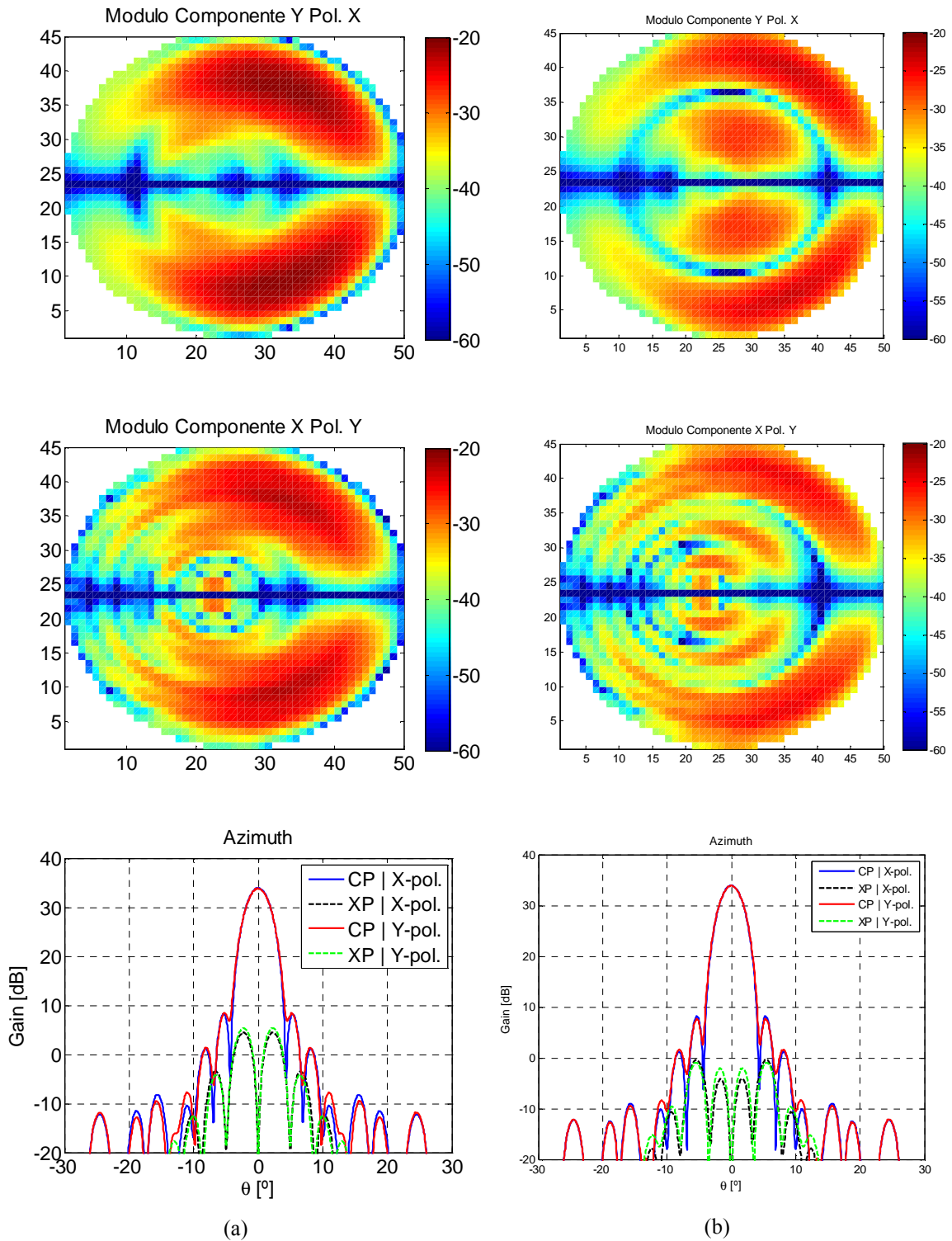


Fig. 4-74. Module of crosspolar component of reflected field for the main-reflectorarray and azimuth cut of radiation pattern generated (a) preliminary design (Iteration 1) (b) design with reduction of the crosspolar (Iteration 2)

Table 4-18 points out the gain and the maximum crosspolar level of the radiation pattern, when the cancellation of cross-polarization is applied. A reduction of more than 5 dB in the crosspolar level is achieved for both polarizations.

Table 4-18. Comparison of gain level when reducing the cross-polarization for both V and H polarizations

Gain(dBi)	Iteration 1	Iteration 2
Gain for V-polarization	33.93	33.92
Max. Crosspolar for V-polarization	4.8	-0.33
Gain for H-polarization	33.9	33.92
Max. Crosspolar for H-polarization	5.7	-0.2

The patch dimensions for the top layer are shown in Fig. 4-75. They are related to the dimensions of the patches of the bottom layer through a constant value of 0.7. Fig. 4-76 shows the average error between the phase produced by the designed patches and the goal phases.

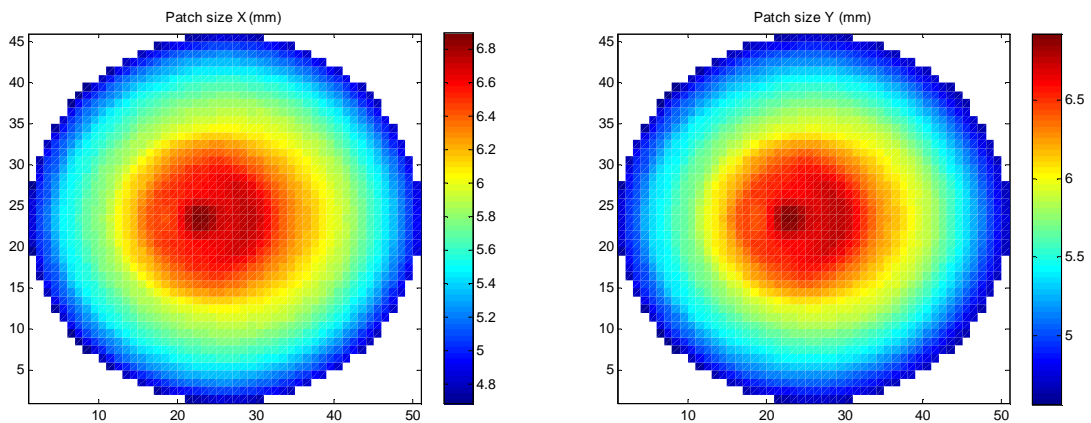


Fig. 4-75. x and y dimensions for the main-reflectarray patches

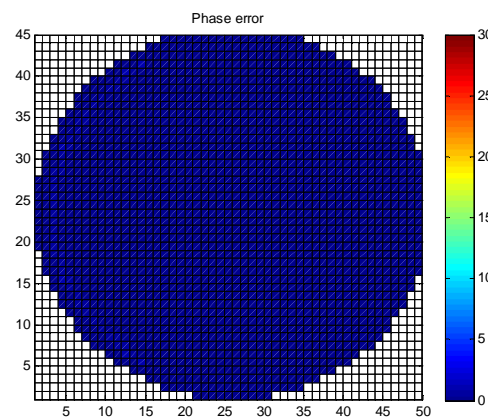


Fig. 4-76. Average error phase for the main-reflectarray patches

As in previous studies, to avoid the errors in the incident angles of the field and perform a more accurate analysis of the structure, the technique consisting on dividing the sub-aperture in sub-arrays is implemented.

Fig. 4-77 shows the crosspolar value of the reflected field when the analysis of the antenna system considers the origin of the incident field on the main reflectarray in the virtual focus, which is the goal case. Fig. 4-78 (a), (b), (c), (d) show the progressive reduction of the cross-polarisation in the reflected field of the main-reflectarray in the following cases: without dividing the sub reflectarray aperture and dividing the sub reflector aperture in 4, 9 and 25 groups respectively. It can be checked how the cross-polarisation gets closer to the expected value shown in Fig. 4-77. The plots of Fig. 4-79 (a), (b), (c), (d) show the radiation patterns for the mentioned cases in the azimuth plane. Table 4-19 and Table 4-20 point out the variation of the maximum crosspolar levels when the sub reflector is divided iteratively in more sub-arrays, getting closer to the goal case and also to the case of considering ideal phases on both printed surfaces, used as reference. Values of XPD better than 40 dB are achieved for both polarizations.

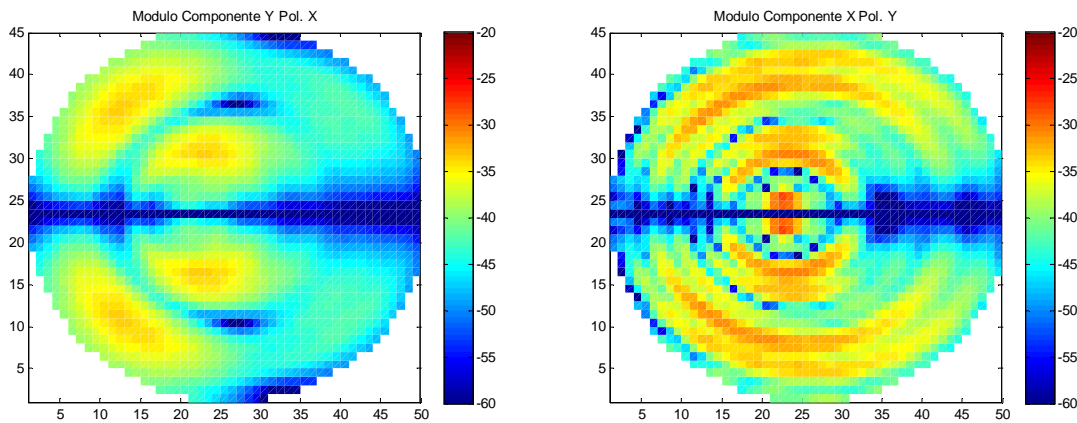


Fig. 4-77. Expected crosspolar value of reflected field on the main-reflectarray

Table 4-19. Comparison of gain level when dividing the main-reflectarray aperture for V-polarisation

Material	Number of groups in the sub-RA aperture	Gain (dBi)	Maximum crosspolar (dBi)
Ideal phases	-	34.73	-10.07
Multilayer structure	1 group	34.53	0.23
	4 groups	34.45	-4.64
	9 groups	34.52	-5.71
	25 groups	34.53	-7.68

Table 4-20. Comparison of gain level when dividing the main-reflectarray aperture for H-polarisation

Material	Number of groups in the sub-RA aperture	Gain (dBi)	Maximum crosspolar (dBi)
Ideal phases	-	34.73	-10.07
Multilayer structure	1 group	34.55	0.33
	4 groups	34.58	-2.31
	9 groups	34.59	-5.26
	25 groups	34.63	-5.86

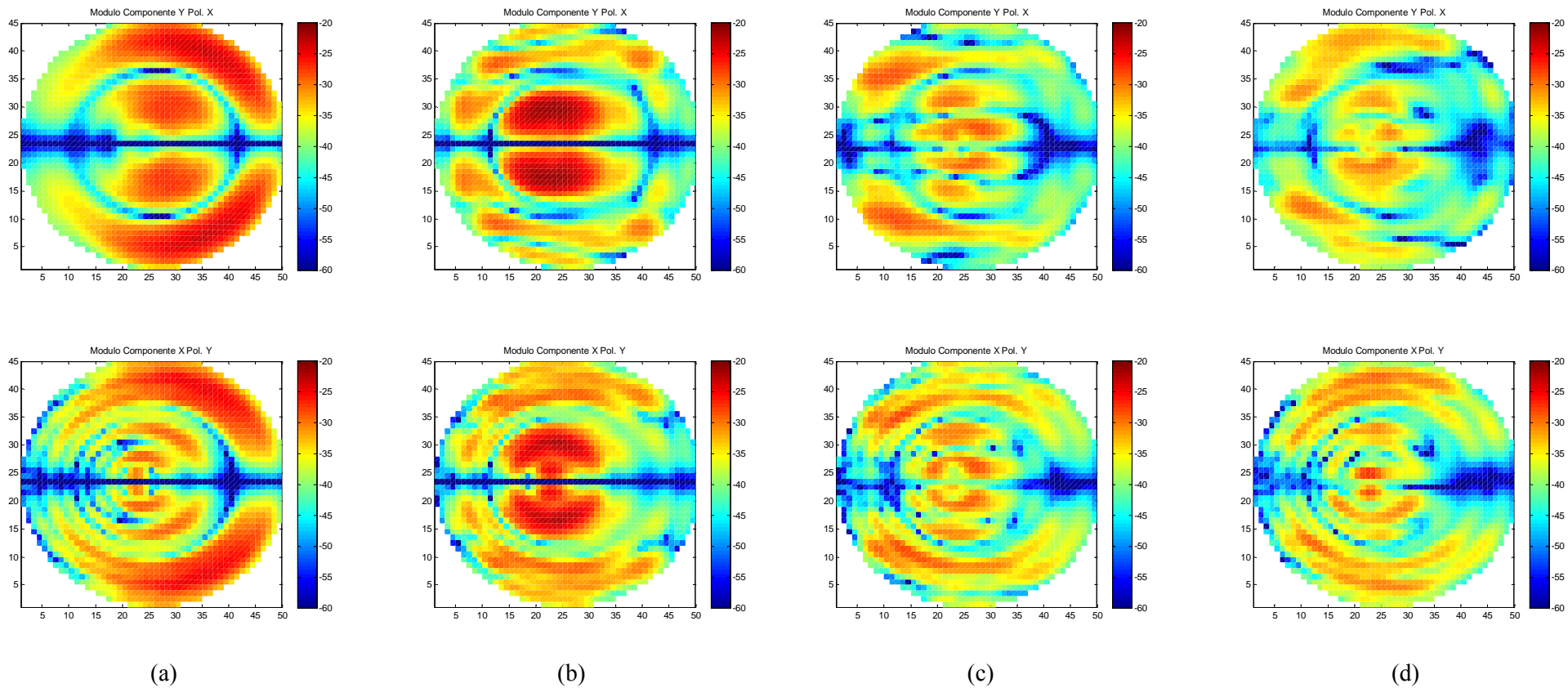


Fig. 4-78. Module of crosspolar component of reflected field for the main-reflectorarray (a) without dividing the sub reflectarray aperture (b) dividing the sub reflectarray aperture in 4 groups (c) dividing the sub reflectarray aperture in 9 groups (d) dividing the sub reflectarray aperture in 25 groups

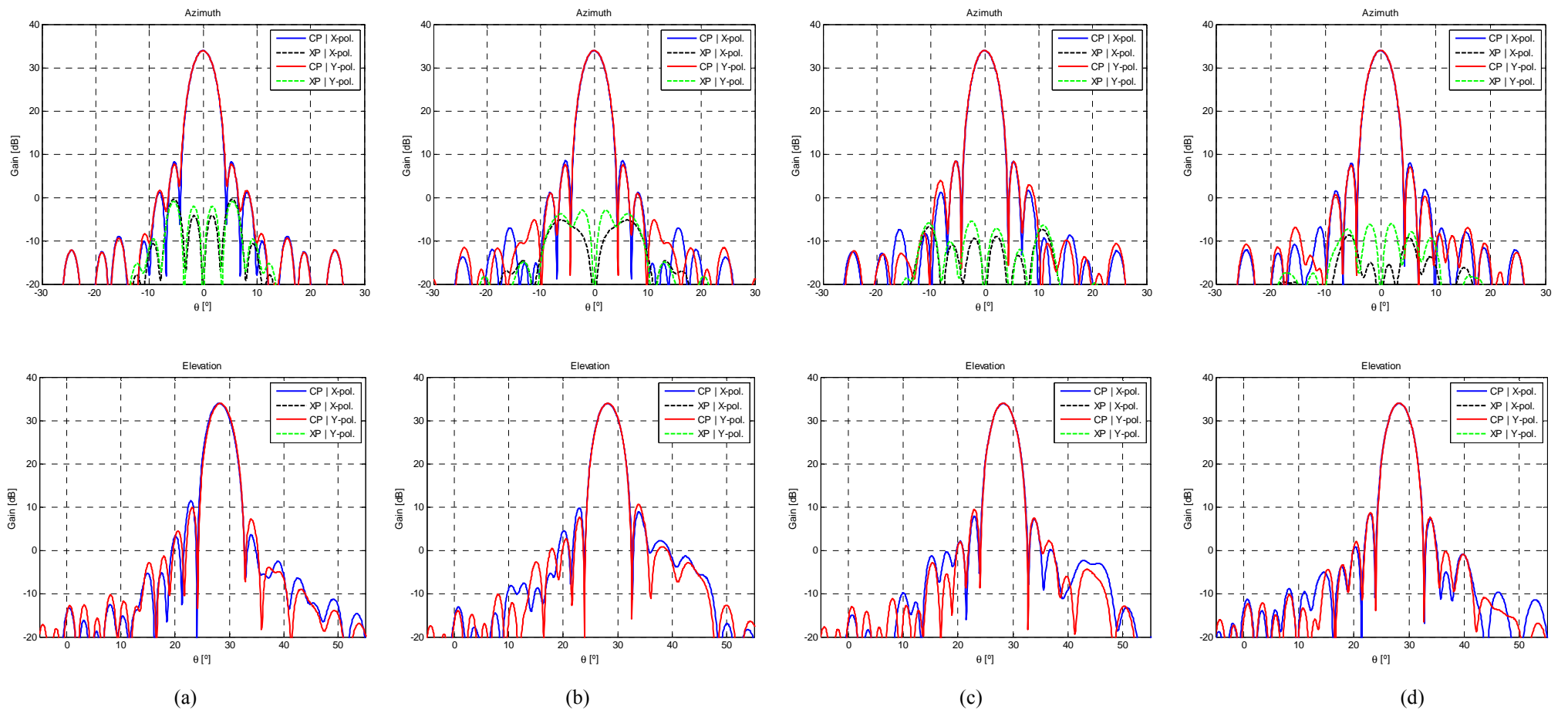


Fig. 4-79. Cuts in elevation and azimuth (a) without dividing the sub reflectarray aperture (b)dividing the sub reflectarray aperture in 4 groups (c) dividing the sub reflectarray aperture in 9 groups (d) dividing the sub reflectarray aperture in 25 groups

In Fig. 4-80, the radiation patterns are compared for the cases considered in the analysis. For the goal case, the main reflectarray is analysed assuming the incident field coming from the virtual focus. For the approximate case, the origin of the field is located in the centre of the sub reflectarray. For the other cases the origin for the incident field on the main reflectarray is assumed to be in the centre or each sub-group, in which the sub reflectarray aperture is divided (4, 9 and 25 sub-groups). Fig. 4-81 demonstrates the convergence of the method of analysis when the sub-aperture is divided in 25 groups since it converges to the goal case.

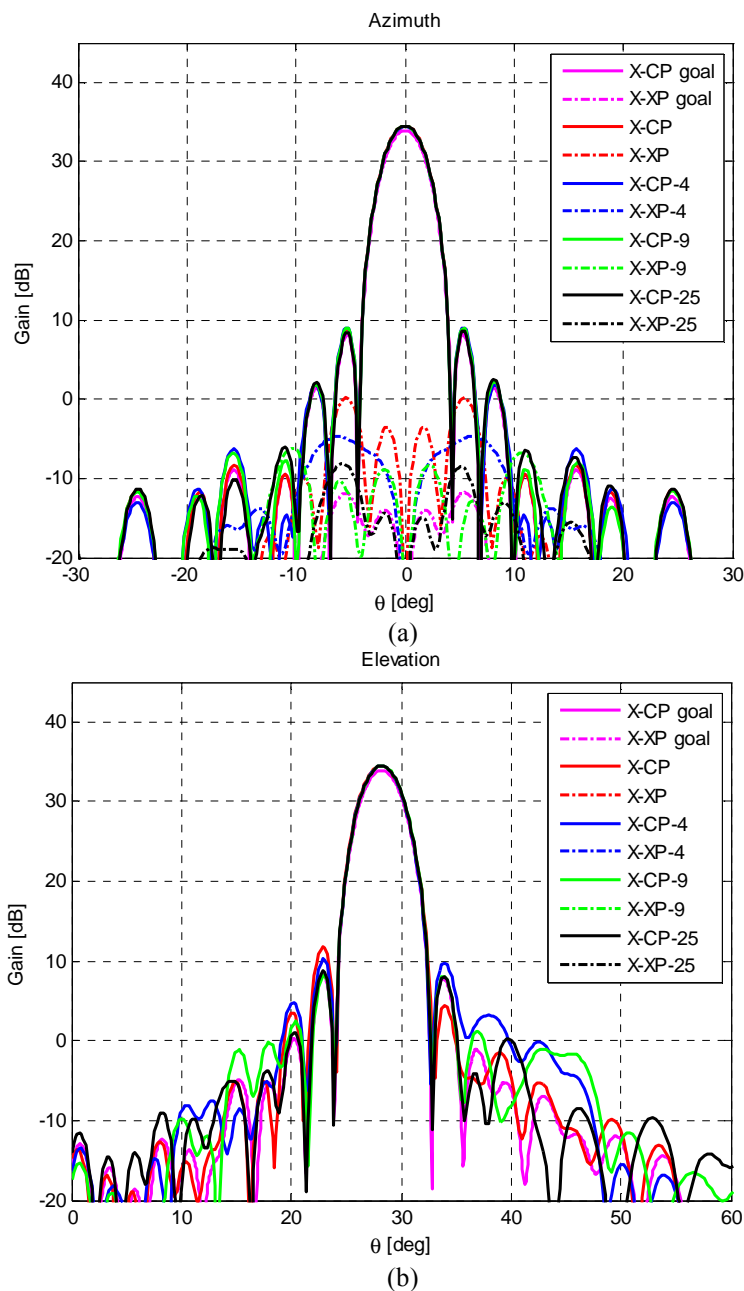


Fig. 4-80. Azimuth (a) and elevation (b) radiation patterns of vertical polarization for the goal case, for the approximate case without dividing the sub reflectarray aperture and dividing the sub reflectarray aperture in 4, 9 and 25 groups

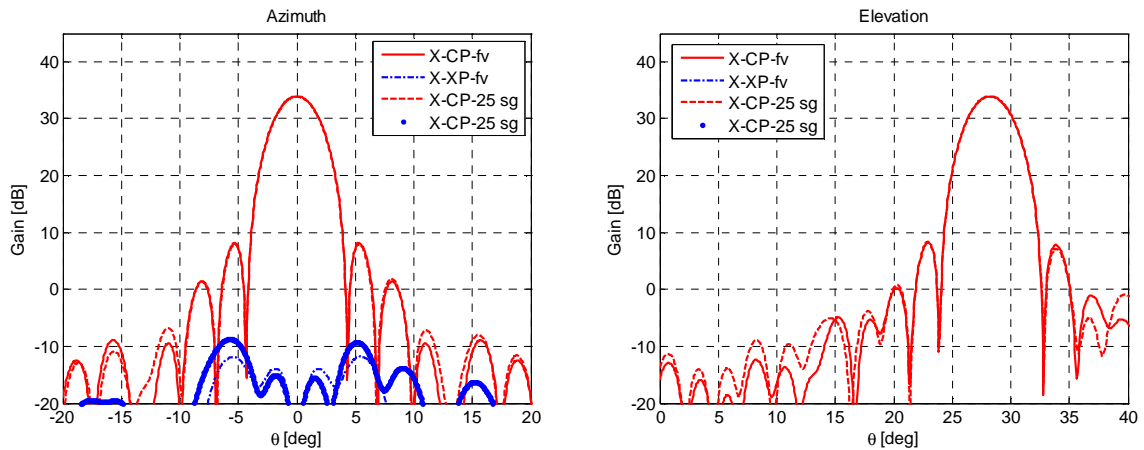


Fig. 4-81. Comparison of radiation patterns for the goal case and for the simulated patterns when dividing the sub-aperture in 25 groups

The main reflectarray does not increase the crosspolar already introduced by the sub reflectarray but reduces this component. The radiation pattern when the antenna is analyzed using ideal phase shift for the main-reflectorarray and when the antenna is analyzed using patches designed to reduce the crosspolar (considering the virtual focus as the origin of the field) are compared in Fig. 4-82.

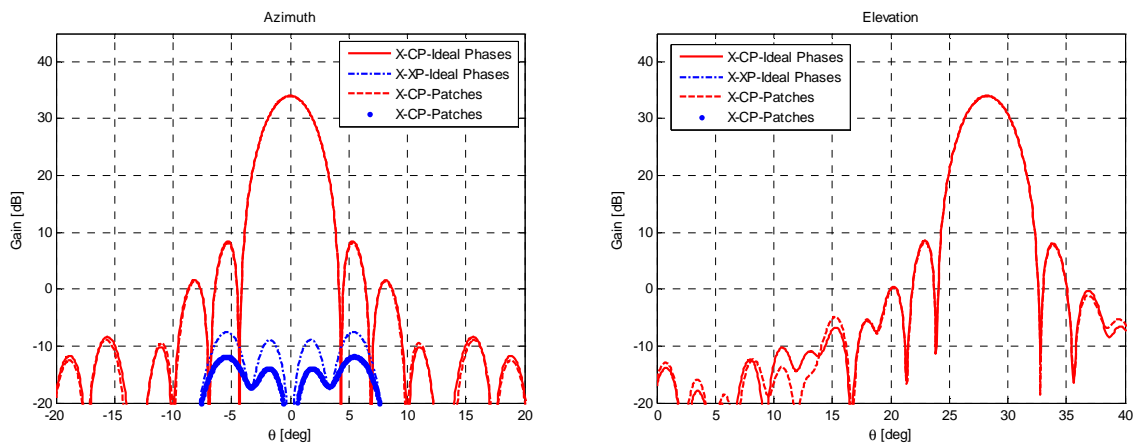


Fig. 4-82. Comparison of radiation patterns analyzing the antenna with ideal phases distribution on main and with the designed patches

Finally, the patterns at different frequencies are compared. Fig. 4-83 shows the radiation patterns at 12.2, 12.975, 13.75, 14 and 14.25 GHz for V polarization. All patterns show similar behaviour at different frequencies, showing how the antenna can work in a wide frequency band. All the plots are computed in gain, assuming the dissipative losses in the reflectarrays. The patterns are referred to the main reflectarray coordinate system. These simulations are run considering that the sub reflectarray aperture was divided in 25 groups and taking 9 samples per patch.

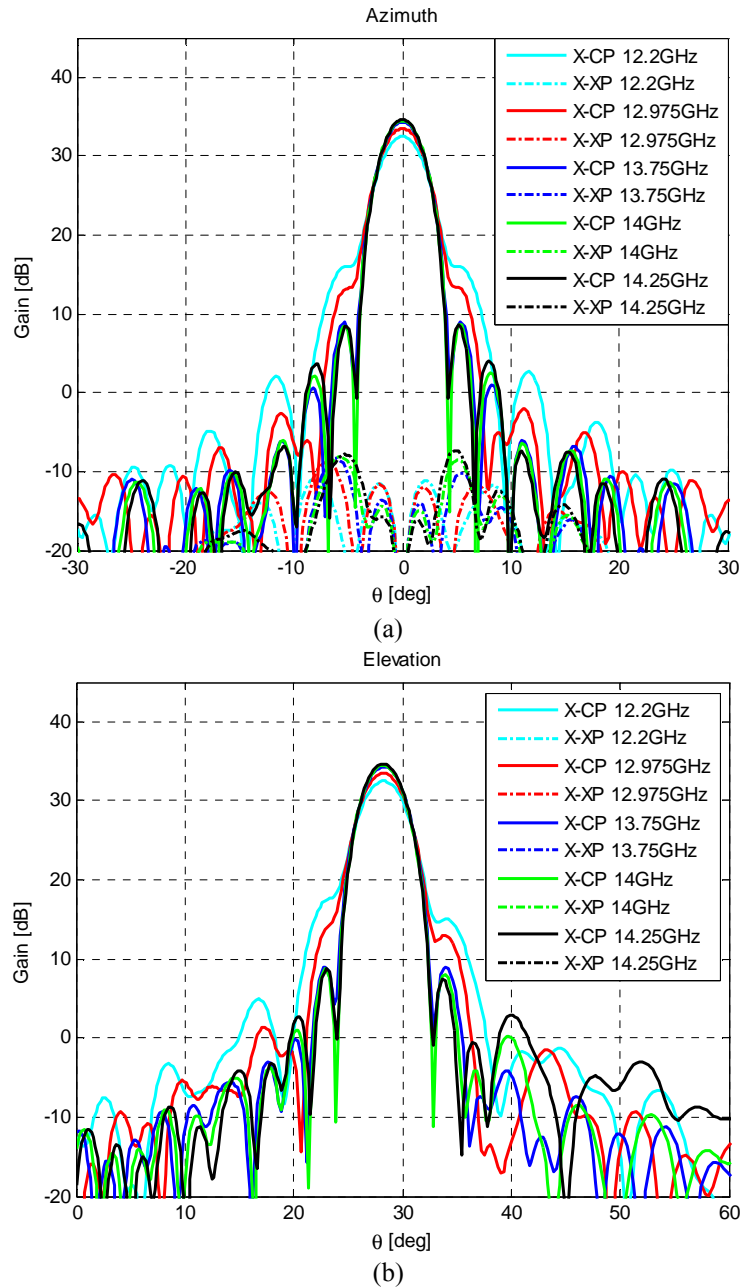


Fig. 4-83. Azimuth (a) and elevation (b) radiation patterns for vertical polarization at 12.2, 12.975, 13.75, 14 and 14.25GHz

4.5.3 Photo-etching masks

The photo-etching of the patches on the Arlon substrates is carried out in a single piece for both layers of main. The two masks corresponding to the two layers, the bottom and the top layers are depicted in Fig. 4-84 and Fig. 4-85 .

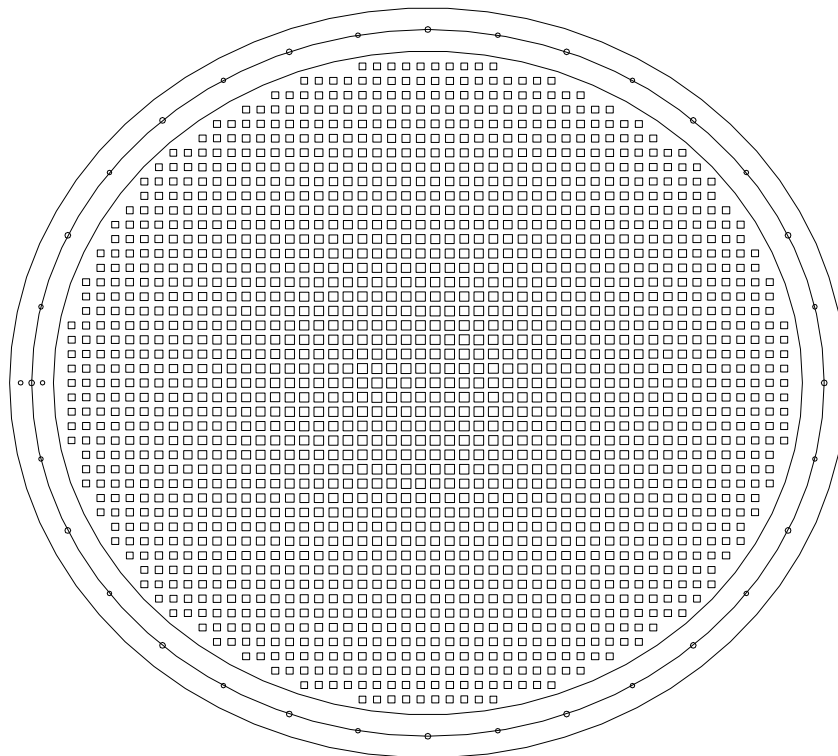


Fig. 4-84. Photo-etching mask of bottom layer for the main-reflectarray

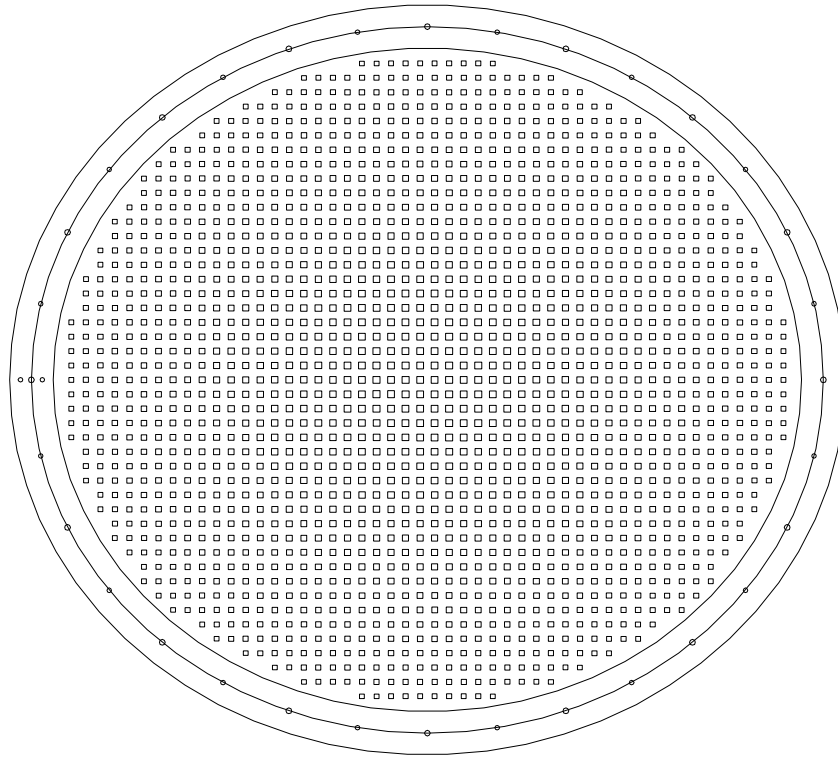


Fig. 4-85. Photo-etching mask of top layer for the main-reflectorarray

4.5.4 Conclusions

A dual-reflectorarray antenna with compact optics has been proposed to generate a focused beam. The antenna has been designed in dual linear polarization and the patches have been adjusted to cancel the cross-polarization levels of the dual-reflectorarray antenna. A reduction of 12 dB in the levels of cross-polarisation is achieved, providing a cross-polar discrimination better than 40 dB.

4.6 Contoured-Beam Dual-Reflectarray Antenna for DBS Applications

A dual-reflectarray configuration is proposed for the synthesis of a contoured beam that provides an European coverage for DBS. The antenna geometry is very similar to the dual-offset configuration presented in the previous two sections. The beam shaping is achieved by synthesizing the phase distribution on the main reflectarray while the sub reflectarray emulates an equivalent hyperbolic sub reflector.

4.6.1 *Coverage requirements and antenna definition*

The chosen European coverage is referred to a satellite in the position: 10°E longitude, 0° latitude. The specifications consist of a 25 dBi minimum gain level at the borders of the coverage region defined by the grey line in Fig. 4-86 in a frequency band centered at 14GHz. The coverage is enlarged by taking into account typical satellite pointing errors; see black line in Fig. 4-86.

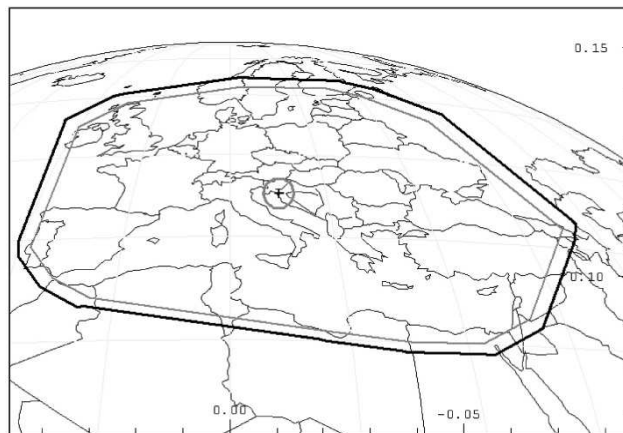


Fig. 4-86. Required European Coverage at 14 GHz.

In order to synthesize the required radiation pattern, the antenna configuration shown in Fig. 4-87 is proposed, which has been derived from a compact range dual-reflector antenna. The antenna is made up of three components: a primary feed and two reflectarrays composed of a circular sub reflectarray (SRA) and an elliptic main-reflectorarray (MRA). The main parameters of the geometry have been summarized in Table 4-21.

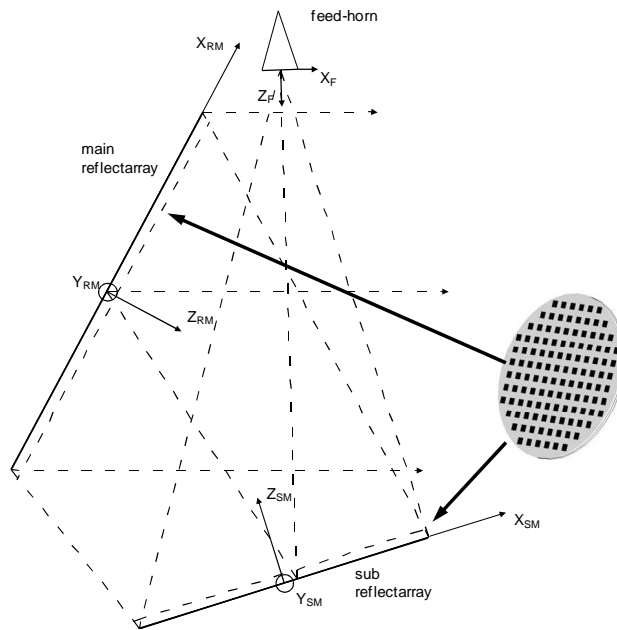


Fig. 4-87. Top view of the antenna configuration.

Table 4-21. Main data of the antenna geometry

Main Reflectarray	
Main reflectarray size	500mm × 450mm 40 × 36 elements
Periodicity	12.5mm × 12.5mm
Sub reflectarray (data in main-reflectarray coordinate system)	
Centre	(-217, 0, 370)mm
Direction cosines matrix Relation between MRA and SRA Coordinate Systems	$\begin{bmatrix} 0.715 & 0 & 0.698 \\ 0 & -1 & 0 \\ 0.698 & 0 & -0.715 \end{bmatrix}$
Sub reflectarray size	375mm × 375mm 30 × 30 elements
Periodicity	12.5mm × 12.5mm
Feed-Horn (data in sub reflectarray coordinate system)	
Phase centre	(188, 0, 616)mm
Pointing (on the sub reflector surface)	(15, 0, 0)mm

The sub reflectarray is illuminated by a horn antenna. In this case a simple model based on $\cos^q(\theta)$ function with $q=36$ is used, providing an illumination taper of -12.3 dB and -16.9 dB at the sub and main-reflectarray edges respectively. However, the elements of the sub reflectarray are not in the far-field region of the feed and the near-field radiated by the horn should be used for a more accurate analysis, as shown in [49].

The two reflectarrays used as sub and main reflectors are considered as planar arrays in rectangular lattices of printed stacked patches of variable size above a ground plane. The geometry is derived from a compact range configuration, made up of a paraboloid and a hyperboloid with negative eccentricity ($e = -2$) as main and sub reflector respectively. As a first step, both reflectarrays are defined to emulate the equivalent reflectors and the required phase shift on the main and sub reflectarrays are shown in Fig. 4-88. This configuration produces a focused beam directed to the center of the coverage.

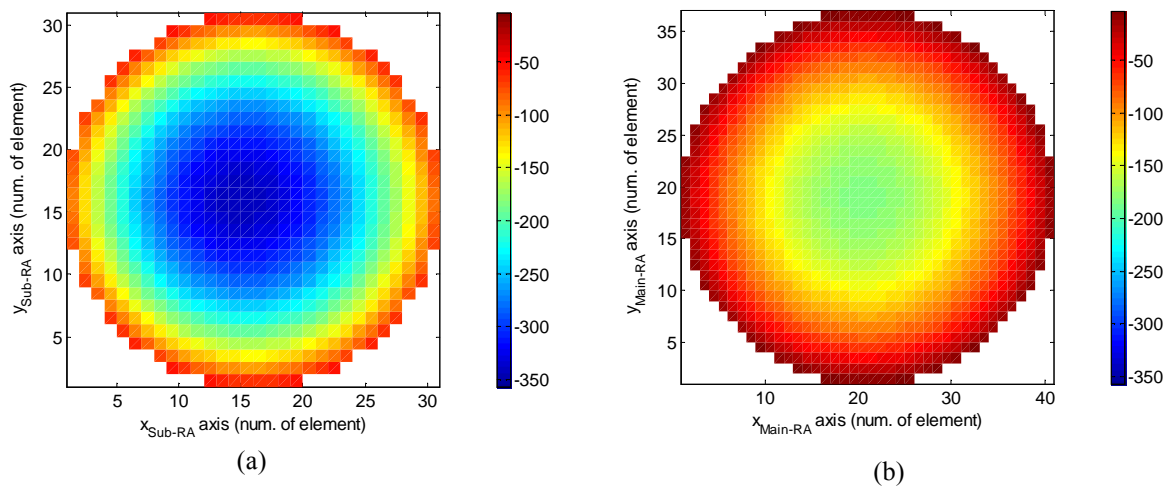


Fig. 4-88 Phase-shift distribution of the sub reflectarray (a) and main reflectarray (b) to produce a focused beam.

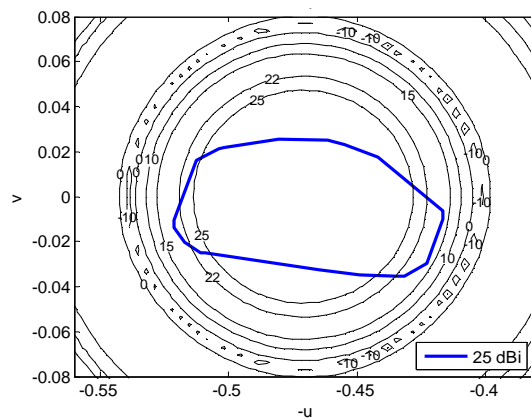


Fig. 4-89. Copolar radiation pattern at 14GHz for a focused beam.

The geometry defined by data in Table 4-21 has been analyzed by the technique described in Chapter 2, assuming ideal reflectarray elements that provide the phases shown in Fig. 4-88. The resulting copolar radiation pattern is shown in Fig. 4-89 superimposed to the mask for gain requirements (in blue). The resulting gain for the

pencil beam in the boresight direction is 33.8 dBi. Note that the boresight direction in the antenna reference system corresponds to $\theta_0 = 28.2$ degree ($u = 0.472$) in the main reflectarray reference system, see Fig. 4-87.

4.6.2 *Contoured beam synthesis*

In this configuration there are two surfaces that can be used to synthesize a contoured beam: the sub and the main reflectarray. In this case, the phase distribution on the sub reflectarray emulates the equivalent hyperboloid and the phase distribution of the main reflectarray is synthesized to obtain the required coverage. The synthesis tool is based on the intersection approach method [65], which has been demonstrated in the design of shaped-beam reflectarrays for DBS applications [39], [40]. Usually the initial phase distribution is important to avoid local minima. To obtain a suitable starting point for the synthesis, the phase distribution associated to the parabolic surface (shown in Fig. 4-90) is changed by the one shown in Fig. 4-90 that corresponds to a parabolic cylinder, which is uniform in x-direction, in order to broaden the beam of Fig. 4-90 in the y axis.

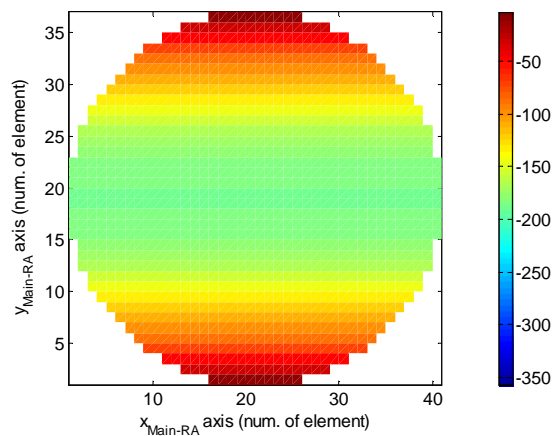


Fig. 4-90. Phase distribution on the main reflectarray to emulate a parabolic cylinder

Using the new phase distribution on the main reflectarray, and after several iterations in a single-stage optimization, the required coverage is achieved. The phase distribution obtained from the optimization process is depicted in Fig. 4-91 and the resulting radiation patterns are shown in Fig. 4-92 and Fig. 4-93. As shown, the copolar radiation pattern fulfills the requirements and the maximum value of crosspolar is -8dBi but the radiation pattern does not fit into the mask accurately because of the limited size of the antenna (demonstrator). However, the side lobes are very low, see Fig. 4-93.

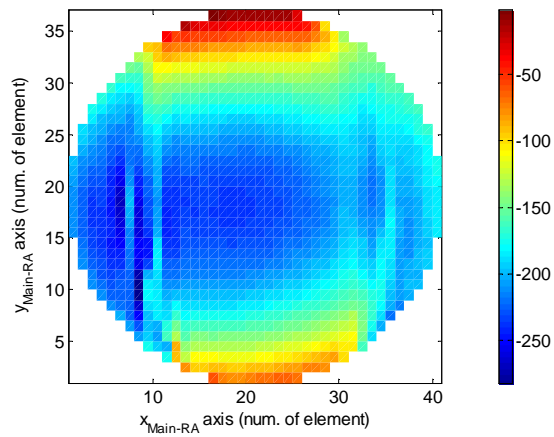


Fig. 4-91. Phase distribution synthesized on the main reflectarray for the contoured beam.

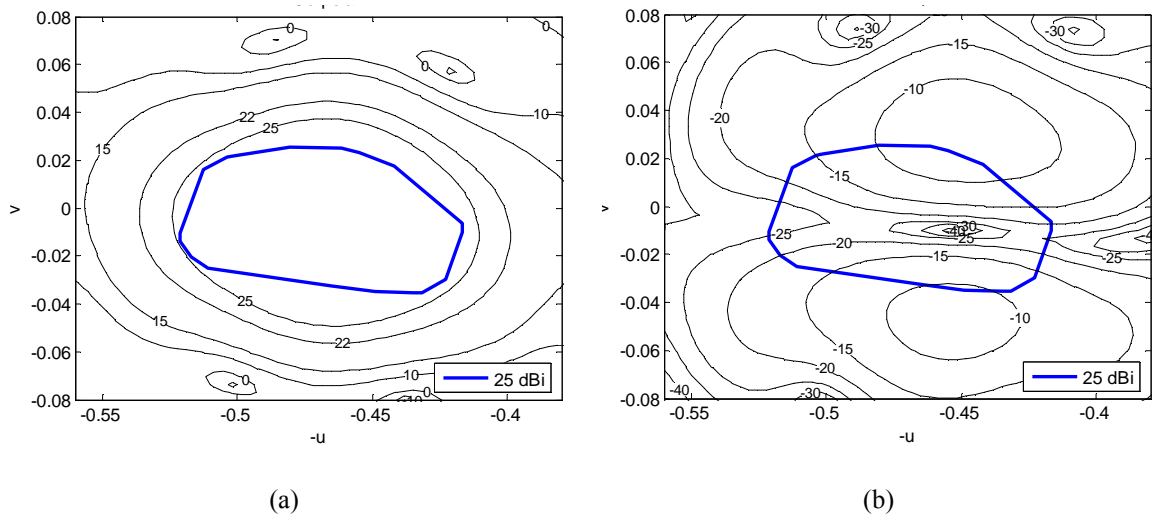


Fig. 4-92. Contoured beam in dB after the optimization process for Horizontal polarization. Copolar (a) and crosspolar (b) patterns.

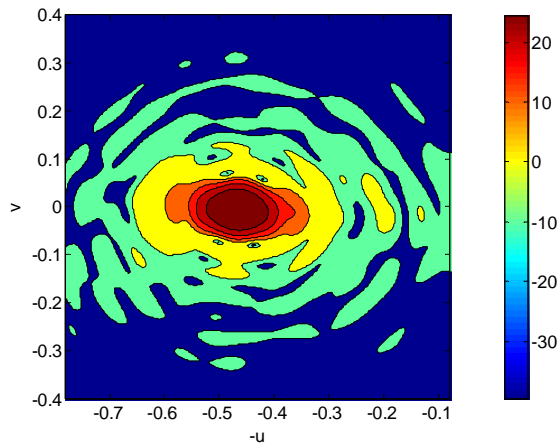


Fig. 4-93. Copolar 3D radiation pattern in dB.

4.6.3 Antenna design

The sandwich configuration used for the design of the main-reflectarray to generate a contoured beam consists of two-layers of copper patches printed on a 60-mil dielectric substrate (DiClad880B). Both layers are glued using two layers of thermoplastic bonding film (Cuclad6250).

In the two-layer main-reflectarray, the patches are distributed in a rectangular lattice with an elliptical shape of 500 mm \times 450 mm. The selected period is 12.5 mm in x and y axes, thus the main reflectarray is arranged in 40 \times 36 elements. Fig. 4-94 shows the patch size in x and y dimensions and Fig. 4-95 points out the photo-etching masks for both layers of the main reflectarray

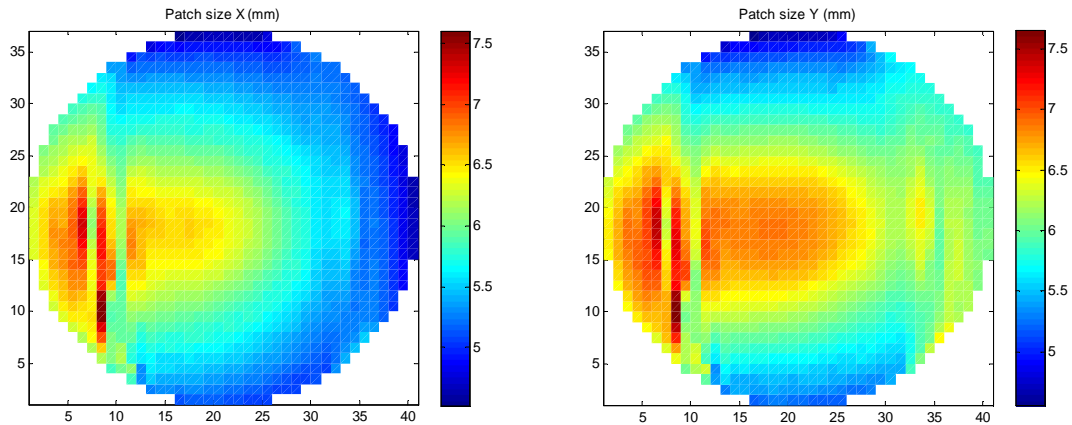
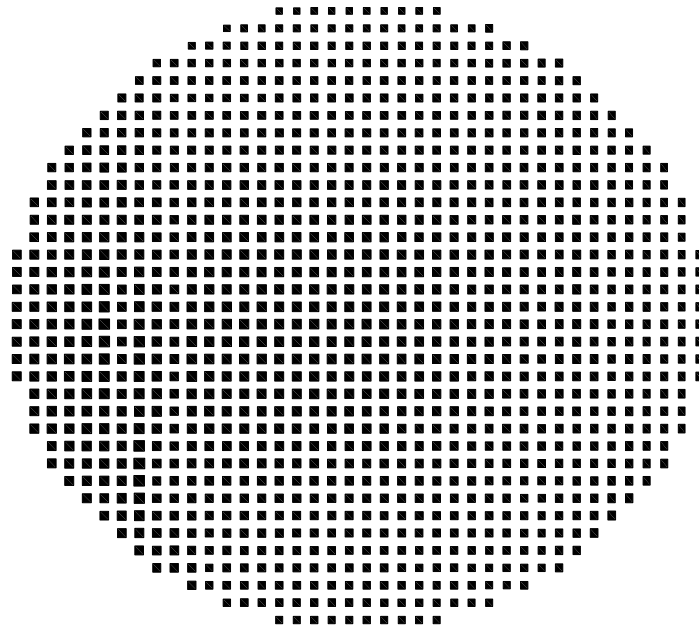
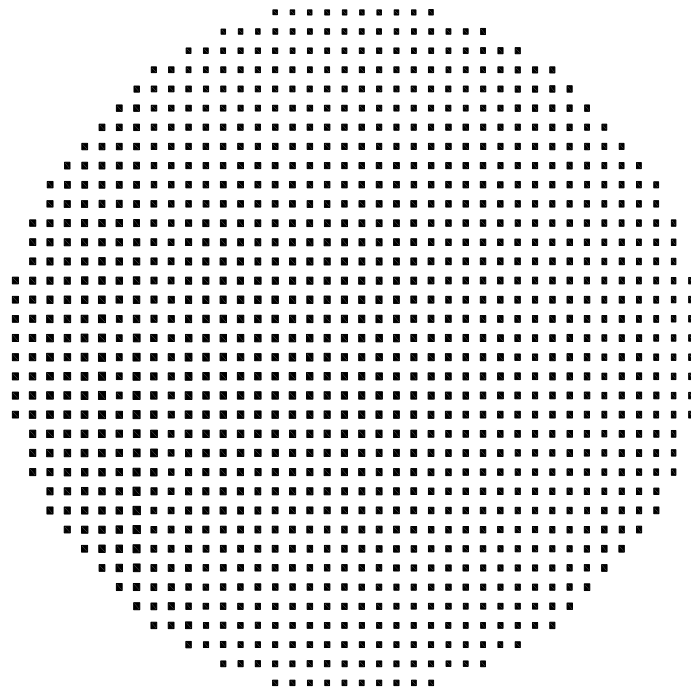


Fig. 4-94. x and y dimensions for the main reflectarray patches



(a)



(b)

Fig. 4-95. Photo-etching masks of the main-reflectorarray: (a) bottom layer, (b) top layer

The radiation pattern obtained when the antenna configuration is analysed considering the virtual focus as origin of the incident electric field is shown in Fig. 4-96 and Fig. 4-97. Then, the antenna is analysed dividing the sub reflectarray in several groups of

elements. Fig. 4-98 shows the progressive convergence of the radiation pattern to that shown in Fig. 4-93, when using the analysis technique explained in Chapter 2. Finally a frequency analysis is performed and shown in Fig. 4-99. As it can be checked the behaviour of the antenna is very stable in the required transmit frequency band from 13.75 GHz to 14.25 GHz.

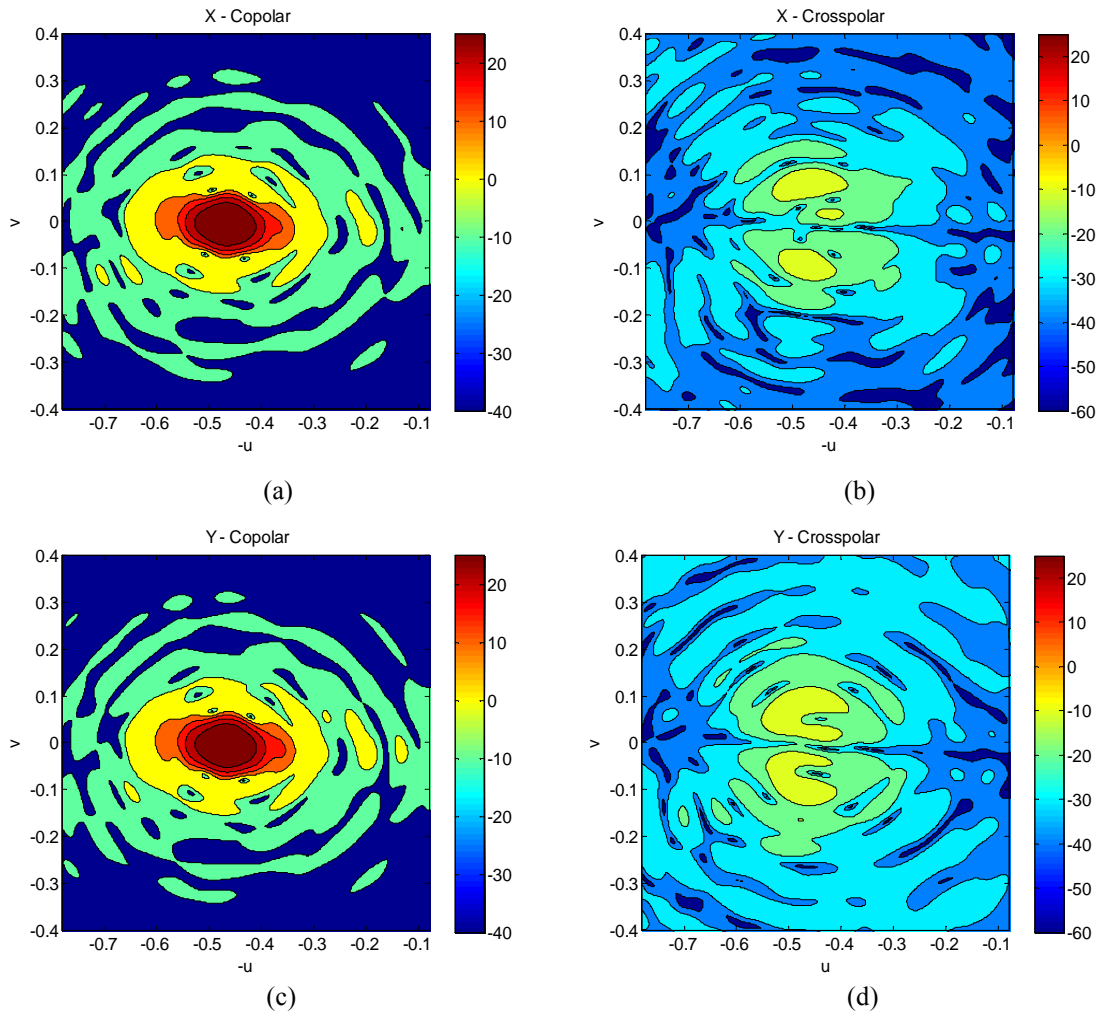


Fig. 4-96. 3D radiation pattern of the contoured beam for Vertical (X) polarization: (a) copolar and (c) crosspolar components and for Horizontal (Y) polarization: (b) copolar and (d) crosspolar components, when using the virtual focus as the origin of the field.

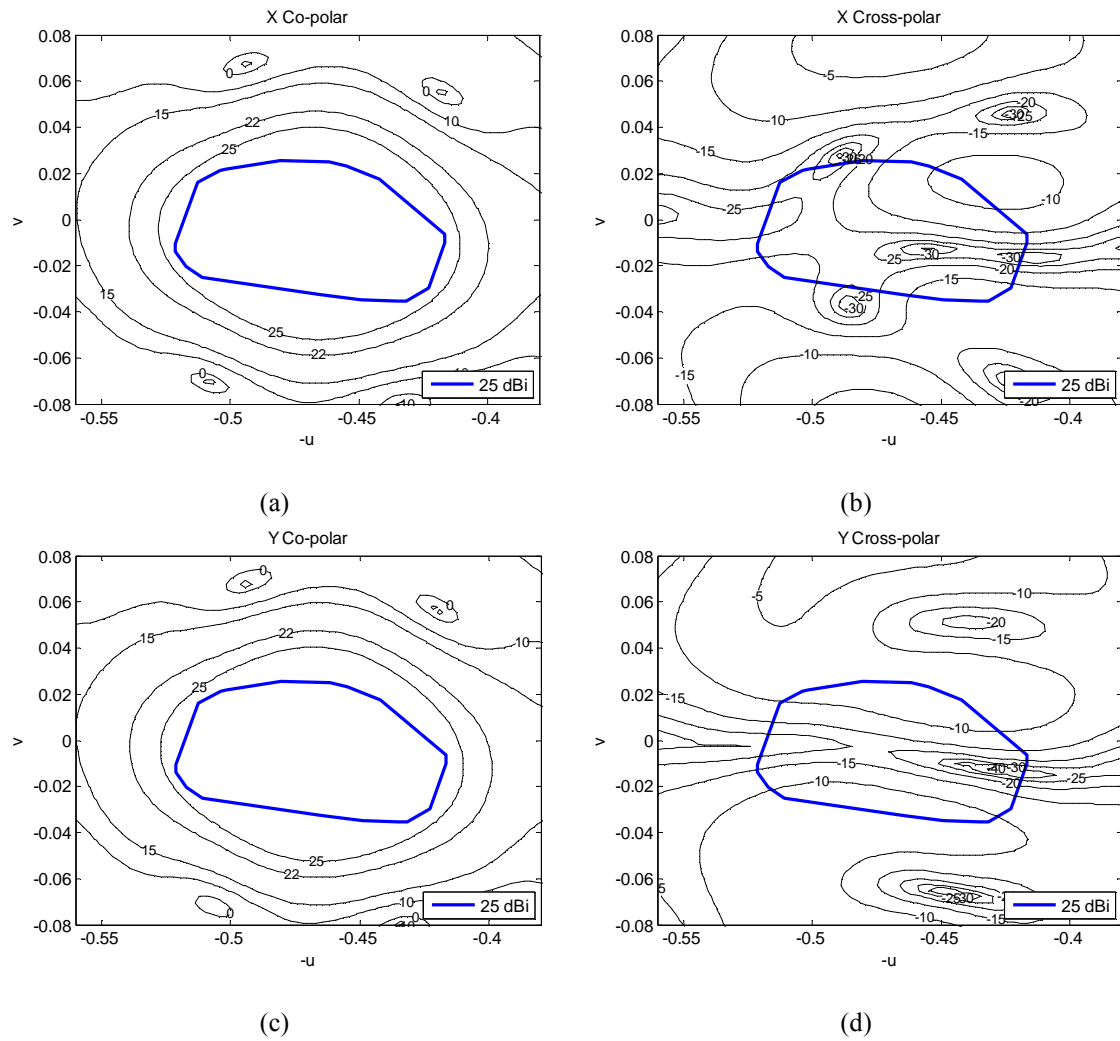


Fig. 4-97. Contoured beam in dBi after the optimization process for Vertical (X) polarization: (a) copolar and (c) crosspolar components and for Horizontal (Y) polarization: (b) copolar and (d) crosspolar components

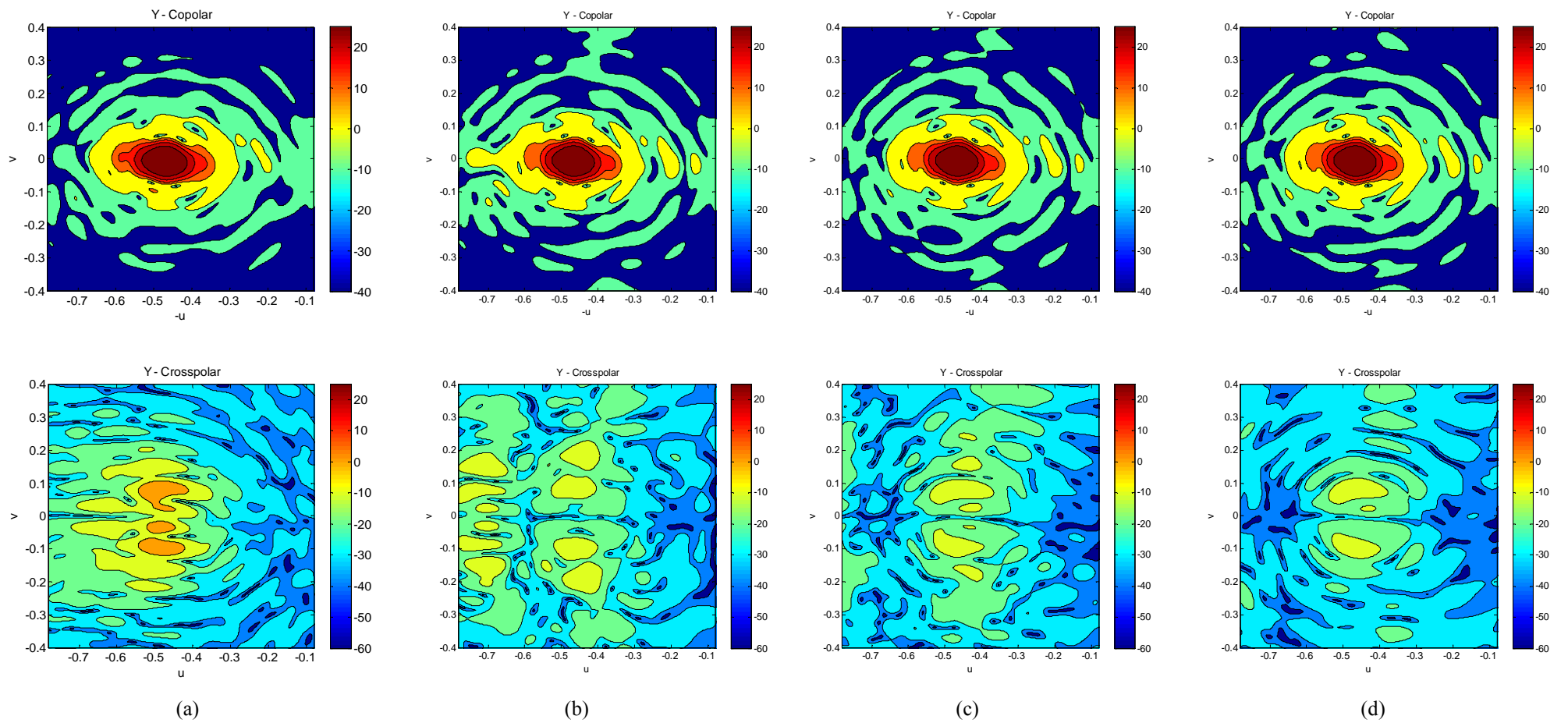


Fig. 4-98. Module of copolar and crosspolar components of 3D radiation pattern for Horizontal polarization (a) without dividing the sub reflectarray aperture (b) dividing the sub reflectarray aperture in groups of 7x13 cells (c) dividing the sub reflectarray aperture in groups of 4x8 cells (d) dividing the sub reflectarray aperture in groups of 2x4 cells

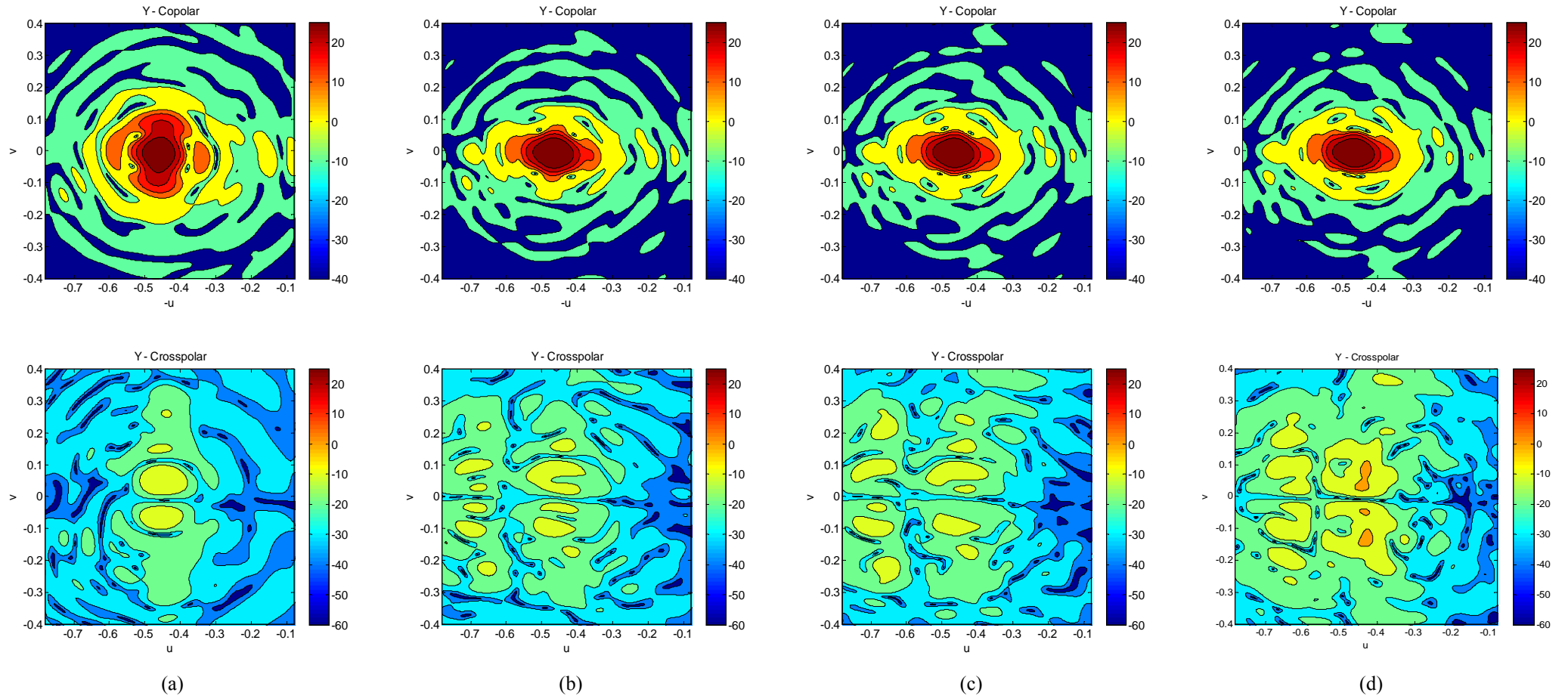


Fig. 4-99. 3D radiation patterns for Horizontal polarization at: (a) 12.2 GHz (b) 13.75 GHz (c) 14 GHz and (d) 14.25 GHz

4.6.4 Conclusions.

A dual-reflectarray antenna has been proposed to generate a contoured beam for DBS coverage. The antenna is derived from a compact range dual-reflector antenna, where the sub reflectarray emulates a hyperbolic sub reflector. The phase distribution on the main reflectarray has been synthesized to provide the required European coverage. The antenna was designed for dual linear polarization and the resulting patterns fulfill the coverage requirements.

4.7 Conclusions

A dual-reflectarray antenna characterized by its compact optics, has been designed, manufactured and tested to generate a focused beam. The antenna demonstrator was designed to reduce the cross-polarization, by producing some cancelation of the cross-polarization introduced by the patches. The antenna was designed using two layers of varying-sized patches for the sub reflector and a single layer for the main reflector, because the required range of phase was smaller. The comparison of the simulated results with the measurements shows good agreement, however, some slight differences in the side lobe level are observed as consequence of the tolerance errors of the manufacturing process. The antenna provides a cross-polar discrimination better than 35 dB and a very wide frequency bandwidth, from 12.2 GHz to 15 GHz.

A further improvement in both bandwidth and cross-polarization was introduced by designing the main reflectarray also using two-layers of varying-sized patches. The nulls and change of sign of the cross-polarization for certain patch dimensions are used to cancel the cross-polarization levels of the dual-reflectarray antenna. A substantial reduction in the levels of cross-polarization is achieved, providing a cross-polar discrimination better than 40 dB for both polarisations.

A third configuration based on the same geometry as in the two previous antennas is designed. In this case, the phase distribution on the main reflectarray has been synthesized to provide the required European coverage. The antenna can work in dual linear polarization and the resulting patterns fulfill the coverage requirements in the transmission frequency band.

The results presented in this chapter show the capabilities of this dual-reflectarray configuration to fulfill the requirements of DBS antennas in transmit and receive bands.

CHAPTER 5

5 Dual reflectarray for beam scanning in Ku-band

5.1 Introduction

This chapter describes two possible architectures for a Ku-band antenna based on a dual planar reflectarray configuration that provides electronic beam scanning in a limited angular range. In the first architecture, the main reflectarray is passive and the beam scanning is achieved by introducing a phase-control in the elements of the sub reflectarray. A second alternative is also studied, in which the beam scanning is produced using 1-bit control elements on the main reflectarray, while a passive sub reflectarray is designed to provide a large focal distance within a compact configuration. Both designs have been developed in the context of the RESKUE project (ESA contract n° 22078/08/NL/ST) in collaboration with the European Space Agency (ESA) and RF-Microtech.

The system aims to develop a solution for bi-directional satellite links for emergency communications that may take place in remote locations, where other telecommunication infrastructures may be either not available or inadequate. In both proposed architectures, the objective is to provide a compact optics and simplicity to be folded and deployed. The system should provide automatic pointing to a geo satellite in a limited angular range. The antenna is designed to provide a directive beam in receive

(10.70-12.75 GHz) and transmit (14.0-14.5GHz) frequency bands with electronic scanning capabilities within a limited angular range.

5.2 Dual-reflectarray antenna for beam scanning with phase control on the sub reflectarray

An offset dual reflector antenna using a reflectarray sub reflector and a parabolic main reflector has been proposed for beam steering in a limited range by implementing a progressive phase on the sub reflectarray [61]. This antenna configuration combines the high gain capabilities of the parabolic main reflector with the simplicity of fabricating a small reconfigurable sub reflectarray, which could be constructed using MEMS switches to provide electronic beam scanning [66] . In the present work the main parabolic reflector is substituted by a flat reflectarray.

5.2.1 Antenna definition

In the dual-reflector configuration, the main reflector is a flat passive reflectarray designed to focus the beam. When compared with conventional dual-reflector antennas, the dual-reflectarray configuration shown in Fig. 5-1 exhibits some advantages, both from a mechanical point of view, such as a reduced volume and ease for folding; and also from electrical features, offering capabilities to scan or reconfigure the beam. Furthermore, the proposed dual-reflectarray configuration provides phase control on both reflectarray surfaces [67], which can be used to improve the antenna performances for multiple beams or for beam scanning.

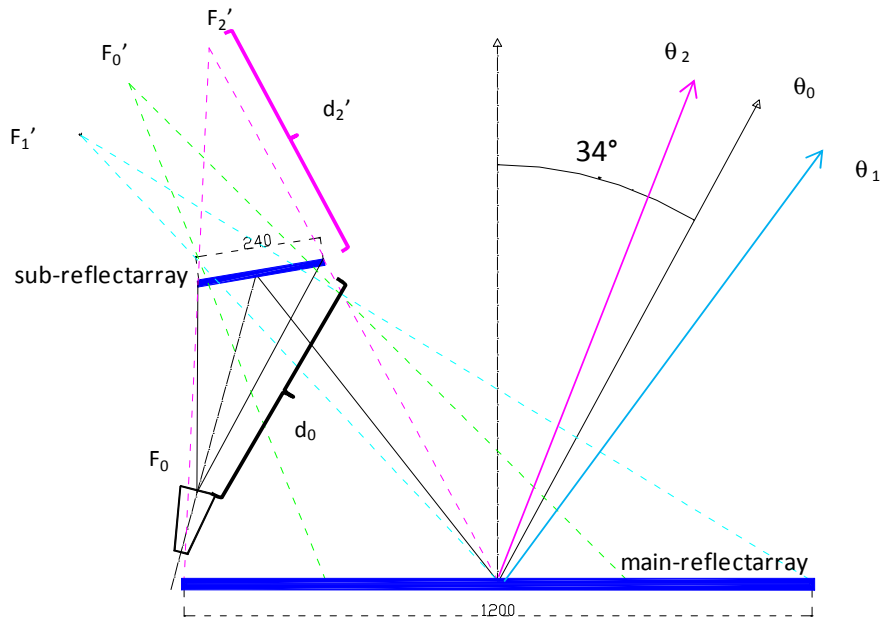


Fig. 5-1. Lateral view of the dual-reflectarray configuration.

Table 5-1. Main data of the antenna geometry

Main Reflectarray	
Main reflectarray size	1175mm × 962mm 94 × 76 elements
Periodicity	12.5mm × 12.5mm
Sub reflectarray (data in main-reflectarray coordinate system)	
Centre	(-453, 0, 560)mm
Direction cosines matrix Relation between MRA and SRA Coordinate Systems	$\begin{bmatrix} 0.987 & 0 & 0.158 \\ 0 & -1 & 0 \\ 0.158 & 0 & -0.987 \end{bmatrix}$
Sub reflectarray size	250mm × 225mm 20 × 18 elements
Periodicity	12.5mm × 12.5mm
Feed-Horn (data in sub reflectarray coordinate system)	
Phase centre	(356, 0, 616)mm
Pointing (on the sub reflector surface)	(15, 0, 0)mm

The antenna configuration has been selected to provide beam scanning on the elevation plane (XZ) in a range of 13 degrees using elliptical reflectarrays of axes (1175 mm, 962mm) for the main and (250 mm, 225 mm) for the sub reflectarray. For a preliminary evaluation of the beam scanning performance, a phase is introduced on the sub reflectarray to emulate the optics corresponding to different virtual foci, associated to each beam direction, as shown in Fig 5.1. The virtual foci determine a progressive phase

along a dimension of the reflectarray, $\phi_{RA}(p, q)$, being p and q the indexes of the sub reflectarray cells, see Eq. 5-1

$$\phi_{RA}(p, q) = f(d_i'(p, q) - d_0(p, q)) \quad (5-1)$$

The main reflectarray is designed to emulate the behaviour of a parabolic reflector, producing a focused beam in θ_0 direction when the phase distribution on the sub reflectarray is uniform, while the sub reflectarray is used to introduce the appropriate progressive phase in order to scan the beam.

5.2.2 *Antenna design and analysis*

The passive main reflectarray can be designed using stacked variable-sized patches [68] in a prescribed frequency band as done in the case of the demonstrator shown in chapter 4, however in this case ideal phases will be considered for the main-reflectarray. The periodic cell has been chosen as $12.5 \text{ mm} \times 12.5 \text{ mm}$ for both reflectarrays. The reflectarray element for dual polarization proposed for the sub reflectarray is shown in Fig. 5-2, which is based on two stacked printed patches aperture-coupled to delay lines. This reflectarray element has been designed to provide the required phase variation in the frequency bands 10.7-12.75 GHz and 14-14.5 GHz [69]. The phase control on the sub reflectarray can be implemented by a 3-bit phase-shifter in the delay lines corresponding to each polarization. Fig. 5-3 shows the phase-curves of the element for a 10.7 GHz, 12.0 GHz and 14.0 GHz.

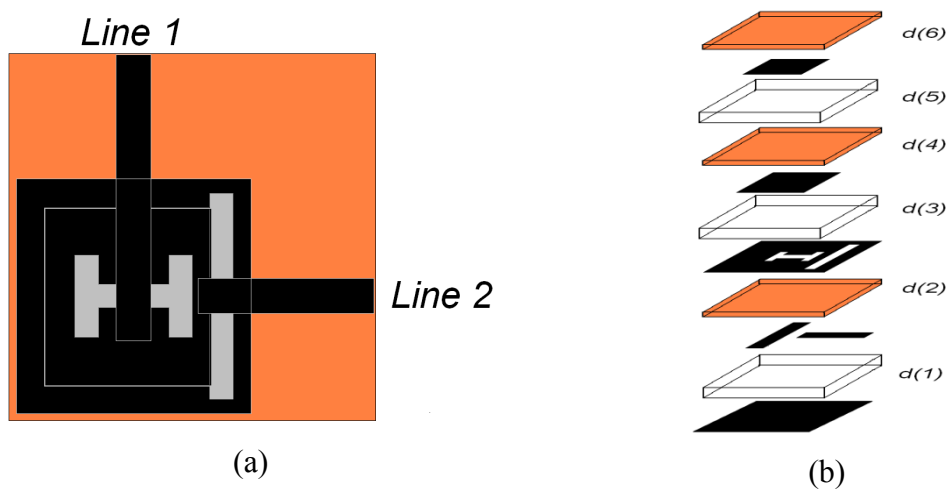


Fig. 5-2. Top view of the aperture coupled cell (a). Lateral view of the cell (b)

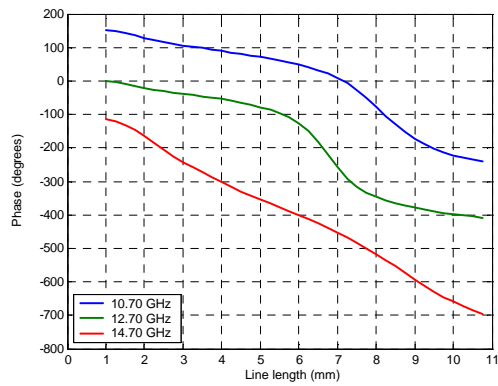


Fig. 5-3. Required phase shift of the aperture coupled element

To evaluate the beam scanning performance, the phase distributions required on both the main and sub reflectarrays have been computed for various scan angles. The phase distribution required on the main reflectarray to emulate the behaviour of a parabolic reflector at 12 GHz is shown in Fig. 5-4 (a). The phase distribution on the sub reflectarray required to produce a beam scan of 5 degrees and -8 degrees in elevation (θ_1 and θ_2 in Fig. 5-1) is shown in Fig. 5-4 (b) and Fig. 5-4 (c) respectively.

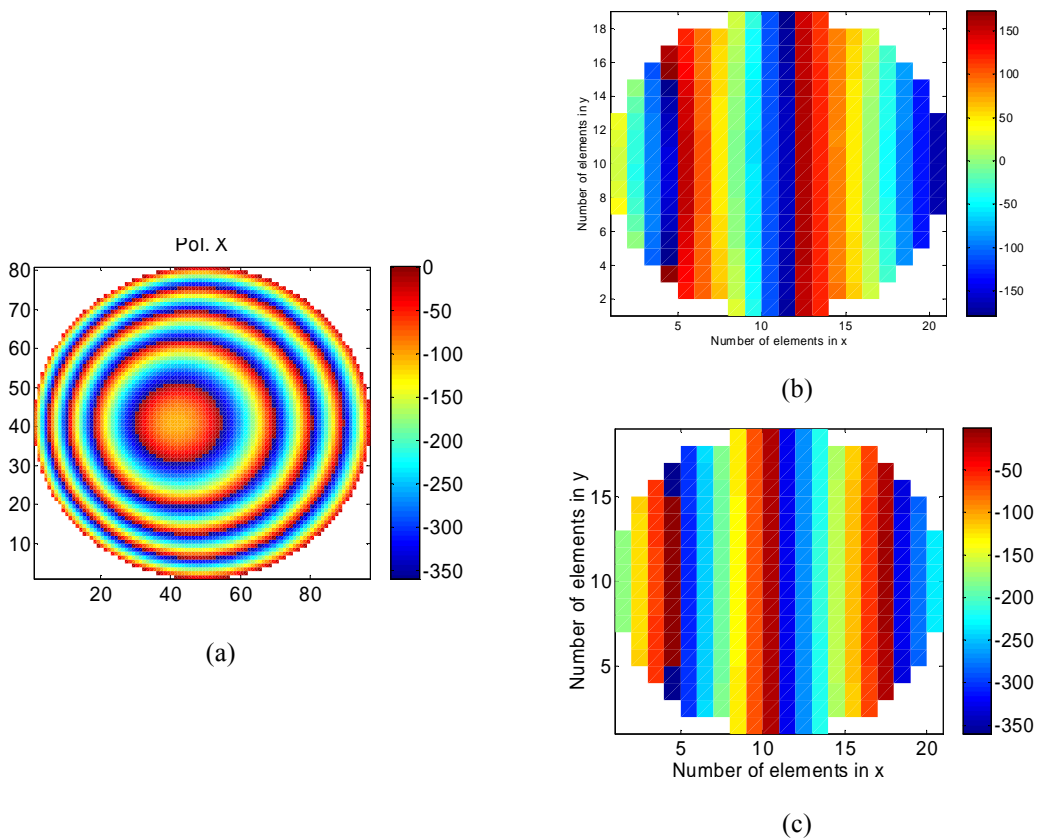
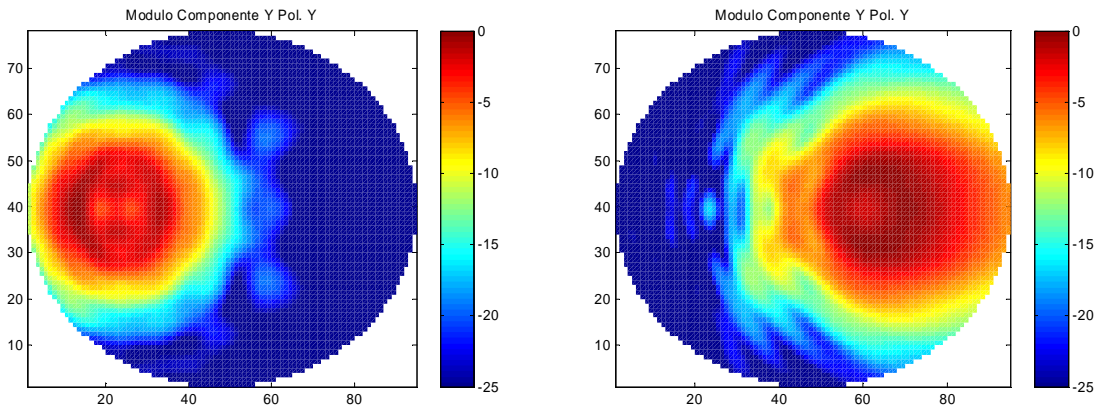
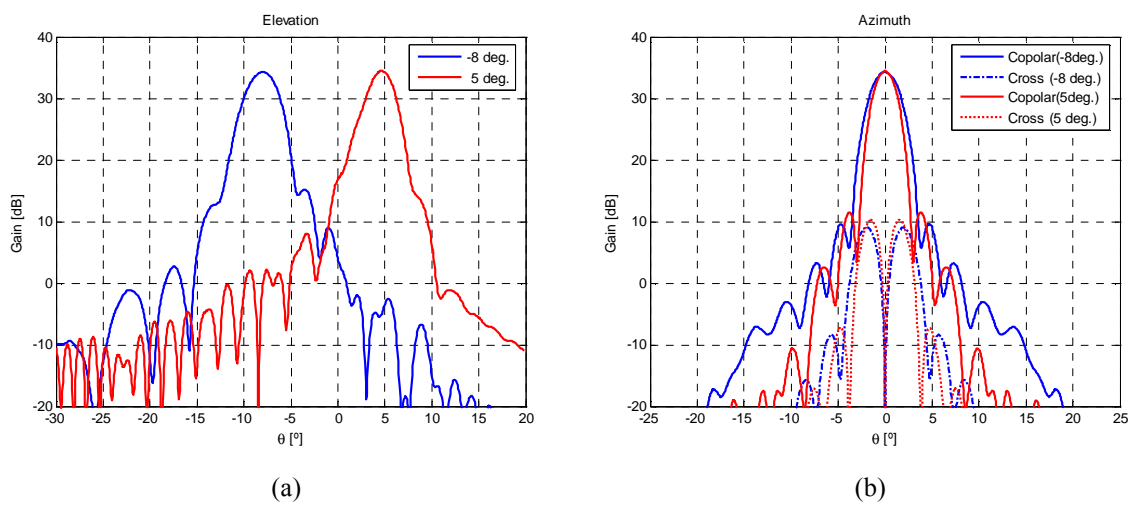


Fig. 5-4. Required phase distribution on main reflectarray (a). Required phase for 5° beam deviation on sub reflectarray (b) and required phase for -8° beam deviation on sub reflectarray (c)

As a first step to analyse the antenna designed to steer the beam in a range of 13 degrees, ideal phases for both sub and main reflectarray are considered. By varying the progressive phase distribution on the sub reflectarray, the beam is steered from -8 degree to 5 degree with practically no distortion on the radiation patterns, as shown in Fig. 5-6. Fig. 5-5 shows the module of the incident field on the main reflectarray and Fig. 5-7 the 3D radiation patterns of the antenna. Note that to achieve beam scanning by adjusting the phase-distribution only on the sub reflectarray, the dimensions of the main passive reflectarray have been oversized, so that the beam radiated by the sub reflectarray is impinging in only one part of the main reflectarray, depending on the scan angle. The beam scanning performance can be further improved by optimizing the phase distribution on the main passive reflectarray in order to minimize the pattern distortions in the whole range of scan angles.



(a) (b)
Fig. 5-5. Illumination on the main-reflectarray for -8° (a) and 5° (b)



(a) (b)
Fig. 5-6. Radiation patterns for the ideal phase distribution at 12 GHz (beam scan -8°, 5°) in elevation (XZ plane) and azimuth (orthogonal plane)

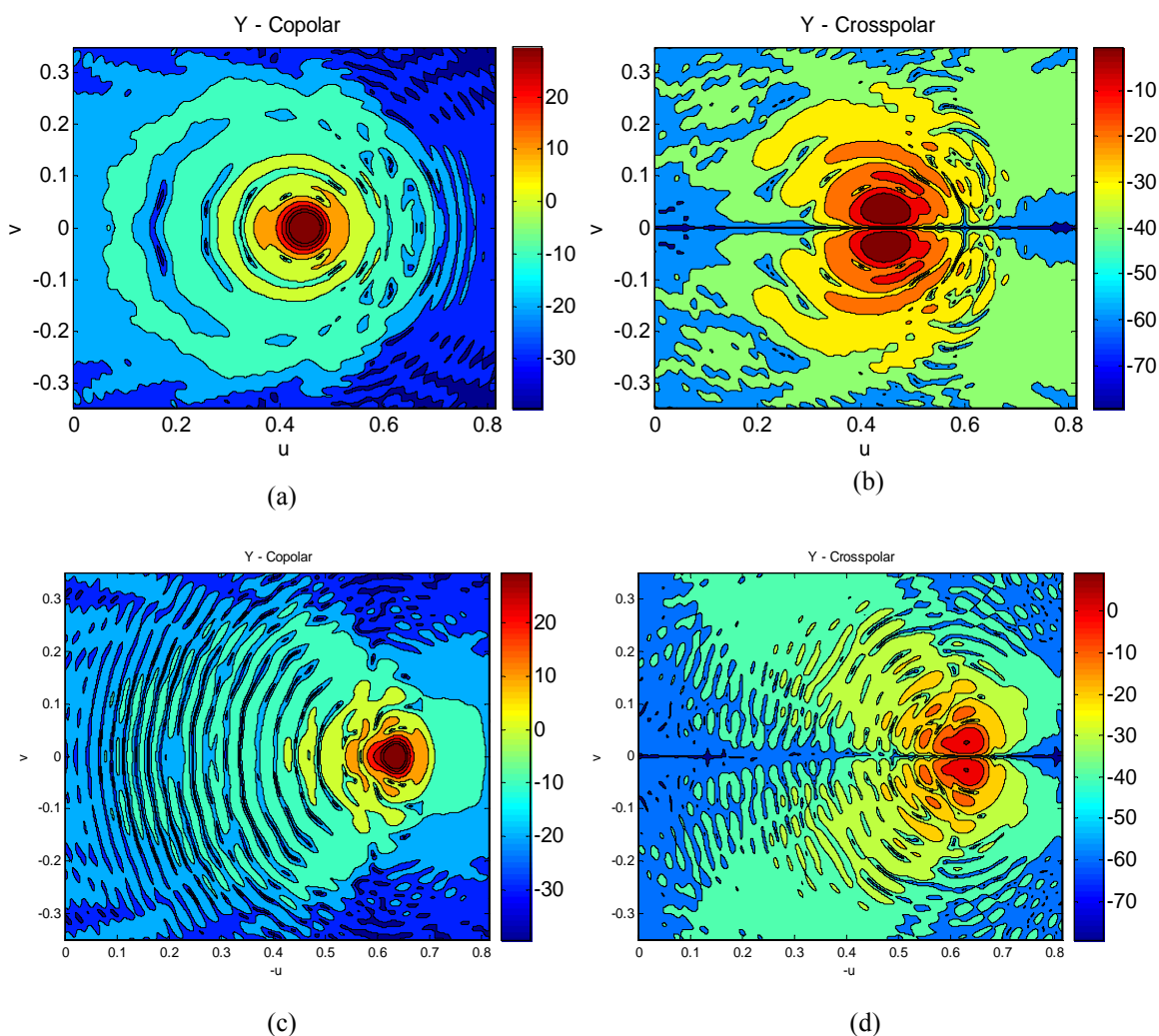
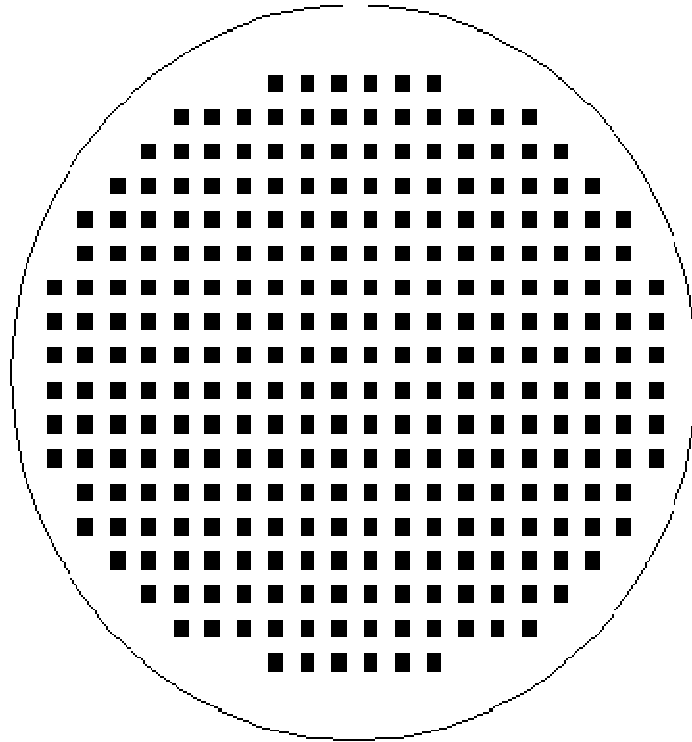
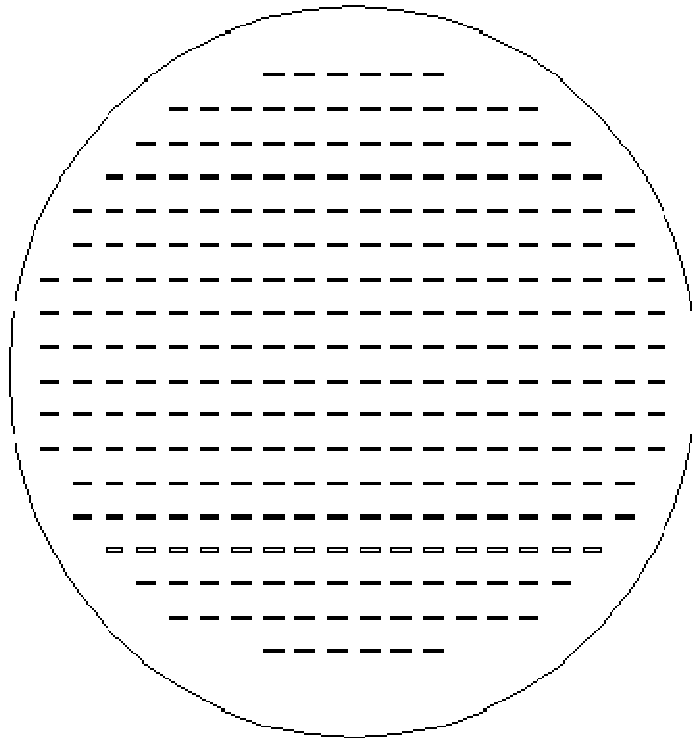


Fig. 5-7. Radiation patterns for -8° scan: co-polar (a) and cross-polar (b) and for 5° scan: co-polar (c) and cross-polar (d)

As a second step to evaluate the antenna performance, the real effect of the sub reflectarray elements based on aperture-coupled elements is considered. The reflectarray sub reflector has been designed by adjusting the lengths of the lines for each polarization to provide the required phase distribution associated to each scan angle. Then, the required line lengths should be adjusted by MEMS switches in a real implementation. However, the effect of the MEMS devices has been neglected in this study, being the antenna analyzed assuming the sub reflectarray elements shown in Fig. 5-2. The appropriate line lengths have been used to provide the required phasing on the sub reflector and considering ideal phases on the main reflectarray. Fig. 5-8 shows the photo etching masks of the three layers of printed patches for the sub reflectarray.



(a)



(b)

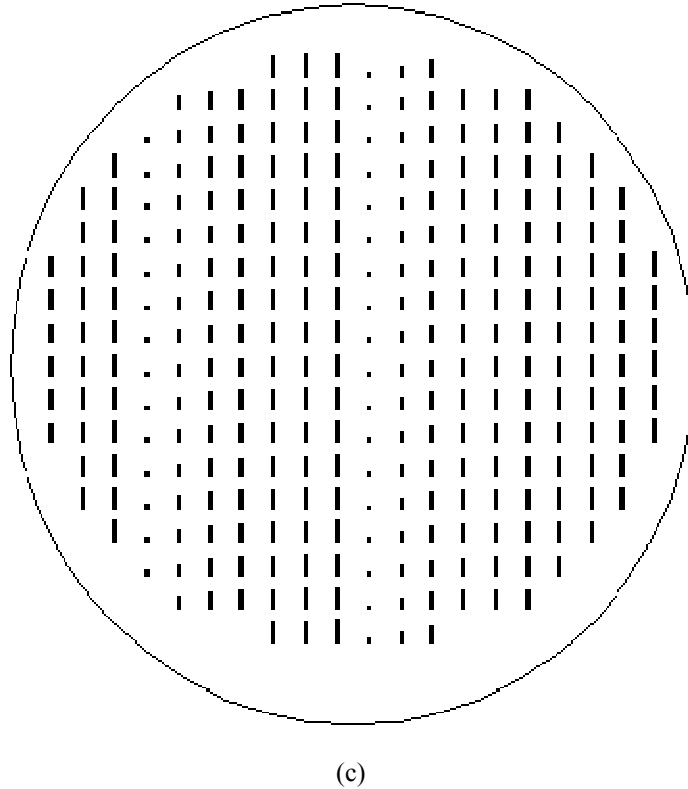


Fig. 5-8. Mask of the sub reflectarray: (a) first layer of patches, (b) slots and (c) lines

This analysis includes the variation with frequency of the reflectarray elements and provides a preliminary estimation of the antenna performance. Considering the sub reflectarray designed for 5° beam scan at 12 GHz, the antenna has been analyzed at other frequencies (10.7 and 14 GHz). Fig. 5-9 shows the radiation patterns in the main planes at 10.7 GHz and at 12 GHz with no distortion in azimuth and slight distortion in elevation. Fig. 5-10 shows the radiation pattern at 14 GHz, showing some distortions in elevation. Note that the beam is radiated at 4° , therefore a beam squint is produced. These distortions, not observed when ideal phases are used, are produced because the response of the aperture-coupled element is not appropriate for such a wide frequency band, from 10.7 GHz to 14.5 GHz. Therefore the reflectarray element for the reconfigurable sub reflectarray has to be redesigned.

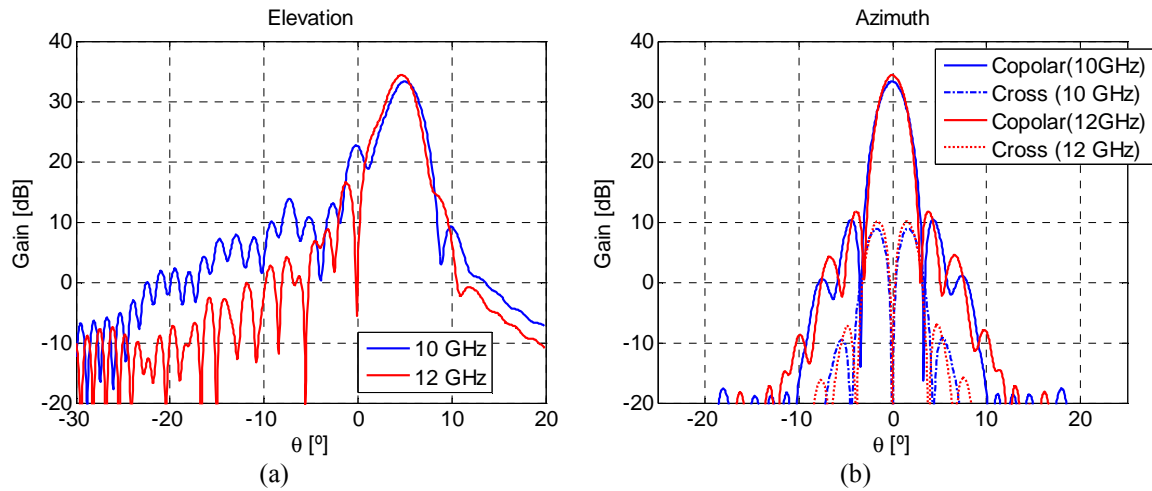


Fig. 5-9. Radiation pattern for the sub reflectarray based on aperture-coupled elements designed for 5° beam scan at different frequencies in elevation (XZ) (a) and azimuth (b) (orthogonal) planes

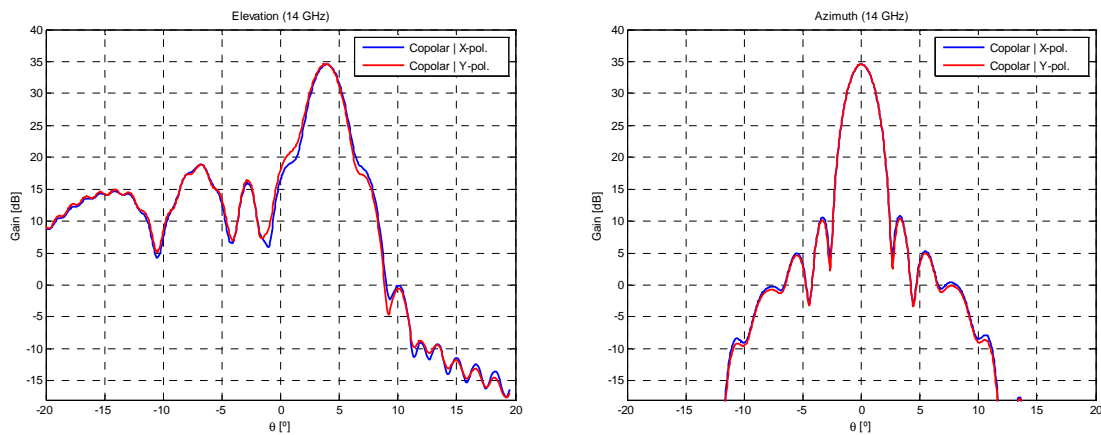


Fig. 5-10. Radiation pattern for the sub reflectarray based on aperture-coupled elements designed for 5° beam scan at 14 GHz in elevation (XZ) and azimuth planes

5.2.3 Conclusions

The proposed dual-reflectarray configuration provides phase control on both reflectarray surfaces [67], which is used to improve the antenna performance for multiple beams or for beam scanning. A dual-reflectarray antenna in Ku-band has been designed to steer the beam in a range of 13 degrees (-8 to 5 degrees). The preliminary simulated results obtained show acceptable beam scanning capabilities in a frequency band larger than a 10 %. The radiation patterns present a good behaviour in azimuth and a little distortion in elevation. A beam squint of approximate 1 degree has been observed from 10 to 14 GHz, which must be compensated in the design. The effect of

the MEMS devices has been neglected, assuming the reflectarray elements with the appropriate line lengths to provide the required phasing on the sub reflector.

In this preliminary study, the beam scanning requirements for bandwidth and beam pointing were not met for both transmit and receive frequency bands. Since the simulated results obtained by the analysis technique proposed in the second chapter show acceptable beam scanning capabilities in a frequency band larger than a 10 %, another alternative is to design the antenna for transmitting in one polarization and use the orthogonal polarization for receiving. In this case the bandwidth requirements of the reflectarray elements would be relaxed

Another alternative antenna configuration, which considers a simple 1-bit control on the main reflectarray and a passive sub reflector, is considered in the following section.

5.3 Dual-reflectarray antenna for beam scanning with 1-bit phase control on the main reflectarray

5.3.1 Antenna geometry

The antenna architecture for a single offset configuration using a 1-bit reconfigurable reflectarray analysed here was reported in [71]. It should accomplish the requirements on EIRP over RF transmit band (32 dBW/40KHz, Regulations mask ETSI EN 301.428 and ITU-R S.728.1).

The proposed main reflector is a pentagon, as shown in Fig. 5-11(a), with dimensions $3B/2=750$ mm and $2A=1200$ mm, which corresponds to $A=600$ mm and $B=500$ mm. This reflectarray comprises 5250 elements distributed in 75 row and 120 columns. The patches are assumed in a lattice with a period of $10\text{ mm} \times 10\text{ mm}$. The position of the feed is defined by $h=3000$ mm, $d_f=2518$ mm and the angle $\theta=40^\circ$, taking into account that the feed axis is directed to a point in the reflectarray 350 mm from the right edge. See Fig. 5-11 (b)

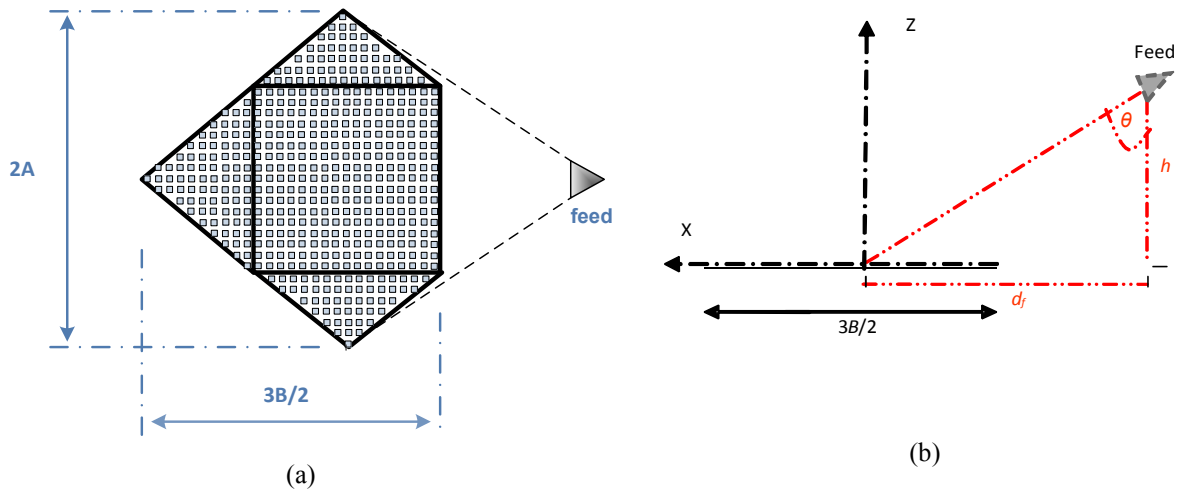


Fig. 5-11. Single offset antenna configuration. Top view (a) and lateral view (b).

In order to facilitate the folding of the antenna for transportation and to reduce the antenna dimensions, a flat sub reflectarray is designed to produce the same performance of the equivalent single-offset antenna shown in Fig. 5-11 (b) , as it can be seen in Fig. 5-12. Several configurations have been studied to improve the performance of the dual-reflectarray antenna.

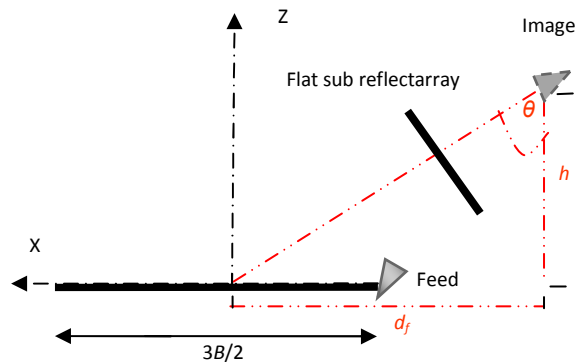


Fig. 5-12: Lateral view of the dual-offset antenna configuration

For this application, the dimensions of the sub reflectarray are limited to 500 mm × 600mm (being the expected dimensions of the suitcase that would contain the packed antenna 700 mm × 700 mm × 400 mm). Fig. 5-13 shows a CAD drawing of the entire antenna system.

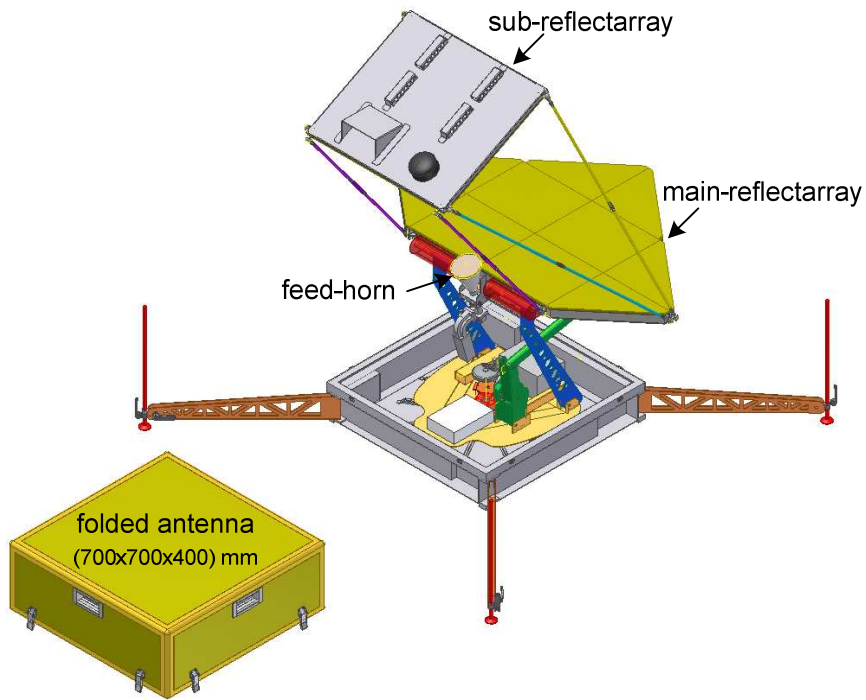


Fig. 5-13. CAD scheme of the antenna

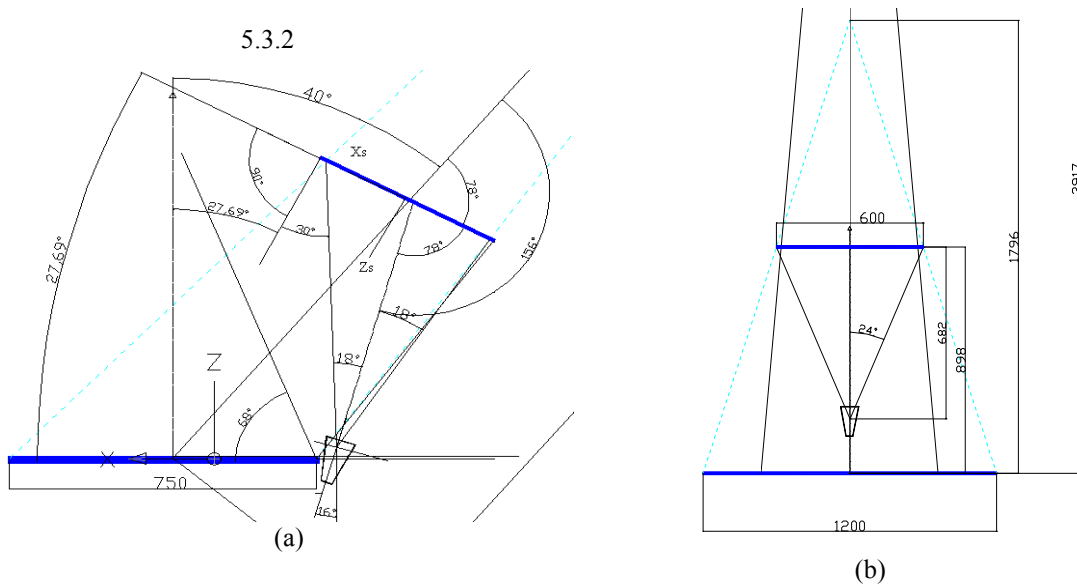


Fig. 5-14. Antenna configuration with reflectarray sub reflector. (a) Lateral view, (b) front view for focal distance of 1.8m.

The best way to illuminate the entire reflectarray surface with a sub reflectarray of dimensions $475 \text{ mm} \times 600 \text{ mm}$ is to reduce the “equivalent” focal distance to 1800 mm in the front plane while keeping the 3 m focal distance in the offset plane, see Fig. 5-14 and Fig. 5-13. The sub reflectarray forms an angle of 27.69° with respect to the X-axis of the main reflectarray and it is placed with its centre at coordinates $(-473, 0.0, 690)$

mm referred to the main coordinate system. The phase centre of the feed-horn is located at coordinates (300, 0, 30) mm referred to the main reflectarray coordinate system, see Fig. 5-14 (a). The sub reflectarray is illuminated under an angle of 48° in the YZ plane of the feed, and 36° in XZ plane.

5.3.3 *Feed-horn*

In order to illuminate properly the main reflectarray, a rectangular or elliptical horn with different beam-width in the two principal planes has been considered. However, a simplified model of the horn has been used in the preliminary results shown in this chapter. For the XZ plane of the feed coordinate system, the model used corresponds to $\cos^{q_x}\theta$ and for the YZ plane to $\cos^{q_y}\theta$. The q_x and q_y factors are defined, in order to provide the following illumination values at the edge of the main reflector at each frequency:

- Between -10dB and -8 dB at $f=10.7$ GHz
- Between -13dB and -10 dB at $f=12.75$ GHz
- Between -18dB and -12 dB at $f=14.25$ GHz

Table 5-2 includes the values of both parameters: q_x and q_y , for three frequencies: 10.7 GHz, 12.75 GHz and 14.25 GHz. These are the values needed to illuminate the main reflectarray according to the ranges mentioned before. The table also provides the illumination levels at the edges of the sub reflectarray.

Table 5-2. Values of the q_x and q_y for each frequency

Feed-horn: $\cos^q \theta$	Frequency (GHz)		
	10.7	12.75	14.25
q_x	22	28	36
q_y	16	18	24
Edge taper in XZ (dB)	-11	-13	-17
Edge taper in YZ (dB)	-12	-13	-18

5.3.4 Phase distribution for both reflectarrays.

5.3.4.1 *Phase distribution for the sub reflectarray*

Considering a sub reflectarray of 38×48 elements with a periodic cell of $12.5\text{mm} \times 12.5\text{mm}$, the phase distribution that should be implemented on the sub reflectarray at different frequencies is shown in Fig. 5-15. These phases have been calculated using geometrical optics.

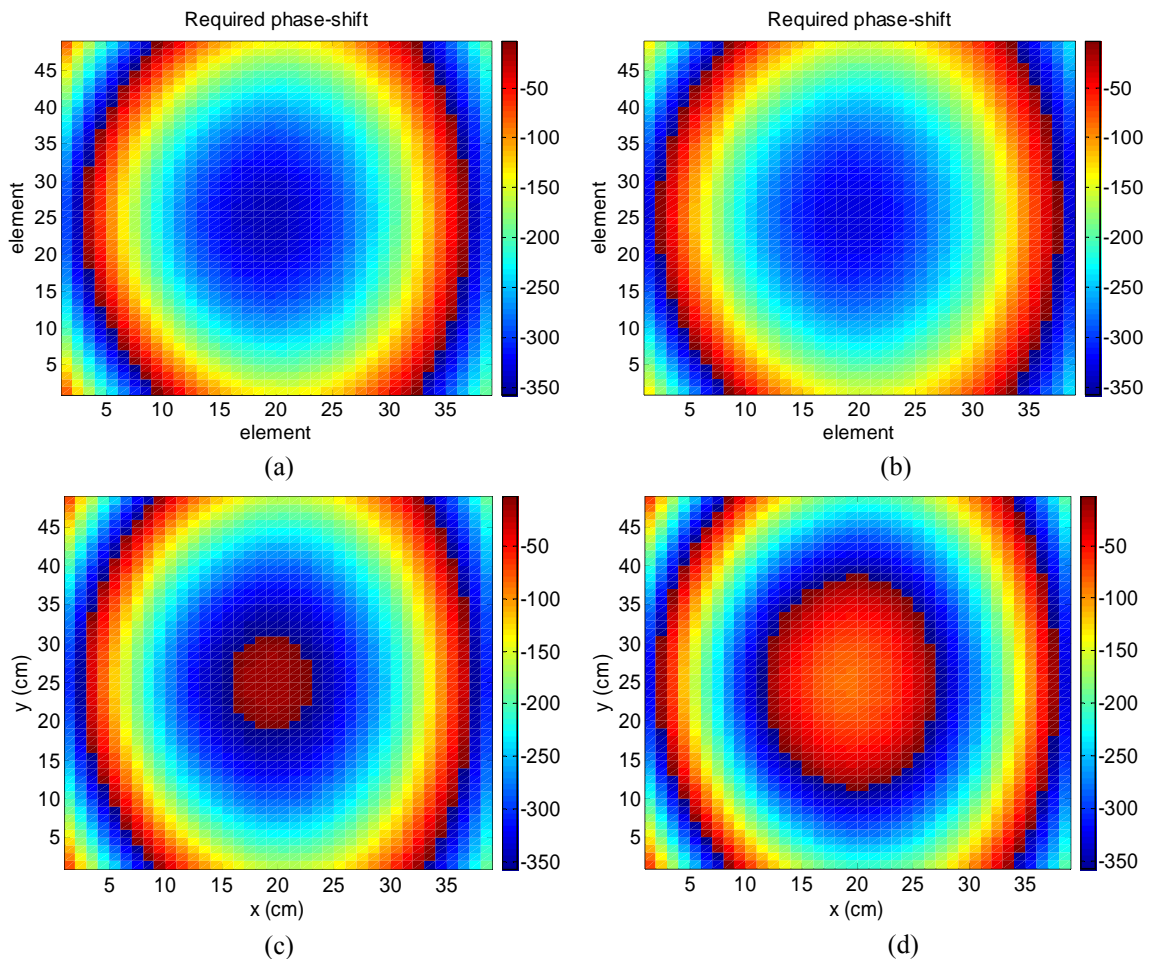


Fig. 5-15. Phase distribution to be implemented on the sub reflectarray of $47.5\text{cm} \times 60\text{cm}$ at different frequencies: 12 GHz (a), 10.7 GHz (b), 12.75 GHz (c) and 14.25 GHz (d).

The incident and reflected field (amplitude and phase) on the reflectarray sub reflector are shown in Fig. 5-16. These plots correspond to an x-polarized field when using the simplified " $\cos^{\alpha}\theta_x \cos^{\alpha}\theta_y$ " model, being the field distributions for the y-polarised field very similar.

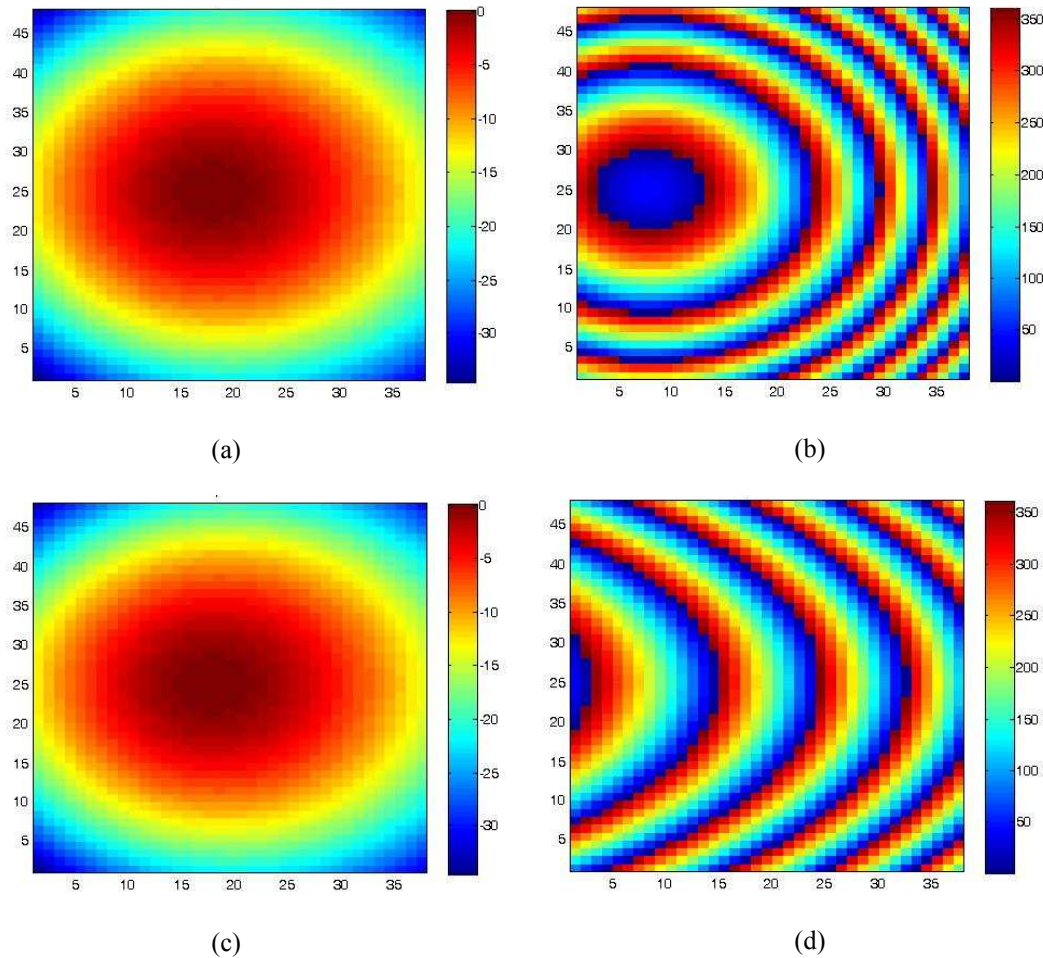


Fig. 5-16. Field distribution on the sub reflectarray at 12 GHz for x-polarisation. Amplitude (a) and phase (b) of the incident field, amplitude (c) and phase (d) of the reflected field .

5.3.4.2 Phase distribution of the main-reflectarray

In this section, the dual reflectarray antenna is analyzed to compute the incident field on the main reflectarray at different frequencies. This incident field is used to evaluate the beam scanning performance when implementing the 1-bit control on the main reflectarray. This limitation is imposed by the element of the main reflectarray in order to reduce the complexity and cost of the antenna. The dual-offset reflectarray is analyzed considering ideal phase distributions in both surfaces at three frequencies in Tx and Rx bands (10.7, 12.75 and 14.25 GHz). This analysis is a first evaluation of the antenna performance.

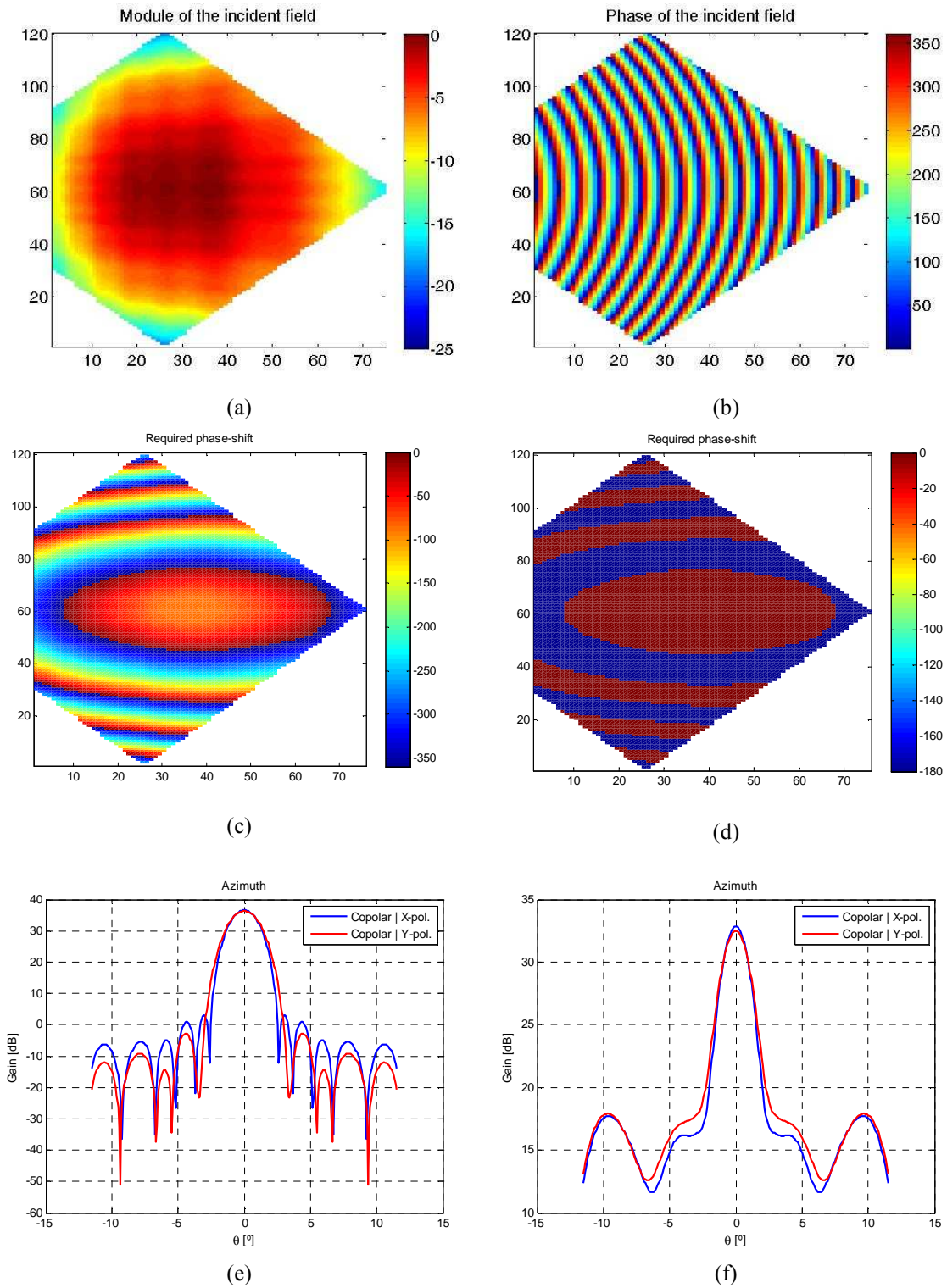


Fig. 5-17. Field distribution and radiation patterns at 10.7 GHz. Amplitude (a) and phase (b) of the incident field. Required phase distribution (c) and required phase distribution for 1-bit (d) to produce a focused beam at 40° from roadside. Azimuth cut of radiation patterns for both polarizations when the exact required phase distribution (e) and 1-bit phase distribution (f) are used in the main reflectarray.

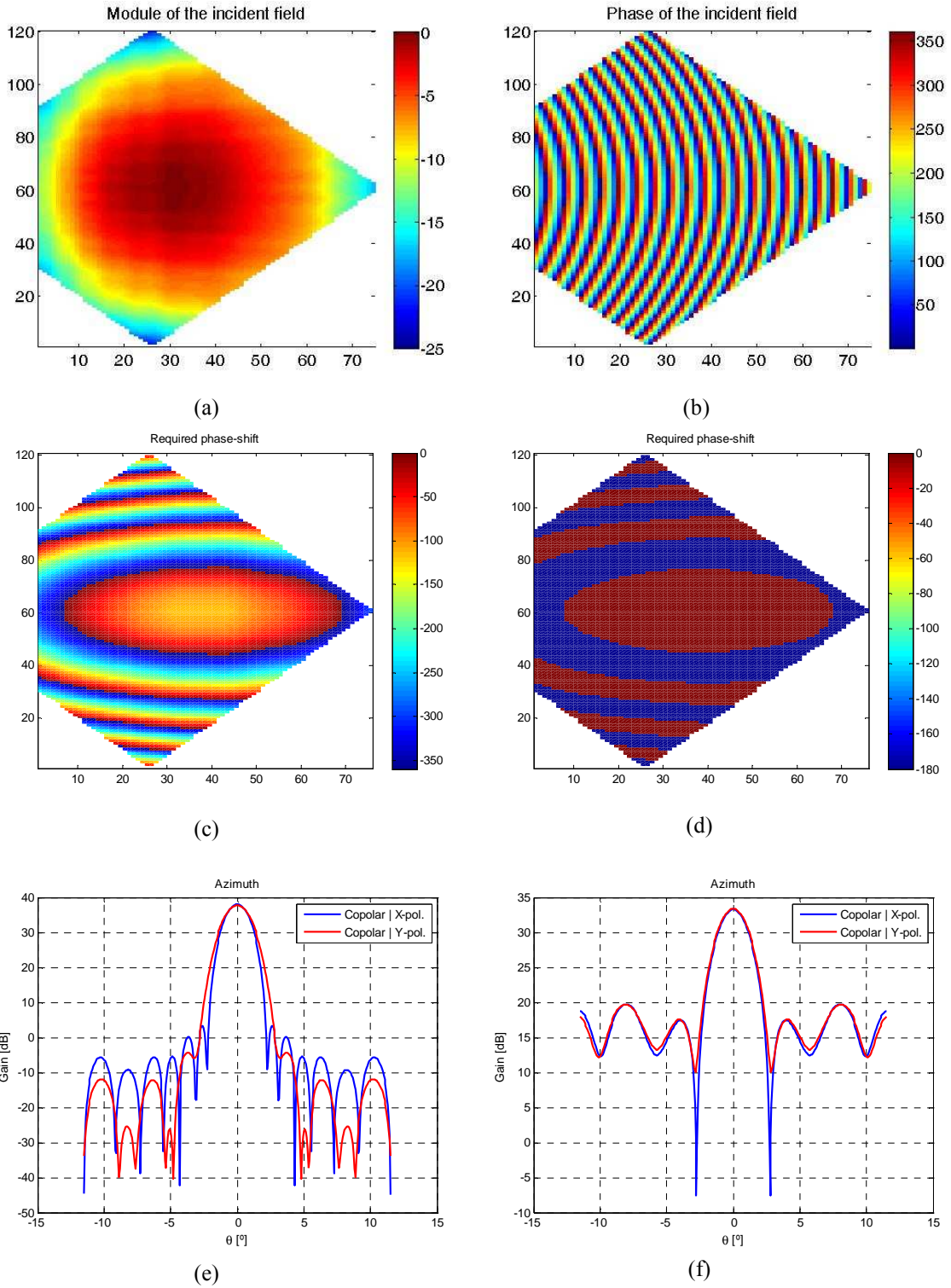


Fig. 5-18. Field distribution and radiation patterns at 12.75 GHz. Amplitude (a) and phase (b) of the incident field. Required phase distribution (c) and required phase distribution for 1-bit (d) to produce a focused beam at 40° from boadside. Azimuth cut of radiation patterns for both polarizations when the exact required phase distribution (e) and 1-bit phase distribution (f) are used in the main reflectarray.

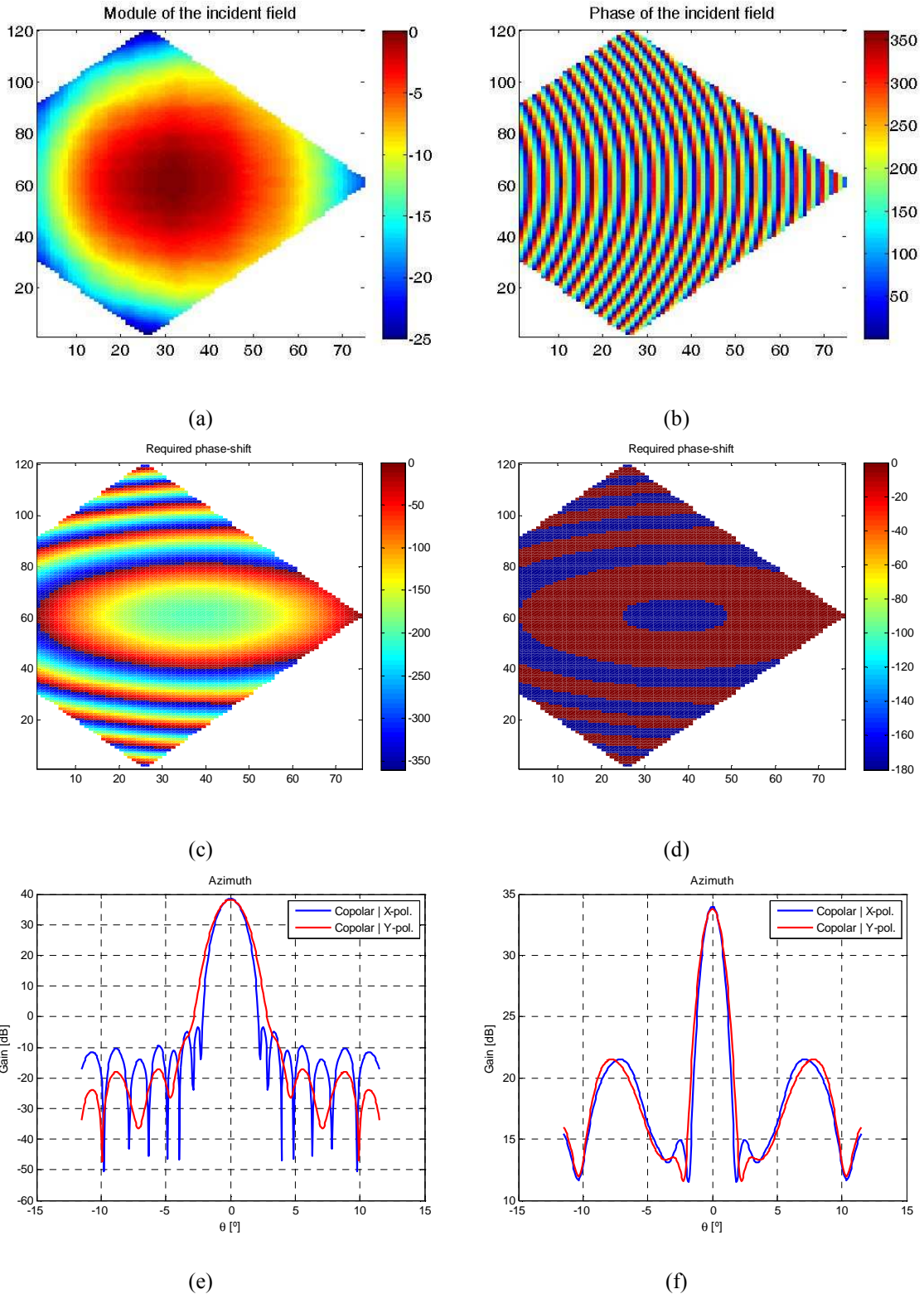


Fig. 5-19. Field distribution and radiation patterns at 14.25 GHz. Amplitude (a) and phase (b) of the incident field. Required phase distribution (c) and required phase distribution for 1-bit (d) to produce a focused beam at 40° from boadside. Azimuth cut of radiation patterns for both polarizations when the exact required phase distribution (e) and 1-bit phase distribution (f) are used in the main reflectarray.

The amplitude and phase of the incident field on the main reflectarray for x-polarization when the ideal phase distribution is considered in the sub reflectarray, is shown in Fig. 5-17, Fig. 5-18 and Fig. 5-19. When the main reflectarray is designed to produce a focused beam at 40° from broadside, the phase-shift distribution that must be implemented in the main-reflectarray and the phase of the reflected field are shown in the reception band (10.7 GHz and 12.75 GHz) and in the transmission band (14.25 GHz). As it can be checked in Fig. 5-17, Fig. 5-18 and Fig. 5-19, the radiation patterns for both X and Y polarizations are very similar, so in the rest of the chapter the plots of the radiation patterns will include only the copolar and crosspolar components of the X-polarization. Note that in Fig. 5-17 to Fig. 5-19, the phase distribution on the main reflectarray surface is shown for two cases: continuous phase control and 1-bit control (2 level quantification)

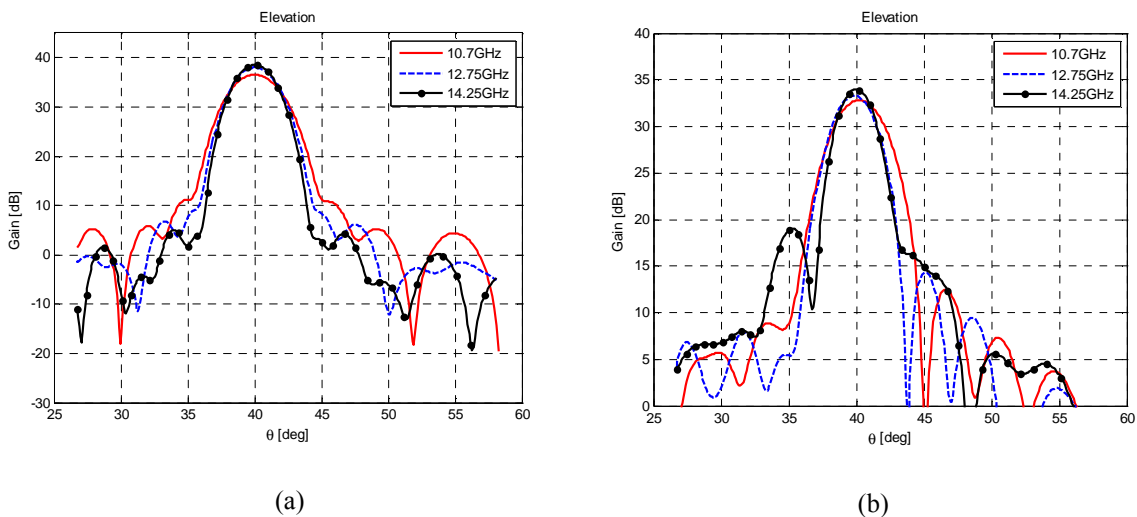


Fig. 5-20. Comparison of the elevation cut for the three frequencies studied. Using continuous phase control (a) and 1-bit phase control (b)

The beam squint has been evaluated for the three frequencies in the case of using continuous phase control in the main reflectarray resulting in 0.08345° . For the case of 1-bit control, the value of the beam squint is 0.50115° , see Fig. 5-20.

The antenna configuration is simulated to evaluate its performance in terms of gain in Rx band (10.7 – 12.75 GHz) and in Tx band (14 – 14.5 GHz). The gain is evaluated in the lower frequency of Rx band (10.7GHz) while the EIRP is computed considering the central frequency of Tx band (14.25GHz) and a bandwidth of 40KHz. Three pointing

directions are simulated to consider the performance of the antenna also as a function of the pointing angle, two of them are the extreme scanning angle defined by specification (1st direction: elevation=36.8° and azimuth=-5°, 2nd direction: elevation=31° and azimuth=0°, 3rd direction: elevation=25° and azimuth=5°).

Table 5-3 show the directivity, the maximum of cross-polarization, the angle of radiation for a 40° beam and the beam squint obtained, considering both cases: continuous and ideal 1-bit phase control. These results, only obtained for the beam radiated at 40 ° from broadside, show very low values of beam squint for both cases, better than the antenna requirements. However the beam squint is increased when the antenna is scanned to other directions, see Table 5-4.

Table 5-4 points out the beam squint calculated for a set of 5 different pointing angles for the extreme working frequencies (10.7 GHz and 14.25 GHz) considering the phase distribution discretized to 1-bit. The values of the gain and the EIRP are also included.

Table 5-3. Directivity, maximum of cross-polarisation, angle of radiation for a 40° beam and beam squint obtained for the exact phase distribution on the main reflectarray

Phases	f (GHz)	Xcp (dB)	Xxp (dB)	θ ₀ (°)
Continuous Phases	10.7	36.55	6.4	40.085
	12.75	38.03	11.14	40.00155
	14.25	38.51	12.16	40.01505
	Beam squint (10.7GHz - 12.75GHz - 14.25GHz) → 0.08345°			
1-bit Ideal Phases	10.7	32.84	234	40.20245
	12.75	33.31	5.92	39.7013
	14.25	33.99	8.13	39.9766
	Beam squint (10.7GHz - 12.75GHz - 14.25GHz) → 0.50115°			

Table 5-4. Beam squint, values of gain and EIRP for different pointing angles the at 10.7GHz and 14.25GHz

Pointing angle: (θ,φ).	Resulting pointing angle at 10.7GHz	Resulting pointing angle at 14.25GHz	(Δθ, Δφ) (Beam squint in θ and φ)	Gain (dB) @10.7GHz	EIRP (dBW/40kHz) @14.25GHz
(25.1°, -5°)	(22.8°, -6.4°)	(26.5°, -4.4°)	(3.7°, 2°)	30.42	27.31
(31°, 0°)	(29.65°, 0°)	(31.7°, 0°)	(2.1°, 0°)	31.47	31.7
(36.8°, 5°)	(36.25°, -5.8)	(36.75°, -4.25°)	(0.5°, 1.55°)	30.91	27.13
(42.5°, 0°)	(43°, 0°)	(41.75°, 0°)	(1.25°, 0°)	31.87	24.81
(48.3°, -5°)	(50.2°, 5.6°)	(47°, 4.5°)	(3.2°, 1.1°)	31.39	22.91

5.3.5 Analysis considering a real sub reflectarray

5.3.5.1 Sub reflectarray periodic cell

The reflectarray elements are based on multilayer variable-sized patches, as shown in Fig. 5-21. In order to simplify the manufacturing process and to reduce the cost, a two-layer configuration is selected for the sub reflectarray. In the proposed configuration, the patches are printed on 0.305 mm substrate, which is bonded to 3 mm separators, according to the sandwich defined in Table 5-5.

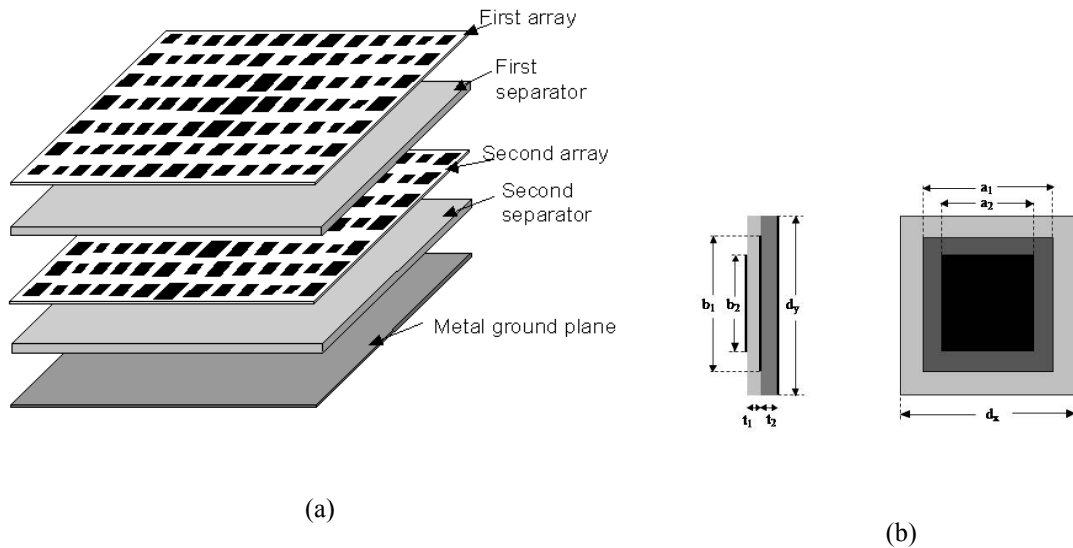


Fig. 5-21. Multi-layer reflectarray made of varying-sized patches (a)Two-layer periodic cell (b)

Table 5-5. Sandwich definition for a two-layer reflectarray

ARLON 25N (patches on bottom surface)	0.305mm	DK: 3.4, LT: 0.004
ECCOBOND 45A (Bonding film)	0.050mm	DK: 3.4, LT: 0.04
ECCOSTOCK SH-8 (separator)	3mm	DK: 1.12, LT: 0.002
ECCOBOND 45A (Bonding film)	0.050mm	DK: 3.4, LT: 0.04
ARLON 25N (patches on bottom surface)	0.305mm	DK: 3.4, LT: 0.004
ECCOBOND 45A (Bonding film)	0.050mm	DK: 3.4, LT: 0.04
ECCOSTOCK SH-8 (separator)	3mm	DK: 1.12, LT: 0.002
ECCOBOND 45A (Bonding film)	0.050mm	DK: 3.4, LT: 0.04
Aluminium plate	2.000 mm	

The phase curves and the difference in phase delay at extreme frequencies in Rx and Tx bands are shown in Fig. 5-22 for normal incidence. The curves have also been

computed for other angles of incidence, showing small variations with the incidence angle. However, the real angle of incidence is taken into account in the design of the reflectarray.

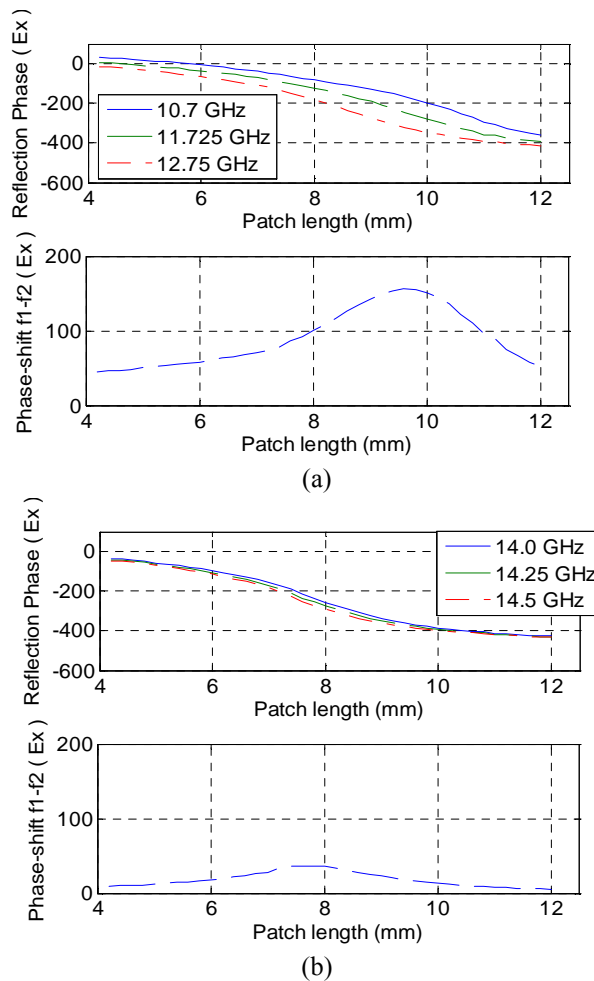


Fig. 5-22. Phase curves and difference of phase delay in the extremes of the Rx (a) and Tx (b) bands.

5.3.6 *Sub reflectarray design*

The reflectarray has been designed by using an iterative routine that adjusts the dimensions of the patches in each reflectarray element by calling an analysis routine until the required phase at each frequency and polarization is achieved. The reflectarray analysis is based on Spectral-Domain Method of Moments assuming local periodicity. As a first step in the design, the patch dimensions were determined, keeping the same ratio between layers ($a_2=0.9 a_1$, $b_2=0.7 b_1$), to fulfill the required phase distribution at 11.725 GHz. To design the reflectarray in two frequency bands, the patch dimensions are adjusted to match the required phase-shift distribution at central and extreme frequencies in each of the Tx and Rx bands (10.7, 11.725, 12.75, 14.0, 14.25 and 14.5

GHz), starting from the patch dimensions obtained by the design at 11.725 GHz. This step is carried out element by element, using an optimization routine based on Fletcher-Powell algorithm which adjusts all the dimensions of the stacked patches simultaneously, to match with a minimum error the required phase at central and extreme frequencies considered. Once the dimensions of all the patches are obtained for both polarizations, the phase distribution and the errors obtained at each frequency are evaluated. The photo-etching masks for the two layers of patches are shown in Fig. 5-23 and Fig. 5-24.

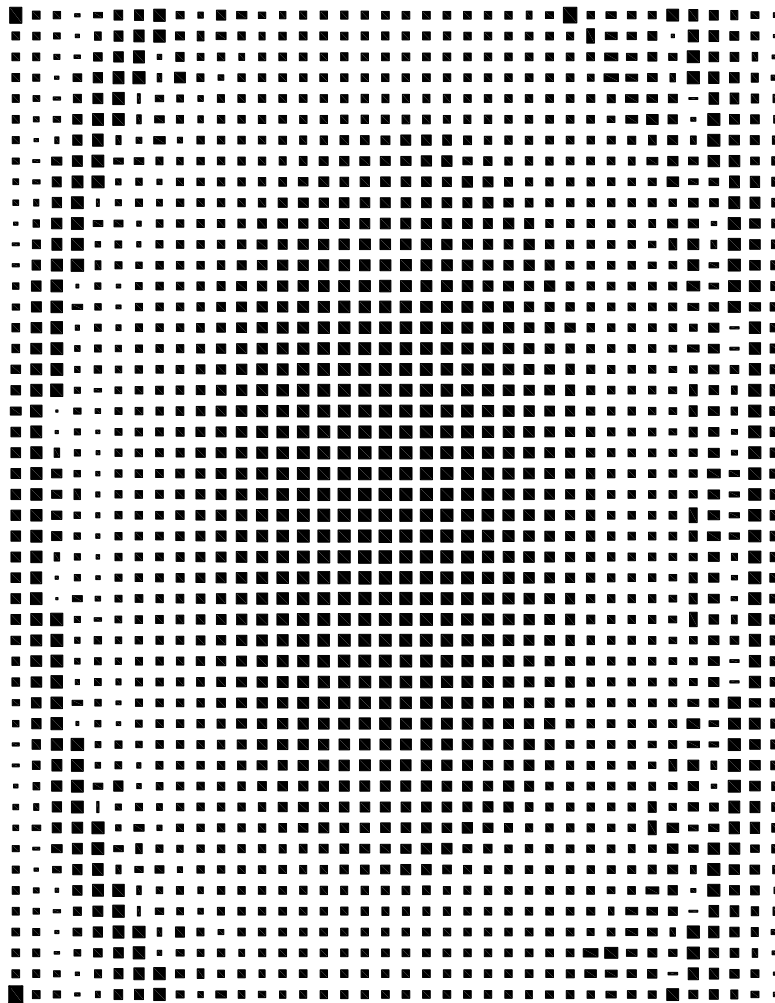


Fig. 5-23. Mask of reflectarray for the second layer of patches (top layer)

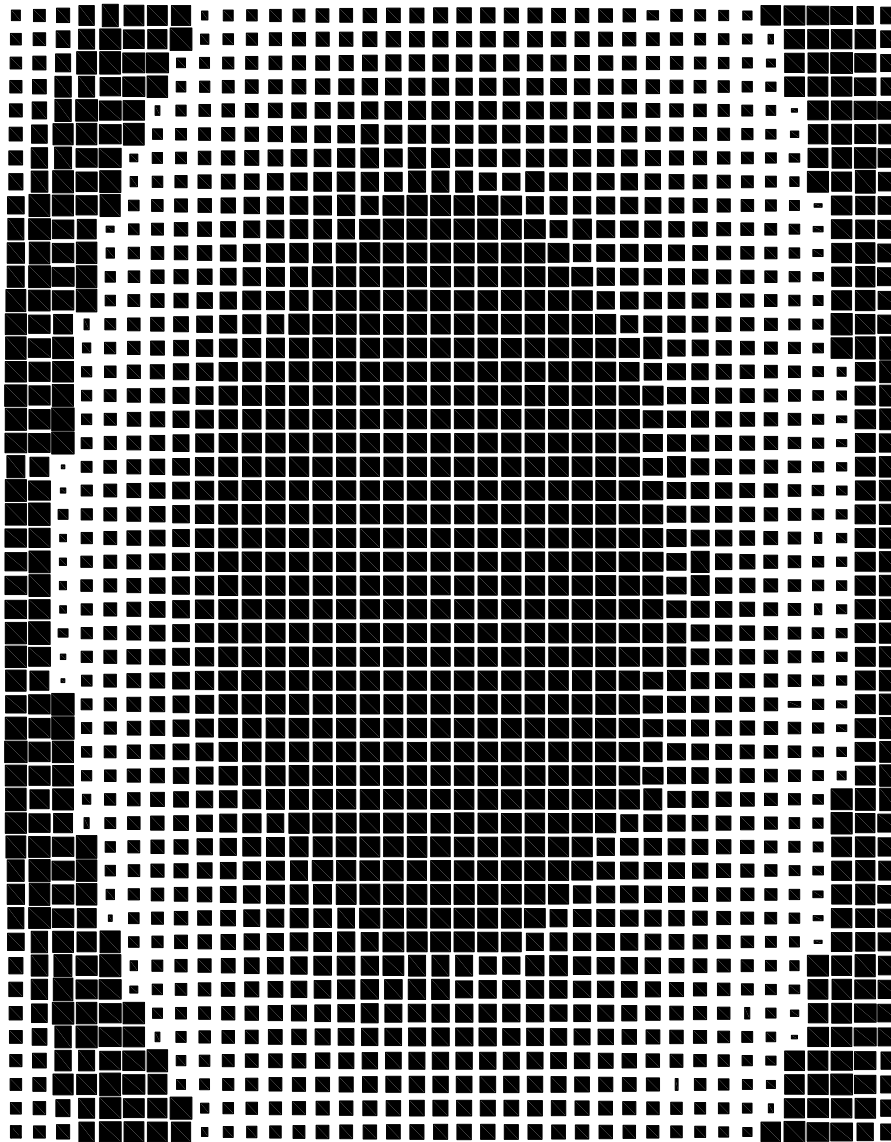


Fig. 5-24. Mask of reflectarray for the first layer of patches (bottom layer)

The phase-shift introduced by the optimized reflectarray is computed and compared with the objective phase distribution at each frequency, see Fig. 5-25 to Fig. 5-28. As shown in the figures, there are slight discrepancies between the required phase distribution at each frequency and the one obtained by analyzing the optimized reflectarray. The errors in phase in Rx and Tx band are shown in the figures Fig. 5-25 to Fig. 5-27. The errors in Fig. 5-26 and Fig. 5-28 represent the error in the difference of phase delay (dispersion of phase with frequency) computed between central and extreme frequencies in each band for x-polarization. The corresponding plots for y-polarization are very similar. Note that these errors are proportional to the phase error at extreme frequencies. It has been checked that only in 2% of the elements the error is

larger than 30° for the Tx band (14.0-14.5 GHz), while 18% of the elements exhibit this error in Tx band (10.7-12.75 GHz). These errors can be significantly reduced if a third layer of patches is added to the reflectarray.

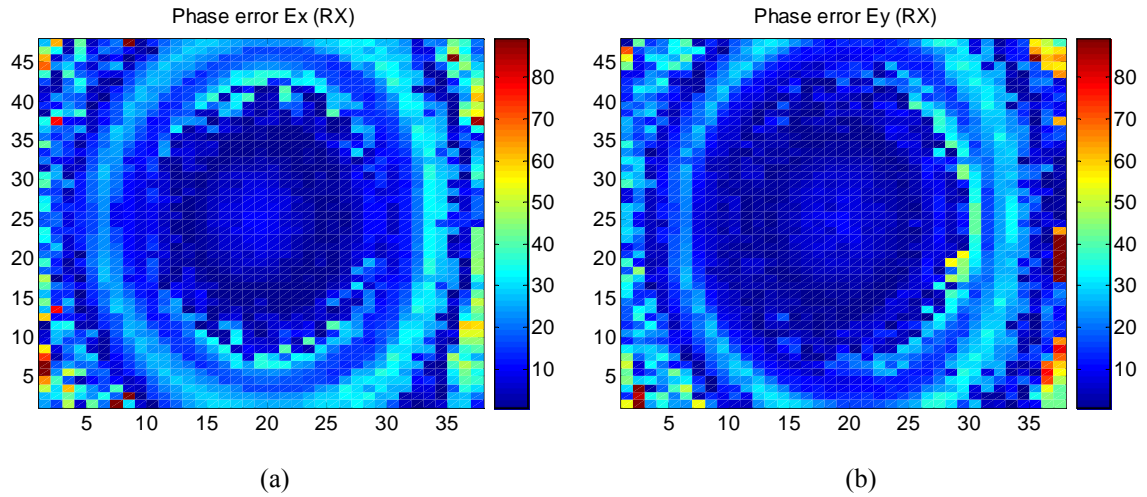


Fig. 5-25. Error in phase (difference between required and computed phases) at central frequency in Rx for X (a) and Y (b) polarisation

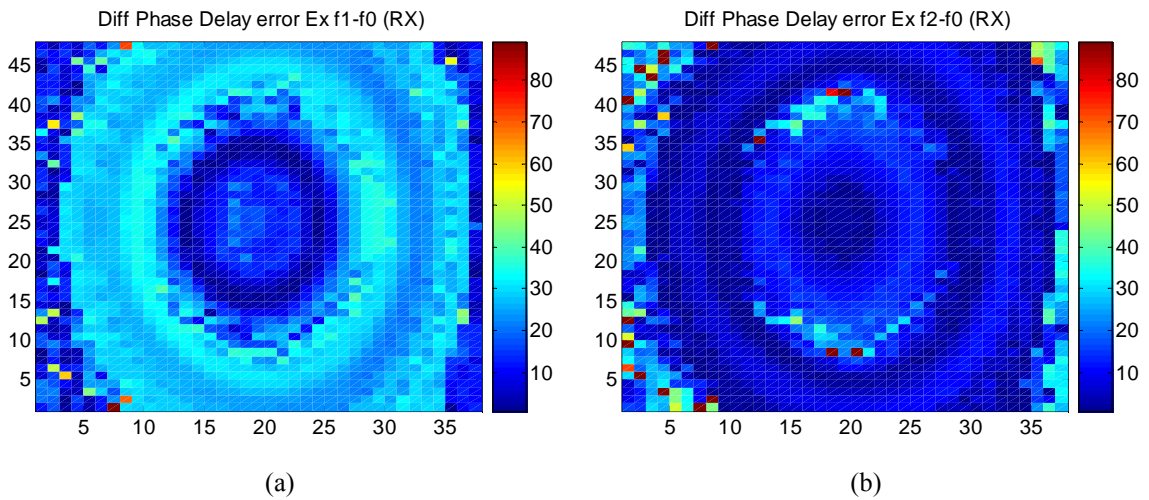


Fig. 5-26. Error in difference of phase-delay between central and extreme frequencies in Rx for X-pol. For 10.7 GHz (a) and 12.75 GHz (b).

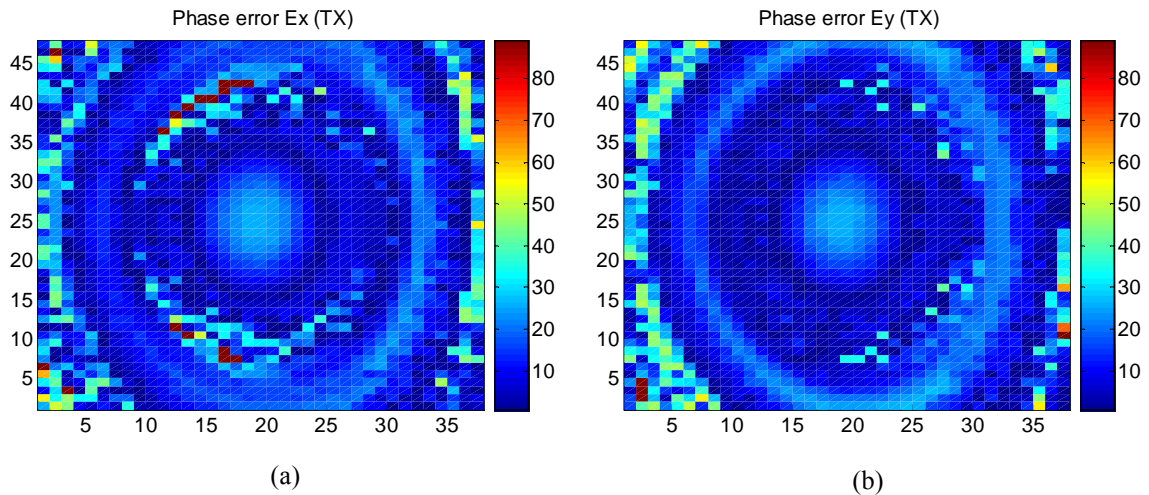


Fig. 5-27. Error in phase (difference between required and computed phases) at central frequency in Tx (14.25 GHz) for X (a) and Y (b) polarisation (b).

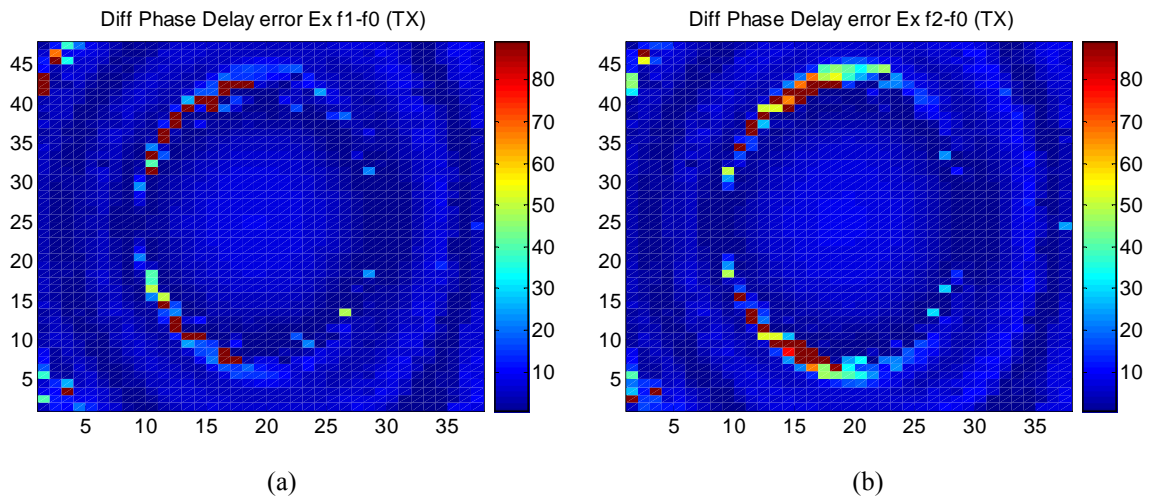


Fig. 5-28. Error in difference of phase-delay between central and extreme frequencies in Rx for X pol. For 14 GHz (a) and 14.5 GHz (b).

5.3.7 Main-reflectarray element

The element developed for the main reflectarray is a wideband (10.7 GHz - 14.5 GHz) dual polarization element that can be reconfigured through PIN diodes. The elementary cell consists of a circular patch coupled to a phase shifting circuit with 1-bit phase resolution (0° - 180°), which was demonstrated to be workable to simplify large reconfigurable reflectarrays [72], [73]. The 1-bit cell proposed in [74] provides a flat phase shift over a broadband.

5.3.8 Analysis of dual reflectarray including the two-layer sub reflectarray

The analysis previously performed using ideal phase distributions in both reflectarray surfaces, is now repeated at 10.7 GHz, 12.75 GHz (Rx) and at 14.25GHz (Tx) using the designed two-layer sub reflectarray. The amplitude and phase of the incident field for both polarizations are shown in Fig. 5-29 to Fig. 5-31. The continuous phase-shift distribution that must be implemented in the reflectarray and the azimuth cut of the radiation pattern are also shown for a beam radiated at 40 degree from broadside.

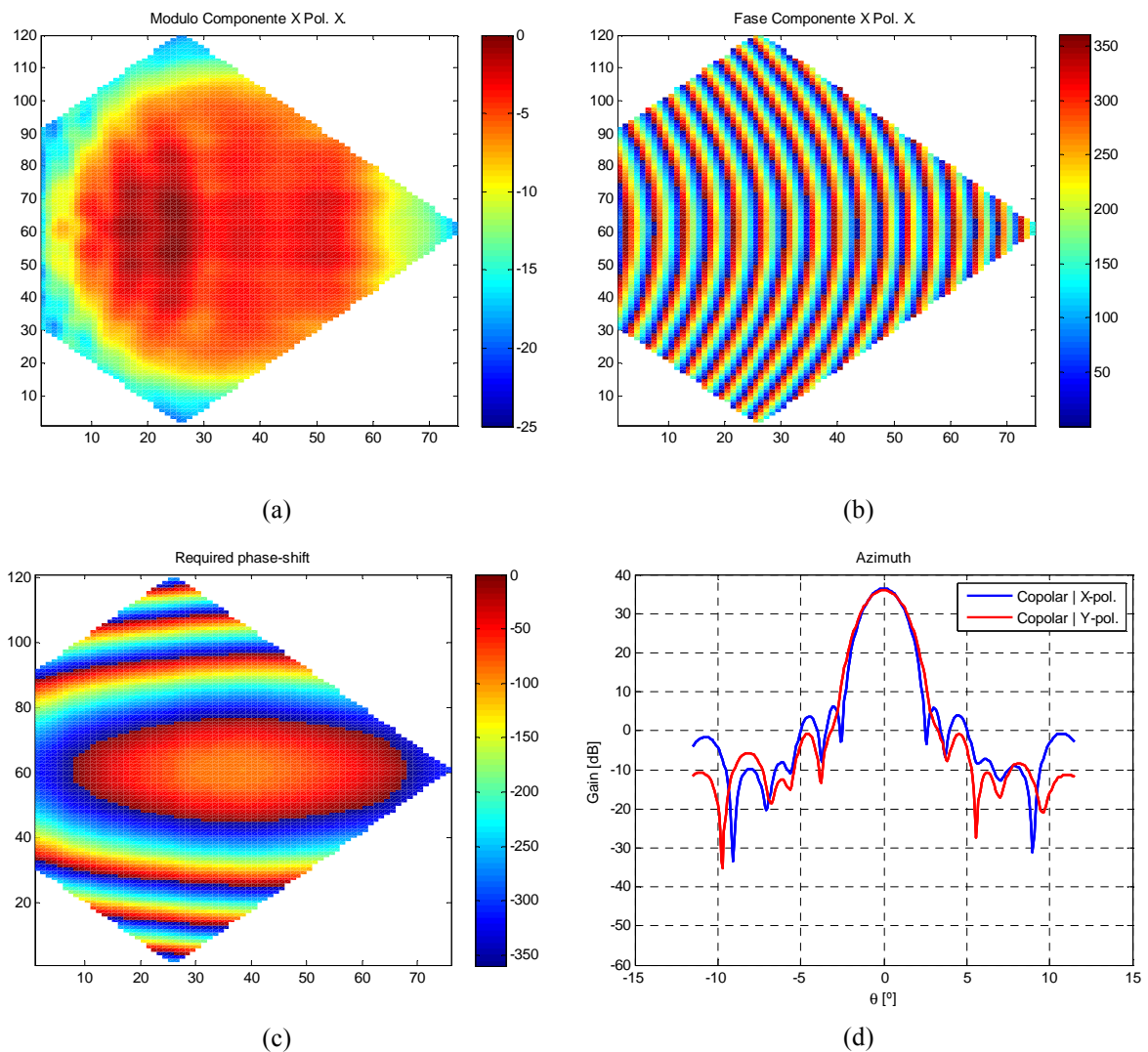


Fig. 5-29. Field distribution on the main reflectarray and radiation patterns at 10.7 GHz, considering the two-layer sub reflectarray. Amplitude (a) and phase (b) of the incident field. Required phase distribution (c) and azimuth cut of radiation pattern for x-polarisation.

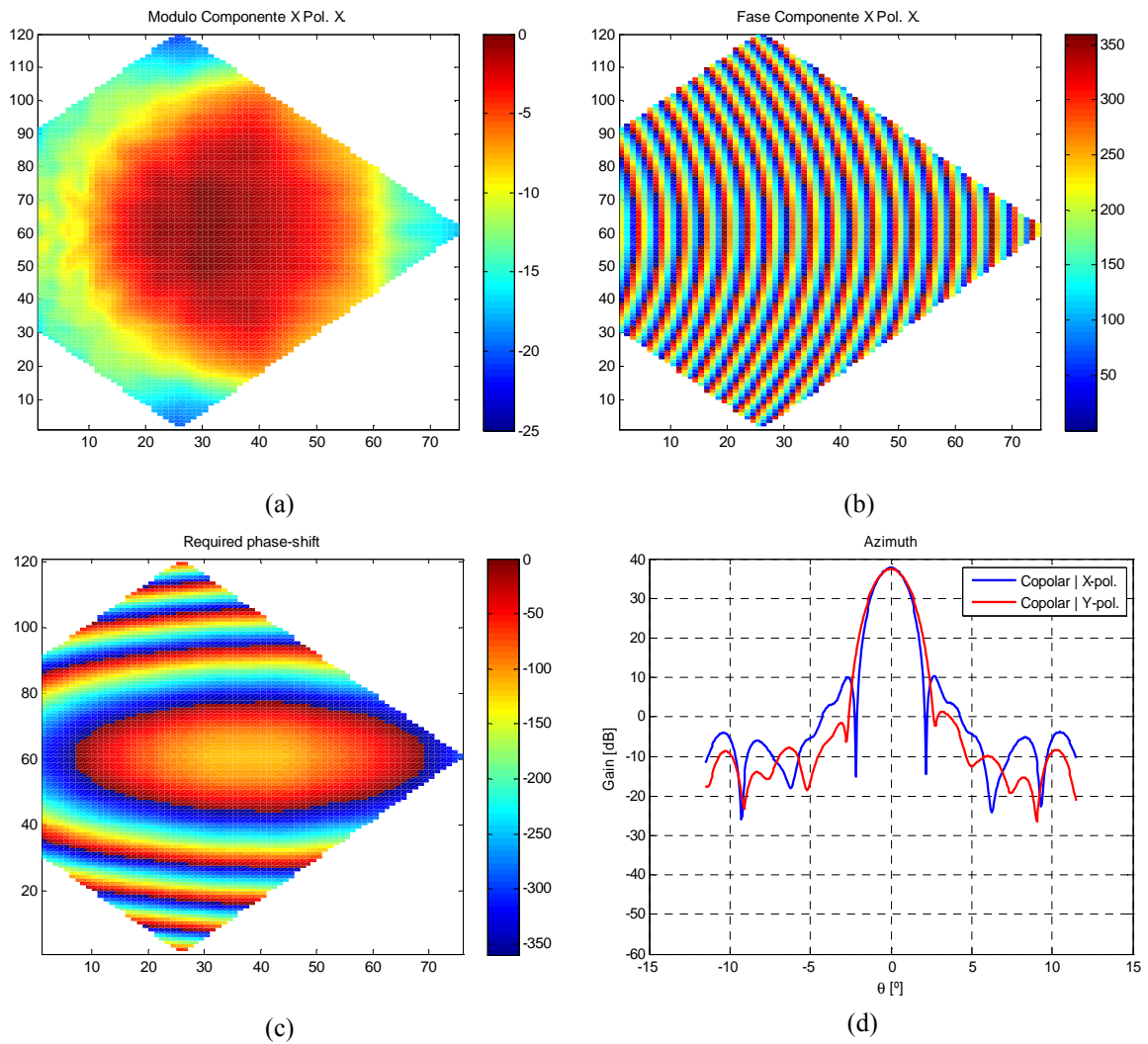


Fig. 5-30. Field distribution on the main reflectarray and radiation patterns at 12.75 GHz, considering the two-layer ssb reflectarray. Amplitude (a) and phase (b) of the incident field. Required phase distribution (c) and azimuth cut of radiation pattern for x-polarisation..

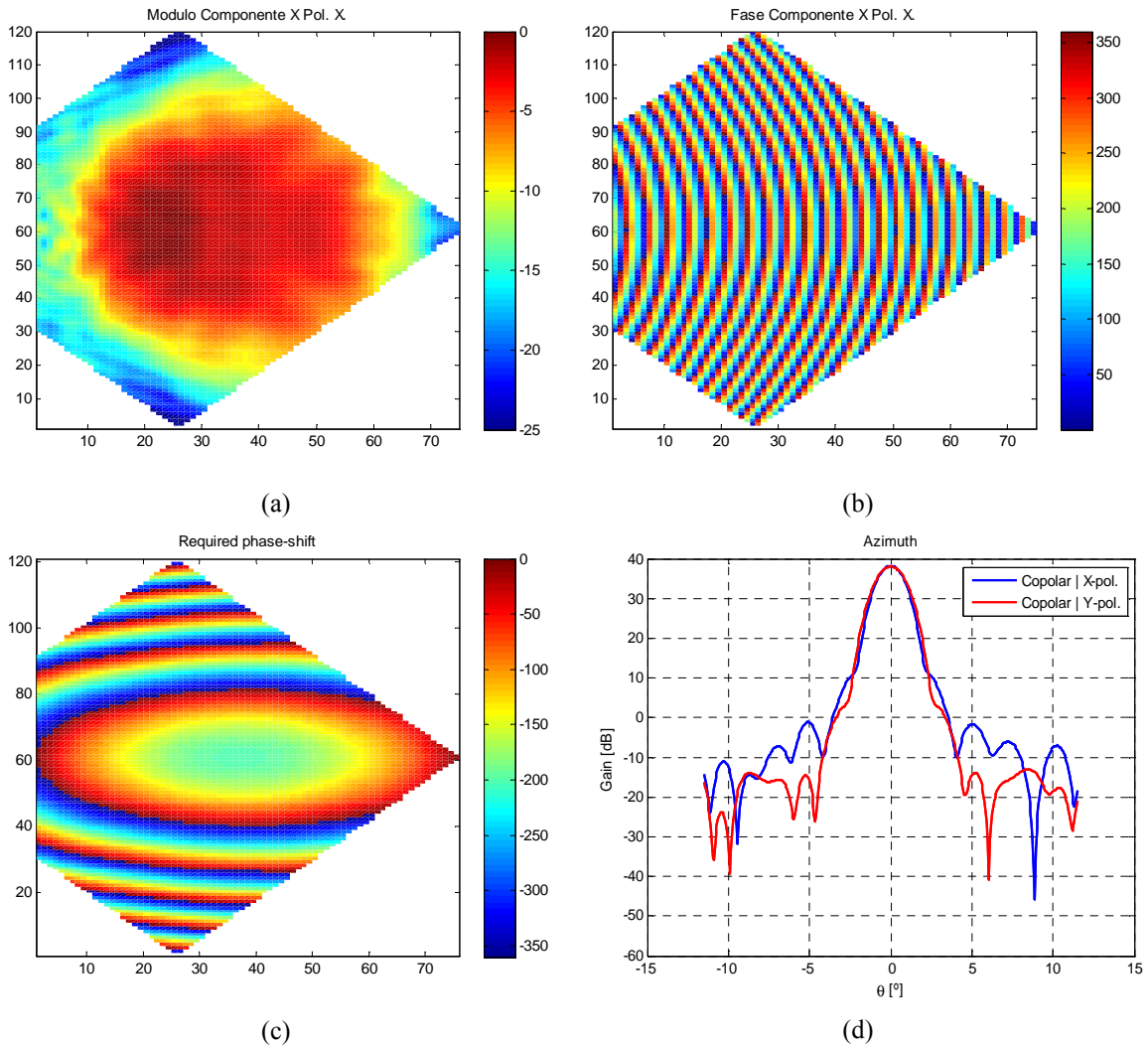


Fig. 5-31. Field distribution on the main reflectarray and radiation patterns at 14.25 GHz, considering the two-layer sub reflectarray. Amplitude (a) and phase (b) of the incident field. Required phase distribution (c) and azimuth cut of radiation pattern for x-polarisation.

In a second step, the appropriate states of all the 1-bit reconfigurable elements are determined to provide a focused beam in a given scan direction. Then, the radiation patterns of the antenna are computed taking into account the real dispersion of the reconfigurable reflectarray element. These computations are repeated for different scan angles and for different frequencies. The co and crosspolar radiation patterns for a beam radiated at 30° from broadside in XZ-plane at 10.7GHz, 12.75 GHz (Rx) and 14.25 GHz (Tx) are shown in Fig. 5-32. The value of the EIRP is larger than 31dB for all frequencies.

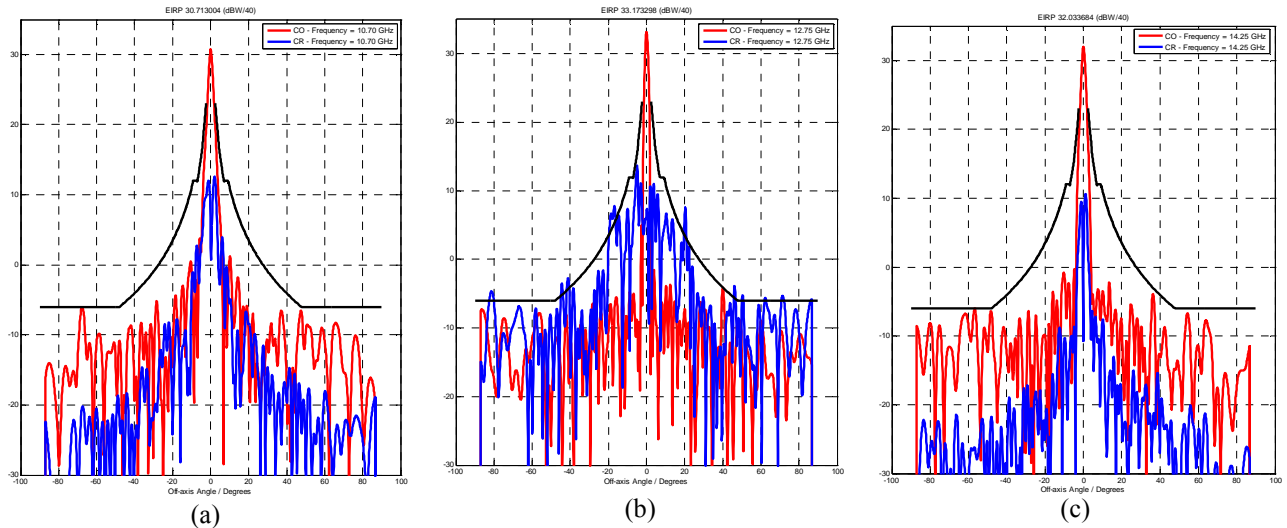


Fig. 5-32. Radiation pattern superimposed with the mask of requirements at 10.7GHz (a), 12.75GHz (b) and 14.25GHz(c)

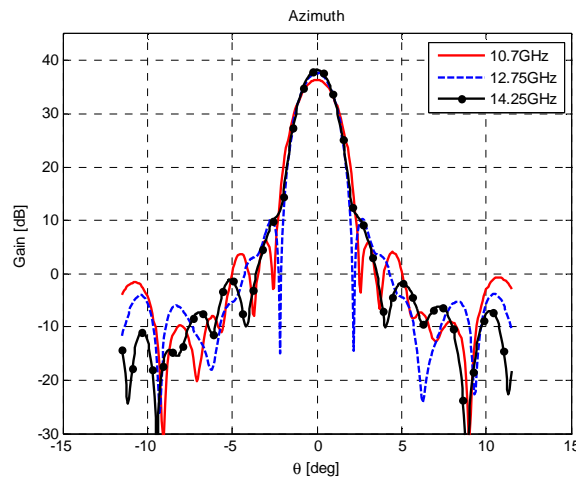


Fig. 5-33. Comparison of the elevation cut for the three frequencies studied.

The beam squint calculated for the three frequencies in the case of continuous phase control in the main reflectarray and a two layer sub reflectarray is **0.161°**, see Fig. 5-33.

5.4 Conclusions

Two different dual-reflectarray configurations have been studied in order to provide electronic beam steering in portable systems for Ku-band satellite links with automatic pointing capabilities. In the first architecture, the main reflectarray is passive and the beam scanning is achieved by introducing a phase-control in the elements of the sub reflectarray. The main drawbacks observed in this configuration are that the main reflectarray has to be oversized and it is difficult to design a reflectarray element in dual polarization that covers both transmit and receive bands. To overcome these problems, a

second configuration, which comprises a passive sub reflectarray and a main reflectarray with 1-bit electronic control, has been studied. A two-layer reflectarray has been designed for the sub reflector. The small errors in phase have been evaluated at different frequencies. If necessary, to improve the antenna performance these errors can be reduced by adding a third layer in the passive reflectarray sub reflector. The preliminary results show a satisfactory antenna performance in the prescribe frequency bands for transmit and receive.

CHAPTER 6

6 Dual-Reflector configuration with parabolic main reflectarray

An alternative dual reflectarray antenna consist of replacing the main flat reflectarray by a reflectarray printed on a parabolic surface, or in general in a curved surface. The alternative antenna configuration proposed in this chapter is made of three components: a primary feed, a flat sub reflectarray and a parabolic main reflectarray, as shown in Fig. 6-1. In this antenna, only slight adjustments of the phase shift is required on the main reflectarray since the parabolic surface focusses the field itself. In principle a dual-offset configuration is considered and a horn antenna is used as the primary feed. In general, the two reflectarrays used as sub and main reflectors are considered as arrays in rectangular lattices of printed stacked patches of varying size above a ground plane [2].

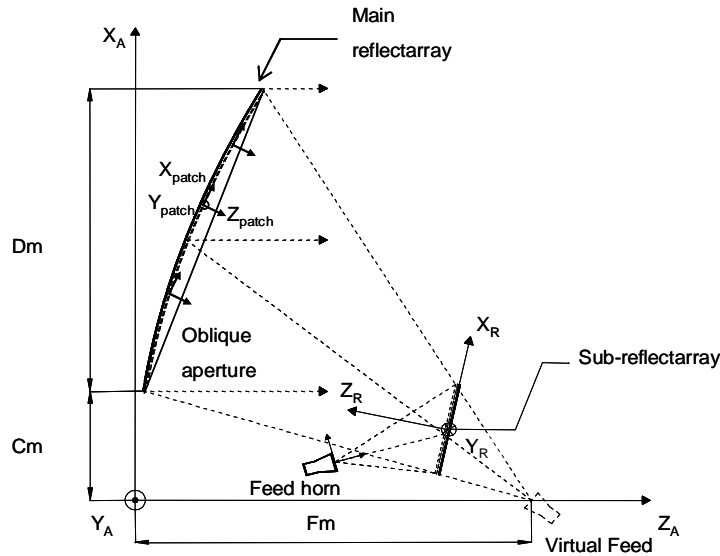


Fig. 6-1. Scheme of a dual-reflectorarray structure analysis

For the analysis of this antenna, five coordinate systems are required: the feed reference system, (x_F, y_F, z_F) , which is centred at the phase-centre of the primary feed; the sub reflectarray reference system, defined by (x_{SR}, y_{SR}, z_{SR}) , its origin is placed at the centre of the sub reflectarray surface, the element reference system $(x_{epq}, y_{epq}, z_{epq})$, which is placed at the centre of each element of the parabolic main reflectarray, defined by the subindexes (m,n) , the aperture coordinate system defined by (x_{ap}, y_{ap}, z_{ap}) and its origin, is at the center of the aperture and the antenna coordinate system (x_A, y_A, z_A) , with the Z_A axis on the direction of the shaped beam, as usual in reflector antennas.

The elements of the flat sub reflectarray and the main parabolic reflectarray are analysed through the general technique implemented for multilayer reflectarrays [2], which has been demonstrated to be accurate and time-efficient [39]. Each reflectarray is analysed by computing the total reflected field on each cell by a full-wave analysis based on MoM, assuming that each cell is in a periodic environment, [2],[3]. The calculation of the reflected field includes dissipative losses on the reflectarray and the cross polarisation produced by the printed patches and by the antenna geometry.

This antenna configuration is analysed in a similar way than the case of the dual flat reflectarray antenna: First, the field radiated by the feed horn is considered as an incident field on each sub reflectarray element. In some cases, a conventional $\cos^q(\theta)$ can be used to model the feed with good accuracy [62]. In general, the sub reflectarray elements are placed in the Fresnel zone of the primary feed and therefore the near field

of the feed must be taken into account, which can be obtained through full-wave simulations or measurements of the feed, [19],[49].

In general the feed will radiate dual linear polarisation, vertical and horizontal, with the electric field on the X_F and Y_F directions, respectively. The incident field must be computed on the sub reflectarray surface at the centre of each reflectarray cell and then transformed into the sub reflectarray reference system. Note that although the polarisation of the feed is pure-linear, the incident field has two components, since the antenna geometry produces a small cross-polar component.

In the second step, the sub reflectarray is analysed element by element, considering the same assumptions as for the case of flat reflectarrays.

$$\mathbf{E}_{ref}(p, q) = \mathbf{R}^{p,q} \cdot \mathbf{E}_{in}(p, q) \quad (6-1)$$

The matrix $\mathbf{R}^{p,q}$ relates the Cartesian components of the incident and the reflected fields.

$$\mathbf{R}^{p,q} = \begin{pmatrix} \rho_{xx}^{p,q} & \rho_{yx}^{p,q} \\ \rho_{xy}^{p,q} & \rho_{yy}^{p,q} \end{pmatrix} \quad (6-2)$$

The main reflectarray is analysed using the same technique as for the sub reflectarray. Although the cells of the main reflectarray are located in the Fresnel zone of the sub reflectarray, they are placed in the Far-Field region of the sub reflectarray cells (small apertures). Thus, the computation of the incident electric field on the main reflectarray surface can be computed as the superposition of all the contributions from the sub reflector elements. For a very accurate analysis of the main reflectarray, the reflected field on each element of the main should be computed for the contributions of each sub reflectarray cell. Nevertheless, the incidence angles for different contributions of the sub reflectarray cells on the elements of the main reflectarray are only slightly different, as it happens in the case of a flat main reflectarray. Therefore an approximation can be applied, considering the same incidence angle for all the contributions of the sub reflectarray. This simplification produces a significant reduction in the computation time.

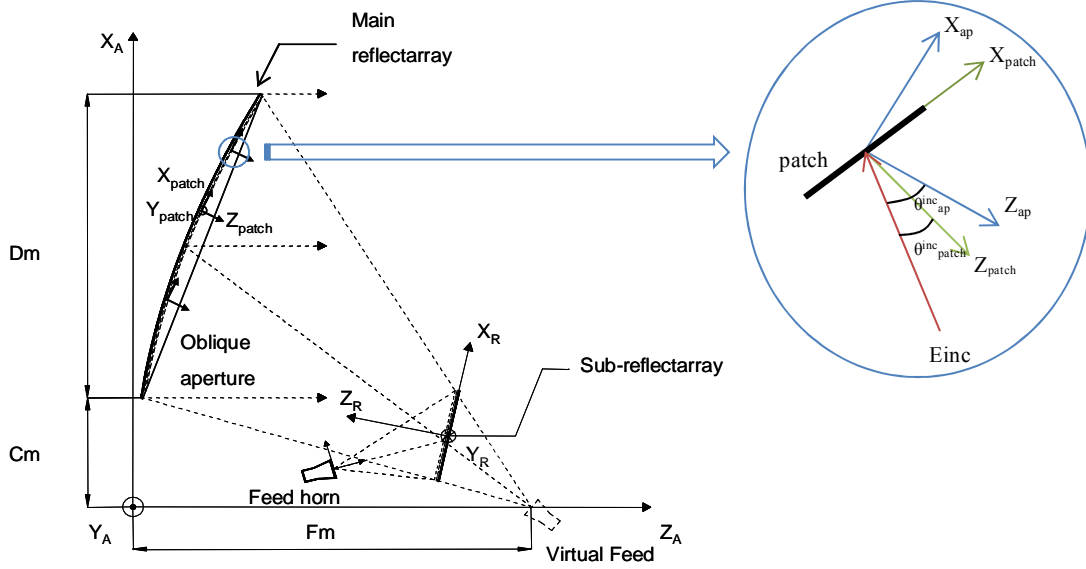


Fig. 6-2. Scheme of a dual-reflector structure analysis with patch coordinate system detail

The calculation of the incident angle in every cell of the main reflectarray has been done considering a local coordinate system. Every x_{patch} axis has been defined according to the direction of the patch in the XZ plane. The fact of using a different coordinate system for analysing each patch instead of using a common coordinate system for all of them, provides a more appropriate calculation of the incident angle since the inclination effect of each patch produced by the curvature can be taken into account, see Fig. 6-2.

After calculating the incident field, the field scattered at each element of the main reflectarray is computed again by SD-MoM.

$$\mathbf{E}_{ref}^{X/Y}(m, n) = \mathbf{R}(m, n) \cdot \sum_p \sum_q \mathbf{E}_{inc(p,q)}^{X/Y}(m, n) \quad (6-3)$$

where

$$\mathbf{R}(m, n) = \begin{pmatrix} \rho_{xx}^{m,n} & \rho_{yx}^{m,n} \\ \rho_{xy}^{m,n} & \rho_{yy}^{m,n} \end{pmatrix} \quad (6-4)$$

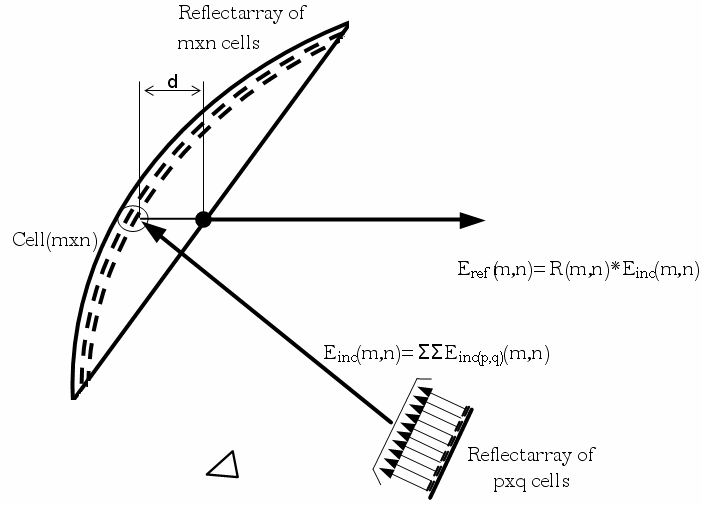


Fig. 6-3. Scheme of a dual-reflectarray structure with a parabolic main reflectarray for the method of analysis

Once the reflected electric field on the curved surface is known, it is projected to the oblique aperture of the curved reflectarray, defined by the contour of the parabolic reflector, as:

$$\mathbf{E}_{ref\ ap}^{X/Y}(m, n) = \mathbf{E}_{ref}^{X/Y}(m, n) \cdot e^{j\phi} \quad (6-5)$$

by using the phase displacement,

$$\phi = k_0 d = k_0 (z - z_{ap}) \quad , \quad (6-6)$$

d is the distance between the z components of the paraboloid and the oblique aperture, and ϕ is the phase factor introduced because of the displacement from the reflector to the integration plane [75] , see Fig. 6-3.

Finally the radiation patterns of the entire antenna are computed starting from the electric field on the aperture of the main reflectarray in a similar maner as for the main flat reflectarray, using an algorithm based on the FFT. The radiation patterns are computed in gain taking into account the total power radiated by the feed, the ohmic losses in the reflectarray as well as the spillover and aperture efficiencies.

6.1 Analysis of a parabolic reflectarray in a dual reflector configuration

The analysis technique described here has been applied to accurately analyse the single offset parabolic reflectarray designed in [9] for a South American coverage. Although the analysis tool has been developed for dual-reflectarray antennas, the reflectarray sub reflector is substituted by a flat metal plate, in order to analyse the single offset parabolic reflectarray reported in [9].

6.1.1 *Antenna geometry*

To analyze the single parabolic reflector, a flat sub reflectarray that introduces a constant phase distribution (acting as a metal plate) is considered, resulting a geometry equivalent to the one reported in [9], see Fig. 6-4 gives the data of the antenna geometry, including the flat sub reflector considered in the analysis. Table 6-1 shows the main parameters of the antenna geometry.

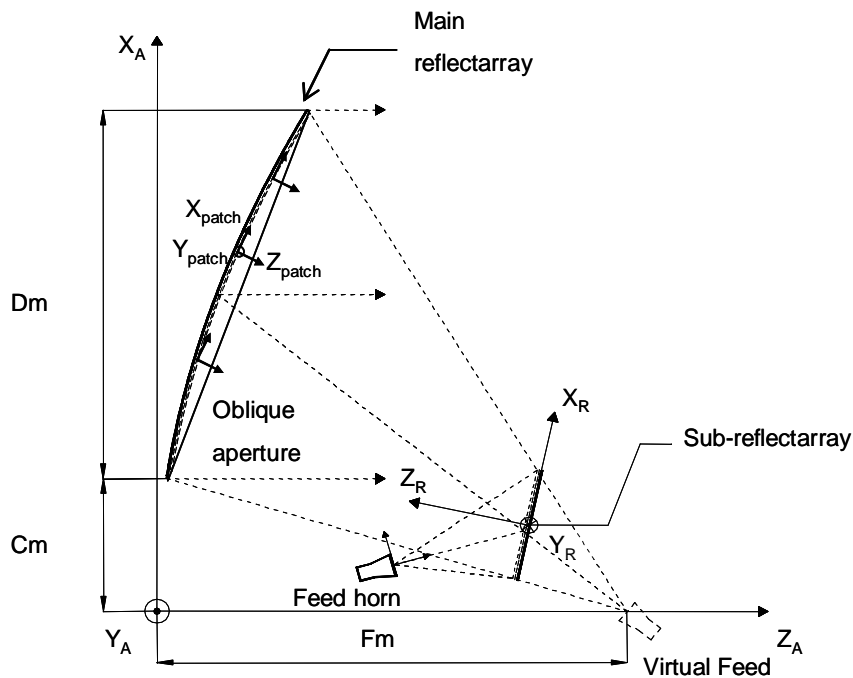


Fig. 6-4. Scheme of a dual-reflectarray structure analysis

Table 6-1. Main data of the studied geometry

EQUIVALENT PARABOLIC GEOMETRY	
Diameter of the projected aperture (Dm)	1500mm
Clearance (Cm)	200mm
Focal distance (Fm)	1800mm
MAIN REFLECTARRAY <i>(data in antenna coordinate system)</i>	
Main reflectarray dimensions	1551 x 1500mm
Matrix of direction cosines <i>(Relationship between Antenna and Main reflectarray Coordinate Systems)</i>	$\begin{bmatrix} 0.9669 & 0 & 0.2551 \\ 0 & 1 & 0 \\ -0.2551 & 0 & 0.9669 \end{bmatrix}$
FLAT SUB REFLECTOR <i>(data in antenna coordinate system)</i>	
Centre (x _{fm} , y _{fm} , z _{fm})	(406, 0.0, 1175) mm
Sub reflectarray size	598 × 559 mm
Matrix of direction cosines <i>(Relationship between Antenna and Sub reflectarray Coordinate Systems)</i>	$\begin{bmatrix} 1 & 0 & 0 \\ 0 & -1 & 0 \\ 0 & 0 & -1 \end{bmatrix}$
FEED-HORN <i>(data in sub reflectarray coordinate system)</i>	
Phase centre	(-329, 0, 437)mm
Pointing <i>(on the reflectarray surface)</i>	(-78, 0, 0)mm
Illumination level at the sub reflectarray edges	-18 dB

The phase-shift distribution necessary to obtain the required South-American coverage was obtained in [9] using geometrical optics, and it is shown in Fig. 6-5. To implement this phase distribution, a unit cell with two stacked rectangular patches has been used as reflectarray element. The patches arranged in a periodic lattice of 13 mm × 13 mm are assumed to be printed on a 125-micron Kapton film bonded to a Quartz fabric composite layer and separated by Quartz honeycomb separators of thickness 3.5 mm. Patch dimensions, shown in Fig. 6-6, were adjusted to provide the required phase distribution to shape the beam [9], and the result masks are shown in Fig. 6-7.

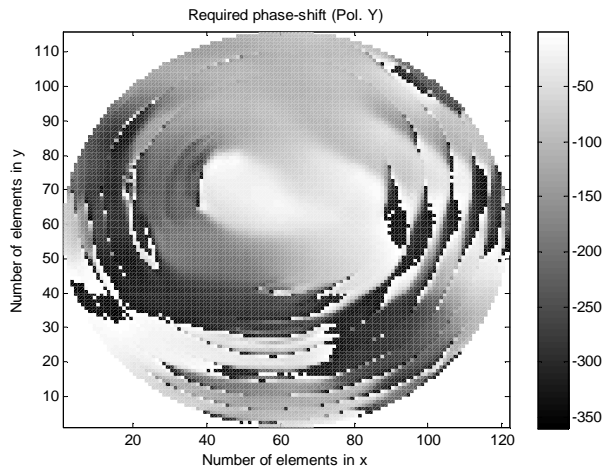
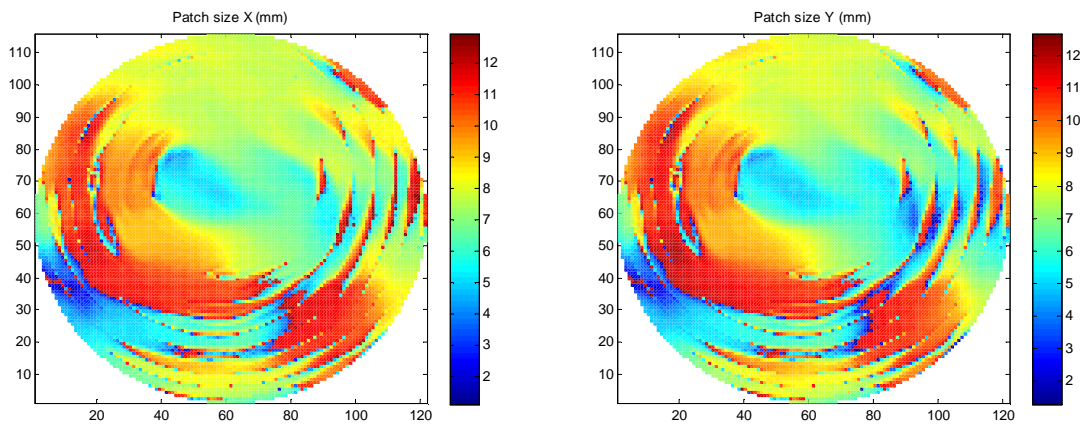


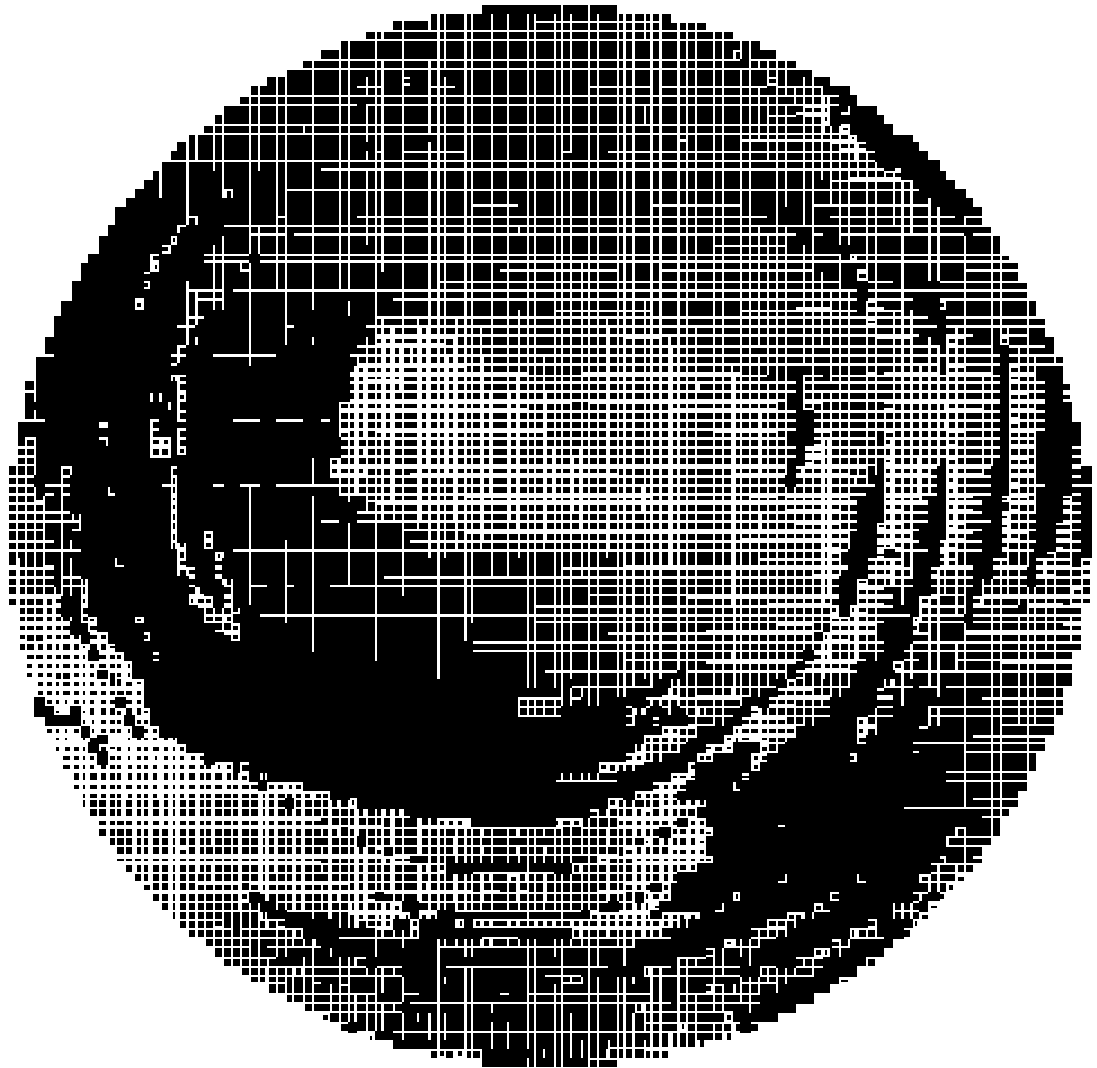
Fig. 6-5. Required phase-shift for a 1.5-m parabolic reflectarray at 11.95 GHz, $F/D=1.2$



(a)

(b)

Fig. 6-6. X-dimensions (a) and Y-dimensions (b) of the main parabolic reflectarray



(a)

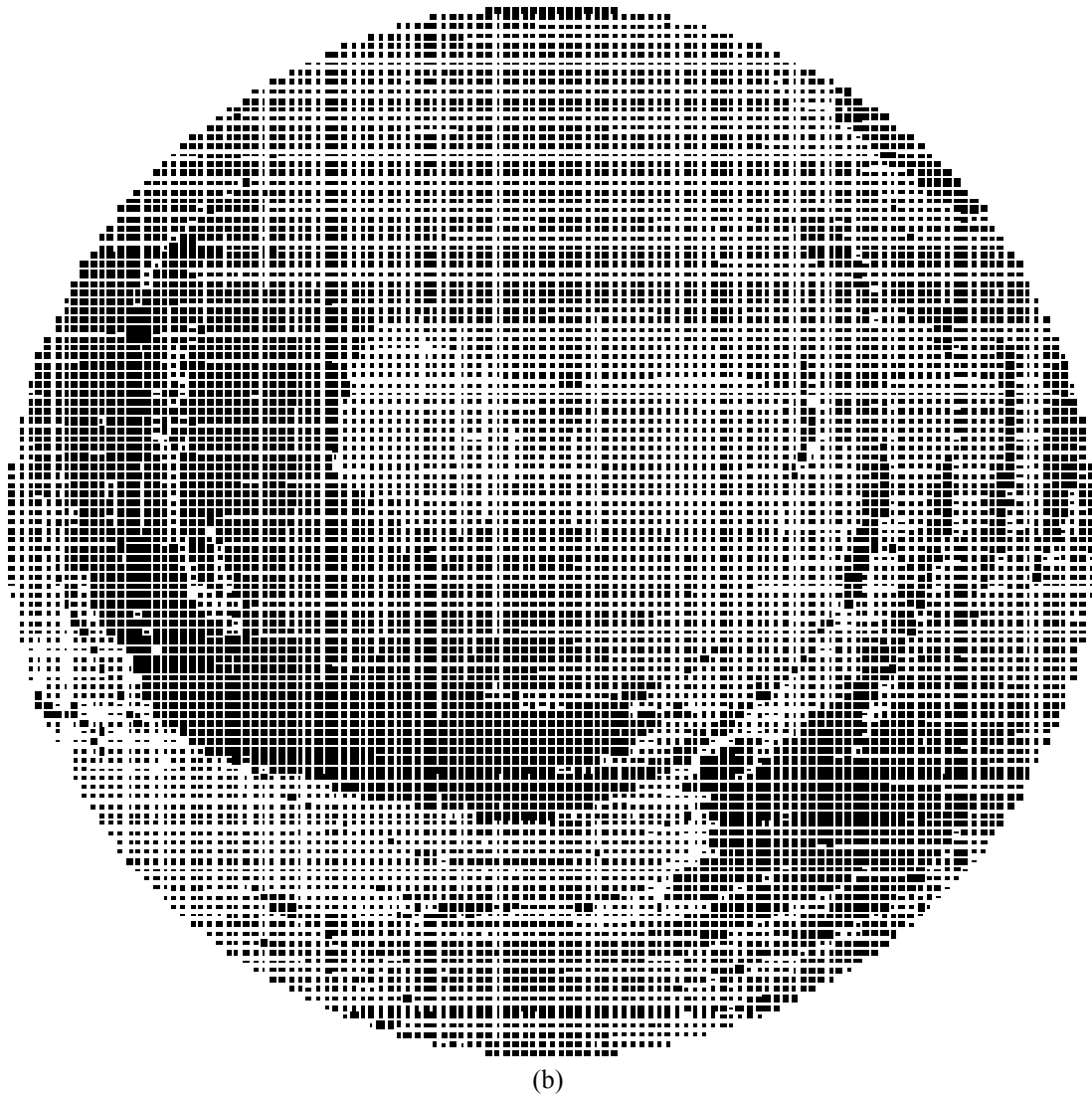


Fig. 6-7. Mask of parabolic main- reflectarray (a) bottom layer (closer to the ground plane) (b) top layer

6.1.2 *Antenna analysis*

The radiation patterns have been calculated by using the previously describe analysis technique at three frequencies: 11.7, 11.95 and 12.2 GHz, corresponding to the central and extreme frequencies of the defined transmission band (TX). Both co and crosspolar patterns are depicted in Fig. 6-8 to Fig. 6-10, showing that the contoured patterns are close to fulfill the coverage requirements (also shown in the figures as coloured polygons) at the three frequencies. Only two small holes on the border of the 28.81 dBi contour are found. Note that the antenna gain is slightly reduced in the areas of higher gain (28.81 dBi) because of ohmic losses and phase errors produced as a result of the

approximate design technique used in [9], in which the pattern synthesis is applied on the planar aperture and the required phase distribution is obtained by geometrical optics.

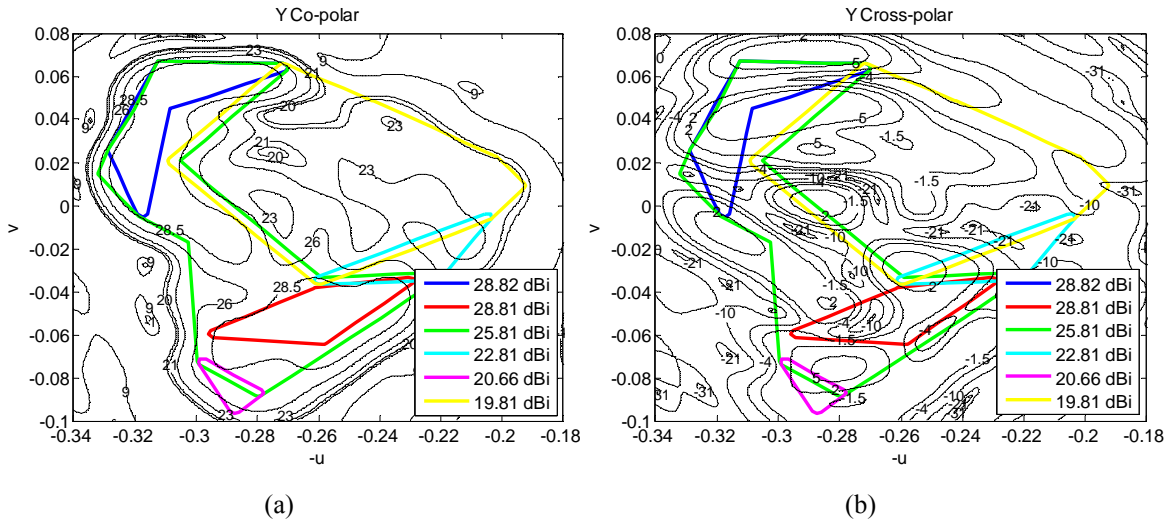


Fig. 6-8. Radiation patterns obtained by MoM for a two-layer reflectarray in Tx band, 11.95 GHz. (a) Copolar component. (b) Crosspolar component.

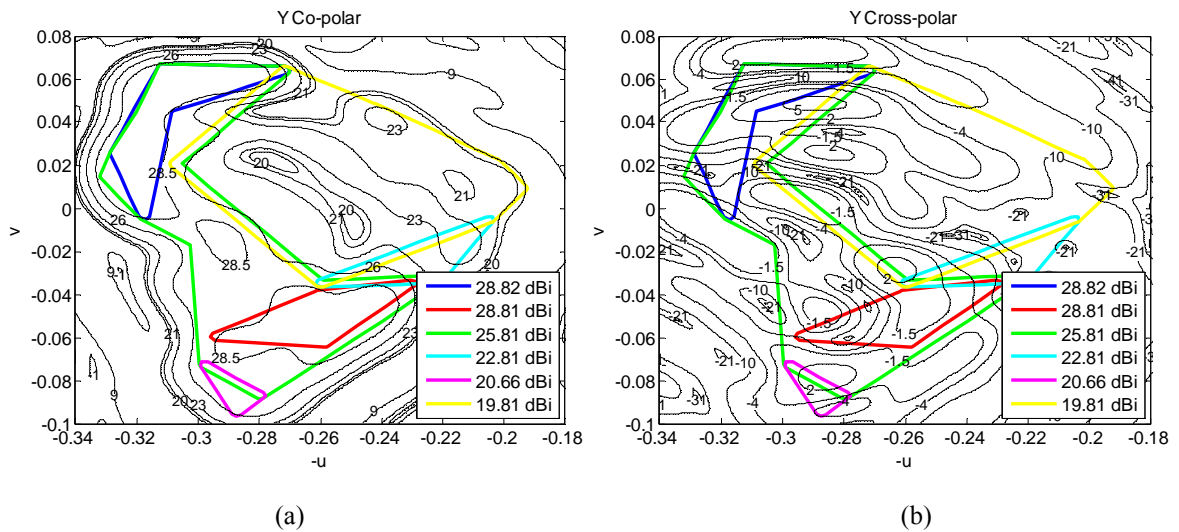


Fig. 6-9. Radiation patterns obtained by MoM for a two-layer reflectarray in Tx band, 11.7 GHz. (a) Copolar component (b) Crosspolar component

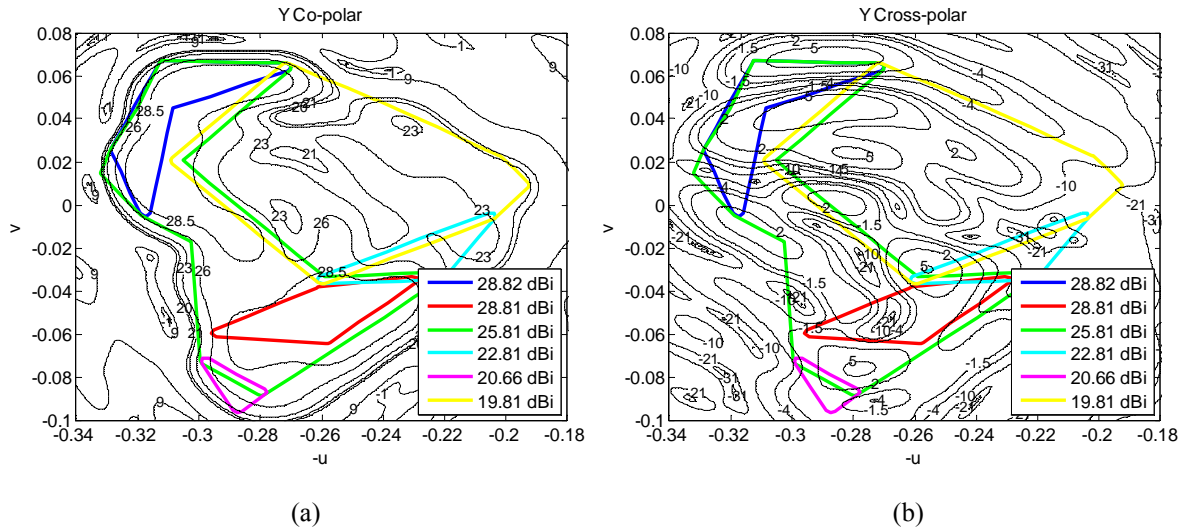


Fig. 6-10. Radiation patterns obtained by MoM for a two-layer reflectarray in Tx band, 12.2 GHz. (a) Copolar component (b) Crosspolar component

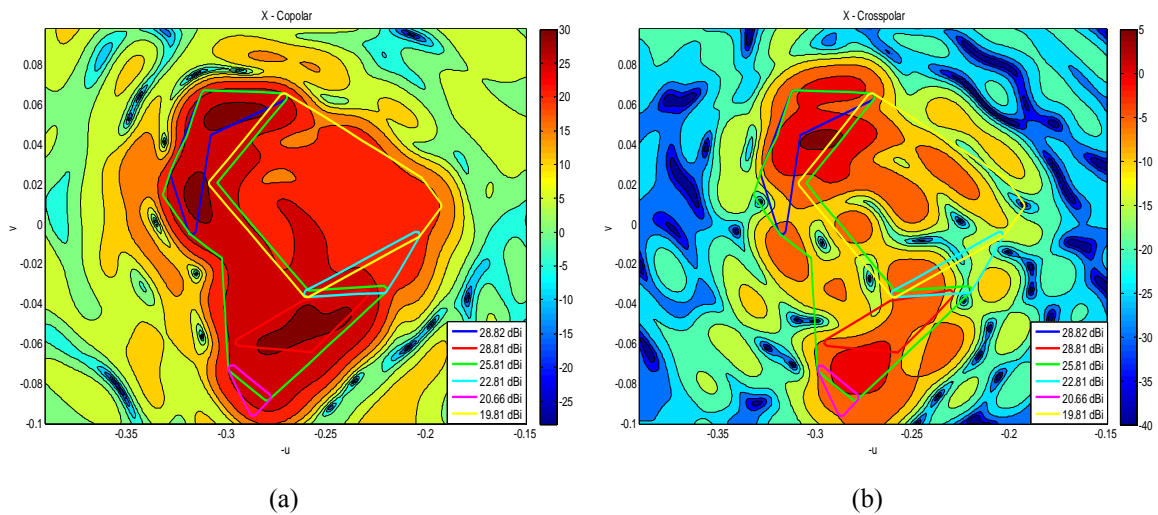


Fig. 6-11. Radiation patterns at 12.2 GHz in dB (a) Copolar component (b) Crosspolar component

The contoured patterns can be improved by a suitable pattern synthesis taking into account the curved surface. The analysis technique provides an accurate prediction of the cross polarization pattern performances, because it takes into account the cross-polarisation produced by the printed patches and by the offset reflector. The cross-polarisation shown in Fig. 6-11 is too high to be compliant with typical requirements in Telecommunication satellite missions, but it can be reduced by using the sub reflector, as in classic dual-reflector antennas.

6.1.3 Conclusions

The analysis technique described in chapter 2 has been extended in this chapter to analyse a dual-reflector antenna including main reflectarray on a parabolic surface and a flat reflectarray sub reflector. The technique can also be applied to analyse a more general dual-reflectarray antenna, in which the sub reflectarray, the main-reflectarray, or both can be printed on other type of curved surface. As a particular case, a single offset parabolic Reflectarray previously designed to provide a South American coverage has been analysed. The results show that the radiation patterns are close to the contour requirements. The lack of compliance in the coverage requirements is because of the simplifications carried out in the design process used in [9], although it can be improved in the future by applying a pattern synthesis technique that takes into account more accurately the parabolic surface.

The main drawback of the present configuration is the cross-polarisation, which is produced by the offset parabolic reflector and by the printed patches. The reflectarray sub reflector, considered in the analysis tool but not in the antenna reported in [9], will be optimised in a future work to reduce the cross polarisation of the antenna.

CHAPTER 7

7 Conclusions and future research lines

7.1 Conclusions

This thesis comprises the development of a general modular technique for the analysis of dual-reflectarray antennas. A detailed description of the methodology is discussed and a validation of the analysis technique is carried out in two parts. First, two dual-reflectarray antennas have been designed to be equivalent to dual-reflector antennas composed of a main parabolic reflector and a reflectarray acting as sub reflector, being the simulations of the dual-reflectarray antennas in good agreement with those of the reference antennas previously reported. Second, the design, manufacture and test of a very challenging dual-reflectarray antenna has been carried out, which shows the main capabilities of the system: large bandwidth and reduction of cross-polarization. Finally, two potential applications are evaluated. One of the applications proposed is a dual-reflectarray for beam scanning, by using a compact geometry that can be folded and deployed easily. Another application is DBS missions, based on dual-reflectarrays for contoured-beam antennas.

For the first time, a technique to analyze a general dual-reflectarray antenna is proposed, this comprises the analysis of the feed and the two reflectarrays. All the field

contributions radiated by the sub reflectarray elements are considered for an accurate computation of the incident field on the cells of the main reflectarray. The field reflected by the main reflectarray cells is computed through MoM considering local periodicity. A simplification has been introduced in the analysis method, consisting on using the same angle of incidence for the contributions from all the elements of the sub reflectarray. This incidence angle is calculated using the centre of the sub reflectarray as the origin of the field. This simplification yields a drastic reduction in the computation time and provides accurate results in many practical configurations as presented in this thesis. When the main-reflectarray is located in the near field of the sub reflectarray, the sub reflectarray elements are grouped in small arrays of elements, to provide a more accurate analysis of the dual offset configuration. Then, the field is decomposed in waves radiated by each sub reflectarray with different incident angles on the main reflectarray elements. Once the field reflected on the main reflectarray is calculated, the radiation patterns are computed using the Fast Fourier Transform to improve the numerical efficiency.

The method has been applied to design and analyse several dual-reflectarray antennas and their results are compared with those corresponding to other dual-reflector geometries with a reflectarray sub reflector, reported in previous works and considered as reference antennas. In this work, the main reflector is replaced by a main reflectarray to demonstrate that the antenna performance in terms of gain, efficiency and radiation patterns are equivalent. The first antenna consists on two flat reflectarrays in a dual offset configuration, that generates a pencil beam in Ku-band. In the second case, the main reflectarray focuses the beam and a sub reflectarray introduces a progressive phase to tilt the beam by 5 °. In this case, the near field radiated by the feed-horn has been included in the analysis to achieve accurate results. This improvement enables an accurate analysis of reflectarrays illuminated in the Fresnel zone of the primary feed.

Then, a dual reflectarray demonstrator has been designed, manufactured and tested for a full radiation of the analysis technique. The optics of the antenna is based on a compact range dual-reflector antenna, which produces low crosspolar radiation. The phase distribution of the sub reflectarray is defined to simulate an equivalent hyperbolic sub reflector with negative eccentricity. The antenna produces a pencil beam at $\theta=28^\circ$ and works in the Ku-band. A spherical wave expansion of the field radiated by the feed-horn

was used to compute accurately the incident field on the sub reflectarray elements, which is located in the Fresnel zone of the feed-horn. The cross-polarization generated by the antenna is due to two facts: the optics of the antenna and the crosspolarization introduced by the patches. The antenna geometry is heritaged from a dual offset parabolic system which fulfills Mizugutchi conditions, which reduces the crosspolar contribution. The crosspolar component generated by the patches is reduced locating a null of the phase curve on the area of the reflectarray where the maximum contribution of crosspolarization is produced. A breadboard of this design is manufactured and tested, achieving a good agreement between simulations and measurements. Other two designs are carried out based on the same antenna optics. A second design of the main-reflectarray based on a two layer configuration is performed. The goal of this design consists on the cancellation of the cross-polarisation introduced by the geometry and the patches of both the sub and the main reflectarray. In this case, the level of crosspolarization was even lower than the one obtained using ideal phases on the reflectarray elements, which means no cross-polarization introduced on the patches. The consequence of these results is that the method for reducing the cross-polarization is effective, because it produces a partial cancelation of the cross-polarization introduced by the geometry. A third design based on the same antenna optics is carried out to generate a contoured beam for DBS European coverage.

The beam scanning capabilities of dual-reflectarray configurations have been also studied. The preliminary results of a dual reflectarray antenna designed to provide electronic beam steering in portable systems for Ku-band satellite links with automatic pointing capabilities are presented. Two dual-reflectarray architectures have been studied. In the first one, the main reflectarray is passive and the beam scanning is achieved by introducing a phase-control in the elements of the sub reflectarray. In a second alternative, the antenna comprises a passive sub reflectarray and a main reflectarray with 1-bit electronic control to provide a pencil beam steerable in a $\pm 5^\circ$ angular range. The results show a satisfactory antenna performance in the prescribed frequency bands for transmit and receive links.

Finally, the analysis technique has also been applied to analyze a 1.5 m parabolic reflectarray antenna designed to generate South American coverage. Although the results can be improved in the future by applying a pattern synthesis technique, the

resulting radiation patterns are close to the coverage requirements. These results show the feasibility of dual-reflectarray antennas, which can be designed to improve the antenna performance by properly adjusting the phase on both reflectarray surfaces.

7.2 Original contributions

- 1) In this thesis, **it is proposed, implemented and validated for first time a general tool to analyze dual-reflectarray antennas, in which both, the sub reflector and the main reflector are reflectarrays.** The phase adjustment in both reflective surfaces can be used to achieve a significant improvement of the antenna performance in applications such as multi-beam, scanning beam or beams forming.
- 2) For the analysis of the dual-reflectarray configurations, **an approach that reduces drastically the computation time** has been proposed and validated. With this approach, the incident field is calculated by summing the contributions of the field radiated by each cell of the sub reflector and the angle of the field from the sub reflector is defined by assuming its origin in the sub-center of the reflectarray. This does not reduce the accuracy in the analysis of the main reflector, if the variation in the incident angle of the several elements of the sub reflectarray does not produce a significant variation of the phase shift of the main-reflector. This condition depends on the optics of the antenna and the sensitivity of the angle of incidence.
- 3) For those cases in which the previous approach is not accurate enough, **a more accurate technique** has been implemented, **which consist of dividing the reflectarray sub reflector in several groups** and computing the response on each element of the main reflectarray independently for each group. The number of groups in which the sub reflectarray is divided is maintained as a parameter in analysis tool, so that it can be adjusted, in order to have a better accuracy (more groups) or a better numerical efficiency (less number of groups). It has been checked and experimentally validated that the radiation patterns converges to the measurements when the number of groups is sufficient. The required number of groups depends on both, the

antenna configuration and the sensitivity of the reflectarray elements on the main reflectarray to the angle of incidence. It was checked that in most cases a division of the sub reflectarray in 9x9 groups is enough to provide accurate radiation patterns and good numerical efficiency.

- 4) **A dual-reflectarray antenna demonstrator has been designed, manufactured and measured for first time.** The antenna demonstrator is very challenging, because the sub reflector is located in the near field of the main reflector, violating the far field conditions, and because the sub reflector has also a large size with respect to the main-reflector. Therefore, the conventional approximations of far field are not suitable for the analysis of the antenna. The purpose of choosing this geometry was mainly to be used as benchmarking for the proposed analysis tool in very stringent conditions. To carry out the analysis, a spherical wave expansion of the feed-horn was implemented to calculate the incident field on the sub reflectarray. Because of the large size of the sub reflectarray, the elements of the sub reflectarray are grouped in sub-arrays for an accurate and efficiency analysis. The measured radiation patterns of the demonstrator have fully validated the analysis technique developed in the present thesis, under stringent conditions.
- 5) **Experimental demonstration of a previously proposed technique to reduce the cross-polarization in reflectarray antennas.** A technique consisting on the cancelation of the cross-polarization produced by the printed patches has been implemented in the antenna demonstrator. In addition, the cross-polarization has been reduced by applying Mizuguchi conditions to define the optics of the system. As a result, the antenna demonstrator provides very low levels of cross polarization (XPD oscillates between 32 dB and 40 dB for both polarizations in the frequency band from 12.2 GHz to 15GHz).
- 6) **To demonstrate that dual-reflectarray antennas provide broad-band operation.** The antenna demonstrator provides a 25% bandwidth, for a gain variation of 1 dB (from 12.2 GHz to 15 GHz). These results show that the

dual-reflectarray antenna can cover both transmit and receive bands in satellite Ku-band communications.

- 7) **To demonstrate that dual-reflectarray antennas can be used to provide beam scanning.** Some simulation results have been shown to demonstrate that a dual-reflectarray antenna can be used to scan the beam in a limited angular range. The results were validated by comparing the experimental results of a reference dual-reflector reflector-antenna (with a reflectarray sub reflector to deflect the beam) and a dual-reflectarray, where a reflectarray was designed to emulate the main parabolic reflector in the reference antenna
- 8) **To demonstrate that dual-reflectarray antennas can be used to provide contoured beams.** A relatively simple, but realistic, European coverage has been achieved by appropriate adjusting the phase distribution on the main reflectarray. The proposed dual-reflectarray antenna can be used to design DBS antennas, including the requirements of gain in the coverage region, cross-polarization and bandwidth.
- 9) **The analysis tool has been extended to curved reflectarrays.** An antenna system with a curved reflectarray as main reflector and a flat reflectarray as sub reflector has also been analyzed. In this case the curvature of the main reflector has been used to focus the beam in a large bandwidth, while the reflectarray patches produce the required shaping of the beam for an European DBS coverage.

7.3 Future research lines

- *Development and implementation of design techniques for multi-beam antennas or beam scanning using dual-reflectarray configurations.*

The fact of using two reflectarrays introduces an additional degree of freedom with respect to the case of single offset reflectors, enabling the possibility to sweep larger angles. Bifocal reflector antenna systems can be useful to design dual-reflectarray antennas for multiple beams. One of the main drawbacks of bifocal antennas is their larger size. However using an offset configuration could

compensate the blocking effect. The bifocal antenna configuration opens a great spectrum of possible applications and brings a lot of flexibility to the design, being a very promising field of research. Unfortunately, it all comes to the expense of more complex synthesis process.

- *Design of a dual reflectarray with a curved sub reflectarray.*

The target would be to investigate the benefits that a curved sub reflectarray could bring to the overall design. The idea is that the curvature would provide the focus of the beam, while the use of printed patches could shape the illumination on the main reflectarray in order to improve the gain level of the radiation pattern.

- *Synthesis technique applied to both surfaces.*

It is believed that the use of synthesis techniques can be applied to both the main and sub reflectarrays. This is expected to bring better performance of the antenna in terms of cross-polarization, shape and bandwidth. This should be obtained by making a synthesis on the main curve reflectarray, which would provide a phase-synthesis of the shaped beam, while a synthesis in the curve sub reflectarray could be used to improve the illumination on the main-reflectarray. The final result would be a synthesis in amplitude and phase.

- *Design of a dual reflectarray with an electronically reconfigurable sub reflectarray.*

Some demonstrators have already been reported of reflectarrays that can provide electronic scanning or reconfiguration of the beam. The dual-reflectarray antenna configuration can be very appropriate for the implementation of controllable phase-shifters in either the main or the sub reflectarray. Several examples have been provided in chapter 5, including preliminary results for beam scanning. Also this technique can be applied to reconfigure the beam coverage for space applications. A direct application of the already implemented analysis tool and the design techniques proposed in previous paragraphs will be the realization of dual-reflectarray antennas with beam reconfiguration capabilities.

- *Design of a dual reflector system with a reflectarray as sub reflector and a transmitarray as main-reflector.*

In compact range antennas as the one presented in Chapter 4 of this thesis, the possibility of scanning is limited by the geometry. Since, for large angles, the scanned beam may interfere with the feed-horn or the sub reflectarray. However, this scan angle can be increased if the same configuration is implemented with a sub reflectarray and a transmitarray as main reflector.

7.4 List of publications related to this work

7.4.1 Journal papers

- C. Tienda, M. Arrebola, J. A. Encinar and G. Toso: "Analysis of a Dual-Reflectarray Antenna", IET Microwave Antennas & Propagation, Vol.5, no.13, p.1636–1645, October 2011
- Three additional journal papers are being prepared based on the results obtained through the work reported in this Thesis.

7.4.2 International conferences

- C. Tienda, M. Arrebola, J. A. Encinar, G. Toso and C. Mangenot, "Analysis Technique for Double Reflectarray Antenna", 31st ESA Antenna Workshop, 18 - 20 May 2009, ESTEC, Noordwijk, The Netherlands
- J. A. Encinar, C. Tienda, E. Carrasco, M. Arrebola and G. Toso, "Design of Dual-Reflectarray Antenna for Beam Scanning", IEEE Antennas and Propagation Society (AP-S) and CNC/USNC/URSI, 11-17 July 2010, Toronto, Ontario, Canada
- C. Tienda, M. Arrebola, J. A. Encinar and G. Toso, "Analysis of Parabolic Reflectarray in Dual-Reflector Configuration", 4th European Conference on Antennas and Propagation, April 2010, Barcelona, Spain.
- C. Tienda, J.A. Encinar, S. Montori, R.Vincenti Gatti, M.Arrebola and R. Sorrentino, "Dual-Reflectarray Antennas for Bidirectional Satellite Links in Ku-

band”, 5th European Conference on Antennas and Propagation, 11-15 April 2011, Rome, Italy.

- C. Tienda, M. Arrebola and J. A. Encinar, “General Analysis Tool for Reflectarray Antennas in Dual-reflector Configurations”, 5th European Conference on Antennas and Propagation, 11-15 April 2011, Rome, Italy.
- C. Tienda, J. A. Encinar and M. Arrebola, ”Contoured-Beam Dual-Reflectarray Antenna for DBS Application”, IEEE International Symposium on Antennas and Propagation and USNC/URSI National Radio Science Meeting, 3-8 July, 2011, Spokane, Washington, USA
- G. Arista, M. Arrebola, M. Barba, J. Brunetti, F. Cacciamani, A. Cappelli, E. Carrasco, R. Centi, S. Coralluzzo, J. A. Encinar, M. Holzbock, O.Lücke, L. Marcaccioli, R. Midthassel, S. Montori, G. Pandoli, R. Sorrentino, C. Tienda, G. Toso, R. V. Gatti and M. Wener, “Reskue Project: Transportable Reflectarray Antenna for Satellite Ku-band Emergency Communications”, 33rd ESA Antenna Workshop, 18 - 21 October 2011, ESTEC, Noordwijk, The Netherlands
- C. Tienda, J.A. Encinar and M. Arrebola, “Dual-reflectarray Antenna in a Compact-range Configuration”, 33rd ESA Antenna Workshop, 18 - 21 October 2011, ESTEC, Noordwijk, The Netherlands

7.5 Research projects related to this thesis

The work described in previous chapters has produced several contributions to the analysis and design of printed reflectarrays in specific configurations. Part of this work has contributed to the development of several research projects.

- “Análisis, Diseño y Prototipado de Antennas Reflectarray y Tecnologías relacionadas para Aplicaciones de Espacio, Telecomunicaciones y Seguridad”, supported by Ministerio de Ciencia y Tecnología (MCYT). Developed by Department of Electromagnetism and Circuit Theory at Universidad Politécnica de Madrid (UPM). Main researcher: J. A. Encinar (ETC-UPM).
- “Transportable Reflectarray Antenna for Satellite KU-band Emergency Communications”, RESKUE Project supported by ESA (ESA ITT AO/1-

5609/08/NL/ST, ESTEC/Contract Number 22078/08/NL/ST). Developed by RF Microtech Srl (Italy) as prime contract, ELITAL Srl (Italy) and Universidad Politécnica de Madrid.

- “Tecnología de Terahertzios para Aplicaciones de Obtención de Información mediante Sensores Electromagnéticos” TERASSENSE (CSD2008-000068) project supported by Ministerio de Ciencia e Innovación as part of the projects CONSOLIDER-INGENIO 2010. Main researcher: Luis Jofre Roca from Universidad Politécnica de Cataluña with the collaboration of Mariano Barba Gea from Department of Electromagnetism and Circuit Theory at Universidad Politécnica de Madrid (UPM)

8 References

- [1] J. Huang, J. A. Encinar, “Reflectarray Antennas”, Wiley, Nov. 2007.
- [2] J. A. Encinar, “Design of two-layer printed reflectarrays using patches of variable size” IEEE Trans. Antennas Propag., vol. 49, no. 10, pp. 1403-1410, Oct. 2001
- [3] C. Wan and J. A. Encinar, “Efficient computation of generalized scattering matrix for analyzing multilayered periodic structure”, IEEE Trans. Antennas Propag., vol. 43, no. 11, pp.1233-1242, Nov. 1995
- [4] J. Huang, “Bandwidth study of microstrip reflectarray and a novel phased reflectarray concept”, in IEEE Intl. Symp. Antennas Propagat., Newport Beach, California, pp. 582-585, June 1995.
- [5] E.Carrasco, M. Barba and J. A. Encinar, “Reflectarray element based on aperture-coupled patches with slots and lines of variable length”, IEEE Trans. on Antennas and Propag., Vol. 55, No. 3, Pp. -, March. 2007.
- [6] D. M. Pozar, “Wideband reflectarrays using artificial impedance surfaces”, IEE Electron. Lett., vol. 43, no. 3, pp. 148-149, 2007.

- [7] J. A. Encinar, J. A. Zornoza, "Broadband design of three-layer printed reflectarrays", IEEE Trans. on Antennas and Propag. Vol. 51, No. 7, July 2003, pp.1662-1664
- [8] E. Carrasco, J.A. Encinar, M. Barba, "Bandwidth Improvement in Large Reflectarrays by Using True-Time Delay". IEEE Trans. Antennas Propag., vol. 56, no. 8, pp. 2496-2503, Aug. 2008
- [9] J.A. Encinar, M. Arrebola, G. Toso, "A parabolic reflectarray for a bandwidth improved contoured beam coverage", EuCAP 2007, Edimburgh, UK, 11-16 Nov. 2007
- [10] R. Leberer and W. Menzel, "A dual planar reflectarray with synthesized phase and amplitude distribution", IEEE Trans. Antennas Propag., vol. 53, no. 11, pp. 3534-3539, Nov. 2005
- [11] Carey M. Rappaport,, "An Offset Bifocal Reflector Antenna Design for Wide-Angle Beam Scanning", IEEE Transactions on Antennas and Propagation, Issue 11, Nov 1984 Page(s):1196-1204
- [12] J. Agustín Zornoza, Ralf Leberer, Jose A. Encinar, and Wolfgang Menzel, "Folded Multilayer Microstrip Reflectarray With Shaped Pattern", IEEE Transactions on Antennas and Propagation, Vol. 54, Issue 2, pp. 510-518, February 2006
- [13] C. Tienda, J. A. Encinar, S. Montori, R. Vincenti Gatti, M. Arrebola and R. Sorrentino, "Dual-Reflectarray Antenna for Bidirectional Satellite Links in Ku-band." Proceedings of the 5th European Conference on Antennas and Propagation (EUCAP), 11-15 April 2011
- [14] H. M. Braun, P. E. Knobloch, "SAR on Small Satellites- Shown on the SAR-Lupe Example" Proceedings of the International Radar Symposium 2007 (IRS 2007), Cologne, Germany, Sept. 5-7, 2007
- [15] R. J. Martin and D. H. Martin, "Quasi-optical antennas for radiometric remote-sensing", IEE Electron. & Comm. Eng. J., vol. 8, pp. 37-48, Feb. 1996

- [16] W. Hu, R. Cahill, J. A. Encinar, R. Dickie, H. Gamble, V. Fusco and N. Grant, "Design and Measurement of Reconfigurable mm Wave Reflectarray Cells with Nematic Liquid Crystal", *IEEE Trans. on Antennas and Propagat.*, vol 56, Issue 10, pp.3112 – 3117, Oct. 2008
- [17] Moessinger R, Marin J, Freese S, Mueller S, Manabe A, and Jakoby J, '77 GHz reconfigurable reflectarray with nematic liquid crystal', *Proc. 2nd European Conference on Antennas and Propagation, EuCAP*, Edinburgh, November 2007
- [18] W. Hu, M. Y. Ismail, R. Cahill, J. A. Encinar, R. Dickie, H. S. Gamble, V. F. Fusco, D. Linton, S. P. Rea, and N. Grant, "Liquid crystal based reflectarray antenna with electronically switchable monopulse patterns", *Electron. Lett.*, vol.43, no.14 pp. 744- 745, 2007.
- [19] W.Hu, M. Arrebola, R. Cahill, J.A. Encinar,V. Fusco, H. Gamble, Y. Alvarez, F. Las-Heras, "94 GHz Dual-Reflector Antenna with Reflectarray Sub reflector", *IEEE Trans. Antennas Propag.*, vol. 57, no. 10, part 2, pp. 3043-3050, Oct. 2009.
- [20] J. M. Colin, "Phased array radars in France: present and future , " *IEEE symposium on Phased Array System and Technology*, Boston, Massachusetts, October 1996 , pp. 458 – 462.
- [21] D. M. Pozar and T. A. Metzler , " Analysis of a reflectarray antenna using microstrip patches of variable size , " *Electronics Letters* , April 1993 , pp. 657 – 658 .
- [22] A. Kelkar , " FLAPS: conformal phased reflecting surfaces , " *Proc. IEEE National Radar Conf .*, Los Angeles , California , March 1991 , pp. 58 – 62.
- [23] Y. T. Gao and S. K. Barton , " Phase correcting zonal reflector incorporating rings , " *IEEE Trans. Antennas Propagat .*, Vol. 43 , April 1995 , pp. 350 – 355.
- [24] J. A. Encinar, and J. A. Zornoza, "Three-layer printed reflectarrays for contoured beam space application", in *IEEE Trans. Antennas Propag.*, vol. 52, no. 5, pp. 1138-1148, May 2004.

- [25] B. Khayatian, Y. Rahmat-Samii and R. Pogorzelski, "An antenna concept integrated with future solar sails", in Proc. IEEE Antennas Propagat. Soc. Int. Symp., pp. 742-745, July 2001.
- [26] S. M. Duffy and S. D. Targonski, "Comparison of two flat reflector-type designs for dualpolarization, dual-band operation", in Proc. IEEE Antennas Propagat. Soc. Int. Symp., pp. 288-291, July 2001.
- [27] D. M. Pozar, "Bandwidth of reflectarrays", Electronics Letters, Vol. 39, Oct. 2003, pp. 1490 – 1491.
- [28] E. Carrasco, M. Barba, and J. A. Encinar, "Aperture-coupled reflectarray element with wide range of phase delay", Electronics Letters, vol. 42, no. 12, pp. 1-2, June 2006
- [29] A. W. Robinson, M. E. Bialkowski and H. J. Song, "A passive reflect array with dual feed microstrip patch elements", Microwave and Optical Technology Letters, pp. 295- 299, December 1999.
- [30] J. Huang, V. A. Faria and H. Fang, "Improvement of the three-meter Ka-band inflatable reflectarray antenna", in Proc. IEEE Antennas Propagat. Soc. Int. Symp., pp. 122-125, July 2001.
- [31] L. Boccia, F. Venneri, G. Amendola, and G. Di Massa, "Application of varactor diodes for reflectarray phase control", IEEE AP - S/URSI Symposium, San Antonio, Texas, June 2002, Vol. 3, pp. 132 – 135.
- [32] S. V. Hum and M. Okoniewski, "An electronically tunable reflectarray using varactor - diode - tuned elements", IEEE AP - S/URSI Symposium, Monterey, California, June 2004, Vol. 2, pp. 1827 – 1830.
- [33] S. V. Hum, G. McFeeters, and M. Okoniewski, "A reflectarray cell based on a tunable MEMS capacitor", IEEE AP - S/URSI Symposium, Albuquerque, New Mexico, July 2006, URSI session 458.
- [34] V. Galindo, "Design of dual-reflector antenna with arbitrary phase and amplitude distribution", IEEE Trans. Antennas Propag, vol. AP-12, pp.403-408, Jul. 1964

- [35] K.A. Green, "Modified cassegrain antenna for arbitrary aperture illumination" IEEE Trans. Antennas Propag., vol. AP-11, pp. 589-590, Sep.1963
- [36] B. S. Westcott and F. Brickell, "Geometric-optics synthesis of dual reflector antennas with distributed sources" Proc.Inst. Elect. Eng. Microw., Antennas Propag., vol. 136, no.5, pt.H, pp. 361-366, Oct.1989.
- [37] J. Hakli, J. Ala-Laurinaho, and A.V. Raisanen, "Numerical synthesis method for designing shaped dual reflector feed system", Proc. Inst. Elec. Eng. Microw. Antennas Propag. Vol.152, no. 5, pp. 311-318, Oct. 2005
- [38] Y. Kim and T. H. Lee, "Shaped Circularly Symmetric Dual Reflector Antennas by Combining Local Conventional Dual Reflector System" IEEE Trans. Antennas Propagat ., Vol. 57 , January 2009 , pp. 47-56.
- [39] J. A. Encinar, et al. "Dual-Polarization Dual-Coverage Reflectarray for Space Applications", IEEE Trans. on Antennas and Propag., Vol. 54, No. 10, Pp. 2827-2837, Oct. 2006.
- [40] J. A. Encinar, M. Arrebola, L. de la Fuente , G. Toso, "Reflectarray Demonstrator for TX/RX Telecommunication Antenna", 32nd ESA Antenna Workshop on Antennas for Space Applications, Noordwijk (The Netherlands), 5-8 Oct 2010.
- [41] D. Pilz and W. Menzel, "Folded reflectarray antenna" Electronics letters, Vol. 34 Issue 9, pp.832-833, 30th April 1998
- [42] B. Khayatian, Y. Rahmat-Samii and J. Huang, "Radiation Characteristics of Reflectarray Antennas: Methodology and Applications to Dual Configurations" First European Conference on Antennas and Propagation- EUCAP 2006, Nice, France, November 6-10, 2006.
- [43] W.Huang and J. R. Lesh, "Reflectarray elements on sub-reflector for fine beam pointing", JPL New Technology Report No. 41562, Dec. 2004.
- [44] J. A. Encinar, M. Arrebola, L. F. de la Fuente, and G. Toso, "A Transmit-Receive Reflectarray Antenna for Direct Broadcast Satellite Applications" IEEE

Transactions on Antennas and Propagation, Vol.59, No 9, September 2011, pp.3255-3264

- [45] M. E. Cooley, T. J. Chwalek, “Method for improving pattern bandwidth of shaped beam reflectarrays”, patent US006031506, 2000
- [46] N. Chr. Albertsen, “Shaped-beam antenna with low cross polarization”, 7th European Microwave Conference, pp.339-342, 1977
- [47] Y. Mizugutch, M. Akawaka and H.Yokoi, “Offset dual reflector antenna” Antennas and Propagation Society International Symposium, pp.2-5, 1976
- [48] J.A. Encinar “Reduction of cross-polarization in contoured beam reflectarrays using a three-layer configuration” Antennas and Propagation International Symposium, 2007 IEEE, 9-15 June 2007 Page(s):5303 – 5306
- [49] M. Arrebola, Y. Alvarez, J. A. Encinar, F. Las-Heras, “Accurate analysis of printed reflectarrays considering the near field of the primary feed”, IET Microw., Antennas Propag., vol. 3, no. 2, pp. 187-194, March 2009
- [50] I. Gonzalez, E. Garcia, F. Saez de Adana and F. Catedra, “Computer tool for the analysis and design of periodic structures taken into account their real size and shape”, in Proc. 29th ESA Antenna Workshop on Multiple Beams and Reconfigurable Antennas, ESAESTEC, Noordwijk, The Netherlands, April 2007
- [51] F. De Vita, P. De Vita, A. Freni, P. Pirinoli, F. Vipiana, and G. Vecchi, “Fast analysis of large finite arrays with a combined multiresolution-fast MoM based techniques”, EuCAP 2007. The Second European Conference on Antennas and Propagation, 2007. Date: 11-16 Nov. 2007
- [52] Y. T. Lo and S. W. Lee, “Antenna Handbook. Vol. I. Antenna Fundamentals and Mathematical Techniques”. Pp. 1-28-1-29. Van Nostrand Reinhold.1993
- [53] K. Pontoppidan, Technical Description of GRASP8 (TICRA)
- [54] J.E. Hansen, ‘Spherical near-field measurements’, IEE Electromagnetics Wave Series 26, Peter Peregrinus Ltd.

- [55] CHAMP User's Manual, Ticra Report S461-01, TICRA Report
- [56] F. Las-Heras, M.R. Pino, S. Laredo, Y. Alvarez, T.K. Sarkar, "Evaluating Near-Field Radiation Patterns of the Commercial Antennas", IEEE Trans. Antennas Propag., vol. 46, no. 8, pp. 2198-2207, August 2006
- [57] Abramovitz and Stegun, 'Handbook of mathematical functions', Dover Publications Inc., USA (1965)
- [58] C. A. Balanis, "Antenna Theory. Analysis and Design." Second Edition. John Wiley&Sons. 1997
- [59] M. Arrebola "Contribution to the analysis and design of shaped-beam printed reflectarrays in complex configurations" PhD dissertation, Departamento de Electromagnetismo y Teoría de Circuitos, Universidad Politécnica de Madrid
- [60] J. A. Zornoza and M. E. Bialkowski, "Australia and New Zealand satellite coverage using a microstrip patch reflectarray", Microwave and Optical Technology Letters, vol. 37, no.5, pp. 321-325, June 2003
- [61] M. Arrebola, L. de Haro, J. A. Encinar, "Analysis of Dual-Reflector Antennas with Reflectarray as Subreflector", IEEE Antennas and Propagation Magazine., Dec. 2008, vol 50, Issue:6 pag:39-51. ISSN:1045-9243
- [62] M. Arrebola, J. A. Encinar and M. Barba, "Multifed printed reflectarray with three simultaneous shaped beams for LMDS central station antenna", IEEE Trans. Antennas Propag., vol. 56, no. 6, pp. 1518-1527, June 2008
- [63] W.V.T. Rush, A. Prata, J.R. Yahya Rahmat-Samii and R. A. Shore: "Derivation and Application of the Equivalent Paraboloid for Classical Offset Cassegrain and Gregorian Antennas" IEEE Trans. Antennas Propag., vol.38, No8, p.1141-1149, August 1990
- [64] A. Frandsen, "Software Package for Analysis of Corrugated and/or Smooth-Walled Horns with Circular Cross-Section" CHAMP User Manual
- [65] Bucci O. et al., "Intersection approach to array pattern synthesis", IEE Proceedings, vol. 137, Pt. H, no.6, pp. 349-57, 1990.

- [66] L. Marcaccioli, B. Mencagli, R. Vincenti Gatti, T. Feger, T. Purtova , H. Schumacher, R. Sorrentino,"Beam Steering MEMS mm-Wave Reflectarrays," MEMSWAVE 2006, Orvieto, Italy, June 27-30, 2006.
- [67] W. Menzel, M. Al-Tikriti and R. Leberer, "A 76 GHz multiple-beam planar reflector antenna", in Proc. 32nd European Microwave Conference, Oct. 2002.
- [68] J. A. Encinar, "Design of two-layer printed reflectarrays using patches of variable size," IEEE Trans. Antennas Propag., vol.49, p.1403-1410, Oct.2001.
- [69] E. Carrasco, J. A. Encinar, M. Barba, R. Vincenti, R. Sorrentino, "Dual-Polarization Reflectarray Elements for Ku-Band Tx/Rx Portable Terminal Antenna", EuCAP 2010, 12-16 April 2010, Barcelona, Spain.
- [70] W. Menzel, M. Al-Tikriti and R. Leberer, "A 76 GHz multiple-beam planar reflector antenna", in Proc. 32nd European Microwave Conference, Oct. 2002.
- [71] H. El Gannudi, R. Gatti, R. Vincenti, C. Tomassoni, R. Sorrentino, "Preliminary design of foldable reconfigurable reflectarray for Ku-band satellite communication" Antennas and Propagation (EuCAP), 2010 Proceedings of the Fourth European Conference on , vol., no., pp.1-5, 12-16 April 2010.
- [72] S. Ebadi, R. Vincenti Gatti and R. Sorrentino, "Linear Reflectarray Antenna Design Using 1-bit Digital Phase Shifters," 3rd European Conference on Antennas and Propagation, EuCAP 2009, Berlin, Germany, March 2009
- [73] R. Sorrentino, R. Vincenti Gatti, L. Marcaccioli, "Recent Advances in Millimetre Wave Reconfigurable Reflectarrays", 3rd European on Conference on Antennas and Propagation, EuCAP 2009, Berlin, Germany, March 2009
- [74] S. Montori, F. Cacciamani, R. Vincenti Gatti, R. Sorrentino, "Wideband Dual-Polarization Reconfigurable Elementary Cell for Electronic steerable RA in Ku-Band," 4th European Conference on Antennas and Propagation, EuCAP 2010, Barcelona, Spain, April 2010.

- [75] J. F. Kauffman, W. F. Croswell and L. J. Jowers, "Analysis of the radiation patterns of reflector antennas," in IEEE Trans. Antennas Propag., vol. AP-24, no. 1, pp. 53-65, Jan. 1976